UNIVERSITY OF LIVERPOOL

Elucidation of the Effects of Hypoxia on DNA Repair Machinery in Brain Tumour Cells

Thesis submitted in accordance with the requirements of the

University of Liverpool

For the degree of Doctor in Philosophy by

Sophie Cowman

September 2018

Acknowledgments

The journey through a PhD can sometimes be a turbulent one, full of laughs, cries and everything in between. It has been an interesting and exciting ride, one that I will never forget. The whole experience wouldn't have been the same without some special people, whom I owe a huge thank you to.

Firstly, I would like to thank my supervisor, Violaine, for her tremendous support throughout this whole process. Her knowledge and guidance have aided me through all my scientific woes, as well as the good parts too. I will be forever grateful to her for her wisdom and teachings that made me into the researcher I am today. Also, thank you to Nigel and Barry who were always there to provide me with insightful tips, tricks and ideas. To Anne and Rosalie, who spent their precious time teaching me exciting new lab techniques that I was eager to learn from my first day, and to Dave, who shared his magical skills and wizardry in image analysis, and made me never forget that 'every day is a school day'. To everyone in Lab B (plus a few from Lab A and E!), you made this whole process a great experience, I will never forget the laughs we shared.

A huge thank you to my parents who were there for me through the good times and bad. To my Mum, whose own career achievements inspired me to aim high and strive for success. To my Dad, whose hardworking and determined attitude has indeed transferred to me. I will be forever grateful for the strength he gave me to carry on even when times were tough. Finally to my Nanna 'cowie' who supported me from day one and was always cheering me on from the side line. All in all, this was an exciting journey and one that I will never forget!

P.S Thank you to those who provided me with the much-needed cups of tea and biscuits. I probably wouldn't have got through the PhD without them!

Abstract

Glioblastoma (GBM) and Medulloblastoma (MB) are the most common brain tumours of adults and children respectively. These tumours are hypoxic as their oxygen levels are lower than the physiological 5-8% O_2 found in the brain. Tumour hypoxia can promote tumour cell invasion, increase metastatic potential and leads to resistance to conventional cancer therapies. Chemotherapeutic agents and irradiation induce excessive DNA damage in order to overwhelm the DNA repair pathways and initiate apoptosis. This thesis aimed to examine the impact of hypoxia on DNA repair mechanisms in GBM and MB, which has not yet been reported. Hypoxic tumours are associated with poor patient outcome, in part due hypoxia-induced resistance to treatment. Work in this thesis showed that, in MB and GBM cells, chronic hypoxia was necessary to induced a resistance phenotype. Downregulation of critical components of the double strand break repair pathway was found to be responsible for treatment resistance in some, but not all hypoxic MB cells. Since hypoxia can directly influence transcription of DNA repair proteins, a NanoString assay was used to obtain a comprehensive assessment of DNA repair gene expression in multiple MB and GBM cell lines exposed to hypoxia. Moderate and severe hypoxic exposure had a variable impact on gene expression, with no clear-cut impact of different oxygen tensions. The level of transcripts of several DNA repair genes were downregulated across multiple GBM cell lines, especially *LIGIV*, which encodes DNA Ligase IV responsible for joining double strand breaks during DNA repair. A multiphoton laser microirradiation protocol was used to assess, in living cells, the functional impact of *LIGIV* downregulation. Reduced double strand break repair efficiency in hypoxia was observed, which may lead to genomic instability that drives tumour progression. Investigations into GBM and MB tumour cell biology, such as that described in this thesis, will aid in the development of new treatment methods, which are desperately needed.

Contents

List of Figures

List of Tables

Abbreviations

2D	Two dimensions
3D	Three dimensions
AF	Acriflavin
AMP	Adenosine monophosphate
APS	Ammonium persulfate
ATO	Arsenic trioxide
BCA	Bicinchoninic acid assay
BER	Base excision repair
bHLH	Basic helix-loop-helix
BrdU	Bromodeoxyuridine
BSA	Bovine serum albumin
CCD	Charged-coupled-device
CMV	Cytomegalovirus promoter
CNS	Central nervous system
CPDs	Cyclobutane-pyrimidine dimers
CTAD	Carboxy-terminal transcriptional activation domain
CV	Crystal violet
DDR	DNA damage response
DE	Differential expression
DGS	Directed global significance
DMEM	Dulbecco's modified eagle's medium
DMOG	Dimethyloxalylglycine
DSB	Double strand breaks
DTT	1,4-dithiothreitol
E.coli	Escherichia coli
EDTA	Ethylenediaminetetraacetic acid
EGFP	Enhanced green fluorescent protein
EGFs	Epidermal growth factors
EGTA	Egtazic acid

EMEM	Eagle's minimum essential medium
EMT	Epithelia-mesenchymal transition
EtOH	Ethanol
FCS	Foetal calf serum
GBM	Glioblastoma
GS	Global significance
HK	House keeping
HRE	Hypoxia responsive elements
HRR	Homologous recombination repair
ICL	Interstrand crosslinks
IMRT	Intensity modulated radiotherapy
IR	Infrared
IRIF	Ionising radiation induced foci
kV	Kilovolts
mA	Milliamps
MB	Medulloblastoma
MDR	Multidrug resistance proteins
MGMT	Methylguanine methyltransferase
MMPs	Matrix metalloproteases
MMR	Mismatch repair
MMS	Methy methanesulfonate
mRNA	Messenger RNA
MSE	Mean squared error
NA	Numerical aperture
NaPyr	Sodium pyruvate
NER	Nucleotide excision repair
NHEJ	Non-homologous end joining
NHS	National Health Service
NSC	Neural stem cells
NTAD	Amino-terminal transcriptional activation domain
ODD	Oxygen dependent domain

PBS	Phosphate buffered saline
PMSF	Phenylmethylsulfonyl fluoride
PNET	Primitive neuroectodermal tumour
Pol	Polymerase
QC	Quality control
RFP	Red fluorescent protein
ROI	Region of Interest
ROS	Reactive oxygen species
RPM	Revs per minute
RT	Radiotherapy
RT-PCR	Real-time polymerase chain reaction
SDS	Sodium doecyl sulfate
SDS-PAGE	Sodium dodecyl sulfate – polyacrylamide gel electrophoresis
SGZ	Subgranular zone
siRNA	small interfering RNA
SOC	Super optimal broth with catabolite repression
SSB	Single strand breaks
SSH	Sonic Hedgehog
SVZ	Subventricular zone
TAGC	The Cancer Genome Atlas Consortium
TAM	Tumour associated macrophages
TBE	Tris/Borate/EDTA
TBS	Tris-buffered saline
TBS-T	Tris-buffered saline with Tween-20
TEMED	N,N,N′,N′-Tetramethylethylenediamine
TME	Tumour microenvironment
TMZ	Temozolomide
UV	Ultra violet
WHO	World Health Organisation
WNT	Wingless
XIR	XRCC4 interacting region

Chapter 1: Introduction

1.1 Human cancers

Cancer is a deadly disease where abnormal cells rapidly divide and invade healthy tissues. Cancer can arise in many areas of the body including the lungs, liver, stomach, brain, bones and skin, leading to organ malfunction and ultimately death. In 2015, 8.8 million people died from cancer globally making it the second leading cause of death. Cancer development is a multi-step process whereby pre-cancerous lesions undergo cellular changes resulting in the formation of a malignant tumour. Lifestyle choices such as poor diet, smoking and alcohol use, can significantly increase risk of developing cancer, yet genetic factors also play a role. Through advances in medical technology and scientific research, the survival rate for some cancers has improved in the last few decades. In the 1970s only four in ten women with breast cancer survived beyond ten years, yet this figure has increased to eight in ten due to enhancements of detection and improved treatment methods. The prevalence of cancer is increasing with an ageing population. Cancer in childhood is rare, and the survival rate is high compared to adults. However, detrimental side effects from treatment can arise (Murphy *et al.*, 2013). For both adult and childhood cancer, the survival remains low, and further research is required to improve detection and treatment.

Through a variety of mechanisms, the majority of cancers acquire a set of functional capabilities that enable the progression and development of cancer. These characteristics are known as the 'Hallmarks of Cancer', first described by Hanahan and Weinberg in 2000. Cancer cells can evade cell death (apoptosis), sustain blood vessel production (angiogenesis), generate growth signals, invade healthy tissue (metastasis) and have limitless ability to replicate (Hanahan and Weinberg, 2000). The identification of these classical properties of cancer has aided the development of targeted therapies and improved understanding of the disease as a whole (Figure 1.1). In 2011, the 'Hallmarks of Cancer' was further updated to include evading the immune system, genetic instability and metabolism reprogramming (Hanahan and

Weinberg, 2011) (Figure 1.1). In part, these characteristics are mediated through interactions with the surrounding environment, known as the tumour microenvironment. The microenvironment can directly influence tumour progression and the response to treatment. Exploration of the implications of a low oxygen (hypoxic) tumour microenvironment on tumour cell biology will be a feature of this thesis.

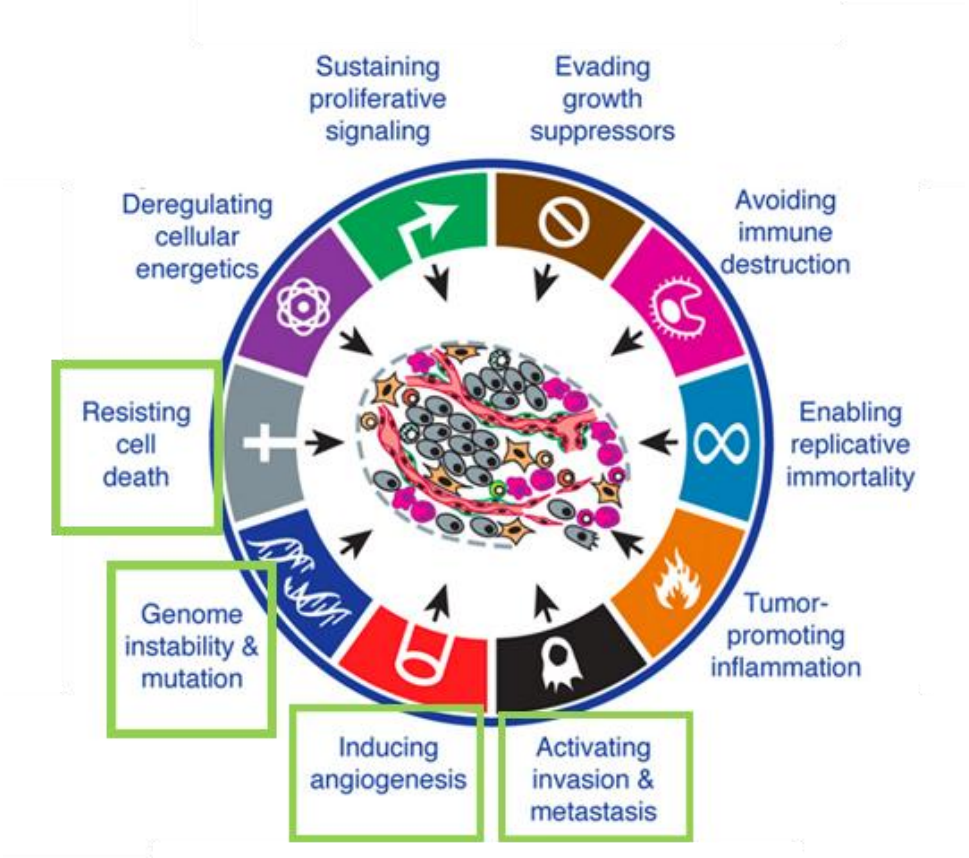

Figure 1.1: The Hallmarks of Cancer. General characteristics of cancer that contribute to tumorigenesis and cancer progression. Highlighted hallmarks are to be discussed in this thesis. Adapted from Hanahan and Weinberg, 2011.

1.2 Brain tumours

The primary site of tumour formation can directly influence patient outcome. Brain tumours, in particular, are linked to poor patient survival. Unlike other cancers such as breast cancer, the outcome of brain tumour has improved very little in the last few decades. Surgery is limited, as removing substantial proportions of healthy tissue can negatively affect patient health. Additionally, the blood-brain barrier restricts the diffusion of chemotherapeutic agents, limiting possible treatment options. These factors directly contribute to the poor outcome of brain tumour patients. Brain tumours are classified into benign low grade (grade I and II) or malignant high grade (grade III and grade IV), and are named based on the cell or region of origin (Louis *et al.*, 2007, 2016). High-grade tumours pose a significant threat to life. Further understanding of the cell biology of these tumours is required to improve the treatment and management of this complex disease.

1.3 Adult glioblastoma

Adult glioblastoma multiforme (GBM) is the most common malignant brain tumour, which arises in the cerebellum. 2,200 new cases are diagnosed in the United Kingdom each year. GBM is primarily found in older patients over 60 with a median diagnosis age of 64 (Dolecek *et al.*, 2012). Survival rates are poor with mean survival for England in 2007-2011 being 6.1 months and a five-year survival rate of 3.4% (Brodbelt *et al.*, 2015). Clinical presentation includes headaches, confusion, memory loss, seizures and changes in personality. Due to the unspecific nature of these symptoms, diagnosis of GBM is usually delayed resulting in detection when a tumour is well established. This, as well as the highly infiltrative and resistant nature of GBM, is responsible for the tragically low survival rates.

1.3.1 Pathology

The WHO classification of central nervous system (CNS) tumours differentiates gliomas into four histology-based grades, segregated by the degree of aggressiveness, anaplasia and un-differentiation (Louis *et al.*, 2007, 2016). GBM is defined as a Grade IV astrocytoma (Figure 1.2) and accounts for 82% of malignant gliomas (Dolecek *et al.*, 2012). Vascularisation and level of necrosis differentiate grade IV (GBM) from grade III astrocytoma. Although GBM is primarily diagnosed using histology, recent advances in sequencing technologies have enabled the identification of molecular signatures of GBM.

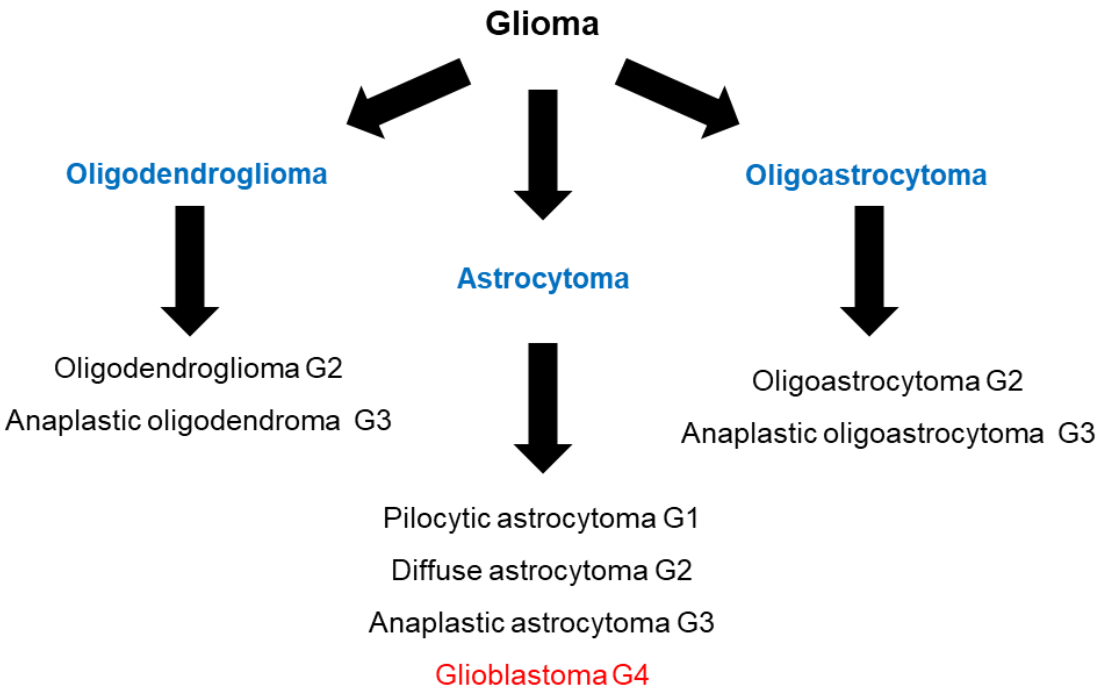

Figure 1.2: Classification of Gliomas. Gliomas fall into three subgroups. These are further categorised into grades based on aggressiveness, anaplasia, un-differentiation and vascularisation. G1 - G4 = WHO Grade I – Grade IV.

The Cancer Genome Atlas Consortium (TCGA) performed transcriptome profiling on over 600 GBM tumours, resulting in the identification of genetic mutations in *TP53*, *EGFR*, *IDH1* and *PTEN* (for brevity abbreviations will be used for genes and proteins, for full names see appendix 1.1), as well as abnormalities in the p53, RB and receptor tyrosine kinase pathways (McLendon *et al.*, 2008; Noushmehr *et al.*, 2010; Verhaak *et al.*, 2010; Brennan *et al.*, 2013; Ceccarelli *et al.*, 2016). This work enabled the molecular classification of GBM into four subtypes; Classical, mesenchymal, neural and proneural (Phillips *et al.*, 2006; Verhaak *et al.*, 2010). However, recent work by Wang *et al.* 2017 using single-cell transcriptomic analysis, suggest that only three subtypes exist as the neural subtype is likely due to contamination with other non-GBM neural tissue (Wang *et al.*, 2017). Proneural GBM has the best outcome, whereas mesenchymal results in a low rate of survival (Phillips *et al.*, 2006). The classical characteristics of the three main GBM subtypes are detailed in Table 1.1. Primary and secondary GBM can frequently be distinguished by the Isocitrate dehydrogenase (IDH) status, with mutated *IDH* genes primarily found in secondary tumours (Ohgaki and Kleihues, 2013). Although histology is still the primary tool for GBM diagnosis, identification of GBM molecular signatures will enable a further understanding of tumour cell biology, which may lead to a personalised medical approach with targeted therapies.

Table 1.1: The common molecular characteristics of GBM subtypes. Information obtained from Veraak et al., 2010

Subtype	Characteristics
Classical	• *EGFR* amplification and increased expression • Chromosome 7 amplification • Chromosome 10 loss • No *TP53* mutations
Mesenchymal	• Loss of *NF1* gene or low expression • Expression of mesenchymal makers
Proneural	• Alterations of *PDGFRA* gene • Mutations in *IDH1* • *TP53* mutations and loss of heterozygosity

1.3.2 Cellular origin of GBM

The specific cell of origin for GBM is unknown, yet the development of GBM mouse models has aided the identification of potential GBM-initiating cell types. Within an adult brain, two neurogenic regions (areas where neurogenesis occurs) are present, the subventricular zone (SVZ) and the subgranular zone (SGZ). Within the SVZ and SGV, neural stem cells (NSC) reside. NSC can self-renew and give rise to progenitor cells (Eriksson *et al.*, 1998; Sanai *et al.*, 2005). Specifically, the SVZ contains glial progenitors, which have limited self-renewal capabilities and commit to specific cell types. Adult NSC, as well as progenitor cells, express nestin (Lendahl *et al.*, 1990;

Zimmerman *et al.*, 1994). Injection of Cre-recombinase adenovirus, under the control of the nestin promoter, into the SVZ of mice with conditional tumour suppressor alleles, *Nf1*, *Trp53, Pten,* enabled the specific targeting of NSC, resulting in the formation of high-grade astrocytoma (Llaguno *et al.*, 2010). Additionally, using a similar Cre-recombinase system targeting adult lineage-restricted progenitor cells, mice formed both grade III and grade IV astrocytomas (Alcantara Llaguno *et al.*, 2015). Whether fully differentiated CNS cells are involved in GBM formation is controversial and has not been fully explored. Taken together, mutations in both NSC and lineage-restricted progenitor cells can give rise to GBM; therefore, different origins could contribute to the heterogeneity of GBM.

1.3.3 Treatment

Current treatment methods of GBM show limited success. Standard protocols involve initial resection of the tumour mass followed by radiotherapy (RT) and chemotherapy. Surgical resection of GBM is challenging, due to the highly infiltrative nature of these tumours, making it difficult to define the exact tumour border. Therefore, RT and chemotherapy are essential. Typically, RT is given as 30 fractions with a 60 Gy dose (Omuro and DeAngelis, 2013). A randomised trial using an escalated irradiation dose found no significant improvement in survival with irradiation doses above 60 Gy (Chang *et al.*, 1983). The alkylating agent temozolomide (TMZ) is used as an adjuvant with RT. This combination results in an increase in mean survival rate compared to RT alone (Athanassiou *et al.*, 2005). However, the effectiveness of TMZ is limited due to the requirement methylguanine methyltransferase (*MGMT*) gene silencing in order to induce DNA damage leading to apoptosis (Brada *et al.*, 1999; Glassner *et al.*, 1999; Esteller *et al.*, 2000; Hegi. *et al.*, 2005). Investigations into alternative treatment protocols are underway to improve survival rates, particularly in non-silenced MGMT patients. For example, Olaparib, a PARP inhibitor used for ovarian cancer, is currently undergoing a phase I trial for GBM. Inhibiting the DNA damage response pathway by

reducing PARP activity may increase the sensitivity of GBM to ionising radiation and temozolomide (Cheng *et al.*, 2005). Additionally, vaccine development is a potentially promising therapeutic option. These vaccines are composed of dendritic cells pulsed with tumour lysate or synthetic peptides, resulting in the initiation of an anti-tumour immune response (Zhang *et al.*, 2004). Initial results from a recent phase III trial found that the vaccine is safe and may extend survival, yet data from this study is only in the preliminary stages of analysis (Liau *et al.*, 2018). Although attempts to improve GBM treatment have been made, survival over five years remains close to zero, highlighting the need for further understanding of the complex biology of these tumours.

1.4 Paediatric medulloblastoma

Medulloblastoma (MB) is a primitive neuroectodermal tumour (PNET) (Grade IV) that arises in the posterior fossa. It is the most common paediatric malignant tumour of the CNS accounting for 15-20% of neoplasms (Hargrave and Zacharoulis, 2007). The peak incidence for MB is 4-7 years with increased prevalence in males, yet MB has been identified in a small proportion of teenage individuals (Pizer and Clifford, 2008). In comparison to GBM, the prognosis of MB is better; however current treatment protocols can have a negative impact on the developing brain of a child.

1.4.1 Pathology

Previously, classification of MB was primarily based on histopathology. However, advances in sequencing technologies have enabled a molecular-based approach (Louis *et al.*, 2007). Recent classification defines MB into four subgroups: Wingless (WNT), Sonic Hedgehog (SHH), Group 3 and Group 4.

1.4.1.1 WNT – 10% of MB

The WNT subgroup of MB is based on activation of WNT signalling through genetic mutations in the Wingless signalling cascade. Commonly, mutations in the *CTNNB1* gene are found which results in stabilisation of β-catenin, leading to aberrant activation of the WNT pathway (Yokota *et al.*, 2002; Ellison *et al.*, 2005; Northcott *et al.*, 2017). Other mutated genes found in WNT MB include *APC, DDX3X, SMARCA4, AXIN1* and *CREBBP* (Dahmen *et al.*, 2001; Yokota *et al.*, 2002; Jones *et al.*, 2012; Pugh *et al.*, 2012; Robinson *et al.*, 2012; Northcott *et al.*, 2017). Chromosomal aberrations such as loss of chromosome 6 has also been observed (Clifford *et al.*, 2006). From a survival perspective, patients with WNT MB have the best prognosis, as these tumours respond well to chemotherapy (Cho *et al.*, 2011; Northcott *et al.*, 2011; Kool *et al.*, 2012; Taylor *et al.*, 2012). Diagnosis of WNT is often by detection of monosomy 6 or *CTNNB1* mutations, yet these are not always present suggesting that some WNT tumours will be missed (Northcott *et al.*, 2017).

1.4.1.2 SSH – 30% of MB

SHH tumours display aberrant activation of the Sonic Hedgehog pathway. This is commonly due to germline or somatic mutations in components of the SHH pathway, for example, *PATCHED1* and *SUFU* (Robinson *et al.*, 2012). Additionally, these tumours tend to have *MYCN* and *GLI2* amplification (Jones *et al.*, 2012; Pugh *et al.*, 2012; Robinson *et al.*, 2012). In a third of SHH tumours, *TP53* mutations have been identified which are thought to be germline mutations resulting in a worse patient outcome (Zhukova *et al.*, 2013).

1.4.1.3 Group 3 – 25% of MB

Group 3 MB are undoubtedly the most aggressive MB tumours, as they are highly metastatic, with tumour dissemination normally observed at initial diagnosis (Kool *et al.*, 2012). Unlike the other MB subtypes, Group 3 has the

fewest recurrent mutations (Jones *et al.*, 2012; Northcott *et al.*, 2012, 2017; Pugh *et al.*, 2012; Robinson *et al.*, 2012), however in 20% of Group 3 MB, *MYC* amplification is found in combination with *PVT1* amplification (Kool *et al.*, 2012; Northcott *et al.*, 2012, 2017). Additionally, TGF-β and NOTCH signalling pathways may be activated (Kool *et al.*, 2012; Northcott *et al.*, 2017). In 40% of patients, 17p loss and 17q gain has been identified (Kool *et al.*, 2012; Shih *et al.*, 2014). Mutation in *TP53* are rare in Group 3 MB (Zhukova *et al.*, 2013).

1.4.1.4 Group 4 – 35% of MB

Group 4 is currently the least understood of the MB tumour subtypes in part due to the current lack of animal models. Group 3 and Group 4 MB present with a high level of molecular similarity, however recent work by Cavalli *et al.* determined they are molecularly distinct (Cavalli *et al.*, 2017). Similar to Group 3, Group 4 MB has amplification of *MYC,* simultaneous loss of 17p and gain of 17q, and *TP53* mutations are rare (Kool *et al.*, 2012; Zhukova *et al.*, 2013; Northcott *et al.*, 2017), Duplication of the *SNCAIP* gene has also been identified. At the time of diagnosis of Group 4 MB, metastatic dissemination is often observed (Kool *et al.*, 2012), however, prognosis is moderately better than Group 3 MB.

A detailed summary of age distribution, sex distribution, metastatic potential, recurrence and prognosis for each subgroup can be found in Table 1.2.

1.4.1.5 Further Subtyping of MB

Although the four subtypes are the MB classification accepted by the World Health Organisation (WHO), recent work suggests there may be up to 12 subtypes: two WNT, four SHH, three Group 3 and three Group 4. Using genome-wide methylation and expression analysis of MB tumours, Cavalli *et al.* were able to identify cytogenetically and clinically distinct subsets of the four main MB subgroups (Cavalli *et al.*, 2017). Whether these 12 subtypes will

be assimilated into the classification of MB, and will play a role in clinical management remains to be seen.

Table 1.2 Comparison of characteristics of medulloblastoma. Infant = 0 – 3 years. Child = 3 – 16 years. Information from Skowron et al., 2015; Taylor et al., 2012.

	WNT	SHH	Group 3	Group 4
Gender distribution	50% M 50% F	50% M 50% F	75% M 25% F	75% M 25% F
Age distribution	100% Child	50% Infant 50% Child	25% Infant 75% Child	10% Infant 90% Child
Rate of Metastasis	Rare	Low	High	High
Recurrence	None	Local	Metastatic	Metastatic
Prognosis	Excellent	Good	Poor	Good

1.4.2 Cellular origin of MB

Understanding the cellular origin of MB has been challenging due to the high level of tumour heterogeneity. Each subgroup of MB arises within different regions of the brain, therefore, are likely to arise from a different tumour initiating cells. Work by Gibson *et al.* determined that the WNT subtype originated from progenitor cells in the dorsal brainstem (Gibson *et al.*, 2011), whereas SSH MB arises from granule neurone precursors cells in the cerebellar hemispheres (Schüller *et al.*, 2008; Yang *et al.*, 2008; Gibson *et al.*, 2011; Perreault *et al.*, 2014). The origins of Group 3 and Group 4 is less clear, yet

evidence suggests that Group 3 may arise from granule neuron precursors, ventricular zone stem cells or other progenitors (Kawauchi *et al.*, 2012; Pei *et al.*, 2012). Whereas, Group 4 MB may originate from deep nuclei precursors in the upper rhombic lip (Lin *et al.*, 2016). Further exploration of the genetic drivers of the MB subgroups will allow for the development of MB mouse models that will give insight into MB origins.

1.4.3 Treatment

Similar to GBM, surgical resection followed by radiotherapy and chemotherapy is the general treatment protocol for MB. Total resection of the tumour may be possible if the tumour has not extensively invaded the brainstem or cerebellum (De Braganca and Packer, 2013). Removal of the whole tumour mass was initially viewed as ideal, however, damage to healthy tissue leads to cognitive defects and issues with motor function (Leland *et al.*, 1996). Recent work determined that there was no observed benefit to progression-free survival when comparing gross total resection and near-total resection for WNT, SHH and Group 3 MB. Therefore, total resection may not be required, and limited resection could reduce unwanted side effects of excessive resection (Thompson *et al.*, 2016).

Chemotherapy is used post-surgery, with cisplatin, cyclophosphamide and vincristine being favoured (Packer *et al.*, 2006; Jakacki *et al.*, 2012). Exploration of other useful chemotherapeutic agents is currently underway. For example, evidence suggests that TMZ in conjunction with radiotherapy is tolerable in paediatric MB patients (Nicholson *et al.*, 2007; Malbari *et al.*, 2012), yet whether this improved survival requires further exploration. Post-surgery RT is specifically directed at the entire craniospinal axis (whole brain and spinal column) due to the dissemination pattern of the tumour (Gold *et al.*, 1999). There is no significant difference in the toxicity of irradiation when using hyper-fractionated (several daily doses) over standard RT (single daily dose) (Câmara-Costa *et al.*, 2015). Alternative RT techniques are under

investigation for MB treatment to reduce the off-target effects and toxicity of standard protocols. Proton beam therapy, has been shown to have a similar positive outcome as standard RT, with acceptable levels of toxicity (Yock *et al.*, 2016). Also, intensity modulated radiotherapy (IMRT) reduces unwanted ototoxicity (toxicity to the ear) compared to standard RT (Huang *et al.*, 2002; Bao *et al.*, 2009; Polkinghorn *et al.*, 2011). The use of RT in infants is unfavourable due to the developmental defects likely to occur. Therefore, in young patients (< 3 years old), chemotherapy alone is preferable post-resection, with radiotherapy introduced when the child is at least three years old (Rutkowski *et al.*, 2008). Molecular classification has enabled a more personalised approach to MB treatment. For example, WNT tumours, which have the best prognosis, may require less RT and chemotherapy for successful treatment. Current trials are underway to understand whether it would be possible to reduce the dose of RT and chemotherapy used for WNT MB (ClinicalTrials.gov Identifier: NCT02724579).

In the era of molecular classification of MB, the development of targeted therapies has begun. In SHH tumours, which present with amplification of *GLI* genes, inhibiting the transcription factor GLI2 presents as a valuable therapeutic option. Arsenic trioxide (ATO) can inhibit the activity of GLI as well as decrease protein expression and stability. In a murine model, daily treatment with ATO inhibited the growth of SHH MB (Kim *et al.*, 2010, 2013). ATO is currently undergoing phase II clinical trials for the treatment of SHH MB. Also, a modified measles virus, can selectively kill MB cells presenting CD46 markers on the tumour cell membrane (Studebaker 2012, 2010), and is currently in a clinical trial to treat recurrent MB (ClinicalTrials.gov Identifier: NCT02962167). The development of future treatment options for MB may help reduce the unwanted developmental defects caused by current methods. This will be driven, in part, by further understanding of the molecular signature of MB.

1.5 Tumour microenvironment

The environment in which a solid tumour resides is a complex milieu of both malignant and non-malignant cells each playing a significant role in tumour promotion or suppression. Many cell types have been identified within the tumour microenvironment (TME), such as immune cells, fibroblasts, pericytes, tumour vasculature and lymphatics (Balkwill *et al.*, 2012). For example, T lymphocytes, such as CD8+ T memory cells, which have cancer-killing properties, can be present (Schietinger *et al.*, 2010). Natural killer cells may also be within the surrounding stroma. Tumour-associated macrophages (TAM) are abundant in most cancers and have pro-tumorigenic properties. For example, TAMs can produce epidermal growth factors (EGFs) which promotes tumour cell migration (Wyckoff *et al.*, 2004). Additionally, transcriptional profiling of TAMs shows enrichment for compounds than are pro-angiogenic (Ojalvo *et al.*, 2009). Overall, TAMs play a significant role within the TME and can result in pro-cancer outcomes. Although cells within the TME can influence tumour progression and metastasis, environmental characteristics can influence tumour cell biology. Specifically, variations in oxygen availability can result in pro-tumorigenic phenotypes.

1.6 Tumour hypoxia

The simplistic definition of hypoxia is the point at which the demand for oxygen outweighs the supply. Within the TME, hypoxia can directly influence tumour cell biology. Tumour hypoxia is caused by 1) reduced blood perfusion due to poor vasculature formation, which is prone to bursts and leaks. 2) Increased diffusion distances (>70 μm) between cells and blood vessels caused by increased cell proliferation (Vaupel *et al.*, 1989; Vaupel and Harrison, 2004). These features of the tumour vasculature results in spatial and temporal heterogeneity in oxygen supply (Figure 1.3).

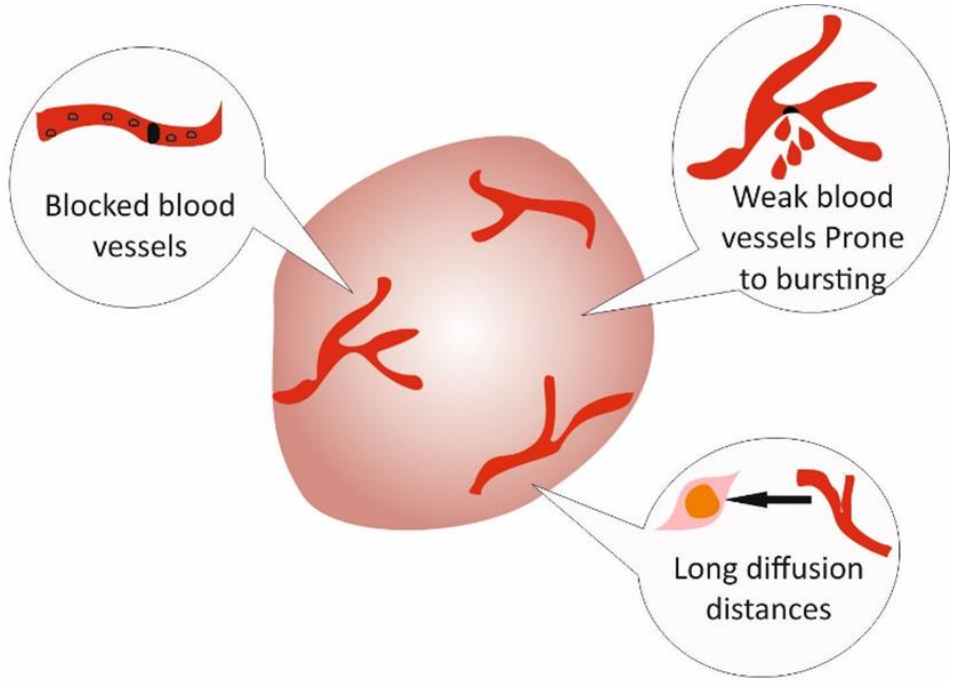

Figure 1.3: Aberrant vasculature contributes to tumour hypoxia. Within a tumour, long diffusion distances, blocked vessels and bursts cause tumour regions to become hypoxic.

The oxygen level in healthy tissue is defined as physioxia, which is highly dependent on proximity to oxygen providing blood vessels. In the brain, oxygen levels are around 5-8%, yet in brain tumours such as MB and GBM, cells are exposed to 0.5% to 3% O_2 (Rampling *et al.*, 1994) (Table 1.3). This leads to cellular adaptions such as the switch to glycolytic metabolism, increased red blood cell production (erythropoiesis) and the development of new blood vessels (angiogenesis) to restore oxygen homeostasis.

Table 1.3: Median oxygen tension in organs, as well as primary tumours. Re-drawn from Muz et al. 2015.

Tissue/Organ	Physoxia (Median % O_2)	Cancer	Hypoxia (Median % O_2)
Brain	4.6	Brain Tumour	1.7
Breast	8.5	Breast Cancer	1.5
Cervix	5.5	Cervical Cancer	1,2
Kidney Cortex	9.5	Renal Cancer	1.3
Liver	4.0-7.3	Liver Cancer	0.8
Lung	5.6	Non-small Cell Lung Cancer	2.2
Pancreas	7.5	Pancreatic Tumour	0.3
Rectal Mucosa	3.9	Rectal Carcinoma	1.8

1.7 Consequences of tumour hypoxia

Tumour hypoxia causes cellular adaptations that can lead to pro-tumorigenic benefits, enabling cancer growth, metastasis and protection from anti-cancer therapy. These changes include increased angiogenesis, increased invasive and metastatic potential, and resistance to chemo- and radiotherapy.

1.7.1 Increased angiogenesis

For tumours to grow, the creation of new blood vessels is required (angiogenesis). However, vessels in solid tumours have an aberrant structure, prone to bursts and leaks, which directly contributes to the hypoxic phenotype. Hypoxia stimulates the production of new blood vessels, through

stimulation of pro-angiogenic factors such as VEGF, EPO, PDGF, FGF (Semenza and Wang, 1992; Krock *et al.*, 2011). Also, hypoxic tumour cells secrete matrix metalloproteases (MMPs) that can degrade the surrounding matrix, aiding the invasion of sprouting vessels into tissue (Yamanaka and Ishikawa, 2000; Ben-Yosef *et al.*, 2002; Choi *et al.*, 2011). This newly formed vasculature within the hypoxic environment is contorted and irregular causing altered blood flow further exacerbating the hypoxic environment.

In an attempt to halt tumour angiogenesis and reduce tumour growth, an anti-VEGF monoclonal antibody, bevacizumab, was developed, which had anti-vascular effects (Willett *et al.*, 2004). This was a promising treatment option for highly vascularised tumours such as GBM. Phase III clinical trials showed that adding bevacizumab treatment to standard GBM therapy (RT and TMZ), resulted in progression-free survival to 10.6 months compared to 6.2 months in the placebo group, although there was no difference in the overall survival rate (Chinot *et al.*, 2014). In contrast, clinical trials for recurrent GBM, investigating treatment with bevacizumab and various chemotherapeutics (TMZ, carboplatin, irinotecan) indicated little patient benefit over standard protocols (Verhoeff *et al.*, 2010; Desjardins *et al.*, 2012; Reardon *et al.*, 2012; Field *et al.*, 2015). Despite these disappointing results, bevacizumab became an FDA approved treatment for recurrent GBM in 2009 (Cohen *et al.*, 2009). Anti-VEGF therapy can successfully reduce angiogenesis, however increased tumour cell invasion has been observed, attributed in part, to the hypoxic environment created as a result of reduced blood supply (Keunen *et al.*, 2011). The invasive side effect of bevacizumab may be reversed by integrins inhibition. Ishida *et al.* determined that treatment of cells with and the integrin inhibitor, celingitide, reduced cell invasion caused by bevacizumab (Ishida *et al.*, 2014), yet the immediate clinical applications are not clear. Overall, the use of angiogenesis inhibitors can be beneficial in combating the pro-angiogenic phenotype of hypoxic tumours, yet the added consequence of increased invasion will likely reduce the positive anti-cancer implications.

1.7.2 Increased invasive and metastatic potential

Hypoxia increases tumour cell propensity to invade and metastasise. Pro-angiogenic properties of hypoxic tumours, such as the increased production of MMPs, can enable tumour cell invasion to local tissue (Yamanaka and Ishikawa, 2000; Ben-Yosef *et al.*, 2002; Choi *et al.*, 2011). In gliomas, activation of TGF-β2 signalling upregulated the expression of MMP -1, -2, -9 leading to increased tissue invasion (Wick 2011). Also, these highly invasive hypoxic cells have increased ability to form a secondary metastasis. In a chick embryo model of neuroblastoma, cells pre-cultured in hypoxia were able to metastasise to chick organs, yet normoxic cells could not (Herrmann *et al.*, 2015). Also, hypoxic myeloma cells injected into mice spread to new bone marrow faster than normoxic cells (Azab *et al.*, 2011). This increased metastatic potential is in part due to epithelial-mesenchymal transition (EMT) induced by hypoxia, whereby tumour cells acquire mesenchymal characteristics. For example, hypoxic myeloid cells have decreased expression of E-cadherin and increased CXCR4 levels, classical mesenchymal attributes (Barbara Muz *et al.*, 2015). Additionally, the driver of EMT, TGF-β, is upregulated in hypoxic cells (Falanga *et al.*, 1991). Other hypoxia-induced changes promoting EMT include the stabilisation of Snail, and upregulation of N-cadherin, Vimentin and SMA (B. Muz *et al.*, 2015; Choi *et al.*, 2017). Exposure of MB cells to intermittent hypoxia induced EMT, highlighted by an increase in N-cadherin, Snail and Vimentin, resulting in increased invasive properties (Gupta *et al.*, 2011). GBM cells cultured in hypoxia have been found to have a mesenchymal phenotype with increased invasive properties as well as increased CDXC4 and VEGF expression (Zagzag *et al.*, 2006; Joseph *et al.*, 2015). Therefore, hypoxia may contribute to the highly infiltrative and invasive characteristics of GBM. Overall, tumour hypoxia can promote the spread of cancer, which is a direct cause of cancer-induced death.

1.7.3 Chemo- and radioresistance

Tumour hypoxia strongly correlates with poor patient survival (Wilson and Hay, 2011), partly due to the chemo- and radioresistance phenotype of hypoxic cells. Hypoxia-induced resistance has been recognised since the 1950's (Deschner and Gray, 1959), yet the molecular mechanisms have only been identified in the last few decades. Hypoxia-induced resistance occurs primarily as a result of the following situations; cell cycle arrest of hypoxic cells, inhibition of apoptosis, induction of autophagy, impaired drug delivery and reduced drug efficacy in a low oxygen environment.

1.7.3.1 Hypoxia-induced cell cycle arrest

Severe hypoxia can induce cell cycle arrest through the upregulation of p21 and p27 (Amellem and Pettersen, 1991; Gardner *et al.*, 2001; Goda *et al.*, 2003). Many anti-cancer therapies require cycling cells to induce sufficient cell death. For example, at the end of S and G2 phase, cells are less sensitive to irradiation compared to the G2/M phase (Pawlik and Keyomarsi, 2004). Also, cells need to be actively synthesising DNA in order to induce lethal double strand breaks, after DNA base damage from TMZ treatment (Zhang *et al.*, 2012). Therefore, cell cycle arrest can lead to indirect resistance to irradiation and TMZ. However, the level of hypoxia required to induce cell cycle arrest may vary. Studies that identified the hypoxia-induced arrest utilised severe hypoxia, with close to anoxic values, however more pathologically relevant levels (1 – 0.1%) fail to induce significant cell cycle arrest in GBM and MB cells (Fan, 2014; Richards *et al.*, 2016). Therefore, the contribution of cell cycle arrest to treatment resistance in GBM and MB is likely to be limited.

1.7.3.2 Inhibition of apoptosis

Hypoxia can downregulate apoptosis signalling, leading to treatment resistance. Reports suggest that Bid and Bax, key pro-apoptotic proteins are downregulated by hypoxia. In human colon carcinoma cells, hypoxia reduced

Bid and Bax expression (Erler *et al.*, 2004). Also, hypoxia-induced phosphorylation of Bax by Pim-1 inhibits apoptosis (J. Chen *et al.*, 2009). MB cells exposed to intermittent hypoxia had reduced expression of pro-apoptotic genes (Bax and Bad) as well as induced expression of anti-apoptotic genes (Gupta *et al.*, 2011). The Bcl-2 protein is directly responsible for regulation of apoptosis, through binding with Bax and inhibiting its activity. Hypoxia can result in upregulation of Bcl-2 in gastric cancer cells contributing to hypoxia-induced chemoresistance (Liu *et al.*, 2008). Overall, alterations of pro-apoptotic systems in hypoxic tumour cells can protect against treatment-induced apoptosis. In contrast, some studies suggest that hypoxia alone can trigger apoptosis and p53 activity (Graeber *et al.*, 1994; Hammond *et al.*, 2002; Hammond, Dorie, *et al.*, 2003). However, these studies used severe hypoxic exposure (<0.2%), whereas moderate hypoxia elicits a protective anti-apoptotic phenotype.

1.7.3.3 Induction of autophagy

Autophagy is an evolutionarily conserved phenomenon triggered when cells are exposed to stressors such as nutrient deprivation or metabolic stress. Autophagy enables the production of ATP and anabolic or catabolic precursors from internal sources to avoid necrosis or apoptosis (Lum *et al.*, 2005). Therefore, cells no longer rely on external oxygen for energy production. Hypoxia can directly induce autophagy, which can protect cells from death (Bellot *et al.*, 2009). Inhibition of autophagy has been shown to increase sensitivity to chemotherapeutic agents (Li *et al.*, 2010; Liu *et al.*, 2011). Recent work suggests that resistance to therapeutic agents is in part, due to hypoxia-induced activation of autophagy (Liu *et al.*, 2010). For example, in glioblastoma hypoxia-induced autophagy promotes tumour cell survival as well as resistance to the anti-angiogenic therapy bevacizumab (Hu *et al.*, 2009). Hypoxic induced autophagy is a protective adaptation, which prevents treatment-induced apoptosis.

1.7.3.4 Impaired drug delivery and reduced drug efficacy

The tortuous vasculature of hypoxic tumours results in altered blood flow to regions of the tumour. Therefore, the delivery of chemotherapeutic agents through the bloodstream is hindered. Also, efflux proteins, such as p-glycoproteins, can remove substrates from the intracellular region to the extracellular space, reducing the internal drug dose. Increased expression of p-glycoproteins (multi-drug resistance proteins, MDR) can cause drug resistance in cancer (Abraham *et al.*, 2015). Hypoxia can indeed upregulate the expression of multi-drug resistance 1 (MDR-1) and multi-drug resistance protein 1 (MPR-1) resulting in chemoresistance (Comerford *et al.*, 2002; Wartenbert *et al.*, 2003; Lv *et al.*, 2015). In glioma cells, hypoxia upregulated MPR-1 gene expression results in reduced sensitivity to etoposide and doxorubicin (Chou *et al.*, 2012). Alterations of MDR expression in hypoxia can directly alter the response to chemotherapy, yet increased MDR by hypoxia is not found in all cell types (Fan, 2014).

A low oxygen environment can directly reduce drug efficacy. Compounds such as alkylating agents (e.g. Melphalan) require molecular oxygen for the mechanism of action, therefore are less active in hypoxia (Teicher *et al.*, 1987). Additionally, irradiation in a normoxic environment results in the reaction of oxygen with the end of broken DNA, making repair more challenging. This phenomenon, known as the oxygen enhancement effect, is lost in low levels of oxygen, making radiotherapy less effective against hypoxic tumours (Chapman *et al.*, 1973).

Overall, hypoxia can result in reduced drug load both extracellularly and intracellularly, as well as causing reduced treatment activity. These characteristics of hypoxic tumours play a significant role in hypoxia-induced tumour resistance.

1.8 HIF – the master regulator of the hypoxic response

The hypoxia-inducible factor (HIF) is responsible for mediating the response to a low oxygen environment by initiating processes such as angiogenesis, erythropoiesis and energy production. Transcriptional activation by HIF was first demonstrated through investigations into the expression of the haematopoietic growth factor, erythropoietin (EPO) (Semenza and Wang, 1992). Since then, HIF has been directly implicated in transcriptional activation of hundreds of genes involved in various cellular processes. HIF is a basic helix loop helix protein, comprising of an oxygen sensitive α subunit and constitutively expressed β subunit. There are three known isoforms, HIF-1, HIF-2 and HIF-3, with HIF-1 being the most studied (Wenger, 2002). The structure of HIF-1α includes a bHLH domain, PAS domain (PER-ARNT-SIM), oxygen-dependent domain (ODD), amino-terminal transcriptional activation domain (NTAD) and carboxy-terminal transcriptional activation domain (CTAD) (Wang *et al.*, 1995) (Figure 1.4). The bHLH domain is essential for DNA binding, and the PAS domain is required for dimerisation with HIF-1β (Wang *et al.*, 1995).

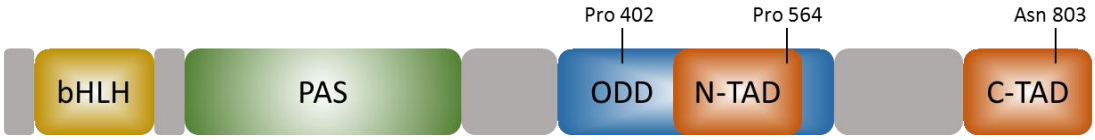

Figure 1.4: Structure of HIF-1α. HIF-1α is a basic helix-loop-helix protein, 826 amino acids in length. bHLH = basic helix-loop-helix, PAS = PER-ARNT-SIM. ODD = oxygen dependent domain, N-TAD = amino-terminal transcriptional activation domain, CTAD = carboxy-terminal transcriptional activation domain, Pro = proline, Asn = asparagine. The key hydroxylation sites are indicated.

HIF-α is constitutively expressed yet the levels are tightly regulated through the activity of prolyl-4-hydroxylase domain proteins (PHD1, 2 and 3). PHDs utilise oxygen as a co-factor in hydroxylation of proline residues in the ODD of HIF-α (Bruick and McKnight, 2001; Epstein *et al.*, 2001). The von Hippel-Lindau protein (pVHL), recognises and polyubiquitinates hydroxylated HIF-α targeting it for destruction by the 26S proteasome (Tanimoto and Makino, 2000; Ivan *et al.*, 2001). Factor inhibiting HIF (FIH), an asparaginyl hydroxylase, can also regulate HIF through hydroxylation of an asparagine residue, preventing interaction with its transcriptional co-activator p300 (Hewitson *et al.*, 2002; Lando *et al.*, 2002; McNeill *et al.*, 2002). The regulatory mechanisms of PHDs and FIHs act together to prevent transcriptional activation of HIF target genes in normoxia. In a hypoxic environment, the activity of both PHDs and FIHs decreases, thus their ability to inhibit HIF is diminished (Bruick and McKnight, 2001; Lando *et al.*, 2002). This enables the HIF-α protein to accumulate in the nucleus where the α and β subunits form a heterodimer (Wenger, 2002), which can interact with co-activators such as p300 (Arany and Huang, 1996). Gene expression is induced through binding to the hypoxia response element (HRE) comprising of a core sequence, 5'-[A/G]CGTG-3', within the promoter of hypoxia-responsive genes (Wenger *et al.*, 2005) (Figure 1.5).

Tight regulation of HIF activity is critical to prevent unwanted transcriptional activation. However, in many cancers, HIF-1α and HIF-2α levels are high (Talks *et al.*, 2000), and significantly contribute to pro-tumorigenic adaptations in hypoxic tumours. Specifically, HIF-1α is upregulated in MB in comparison to the healthy cerebellum (Cruzeiro *et al.*, 2017). Also, mutations in the *IDH1* gene, similar to those found in secondary GBM, can result in the accumulation of HIF-1α (Guerra *et al.*, 2009). Oxygen-independent HIF accumulation in gliomas has been observed, primarily due to activation of EGFR and loss of the tumour suppressors p53 and PTEN. EGFR amplification or overexpression is often found in GBM, which correlates with poor prognosis (Frederick *et al.*, 2000). Overactivation of EGFR signalling leads to initiation

of the PI3K/AKT/mTOR pathway (Clarke *et al.*, 2001), causing the accumulation of HIF-1α. Additionally, loss or mutation of PTEN, the primary inhibitor of the PI3K/AKT pathway, results in the accumulation of HIF and increased vascularization (Zundel *et al.*, 2000). p53 may play a role in HIF regulation, through MDM2-mediated ubiquitination and degradation of HIF. Therefore in *TP53* mutated tumours, HIF may accumulate (Ravi *et al.*, 2000). The accumulation of HIF, through genetic alterations or a hypoxic TME, can lead to the activation of cellular processes, which drive tumour progression contributing to the poor prognosis of hypoxic tumours.

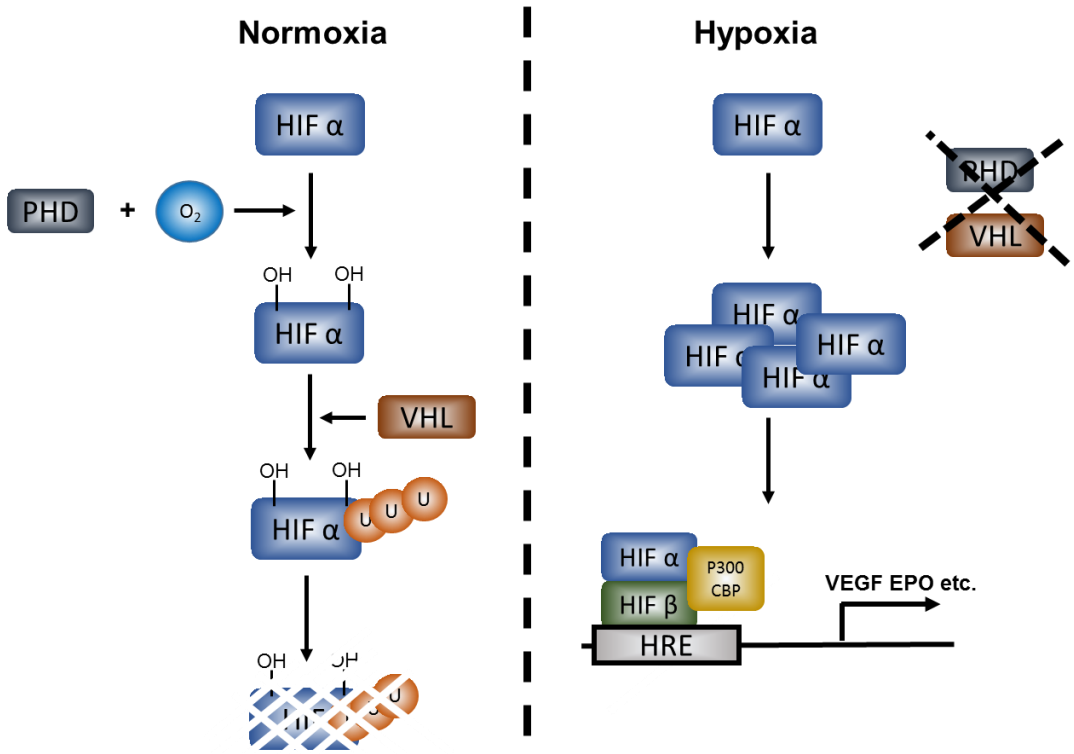

Figure 1.5: Regulation of HIF α in normoxia and hypoxia. In an oxygenated environment, HIF α. Protein levels are tightly regulated through the activity of PHDs and VHL, which target HIF α for destruction. In hypoxia, HIF α accumulates and dimerises with HIF β in the nucleus. HIF activates gene expression through binding at the hypoxia-inducible element (HRE).

1.9 DNA damage response and cancer therapy

It is essential for cells to protect the integrity of their genome and prevent unwanted mutations. However, this is a challenging task, as cellular DNA is constantly under attack from both endogenous and exogenous sources, which actively damage DNA. For example, UV rays from the sun can cause 1 x 10^5 DNA lesions per day (Hoeijmakers, 2009). Also, ionising radiation from both cosmic rays and the sun can result in breakage of the DNA, causing single strand and double strand breaks (SSB, DSB). Internal cellular mechanisms cause DNA damage, such as metabolism, which results in the formation of reactive oxygen species (ROS) that can oxidise DNA and cause SSB. Also, errors in DNA replication can result in mismatched DNA bases which lead to mutations if not repaired (Ciccia and Elledge, 2010). Cellular DNA is being attacked from all angles. However, networks of complex DNA repair mechanisms can repair these DNA lesions and maintain genome integrity. Collectively these mechanisms are known as the DNA damage response (DDR). Although, the repair mechanism employed is specific to the damage type, each of the repair pathways follows a similar set of events, recognition of damage, recruitment of repair proteins, and mechanical repair of the DNA damage (Figure 1.6). If DNA damage cannot be repaired, due to defects in repair mechanism or the overwhelming quantity of DNA damage, activation of apoptosis, through p53 stabilisation, is triggered. This key feature of the cellular response to DNA damage is exploited in cancer therapy. For several decades, radiotherapy has been the primary line of treatment against cancer. RT creates complex DNA damage (SSB, oxidative bases, DSB etc.), which is challenging for cells to repair, therefore cell death is initiated. Additionally, some chemotherapeutic agents directly or indirectly damage DNA. These agents include alkylating agents, crosslinking agents, and inhibitors that trap enzymes at DNA (e.g. topoisomerase inhibitors).

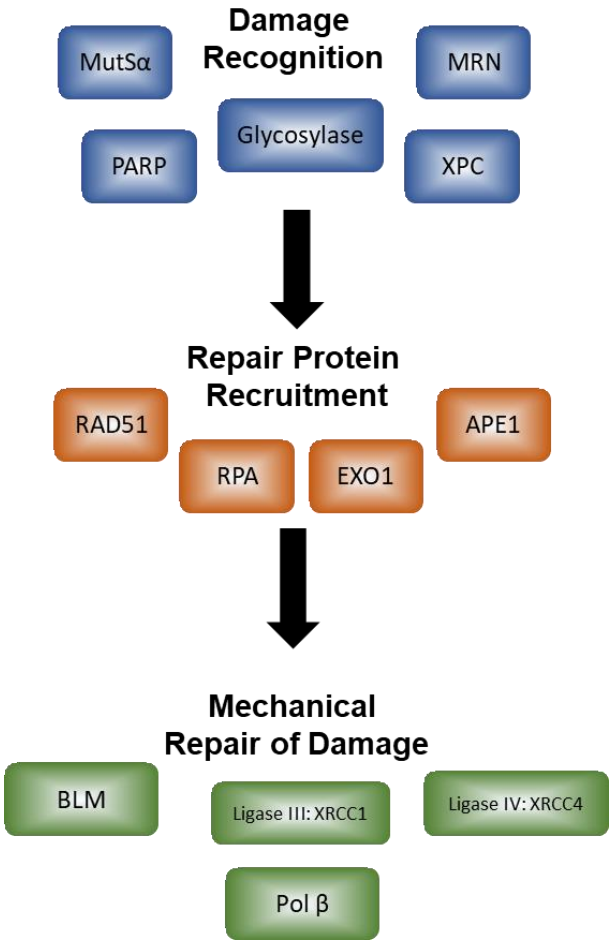

Figure 1.6: The DNA damage response. Stages of the DNA damage response, with examples of the protein complexes involved in each step.

1.9.1 Alkylating agents

The first documented use of alkylating agents as a cancer therapeutic was in the 1940s when Goodman and colleagues trialled the use of nitrogen mustard to treat lymphoma and leukaemia (Goodman *et al.*, 1946). Since then, derivatives of nitrogen mustard have been created, which feature prominently in anti-cancer therapies. Alkylating agents affect DNA by adding alkyl or methyl groups to DNA bases. This results in a bulky adduct which stalls replication, leading to replication fork collapse and the formation of DNA breaks (Roos and Kaina, 2006) (Figure 1.7). Common alkylating agents used

clinically include temozolomide, cyclophosphamide, and melphalan. Temozolomide is the primary chemotherapeutic agent used in GBM treatment (Athanassiou et al., 2005). However, the success of TMZ as a therapeutic agent is highly dependent on the MGMT status of a tumour. MGMT can directly remove the O^6methyl guanine induced by TMZ (Brada *et al.*, 1999; Glassner *et al.*, 1999; Esteller *et al.*, 2000). The presence of alkylated or methylated bases leads to the activation of base excision repair (BER), as well as double strand break repair pathways if the damage is not corrected before replication (Figure 1.7).

1.9.2 Crosslinking agents

Several alkylating agents, including nitrogen mustard, can cause crosslinking of opposite strands of the DNA double helix, known as an interstrand crosslink (ICL). These are thought to be more lethal compared to alkylation alone (Kohn *et al.*, 1966; Wiltshaw, 1979). In the 1960's the discovery of platinum-containing compound, cisplatin, dramatically altered the survival prospect for cancer patients. Cisplatin (Cis-diamminedichloroplatinum(II)) was discovered when a magnetic field generated by platinum electrodes was shown to block *E.coli* cell division (Rosenberg *et al.*, 1965). In the 1970s, cisplatin was slowly adopted as a chemotherapeutic agent, yet with some hesitation (Wiltshaw, 1979). However, since initial testing in the 1970's, the patient survival rate for testicular cancer has dramatically improved, attributed mainly to the adoption of cisplatin as a primary therapeutic strategy (Ansell and Shamash, 2008). Further platinum based compounds have since been developed, including carboplatin and oxaliplatin, which are actively used in the clinic for cancer treatment (Wheate *et al.*, 2010). Cellular repair mechanisms activated to repair ICLs induced by platinum-based compounds include the Fanconi anaemia pathway, homologous recombination repair and non-homologous end joining (Figure 1.7).

1.9.3 Enzyme trapping

DNA-protein complexes form during many cellular processes including transcription, DNA repair and DNA replication. Therefore, trapping these proteins onto the DNA poses a potential option for halting cellular processes. For example, topoisomerases enzymes are responsible for relieving the strain on the supercoiled DNA double helix. The DNA is nicked by the topoisomerase which releases the tension within the helix (Berger *et al.*, 1996). Several inhibitors or 'poisons' of topoisomerases have been developed which trap the enzyme at the DNA, blocking replication and causing the formation of single and double strand breaks (Binaschi *et al.*, 1995; Burden and Osheroff, 1998) (Figure 1.7). Common topoisomerase inhibitors used clinically include etoposide, camptothecin and doxorubicin. Etoposide inhibits topoisomerase II, and is used to treat MB, testicular cancer, lymphoma and lung cancer for example (Wozniak and Ross, 1983). DNA damage induced by topoisomerase inhibitors is repaired by single-strand break repair, homologous recombination repair and non-homologous end joining (Figure 1.7).

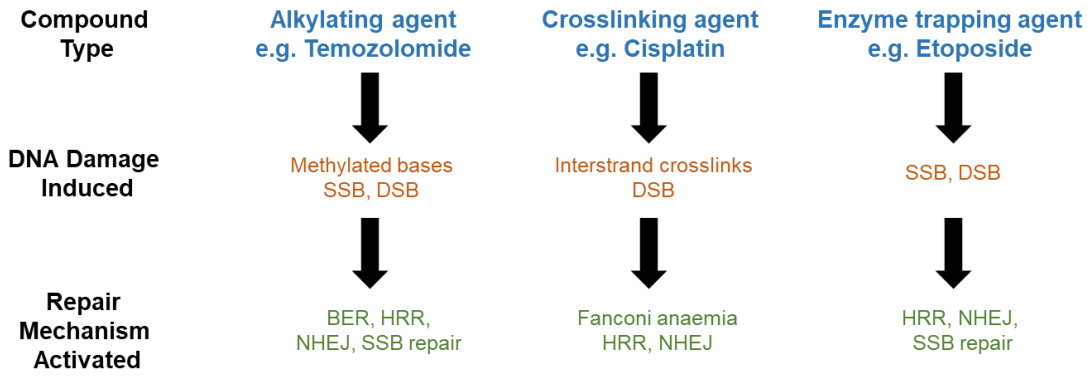

Figure 1.7: Types of DNA damaging agents, the damage they induce, and the repair pathways initiated.

1.10 Repair of DNA damage

Once anti-cancer agents inflict DNA damage, repair mechanisms are activated. Specific mechanisms are employed to repair different types of DNA damage, with crosstalk between some pathways. Three key repair mechanisms are homologous recombination repair, non-homologous end joining and base excision repair (Figure 1.8).

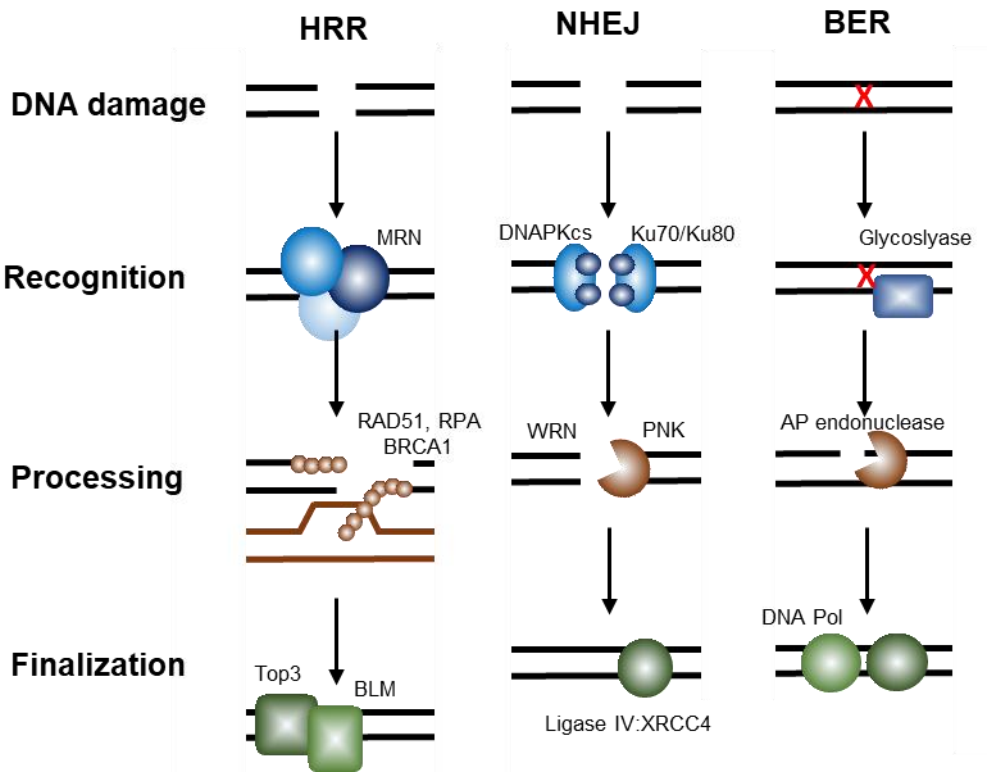

Figure 1.8: Repair steps of HRR, NHEJ and BER. Simplified depictions of the critical steps of homologous recombination repair (HRR), non-homologous end-joining (NHEJ), base excision repair (BER) and the essential protein complexes involved.

1.10.1 Homologous recombination repair

Homologous recombination repair (HRR) is responsible for the repair of DSB as well as other lesions which can cause replication arrest (Lundin *et al.*, 2002). For HRR to occur, the presence of homologous DNA is required, found in G2 and S phase of the cell cycle. In summary, the repair process involves recognition of the break, processing of DNA ends followed by DNA strand invasion, DNA synthesis and resolution of complex structures.

Initially, the MRN complex, composed of MRE11, RAD50 and NBN, recognises the DSB. MRE11 is primarily responsible for end-resection of DNA due to its endonuclease activity (Paull and Gellert, 1998), and both MRE11 and RAD50 can tether DNA ends (De Jager *et al.*, 2001). Upon recruitment to the damage site, NBN is phosphorylated and acts as a beacon for other DNA repair proteins initiating further protein recruitment to the broken DNA (Desai-mehta *et al.*, 2001).

After initial end processing by MRE11, exposed single-stranded DNA (ssDNA) is bound by RPA, followed by the binding of RAD51 forming a nucleoprotein filament. RAD51 is responsible for catalysing the search for homology as well as strand invasion (Pâques and Haber, 1999; Sung, 1994). The RAD51 paralogues (RAD51 B, RAD51 C, RAD51 D, XRCC2, XRCC3) and RAD52 also play a role in these search processes (Kawabata et al., 2005). Both BRCA1 and BRCA2 can interact with RAD51 and play a fundamental role in controlling HRR (Sharan *et al.*, 1997; Wong *et al.*, 1997; Moynahan *et al.*, 1999). Once invasion of the homologous strand has occurred, a D-loop forms, which initiates the synthesis of DNA utilising the homologous DNA as a template. This leads to the formation of a Holliday junction which is resolved by Top3 and BLM (Petr *et al.*, 2012), resulting in ligated DNA strands (Ranjha et al., 2018). Overall, HRR is a complex multistep process involving many essential protein complexes required for efficient repair of the double strand break.

1.10.2 Non-homologous end joining

During the cell cycle, in G0 and G1, HRR is not available due to the lack of homologous DNA stands being present. Therefore non-homologous end joining (NHEJ) is required for DSB repair. NHEJ is a highly error-prone process due to the lack of a homologous DNA template for copying the complementary sequence during DNA synthesis. Initial steps of NHEJ involve the formation of a complex of DNA-PK and Ku (Ku70/Ku80) at the DSB, responsible for recognition of the break (Gottlieb and Jackson, 1993; Kurimasa *et al.*, 1999). Ku is composed of two subunits, Ku70 and Ku80, which form a protein complex with a DNA binding core (Walker *et al.*, 2001). Subsequently, DNA-PKcs is recruited resulting in a geometrical change to the protein complex enabling Ku to translocate along the DNA (Yoo, 1999), this allows the recruitment of further DNA repair proteins to the ends of the DNA for processing.

DNA end processing requires various enzymes including Artemis, PNK, WRN and DNA polymerases (Mahaney *et al.*, 2009). These proteins are responsible for preparing the DNA ends for re-joining. A heterodimer of DNA Ligase IV and XRCC4 is the final complex to be recruited to the damage site. The presence of Ku is essential for this recruitment (Nick McElhinny *et al.*, 2000; Mari *et al.*, 2006). Also, recruitment can be triggered by the interaction of XLF and XRCC4 (Yano *et al.*, 2009). DNA Ligase IV is directly responsible for ligating the two DNA strands together, the final step of NHEJ. Little is known regarding the signals involved in the dissociation of the DNA repair protein complexes from the repaired DNA however in the case of DNA-PKcs, auto-phosphorylation results in its disassociation from DNA (Chan and Less-Miller, 1996; Merkle *et al.*, 2002; Uematsu *et al.*, 2007). Although NHEJ is the primary repair mechanism employed for the repair of DSB, it is a highly error-prone and can result in chromosomal rearrangements and translocation.

1.10.3 Base excision repair

Base excision repair (BER) is responsible for the removal of aberrant bases from DNA, arising from methylation, oxidation or deamination. The causes of these base changes include spontaneous decay of DNA or as a result of an attack from exogenous sources such as chemicals or radiation (Lindahl, 1993). Initiation of BER involves damage recognition by a specific DNA glycosylase which removes the aberrant base creating an abasic site (Stivers and Jiang, 2003; Friedman and Stivers, 2010). AP-endonucleases (e.g. APE1 or APE2) create a nick in the DNA phosphodiester backbone at the abasic site (Demple *et al.*, 1991), which is further processed by DNA polymerase, resulting in a nucleotide-free gap (Sobol *et al.*, 1996). At this stage, the DNA can be processed through short-patch BER pathway or long-patch BER. Pathway choice is poorly understood however ATP levels, type of DNA intermediate produced after AP-endonuclease action or even the cell cycle stage, can influence this decision (reviewed in Fortini and Dogliotti, 2007).

Short-patch BER involves the addition of a single nucleotide to the nucleotide-free gap by pol β or pol λ (Braithwaite *et al.*, 2005). However, long patch BER involves flap displacement synthesis by either pol δ or pol ε, whereby 2-12 nucleotides are replaced by the polymerase resulting in the displacement of part of the DNA strand (Fortini *et al.*, 1996). This 'flap' structure is recognised and removed by FEN1 (Harrington and Lieber, 1994). To seal the nicked DNA, DNA Ligase I aided by PCNA or DNA Ligase III complexed with XRCC1 is required (Caldecott *et al.*, 1994; Hubscher *et al.*, 1998). Additionally, PARP-1 has been shown to have a role in BER by protecting repair intermediates from deterioration as well as preventing the formation of excessive single-strand breaks (Parsons *et al.*, 2005). Overall, BER is a highly efficient method of removal of individual damaged bases.

1.11 Failure of DNA repair mechanisms

When large amounts of DNA damage is induced by anti-cancer treatments, the cell is unable to repair the DNA lesions. This leads to the induction of apoptosis, the primary aim of chemo- and radiotherapy. Apoptosis is initiated through the activities of p53, the 'guardian of the genome'. For example, after the induction of SSB and DSB by ionising radiation, damage recognition complexes recruit ATM and ATR, which phosphorylate further downstream signalling proteins such as Chk1 and Chk2 (Guo *et al.*, 2000; Liu *et al.*, 2000; Matsuoka *et al.*, 2000). This leads to the phosphorylation of p53, which inhibits MDM2 binding and thus prevents p53 degradation (Shieh *et al.*, 1997). p53 is then able to activate pro-apoptotic genes such as Bid and Bax, to trigger apoptosis (Banin *et al.*, 1998; Canman *et al.*, 1998; Epstein *et al.*, 2001; Turenne *et al.*, 2001; Saito *et al.*, 2002). This is a desirable outcome for cancer therapy, as it results in tumour cell death and a decrease in tumour volume. Somatic mutations in *TP53*, the gene encoding p53, are found in cancer, with *TP53* mutations in ~25% of brain tumours (Olivier *et al.*, 2010). These mutations can directly affect p53 functionality and alter the response to anti-cancer therapy. In many tumours, *TP53* mutations are associated with poor prognosis (Robles and Harris, 2009). For MB, *TP53* mutations are enriched in the SHH sub-group and are associated with poor patient outcome in part due to treatment failure (Zhukova *et al.*, 2013). However, the impact of the *TP53* mutation on GBM prognosis is less clear, with conflicting views (Shiraishi *et al.*, 2002; Wang *et al.*, 2014). Overall, alterations to the DDR and p53 can have a negative impact from a treatment perspective. Defective repair mechanism can also have pro-tumorigenic benefits, creating mutations, which drives tumour progression.

1.12 Mismatch repair and pro-tumorigenic benefits

During DNA replication, incorrect nucleotides can be incorporated into DNA resulting in a mismatch. These mismatched errors need to be repaired successfully to prevent a mutation. The repair mechanism responsible for correcting these mistakes is mismatch repair (MMR) (Figure 1.9). Cells with non-functional MMR have an increased rate of spontaneous mutation (Tiraby and Fox, 1973), and are often less sensitive to alkylating agents such as temozolomide and the interstrand crosslinking agent cisplatin (Fink et al., 1998).

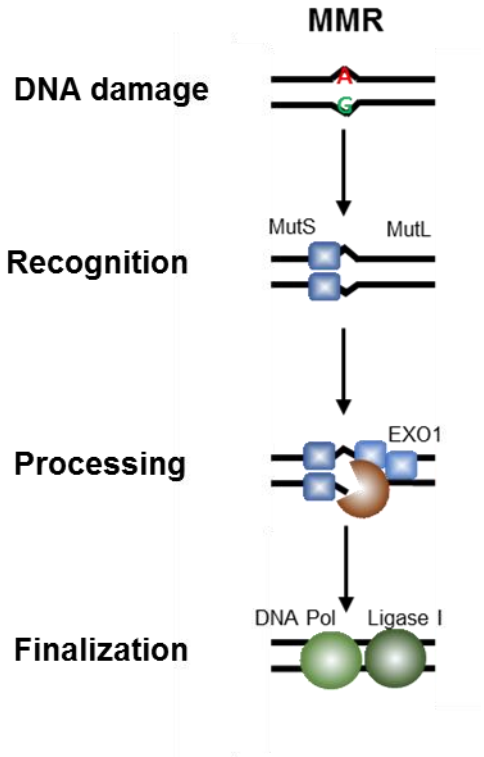

Figure 1.9: Repair steps of MMR. Simplified depictions of the critical steps of mismatch repair (MMR) and the essential protein complexes involved.

The repair protocol for incorrectly inserted nucleotides involves the initial formation of the MutSα protein complex composed of MSH2 and MSH6 (Gradia *et al.*, 1997). MutSα undergoes a conformational change in an ATP dependent manner resulting in the formation of a sliding clamp, which can translocate along DNA (Blackwell *et al.*, 1999; Gradia *et al.*, 1999; Iaccarino *et al.*, 2000). This sliding clamp protein-DNA complex is bound by a second heterodimer, MutLα (MLH1/PMS2), again in an ATP dependent manner (Li and Modrich, 1995), and this large protein complex can translocate bi-directionally along the DNA strands in search of discontinuity in the DNA. EXO1 is responsible for the 5' to 3' excision of nucleotides in stretches of DNA which include the detected mismatch (Zhang *et al.*, 2005). The missing nucleotides are replaced with the correct nucleotide sequence by DNA polymerase δ, and DNA Ligase I repairs nicks (Longley *et al.*, 1997; Zhang *et al.*, 2005). Additionally, PCNA and RFC1 locate to the mismatch site to aid in the synthesis of the corrected nucleotides (Longley *et al.*, 1997; Dzantiev *et al.*, 2004). Correction of the mismatched base is essential as this can lead to point mutations, which can directly contribute to cancer progression. Therefore, deficiencies within MMR will aid tumorigenesis.

1.13 Hypoxia and the DNA damage response

The tumour microenvironment can have a direct impact on the efficiency of DNA repair mechanisms. Specifically, hypoxia can regulate DNA repair through epigenetic modifications, regulation of transcription, translation and post-translational modifications, resulting in changes to DNA repair proteins.

1.13.1 Epigenetic modifications

Hypoxia can result in direct modification of chromatin causing modulation of gene transcription, which can persist long after normoxia is restored. For

example, under severe hypoxia (<0.01%) an increase in H2K4me3 and decrease in H3K27me3 leads to widespread repression of total RNA and mRNA synthesis (Johnson *et al.*, 2008). Also, HIF-1 can directly induce expression of *JMJD1A,* a histone demethylase gene, which reduces histone H3K9 methylation at the adrenomedullin (*ADM*) and growth and differentiation factor 15 (*GDF15*) gene promoters, increasing their expression and promoting tumour growth (Krieg *et al.*, 2010). Therefore, alterations of the chromatin signature can directly affect cancer progression. The DNA repair genes, *BRCA1* and *RAD51* are regulated in hypoxia through chromatin modifications. H3K4 demethylation, H3K9 methylation and H3K9 deacetylation at the *BRCA1* promoter induced by hypoxia results in reduced expression of *BRCA1*. A similar epigenetic signature was also found for *RAD51* (Lu *et al.*, 2011). Alterations in *BRCA1* and *RAD51* transcription could directly affect the functionality of HRR. Hypoxia-induced silencing of the *MLH1* gene, involved in MMR, arises due to decreased H3K4 methylation induced by the H3K4 demethylases, LSD1 and PLU-1 (Lu *et al.*, 2014). Taken together, hypoxia-induced chromatin modifications can directly regulate the expression of DNA repair genes, which may result in lasting changes.

1.13.2 Regulation of transcription

Adaptation to a hypoxic environment is mediated through alteration of transcription. Many gene expression changes are HIF-dependant. The expression of DNA repair proteins in hypoxia has been well studied, with most publications suggesting a decrease in gene expression under a hypoxic environment. For example, several publications by the Glazer group found that hypoxia-induced downregulation of HRR components leading to reduced HRR capacity (Bindra *et al.*, 2004, 2005, 2007; Meng *et al.*, 2005; Bindra and Glazer, 2007; Chan *et al.*, 2008). Specifically, *RAD51* and *BRCA1* expression is downregulated in hypoxia due to binding of the repressive E2F4/p130 complex to E2F sites in proximal promotors (Bindra *et al.*, 2005; Bindra and Glazer, 2007). Also, NBN, a key component involved in DSB recognition, is

downregulated in hypoxia as HIF-1α displaces MYC at the NBN promotor (To *et al.*, 2006). The impact of hypoxia on DNA repair gene expression will be discussed further in Chapter 4.

1.13.3 Regulation of translation

Hypoxia can directly influence protein translation. The translation initiation factor eIF2α is phosphorylated in hypoxia (0-0.2%) resulting in reduced activity and an overall downregulation in mRNA translation (Koritzinsky *et al.*, 2007). Additionally, disruption of the mRNA cap-binding complex eIF4F leads to alterations in translation efficiency in hypoxia (Hernández-Jiménez *et al.*, 2012), Chan *et al.* observed that chronic hypoxia (72 h 0.2%) resulted in reduced BRCA2, RAD54, XRCC3, RAD51. RAD51B and RAD51C protein levels, yet there was no change to mRNA levels. Exploring BRCA2 and RAD51 further, it was determined that there were fewer ribosomes attached to *BRCA2* and *RAD50* mRNA in hypoxia in comparison to normoxia. These changes led to a 3-fold reduction in HRR capacity (Chan *et al.*, 2008). Hypoxia can also reduce the translation of BER proteins leading to reduced BER activity and increased sensitivity to DNA damaging agents (Chan *et al.*, 2014). In addition to reduced translation efficiency, microRNAs, small non-coding RNAs, can reduce the expression of specific proteins. Several microRNAs are induced by hypoxia, creating the 'microRNA signature' of hypoxia. These microRNAs play a role in tumour formation, apoptosis, invasion and proliferation (Kulshreshtha *et al.*, 2007). Hypoxia-induced upregulation of miR-201 and miR-373 in a HIF-dependant manner resulted in downregulation of RAD52 (HRR) and RAD23B (NER), suggesting that microRNAs may play a fundamental role in the regulation of DNA repair pathways in hypoxia (Crosby *et al.*, 2010). Overall, evidence suggests that hypoxia can lead to translational regulation of DNA repair proteins through reduced translation initiation and the induction of microRNAs, which can alter the functionality of DNA repair mechanisms.

1.13.4 Regulation of post-translational modifications

Post-translational modifications of proteins enable rapid control of protein functionality, allowing fast reaction and adaptation to cellular changes or stresses. Protein modifications include phosphorylation, sumoylation, ubiquitination, and acetylation, which can alter protein function, levels and localisation. Under severe hypoxia (0.02%), phosphorylation of ATM and ATR has been observed independent of DNA damage, thought to be triggered by hypoxia-induced replication arrest (Hammond et al., 2003; Hammond et al., 2002; Bencokova et al., 2009). This results in rapid phosphorylation of ATR and ATM targets, including Chk1 and Chk2, leading to phosphorylation of H2AX, 53BP1 and p53. Hypoxia-induced ATR-dependent phosphorylation of p53 could lead to apoptosis in hypoxia (Hammond *et al.*, 2002). Also, activation of the Fanconi anaemia pathway in an ATR-dependant manner may protect from DNA damage induction through stabilisation of the replication forks (Scanlon and Glazer, 2014). Overall, the post-translational modifications of DNA repair proteins in hypoxia are thought to act as a protective mechanism against hypoxia-induced DNA damage. However, for these modifications to occur severe hypoxic stress is required, whether moderate hypoxia is sufficient for these changes needs further investigation.

1.14 Project aims and hypothesis

Brain tumours are complex and challenging diseases. Glioblastoma has a poor patient outcome due to the highly infiltrative nature of GBM and resistance to standard therapies. In contrast, treatment of medulloblastoma is somewhat successful, but high dose chemo- and radiotherapy can lead to developmental difficulties in young patients. To improve treatment protocols for GBM and MB, further understanding of tumour cell biology is imperative. These tumours are hypoxic, resulting in cellular adaptions that can lead to increased invasion and metastasis as well as resistance to conventional cancer therapy. The majority of treatment protocols for GBM and MB aim to create high levels of DNA damage to induce apoptosis. However, hypoxia can have a direct impact on DNA repair mechanisms. To date, there are no publications that examine the impact of hypoxia on DNA repair mechanisms in hypoxic GBM and MB cells, therefore this was the primary aim of the thesis. Previous scientific research focusing on DNA repair and hypoxia has resulted in significant discrepancies between findings, in part due to variations in cell line and hypoxic exposure, with the majority of research being conducted in severe hypoxia (<0.1%). Here, pathophysiological hypoxia (0.1 – 1%) was investigated to give an overall view of the impact of hypoxia on DNA repair in the tumour as a whole. Initially, examination of the double strand break recognition machinery in hypoxic MB cells was undertaken to determine whether hypoxia-induced changes could contribute to treatment resistance (Chapter 3). Next, a focused transcriptomic approach was adopted to gain a global overview of the expression of common DNA repair genes, under hypoxia (Chapter 4). Finally, the functional impact of the observed gene expression changes was investigated (Chapter 5).

Chapter 2: Materials and methods

2.1 Chemicals and reagents

All tissue culture reagents were purchased from Gibco. Chemicals and drugs were from Sigma-Aldrich, unless otherwise stated. Custom designed oligo primers were purchased from Sigma-Aldrich.

2.2 Cell culture

Glioblastoma (Table 2.1), medulloblastoma (Table 2.2), neuroblastoma and HeLa cell (Table 2.3) were maintained at 37°C, 21% O_2 and 5% CO_2 in the appropriate culture medium.

Table 2.1: Summary of glioblastoma cell lines, their p53 status and source.

Cell Line	Culture Medium	p53 Status	Source
U87-MG	EMEM, 10% (v/v) FCS, 1% (v/v) NaPyr	Wild Type	ATCC-HTB-14
D566-MG	EMEM, 10% (v/v) FCS, 1% (v/v) NEAA, 1% (v/v) NaPyr	Mutated	Provided by Professor DD Bigner (Duke University Medical Centre, USA)
U251-MG	EMEM, 10% (v/v) FCS, 1% (v/v) NEAA, 1% (v/v) NaPyr	Mutated	CLS (Eppelheim, Germany)
T98G	EMEM, 10% (v/v) FCS, 1% (v/v) NaPyr	Mutated	ATCC-CRL-1690

Table 2.2: Summary of medulloblastoma cell lines, their p53 status and source.

Cell Line	Culture Medium	p53 Status	Source
D283-MED	EMEM, 10% (v/v) FCS, 1% (v/v) NEAA, 1% (v/v) NaPyr	Wild Type	ATCC-HTB-185
MEB-Med8A	DMEM, 10% (v/v) FCS,	Mutated	Provided by Prof T. Pietsh

Table 2.3: Summary of other cell lines used.

Cell Line	Culture Medium	Source
HeLa (Cervical carcinoma)	EMEM, 10% (v/v) FCS, 1% (v/v) NEAA	ECACC no: 93021013
SK-N-AS (Neuroblastoma)	EMEM, 10% (v/v) FCS, 1% (v/v) NaPyr	ECACC no: 95011817

2.2.1 Cell passaging

Cells were passaged when 80-90% confluent. For adherent cells the culture medium was removed, cells were washed with PBS and incubated for 5 min at 37°C with 1 ml 1 x Trypsin/EDTA. Detached cells were re-suspended in culture medium. For cells grown in suspension, the cells were transferred to a 50 ml falcon tube and centrifuged at 100 g for 5 min. The culture medium was removed and the cells re-suspended in fresh culture medium. Cells were counted using a Bio-Rad TC20 cell counter. Cells were seeded into a T75 flask to maintain the cells (See Table 2.4 for seeding density) or an appropriate vessel for experimentation.

Table 2.4: Seeding densities for cells in 75 cm² flasks

Cell Line	Number of cells seeded per 75 cm² flask
U87-MG	2 – 1 x 10^6
D566-MG	1 x 10^6
U251-MG	1 x 10^6
T98G	2 – 1 x 10^6
D283-MED	10 x 10^6
MEB-Med8A	4 x 10^6
HeLa	1 x 10^6
SK-N-AS	2 – 1 x 10^6

2.2.2 Hypoxic Incubation

Hypoxic culture at 1% O_2 was conducted in a Don Whitley H35 Hypoxystation and at 0.1% O_2 in a New Brunswick Galaxy 48R incubator. The oxygen tension of hypoxic chambers was regularly tested using a Microx 4 fibre Optic Oxygen Meter (PreSens). Additionally, cells incubated in hypoxia were checked when possible for hypoxic markers (GLUT1, VEGF), by RT-PCR, to ensure a hypoxic response was present. 1 day and 5 day hypoxic exposure was used to represent chronic and acute hypoxia. Fan 2014 had previously demonstrated that at these time points, there was a differential impact on HIF levels, drug sensitivity and DNA repair gene expression. Additionally, up to 5 days exposure had little impact on cell proliferation and viability of the chosen cell lines as shown by Fan 2014, Richards *et al* 2016 and experimental observations in this thesis.

2.3 Drug treatment

For survival assays, cells were pre-incubated in the specified O_2 concentration prior to drug application. Etoposide, temozolomide and cisplatin were applied to cells maintained in their designated O_2 condition (with the exception of 0.1% O_2), yet treatment with phleomycin occurred only in 21% O_2. Drug doses and treatment duration were chosen based on preliminary experimental data as well as literature evidence. Dimethyloxalylglycine (DMOG) was utilised as a hypoxia mimetic and applied to cells in normoxic conditions to a final concentration of 0.5 mM. Acriflavin (AF) was applied to cells, which were placed directly in the designated O_2 condition for 24 h. Cells were treated with digoxin for 8 h prior to placing into hypoxia for 24 h.

2.4 X-ray irradiation

Cells were seeded onto 35 mm dishes 24 h prior to irradiation. Cells were cooled on ice before irradiating in a CellRad Faxitron (130-150 kV, 5 mA) at room temperature, 21% O_2. Post-irradiation, cells were again cooled on ice before trypsinization. Cells were counted and seeded in a 96-well plate, before returning the cells to 21% or 1% O_2 for 48 h before assaying for survival.

2.5 MTS assay

The MTS assay (Promega) is a quantitative colorimetric method for determining viable cells in culture. It relies upon the reduction of a tetrazolium compound, 3-(4,5-dimethylthiazol-2-yl)-5-(3-carboxymethoxyphenyl)-2-(4-sulfophenyl)-2H-tetrazolium, by metabolically active cells to a coloured formazan product (Berridge and Tan, 1993). Cells were incubated with 20 µL of MTS reagent in 100 µL of culture medium for 2-4 h before determining absorbance at 492 nm. The absorbance values were proportional to the number of metabolically active cells. Background

subtraction was done using absorbance from wells containing medium only. Absorbance values were normalised to control wells.

2.6 Proliferation assays

Cells were seeded in 24 well plates 24 h before drug treatment. Etoposide was applied at a specified concentration for 24 h, before washing the cells and adding fresh medium. Cells were left to grow for 5 days post-treatment. Cells were then washed with PBS, and stained with a crystal violet solution (0.5% (w/v) in EtOH) for 10 min at room temperature. The crystal violet stain was removed and excess stain washed with H_2O. Plates were left to dry completely, before adding 10% SDS and incubating at 37°C for 1 h. Absorbance at 590 nm was determined which was proportional to the number of crystal violet stained cells. Absorbance values were normalised to the untreated control.

2.7 Transient transfection

Transient transfection was conducted 24-48 h prior to experimental use. Various transfection reagents were used for differing cell lines as described Table 2.5. All transfections were conducted following manufacturers guidelines.

Table 2.5: Details of specific transfection reagents for each cell line.

Cell line	Transfection reagent	Ratio of DNA to reagent	Mass DNA per 3.5 cm^2 dish (µg)
U87-MG	Viromer	1:0.4	2
D566-MG	JetPrime	1:2	1.5
HeLa	Polyethyleneimine	1:2	1

2.8 RNA extraction and reverse transcription

Cells were seeded into 60 mm dishes and incubated in the specified O_2 conditions for the indicated time points. Adherent cells were washed with PBS, lysed in 400 µl of lysis buffer (Roche), and scraped with a cell scraper to detach the cells. For non-adherent cells the cell suspension was centrifuged at 100 g for 5 min, and the cell pellet washed with PBS before a final centrifugation. The cells were re-suspended in 400-500 µl of lysis buffer. Cell lysate was stored at -80°C until use. RNA extraction was performed using High Pure RNA Extraction Kit (Roche) following the manufacturers protocol. RNA purity and concentration was determined using a NanoDrop 1000 Spectrophotometer (Thermo Scientific). 1-2 µg of RNA was utilised for reverse transcription using Superscript Vilo reverse transcription master mix (Invitrogen), following the manufacturers protocol. cDNA was diluted 1:20 with RNase/DNase free H_2O and stored at -20°C before use in RT-PCR.

2.9 Quantitative real-time PCR (RT-PCR)

RT-PCR was performed in a LightCycler480. White 96-wells plates (Roche) were used with the standard well component mix of 10 µl SYBER Green PCR Mix (Roche), 1 µl of 5 mM forward primer, 1 µl of 5 mM reverse primer (Table 2.7), 2 µl cDNA (or H_2O for no template control) and 6 µl H_2O. 3x technical replicates were included for each condition. Cycling parameters are described in Table 2.6. Data analysis was performed using the LightCycler480 SW 1.8 software, utilising a relative quantification method with respect to the housekeeping gene *CYCLOA*. Fold change was determined relative to normoxic controls.

Table 2.6: General cycling parameters for RT-PCR

Step	Temperature (°C)	Time (s)	Number of Cycles
Pre-incubation	50 95	120 600	1
Amplification	95 60 72	10 15 15	40
Melt Curve	95 65 97	5 60 Continuous	1
Cooling	40	10	1

Table 2.7: RT-PCR Primer Sequences

Gene	Forward Primer (5'-3')	Reverse Primer (5'-3')
ABL 1	TGGGGCATGTCCTTTCCATC	GATGTCGGCAGTGACAGTGA
CYCLOA	GCTTTGGGTCCAGGAATGG	GTTGTCCACAGTCAGCAATGGT
ERCC4	CTCCCTCGCCGTGTAACAAA	ACACCAAGATGCCAGTAATTAAATC
FEN1	GTTCCTGATTGCTGTTCGCC	ATGCGAATGGTGCGGTAGAA
GLUT1	GAACTCTTCAGCCAGGGTCC	ACCACACAGTTGCTCCACAT
LIG IV	TCCCGTTTTTGACTCCCTGG	GGCAAGCTCCGTTACCTCTG
MRE11	AGTCCAGCAGTGGGAATTTCT	TCAGTCAAGCTCCTCTGGGA
MSH5	GTTTGCGAAGGTGTTGCGAA	GTCTGAGACCTCCTTGCCAC
NBN	AGAATGGCTTTTCCCGAACT	CAAGAAGAGCATGCAACCA
PARP1	GCCCTAAAGGCTCAGAACGA	CTACTCGGTCCAAGATCGCC
PMS2	AGCACTGCGGTAAAGGAGTT	CAACCTGAGTTAGGTCGGCA
RAD50	TGCTTGTTGAACAGGGTCGT	TCACTGAATGGTCCACGCTC
UBE2T	ATGTTAGCCACAGAGCCACC	ACCTAATATTTGAGCTCGCAGGT
VEGF	CTCCACCATGCCAAGTGGTC	GCAGTAGCTGCGCTGATAGA
WRN	TCACGCTCATTGCTGTGGAT	CAACGATTGGAACCATTGGCA

2.10 Western blotting

2.10.1 Protein extraction

Adherent cells were washed with PBS before adding 150-500 µl of lysis buffer (50 mM pH 7.5 Tris-HCL, 1 mM EDTA, 1 mM EGTA, 0.5 mM Na_3VO_4, 1% (v/v) Triton X-100, 50 mM Sodium flouride, 5 mM Sodium pyrophosphate, 10 mM Sodium B-glycerophosphate, 0.1 mM PMSF, 1 in 100 protease cocktail inhibitor) and scraped with a cell scraper. Suspension cells were centrifuged at 100 g for 5 min, washed with PBS and the centrifugation step repeated to remove the PBS. The cell pellets were re-suspended in 100-200 µl lysis buffer. Cell lysates were frozen at -20°C. Lysates were defrosted at 4°C on a rotary wheel for 1 h, then centrifuged at 13000 g for 15 min. The supernatant was transferred to a fresh 1.5 ml tube on ice. Protein quantification was conducted using Pierce BCA Protein Assay Kit (ThermoFisher) following the manufacturers protocol.

2.10.2 Sample preparation

Protein samples were mixed with 5 x laemmli buffer (250 mM pH 6.8 Tris HCL, 10% (w/v) SDS, 30% (v/v) Glycerol, 5% (v/v) β-mercaptoethanol, 0.02% (w/v) Bromophenol blue), and boiled at 95°C for 5 min. Samples were cooled on ice and centrifuged briefly before loading onto SDS-PAGE gel.

2.10.3 SDS-PAGE for protein separation

20-40 µg of protein was loaded into wells of a 4% stacking gel (0.4 M Tris base pH 6.8, 4% (v/v) Acrylamide, 0.65 ng/µl APS and 0.325% (v/v) TEMED) with a 6% or 10% resolving gel (0.4 M pH 8.8 Tris base, 0.1% (w/v) SDS, 6-10% (v/v) Acrylamide, 0.25 ng/µl APS and 0.125% (v/v) TEMED) cast with Mini-PROTEAN 3 system (Bio-Rad). 10 µl of protein ladder (Precision Plus Protein All Blue Standards, Bio-Rad) was also loaded into the stacking gel. The SDS-PAGE

was run at 100-130 V for up to 1.5 h in running buffer (25mM Tris base, 192 mM Glycine, 1% (w/v) SDS).

2.10.4 Protein transfer

Protein was transferred onto nitrocellulose membrane (0.2 µm, Bio-Rad), in a Bio-Rad tank with transfer buffer (25 mM Tris, 192 mM Glycine, 20% (v/v) ethanol). Transfer was run at 4°C for 1.5 h (300 mA) or overnight (50 mA).

2.10.5 Antibody incubation

Membranes were blocked in 5% (w/v) skimmed milk for 1 h then washed in TBS-T (20 mM Tris, 140 mM NaCl, adjusted to pH 7.6, 0.1% (v/v) Tween-20). Membranes were incubated in primary antibody diluted in 5% (w/v) BSA in TBS-T overnight at 4°C. After primary antibody incubation, the membranes were washed three times in TBS-T and incubated with the secondary antibody, diluted in 5% (w/v) BSA in TBS-T, for 1 h at room temperature. See Table 2.8 for details of antibodies and dilutions.

2.10.6 Developing and analysis

Protein was visualised using Amersham ECL western blotting detection kit (GE Healthcare). Membranes were incubated with 1 ml developer solution and captured with a Syngene gel imaging G-box using GeneSnap image acquisition software. Densitometry analysis of images was conducted using Fiji (Schindelin *et al.*, 2012).

Table 2.8: Antibodies used for western blotting

Antibody	Source	Reference	Species	Dilution
Anti-Mouse-HRP	Abcam	ab6808	Sheep	1 in 5000
Anti-Rabbit-HRP	Cell Signalling	7074S	Goat	1 in 3000
ATM	Abcam	ab32420	Rabbit	1 in 5000
ATM Ser1981	Abcam	ab81292	Rabbit	1 in 2000
β-Actin	Abcam	ab8226	Mouse	1 in 6000
Cyclophillin A	Cell Signalling	2175	Rabbit	1 in 1000
HIF-1α	Bethyl	20960-1-AP	Rabbit	1 in 500
HIF-2α	Bethyl	A700-003	Rabbit	1 in 1000
Histone2B	Abcam	ab1790	Rabbit	1 in 1000
MLH1	Abcam	ab92312	Rabbit	1 in 1000
MRE11	Abcam	ab214	Rabbit	1 in 1000
NBN	Abcam	ab32074	Rabbit	1 in 500
PARP1	Santa Cruz	sc-53643	Mouse	1 in 2500
PCNA	Santa Cruz	sc-9857	Mouse	1 in 1000
PMS2	Abcam	ab110638	Rabbit	1 in 1000
Vinculin	Abcam	ab129002	Rabbit	1 in 10,000

2.11 Immunocytochemistry (ICC)

Cells were seeded onto glass coverslips in 12 well plates 24 h prior to fixing with 4% (w/v) paraformaldehyde at room temperature for 10 min. After fixation cells were washed 3 x with PBS then blocked for 20 min at room temperature in blocking buffer (1% (w/v) BSA, 0.1% (v/v) Triton X-100, and

0.4% (v/v) Tween 20 in PBS). The cells were incubated in primary antibody (diluted in blocking buffer) overnight at 4°C, then washed in blocking buffer before secondary antibody incubation for 1 h at room temperature (see Table 2.9 for antibodies). Coverslips were incubated in To-pro-3 (1 in 1000) (ThermoFisher) for 30 min at room temperature then washed with PBS before mounting onto glass microscope slides with Dako Fluorescent Mounting Medium (Dako UK Ltd). Throughout the procedure, coverslips were protected from light using foil. Slides were imaged on a Zeiss axiovert Epifluorescence microscope using Zeiss 38 HE filter set (GFP) and Chroma 39007 filter set (To-pro-3). Analysis of signal intensity was performed using Fiji (Schindelin *et al.*, 2012). Signal was background subtracted before normalisation to control samples.

Table 2.9: Antibodies used in immunocytochemistry

Antibody	Source	Reference	Species	Dilution
Anti-Rabbit-AlexaFluor488	Invitrogen	A-11008	Goat	1 in 500
γH2AX Ser139	Cell Signalling	9718	Rabbit	1 in 200

2.12 Luciferase assay

Cells were transfected for 24 h with a plasmid containing the luciferase gene (Figure 2.1), before washing with PBS and applying 300 µl of lysis buffer (25 mM pH 7.5 Tris phosphate, 15% (v/v) glycerol, 1% (w/v) BSA, 8 mM $MgCl_2$, 0.1 mM EDTA, 0.03% (w/v) DTT, 1% (v/v) Triton X-100). 80 µl of lysed cells were combined with 200 µl of luciferin working solution (500 µM luciferin, 2.5 mM ATP in lysis buffer), into a single well of a white 96 well plate, in triplicate. Endpoint luminometry measurements were taken using a BMG Labtech FLUOstar Omega plate reader.

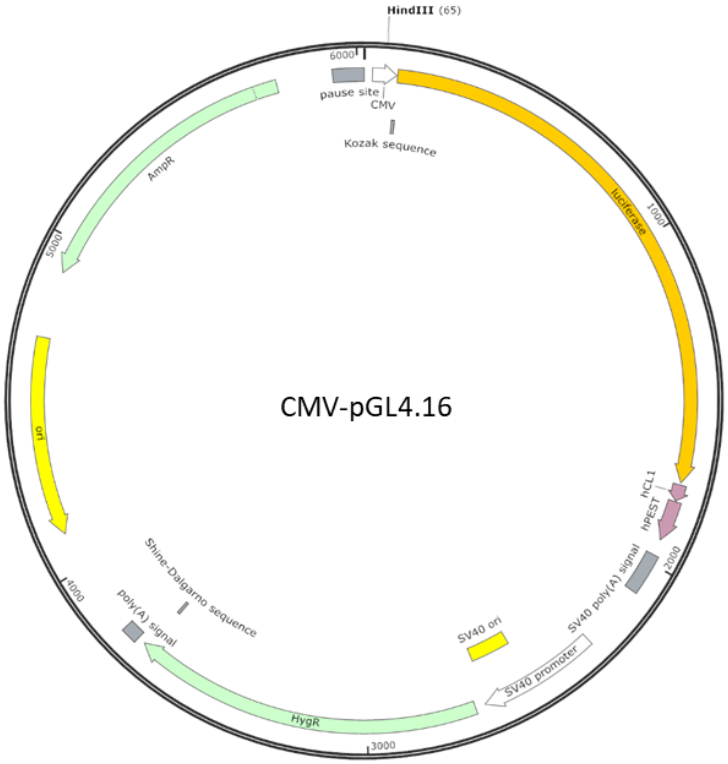

Figure 2.1: Plasmid map of luciferase containing plasmid CMV-pGL4.16. A CMV promotor drives the expression of the luciferase gene. A HindIII restriction site lies directly between the promotor and start codon. Map was drawn using SnapGene (4.1.4).

2.13 NanoString study

NanoString experimentation was conducted using nCounter Vantage™ RNA Panel for DNA Damage and Repair (LBL-10250-03), which contained probes for 192 genes (180 DNA repair genes and 12 housekeeping genes, for a full list of genes see appendix 1.2). For information on cell lines used see Chapter 4 section 4.1.1.

2.13.1 Sample preparation

Cells grown in 60 mm dishes were incubated in either 21%, 1% or 0.1% O_2, and 5% CO_2 at 37°C for 5 days before lysis. Cell lysing, RNA extraction and reverse transcription was conducted as described in section 2.9.

2.13.2 Test for hypoxic markers

To ensure the cells had responded to the hypoxic environments, cDNA was utilised in quantitative RT-PCR experiments to test for the increase in hypoxic markers (*VEGF* and/or *GLUT1*) as described in section 2.10. Only samples with increased hypoxic markers, were used in the NanoString assay.

2.13.3 NanoString hybridisation

Hybridisation reactions were conducted following the NanoString manufacturers protocol. In brief, 100 µg of RNA was mixed with probe solutions as well as hybridisation buffer. Reactions were incubated at 67 °C with a thermal cycler lid temperature of 72 °C for 18 h. Samples were then transferred directly to the NanoString prep station (a multi-channel pipetting robot) for further processing. Steps completed by the prep station include purification of the hybridised samples and immobilisation of molecular labels to the sample cartridge. Once completed, the sample cartridge was sealed and transferred to the Digital Analyzer where the unique molecular identifier for each probe was counted and the data collated.

2.13.4 Data analysis

Data analysis was conducted using the nSolver™ Analysis Software (3.0) with nCounter® Advanced Analysis module (2.0.115). Details of the analysis steps are as follows.

2.13.4.1 Quality control

Before extensive analysis could be performed, several quality control parameters were assessed. Specifically, binding density, and image quality were calculated to determine the ability of the Digital Analyser to count the immobilised molecules (see nSolver 3.0 manual for further details). Additionally, within each experiment, positive controls were included to

assess the efficiency of the assay, the linearity and limit of detection. Negative controls were included to allow for background subtraction to control for noise within the experiment. Probes were also scored as detected or undetected, whereby detected probes have counts that are more than double the median count of the negative controls. Undetected probes were excluded from further analysis.

2.13.4.2 Normalisation

To eliminate technical variation between samples due to any potential deviation in input material (mass and integrity), 12 housekeeping (HK) genes were included in the gene set. To normalise data, each count obtained was divided by the geometric mean of the HK genes. Additionally, before normalisation, rigorous selection of appropriate HK genes was conducted using the geNorm algorithm (Vandersompele, 2002), by calculating the pairwise variation statistic of each gene (Figure 2.2). For each sample the normalisation factor and mean squared error (MSE) of HK genes from expected profile are calculated. A positive normalisation factor indicates higher than average expression of HK genes. Large MSE indicates that expression of HK deviates significantly from the expected profile. This was a key quality control step as it can indicate the run efficiency as well as input material quality or quantity.

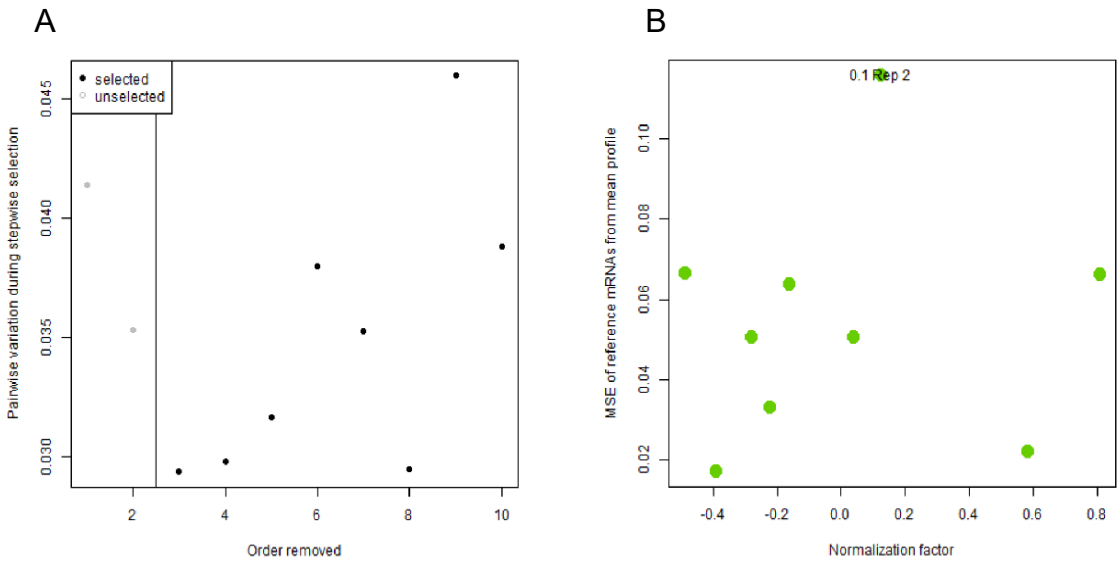

Figure 2.2: Example normalisation output for the NanoString experiment. 12 housekeeping genes (HK) were included in each NanoString reactions. Selection of appropriate HK genes was completed using geNorm algorithm. (A) Visualisation of the geNorm procedure for HK gene selection, where pairwise variation statistics were calculated after removal of individual genes. (B) Summary of normalisation depicting the mean squared error (MSE) for each sample as well as the normalisation factor. Green dots represent each individual sample in a dataset.

2.13.4.3 Differential expression

To determine differential expression of genes, the nCounter® Advanced Analysis Software (2.0.115) utilised multivariate linear regression, whereby oxygen condition was defined as the predictor variables and no confounder variables were specified. Data from samples incubated in 21% O_2 were defined as the reference level of expression. Log_2 fold change of gene expression and associated p-values were determined. To reduce the likelihood of false positive results of significance, a p-value threshold of 0.01 was utilised instead of the commonly used 0.05.

2.13.4.4 DE call

In the situation of too few replicates for differential expression analysis, DE call was used as an alternative. DE call is a test developed specifically for nCounter data, which gives an indication as to whether count values between conditions are larger than can be explained, by noise or background. This is more robust than fold changes alone. Output of this metric is 'yes' or 'no', and can help identify whether the expression level of a gene is likely to be significant.

2.13.4.5 Global and directed significance scoring

The overall extent of differential expression of defined sets of genes (i.e each DNA repair pathway) can be measured with the global significance statistic. This was calculated as the square root of the pathway's average squared t-statistic.

$$\textbf{Global significance statistic} = (\Sigma t_i^2)^{1/2}$$

t_i is the t statistic from the i^{th} pathway gene.

Directed global significance measures the tendency of a pathway to have over or under expressed genes, calculated as the square root of the average sign squared t-statistic.

$$\textbf{Directed global significance statistic} = \textbf{sign}(U)|U|^{1/2}$$

$$\textbf{where } U = \Sigma\, \textbf{sign}(t)_i \cdot t_i^2$$

and where sign(U) is -1 if U is negative or 1 if U is positive.

Formulas were taken from the nCounter Advanced Analysis User Manual.

2.14 Molecular biology techniques

2.14.1 Bacterial transformation

Escherichia coli (*E.coli*) DH5α was subject to a heat shock based transformation protocol for the propagation of plasmids. 5 ng of plasmid DNA was added to competent DH5α and cooled on ice for 30 min. The bacteria were then heat shocked by incubation at 42°C for 45 s, before returning to ice for 2 min. 500 µl of SOC medium (Clonetech) was added and transformed cells were incubated for 1 h at 37°C in a shaking incubator (225 rpm). After recovery, 200 µl of the bacterial mixture was spread across an agar plate containing the appropriate antibiotic for selection of plasmid containing cells. Plates were kept at 37°C overnight to allow for colony growth. Single colonies were picked and added to 5 ml LB broth and left to grow for at least 8 h at 37°C in a shaking incubator (225 rpm).

2.14.2 Plasmid purification

For purification of plasmids, 5 ml of bacterial culture was added to 200 ml LB broth with the appropriate antibiotic. Liquid cultures were grown overnight at 37°C shaking at 225 rpm. Bacteria was then harvested by centrifugation at 6000 g for 30 min in 4°C. Harvesting and purification of plasmid DNA was achieved using a HighPure Plasmid Maxi Prep Kit (Invitrogen) following the manufacturers protocol. The concentration of purified plasmid DNA was measured using a NanoDrop 1000 Spectrophotometer (Thermo Scientific), then diluted to 1 µg/µl with TBE. Plasmid DNA was stored at -20°C until use.

2.14.3 Restriction digest

Plasmid DNA was incubated with restriction enzymes (1 µl/5 µg) and the appropriate buffer for 2 – 4 h at 37°C. DNA fragments were separated on a 1% agarose gel containing Midori Green Nucleic Acid Stain. DNA was visualised under UV light using a Syngene gel imaging G-box.

2.15 Multiphoton laser microirradiation

EGFP-XRCC4 was a gift from Steve Jackson (Addgene plasmid # 46959). Cells were transfected with EGFP-XRCC4 (Figure 2.3) in a 60 mm culture dish. 24-48 h post-transfection, dishes were transferred to a Zeiss LSM 880 (upright) where culture conditions were maintained (37°C, 5% CO_2). An argon laser (488 nm) was used for EGFP excitation with a 40x 1.4 NA water-dipping objective and 5x digital zoom. Laser microirradiation was conducted using a Coherent Chameleon Vision II Ti:Sapphire multiphoton laser. Laser power output was measured at the objective with a laser power meter (ThorLabs), enabling parameters to be adjusted to obtain 10 mW output for 800 nm wavelength. A circular region of the nucleus, 2 µm in diameter, was irradiated with 10 mW 800 nm laser for 20 iterations. Images were subsequently acquired at specified intervals post irradiation.

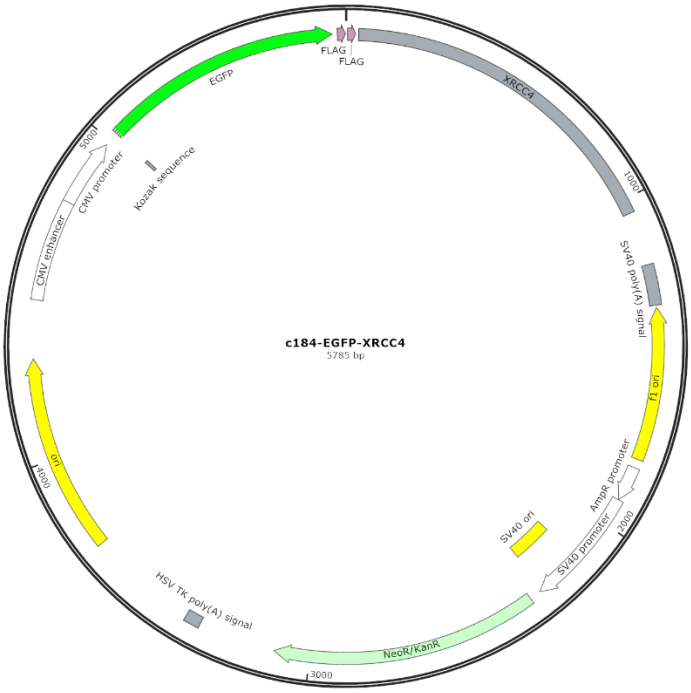

Figure 2.3: Plasmid map of EGFP-XRCC4. The coding sequence of the XRCC4 gene lies directly downstream of the EGFP coding sequence. Gene expression is driven through the CMV promotor. Map was drawn using SnapGene (4.1.4).

2.15.1 Analysis of DNA repair protein recruitment

Registration of acquired movies was completed using StackReg plug-in (Thévenaz *et al.*, 1998) for Fiji (Schindelin *et al.*, 2012). Intensity measurements of the irradiated region (ROI 1), a non-damaged region (ROI 2) and background signal were taken for each frame using Fiji. Subsequent data analysis was completed in Matlab (R2017a) (see appendix 1.3 for custom Matlab script). In brief, average background signal (ROI 3) was subtracted from ROI 1 and ROI 2. Remaining figures were normalised to the average pre-damaged intensity values. Finally, data from the irradiated region (ROI 1) was normalised to the non-damaged region (ROI 2), see Figure 2.4 for analysis workflow. Curves for each individual cell was defined as a 'trace'.

2.15.1.1 Determining recruitment kinetics.

For each trace, a first order response curve $1 - \exp(-\frac{t}{\tau})$ was fitted from the start of the trace to the smoothened maximum intensity (smoothened over a window of 30% of the data set); using the least sum of squares method. Using the curve fitting parameters, the time to 50% of the maximum intensity as well as the kinetic constant τ could be determined (Figure 2.5) (see appendix 1.4 for Matlab scripts).

2.15.1.2 Determining rate of dissociation

For each trace, an exponential decay curve $y = ab^t$ was fitted five datum after the smoothened maximum intensity, using the least sum of squares method. Traces with insufficient points for fitting were excluded from the analysis. Using the curve parameters, the rate of intensity loss as well as the time to 50% loss could be determined (Figure 2.5) (see appendix 1.4 for Matlab scripts).

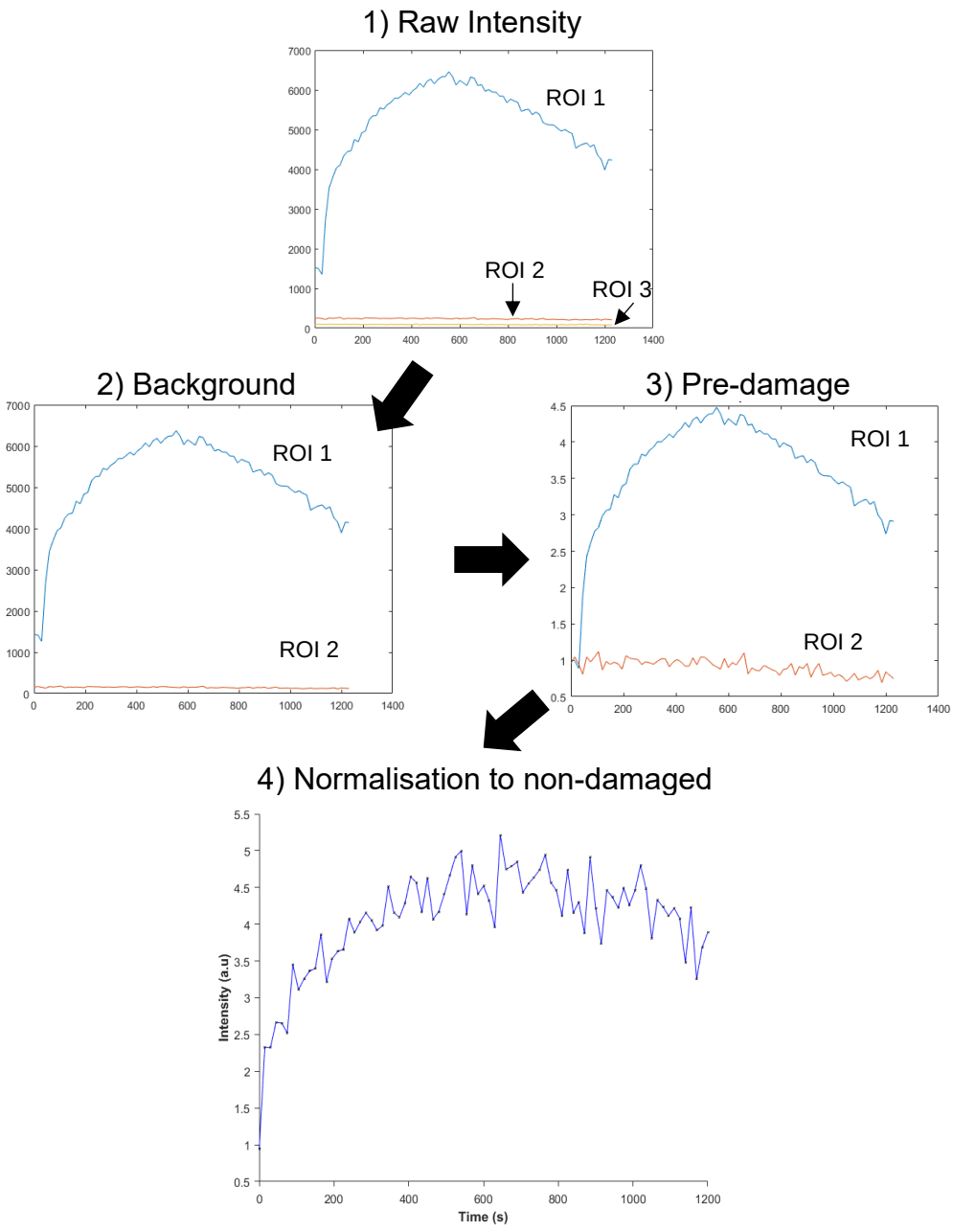

Figure 2.4: Protein recruitment analysis workflow. Custom Matlab scripts were used to perform background subtraction of raw intensity data followed by multiple normalisation steps to obtain finalised intensity data. Graphs are an example of data for a single cell. ROI 1 represents data from damage spot, ROI 2 is from non-damaged region, ROI 3 is background signal.

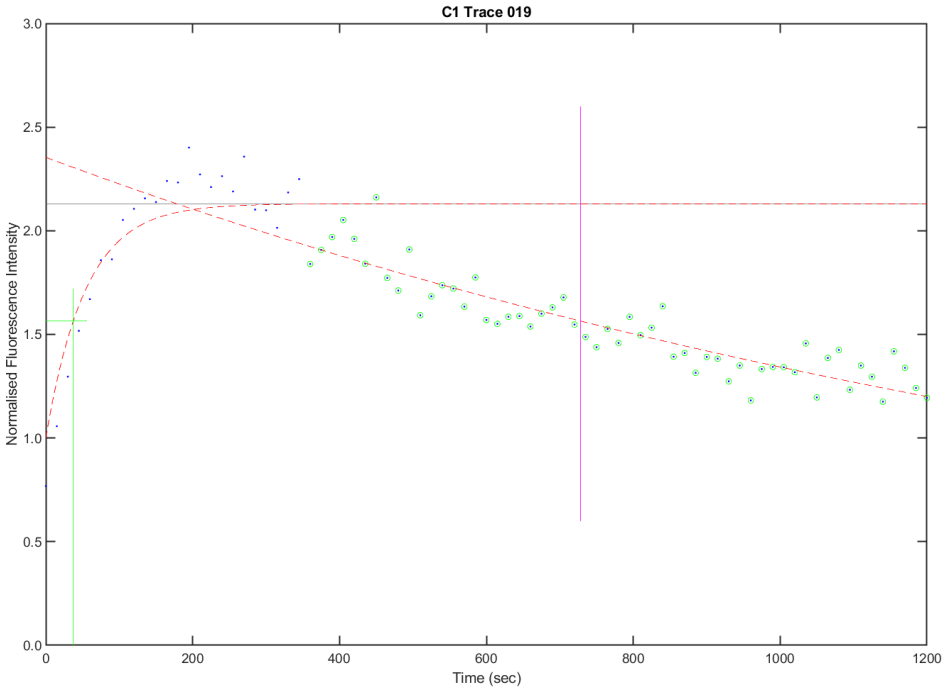

Figure 2.5: Example trace with curve fits. A first order response curve (first dashed orange line) was fitted to an example trace (blue dots = datum). Green intersecting line represents the determined time to 50 % of maximal smoothened intensity (black solid line). An exponential decay curve (second dashed orange line) was fitted to data after the maximal smoothened intensity. Green circles represent data used in exponential decay curve fit. Intersecting magenta line signifies the determined time at which the intensity is reduced by 50%.

2.17 Statistical analysis

Prism 7.0 was used for all statistical analysis unless otherwise stated. A significant threshold of $p<0.05$ was used to define statistical significance.

Chapter 3: The impact of hypoxia on treatment sensitivity and double strand break recognition

3.1 Introduction

Patients presenting with hypoxic tumours have a poor prognosis, in part due to the chemo- and radio-resistant phenotype of these tumours. The tortuous vasculature of solid tumours makes drug delivery to the whole cell population challenging. Yet, the tumour microenvironment itself can have a direct impact on drug efficacy as well as causing cellular adaptations that lead to acquired resistance.

A number of chemotherapeutic agents require oxygen to function efficiently. For example, bleomycin is less effective in a low oxygen environment due to reduced production of reactive oxygen species (Cunningham *et al.*, 1984). Additionally, drugs that require cells to be actively cycling can be rendered ineffective due to hypoxia-induced cell cycle arrest (Amellem and Pettersen, 1991; Gardner *et al.*, 2001). Radioresistance in hypoxia can be attributed to reduced free radical production. Irradiating in a normal oxygen environment causes exposed ends of broken DNA to react with oxygen creating stable organic peroxides, which are less easily repaired. This is known as the oxygen enhancement effect (Chapman *et al.*, 1973). However, in hypoxia, less oxygen is available to react with the ends of DNA, therefore repair of DNA damage is more effective. Overall, hypoxia can have a direct impact on the efficacy of both chemotherapeutic agents and radiotherapy.

Acquired resistance in tumour cells can occur due to hypoxia-induced cellular adaptations. For example, hypoxia can upregulate multi-drug resistance genes, such as MDR-1 and MRP-1 (Comerford *et al.*, 2002; Wartenbert *et al.*, 2003; Lv *et al.*, 2015). Also, hypoxia-induced upregulation of Pim-1, a regulator of apoptosis, results in resistance to cisplatin (J. Chen *et al.*, 2009). Although numerous cellular adaptions have been attributed to hypoxia-induced resistance, these are often tumour type specific. For example, upregulation of the MDR-1 gene by hypoxia was not observed in D283-MED cells, a common medulloblastoma cell line (Fan, 2014). Therefore, further investigations are

needed to fully understand acquired resistance in hypoxic medulloblastoma (MB) and glioblastoma (GBM).

Current treatment protocols for MB and GBM involve the use of DNA damaging agents. For example, temozolomide, the primary drug used against GBM, is an alkylating agent. TMZ treatment creates highly toxic O^6-methylguanine DNA lesions which trigger apoptosis (Roos *et al.*, 2007). Whereas for MB, cisplatin and cyclophosphamide, can crosslink DNA. Radiotherapy, the cornerstone of GBM and MB treatment, results in multiple types of DNA lesions including oxidative bases, single strand breaks and double strand breaks. DNA DSB are highly lethal as an individual DSB can cause cell death (Bennett *et al.*, 1993). However, DSB can be repaired by non-homologous end joining (NHEJ) and homologous recombination repair (HRR) (Takata *et al.*, 1998). The choice between these repair mechanisms is dependent on the cell cycle, with HRR occurring in G2 and S phase when homologous DNA is present, yet NHEJ predominates in G0 and G1.

Acknowledgement of the presence of a double strand break is essential for the repair process and activation of the DNA damage response (DDR). The principle DSB sensor in HRR is the MRN complex composed of meiotic recombination 11 homolog A (MRE11A), RAD50 homolog (RAD50), and Nibrin (NBN or NBS-1). Upon DSB recognition, NBN's primary role is to recruit Ataxia Telangiectasia Mutated (ATM) to the damage site (Lukas *et al.*, 2003; Falck *et al.*, 2005; You *et al.*, 2005). ATM phosphorylates key proteins involved in DNA repair, checkpoint control and apoptosis (You *et al.*, 2005). If the level of DNA damage is too high, phosphorylation of p53 directly or indirectly via ATM occurs leading to the transcription of pro-apoptotic genes and the induction of apoptosis (Banin *et al.*, 1998; Canman *et al.*, 1998; Epstein *et al.*, 2001; Turenne *et al.*, 2001; Saito *et al.*, 2002). Overall, initial recognition of a DSB break is an essential step necessary to trigger downstream signalling in the response to DNA damage.

Previous work in the Sée lab found that, Nibrin (NBN), a key component of the MRN complex, is downregulated in hypoxic D283-MED cells (Fan, 2014). It was hypothesised that this downregulation caused reduced detection of DSB leading to a dampening of downstream damage signalling. This lead to a reduction in p53 stabilisation and activity. Consequently, the hypoxic D283-MB cells were less sensitive to the DNA damaging agent, etoposide (Fan, 2014). The current study aimed to explore this further and to determine whether this mechanism of acquired resistance, involving downregulation ofMRN complex in hypoxia, is universal, occurring in other MB cell lines and GBM cell lines.

3.2 Objectives

The experimental aims for this chapter were as follows:

1. Determine the effect of hypoxia on sensitivity to common DNA damaging agents used in the clinic for MB and GBM.

2. Examine the expression of the main components of the MRN complex (MRE11/RAD50/NBN) under hypoxia.

3. Assess the impact of hypoxia on the upstream regulator ATM, a key signal transducer in the response to double strand breaks.

3.3 Observations of Fan 2014

Previous work by Fan 2014, exploring the impact of hypoxia on MB observed the following in hypoxic D283-MED cells:

1. Resistance to etoposide.
2. Downregulation of NBN (mRNA + Protein) and MRE11 (mRNA).
3. Reduced induction of γH2AX after etoposide treatment.
4. Reduced p53 stability and activity after etoposide treatment.

The aim of the current chapter was to build on the work of Fan 2014, with a particular focus on the following questions:

1. Do hypoxic D283-MED cells display altered sensitivity to other common cancer treatments?
2. Is the observed resistance to etoposide in hypoxia as a result of reduced DNA damage signalling as suggested by Fan 2014?
3. Are these findings universal across other brain tumour cell lines?

Work from both Fan 2014 and the data presented in the current chapter contributed to the production of a publication:

Decrease of Nibrin expression in chronic hypoxia is associated with hypoxia-induced chemoresistance in medulloblastoma cells.

Sophie Cowman, Yuen Ngen Fan, Barry Pizer, Violaine See. 2018 *Under review in BMC Cancer*

(pre-print: https://www.biorxiv.org/content/early/2017/11/30/227207)

3.4 Results

3.4.1 Exploring hypoxia-induced treatment resistance in MB and GBM

Treatment resistance is a common characteristic of hypoxic brain tumours. Fan 2014 determined that chronic hypoxic exposure in D283-MED (MB cells) resulted in resistance to etoposide, a chemotherapeutic agent used to treat many cancers including medulloblastoma, neuroblastoma, lung cancer and testicular cancer. Here, sensitivity to several anti-cancer therapies under normoxic (21% O_2) and hypoxic (1% O_2) environments was examined in MB (D283-MED, MEB-Med8A) and GBM cell lines (U87-MG, U251-MG, D566-MG). Experiments were conducted as described in Figure 3.1 unless otherwise stated.

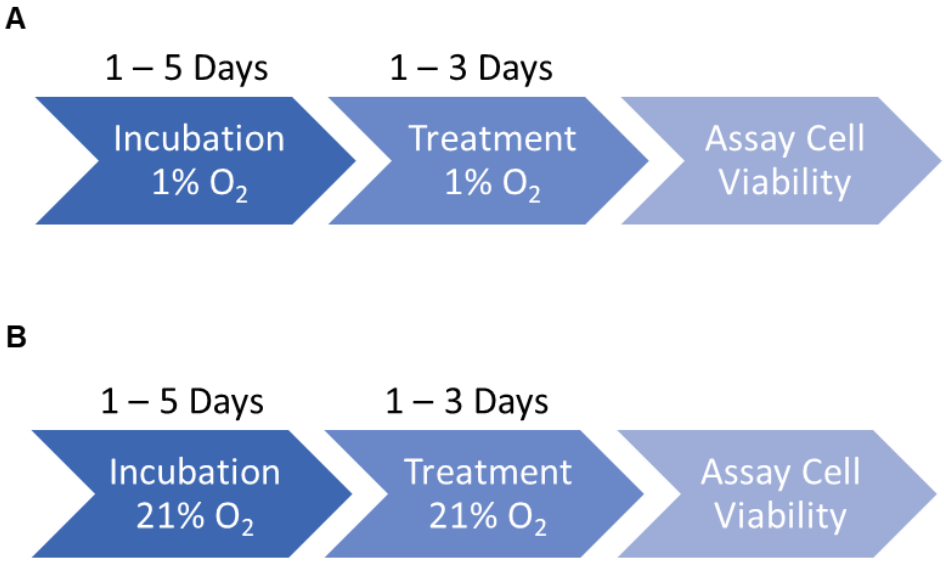

Figure 3.1: Schematic of experimental protocol for treatment sensitivity experiments. (A) Cells that were pre-incubated in 1% O_2 remained in hypoxia throughout treatment yet viability was assayed in normoxia. (B) Cells that were pre-incubated in 21% O_2 remained in normoxia during treatment and viability assay. All hypoxic and normoxic experiments were performed in parallel.

3.4.1.1 Temozolomide is ineffective for inducing U87-MG cell-death *in vitro*

The DNA alkylating agent, temozolomide (TMZ), is the primary drug used to treat GBM in the clinic. Therefore, determining its effectiveness *in vitro* in different oxygen conditions was essential. Unlike its close relative, decarbazine, TMZ does not require metabolic activation, and therefore can methylate DNA at physiological pH (Stevens *et al.*, 1987; Brada *et al.*, 1999). The classical GBM cells line, U87-MG, along with the MB cell line, D283-MED were assessed for their response to TMZ.

TMZ has a short half-life (~2 h); therefore, repeated doses were applied to U87-MG cells. This was not possible for D283-MED as they are in suspension, meaning repeated doses would result in a build-up of toxic DMSO. TMZ had little impact on the viability of U87-MG cells, even with long-term drug exposure (96 h) (Figure 3.2 A, B). Similarly, for D283-MED, sensitivity to TMZ was minimal (Figure 3.2 C, D, E). However, after 72 h and two doses of TMZ (200 µM each), viability decreased to 44%, indicating that TMZ can effectively impact viability for this cell line, yet high doses and long treatment times are required (Figure 3.2 E).

Serum in cell medium can influence the effectiveness of alkylating agents. To understand whether serum removal would improve the ability of TMZ to induce cell death, U87-MG cells were treated with a 200 µM dose of TMZ for 2 h in serum free medium, before a further 72 h incubation in complete medium. Similar to previous experiments, viability of U87-MG cells was not impacted by TMZ, with 96% cells remaining viable (data not shown). In order for TMZ to be effective, the methylguanine transferase enzyme (MGMT) must be silenced by methylation. In U87-MG cells, MGMT is indeed silenced (Qiu *et al.*, 2014), therefore this lack of effectiveness of TMZ cannot be explained by the MGMT status of the cells. However, previous publications have documented the minimal impact of TMZ on U87-MG viability, and the need

for strong doses (up to 2 mM) and long drug exposure (>6 days) to observe cell death (Castro *et al.*, 2015; Akbarnejad *et al.*, 2017; Borhani *et al.*, 2017).

Taken together, TMZ was ineffective for *in vitro* assays performed with U87-MG cells, shown by the high level of viable cells after treatment. D283-MED were more sensitive to TMZ than U87-MG, yet a high dose and long incubation times are necessary to impact cell viability. Based on these results, TMZ was not used further in this work.

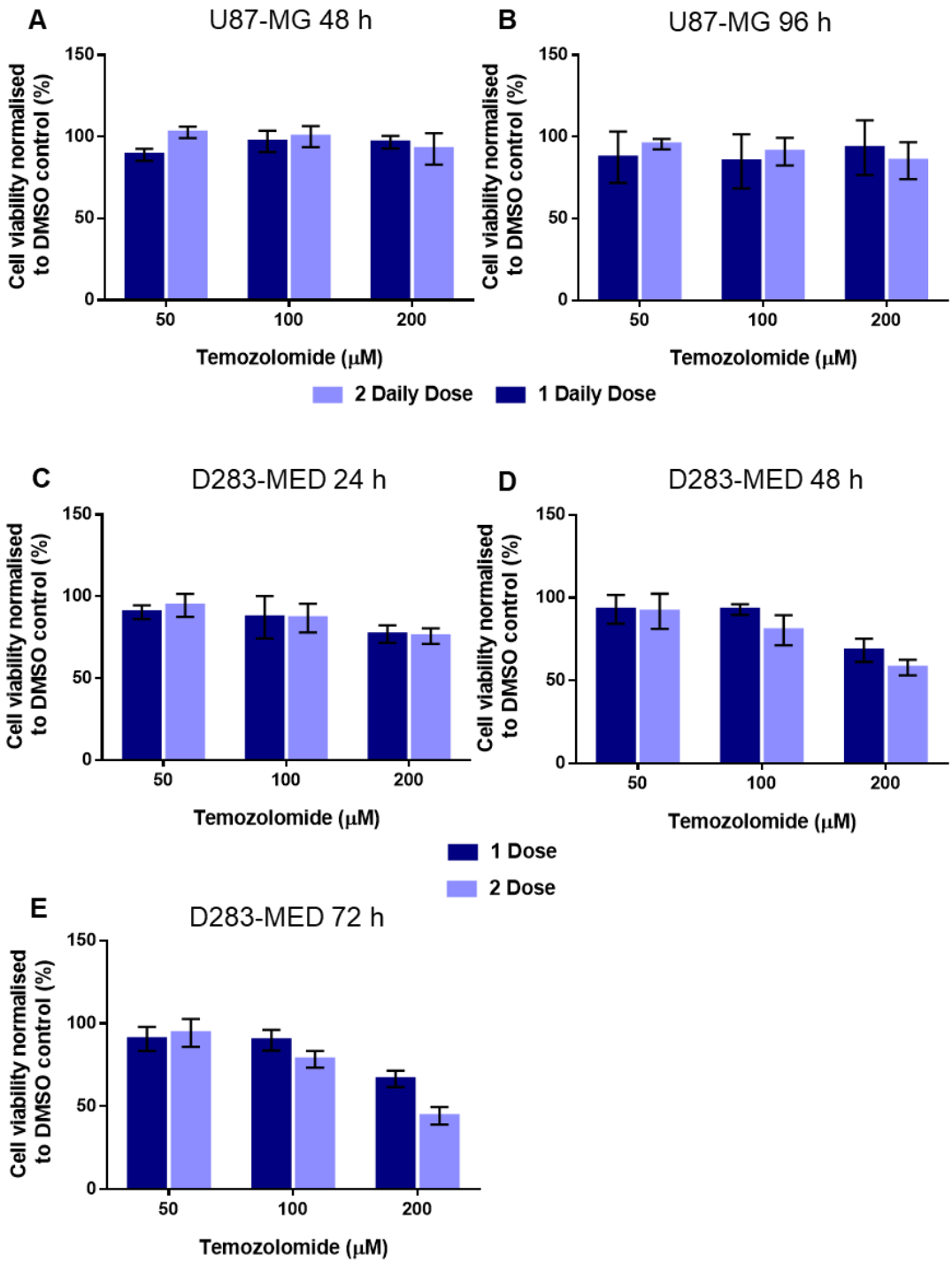

Figure 3.2: Temozolomide-induced cell death is limited in vitro. U87-MG cells were treated with 50-200 μM temozolomide for (A) 48 h and (B) 96 h with 1-2 doses daily. D283-MED were treated on day 1 with 50-200 μM temozolomide with a single dose or two doses. Cells were then incubated for (C) 24 h, (D) 48 h, (E) 72 h. Cell viability was determined using MTS assay with data normalised to DMSO control. Data for (A, B) represents the mean of two independent experiments with SEM, and a single experiment with SD for (C, D, E).

3.4.1.2 Etoposide sensitivity in hypoxic MB and GBM cells

Previous studies determined that the classical MB cell line, D283-MED, displayed sensitivity to the topoisomerase II inhibitor, etoposide, which induces cell death via the p53 pathway (Meley *et al.*, 2010). Pre-incubation of these cell in hypoxia for 5 days reduced sensitivity to etoposide (Fan, 2014). To explore this further, the impact of hypoxia on etoposide sensitivity was investigated in a range of MB and GBM cell lines.

In line with the findings of Fan 2014, for D283-MED cells, pre-incubation in 1% O_2 for 5 days (chronic exposure) resulted in reduced sensitivity to etoposide treatment. For example, treatment with 20 µM etoposide in normoxic cells resulted in 26% viability whereas viability was 74% in hypoxic cells (p=0.003) (Figure 3.3 A). In contrast, acute hypoxic exposure (1 day) had little impact on etoposide sensitivity, with 23% and 26% viability in normoxia and hypoxia respectively with 20 µM etoposide. For the MB cell line, MEB-Med8A, pre-incubation in 1% O_2 did not result in statistically significant alteration of cell viability compared to the normoxic control (Figure 3.3 B). Therefore, the reduced sensitivity to etoposide in hypoxia may be specific to the D283-MED cells.

In comparison to MB cells, GBM cell lines were overall more resistant to etoposide as higher doses and longer treatment durations (48 - 72 h) were required to induce cell death (Figure 3.3 C, D). However, similar to D283-MED, pre-incubation in 1% O_2 for 5 days resulted in reduced sensitivity to etoposide in U87-MG cells (Figure 3.3 C). After exposure to 20 µM etoposide for 72 h, U87-MG viability in normoxia was 39%, yet increased to 67% for hypoxic cells (p=0.006) (Figure 3.3 C). Similar results were obtained for U251-MG cells, with 26% viability for normoxic cells compared to 36% for hypoxic cells (Figure 3.3 D) upon 50 µM etoposide for 48 h. In contrast, in D566-MG cells the sensitivity to etoposide was not altered by hypoxic incubation. (Figure 3.3 D).

Taken together, chronic hypoxic exposure reduced sensitivity to etoposide in the MB cell line D283-MED, and two GBM cell lines U87-MG and U251-MG. Acute hypoxic exposure (1 day) had less effect on etoposide sensitivity in comparison to chronic exposure (5 days).

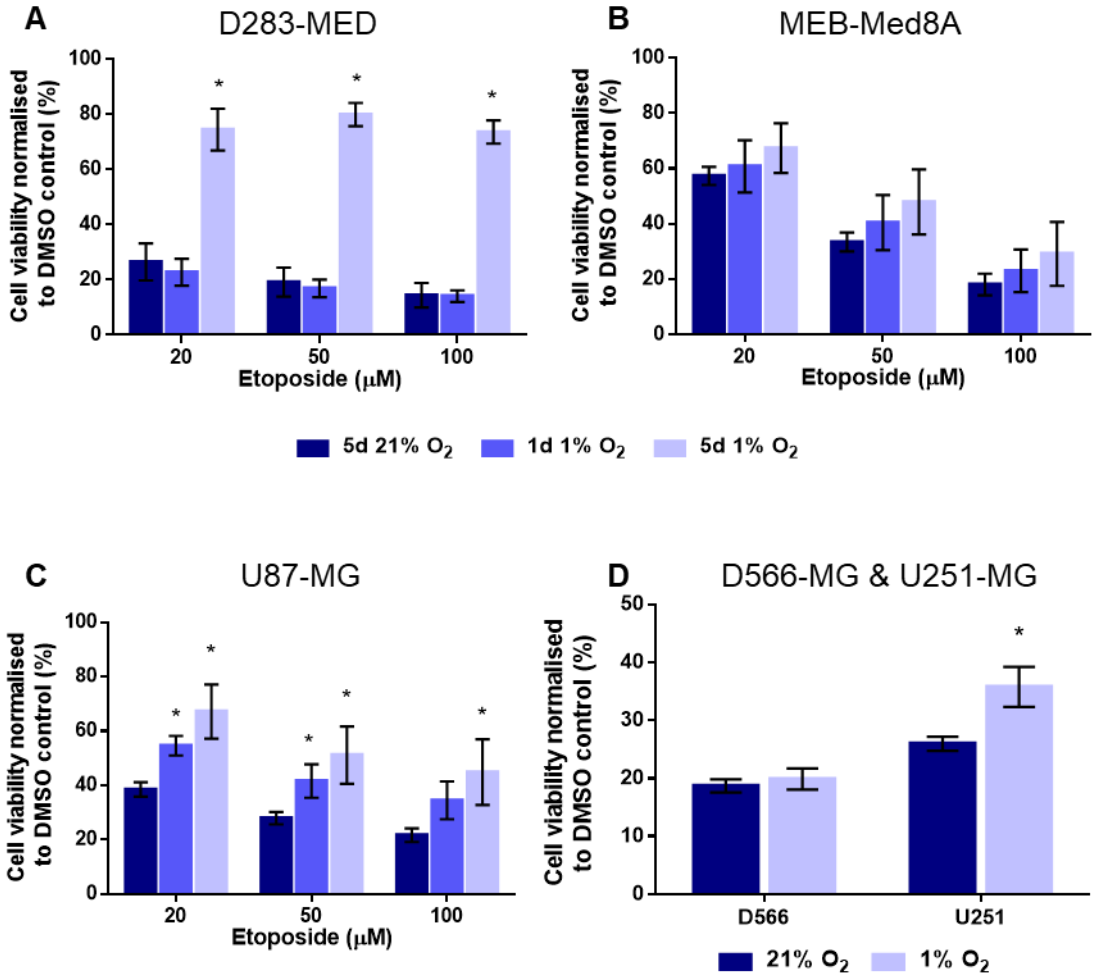

*Figure 3.3: Sensitivity to etoposide in chronic and acute hypoxia. (A) D283-MED, (B) MEB-Med8A and (C) U87-MG cells were pre-incubated in 1% O_2 or 21% O_2 for 1 day or 5 days before treatment with 20-100 μM etoposide. (D) D566-MG and U251-MG were pre-incubated in 1% O_2 or 21% O_2 for 5 days before treatment with 50 μM etoposide. Cell viability was assayed with MTS assay 24 h (D283-MED), 48 h (MEB-Med8A, D566-MG, U251-MG) or 72 h (U87-MG) post-treatment. Absorbance values were normalised to DMSO control. Data is representative of the mean of at least three independent experiments. Error bars represent S.E.M. * denotes significant data where $p<0.05$ indicated by student t-test.*

3.4.1.3 Cisplatin sensitivity in hypoxic MB and GBM cells

Cisplatin is a platinum-based chemotherapeutic agent used to treat MB as well as other cancers such as testicular, ovarian, cervical and breast cancers. This DNA damaging agent creates interstrand crosslinks that can result in the formation of double strand breaks leading to apoptosis (Barry *et al.*, 1990). Previous studies have determined that hypoxia can induce resistance to cisplatin in non-small cell lung cancer (Song *et al.*, 2006; Wohlkoenig *et al.*, 2011; Shin *et al.*, 2014), therefore this concept was explored in GBM and MB cell lines.

D283-MED, MEB-Med8A and U87-MG cells were pre-incubated in 21% or 1% O_2 for 5 days before treatment with cisplatin (Figure 3.4). In D283-MED cells, there was a general trend of increased viability in cells pre-cultured in hypoxia, in comparison to those in normoxia. However, this did not reach statistical significance (Figure 3.4 A). For MEB-Med8A cells, hypoxic pre-incubation resulted in statistically significant reduction in sensitivity to cisplatin, with 36% and 55% viability in normoxic and hypoxia cells respectively after 5 µg/ml cisplatin treatment ($p=0.02$) (Figure 3.4 B). For the GBM cell line, U87-MG, reduced sensitivity to cisplatin in hypoxic cells was observed, yet to a lesser extent compared to MEB-Med8A cells (Figure 3.4 C).

Overall, hypoxia globally reduced the sensitivity to cisplatin in all cell lines tested. This correlates with previous findings in the literature. In non-small cell lung cancer, hypoxia-induced cisplatin resistance is thought to be mediated through SIRT and AMPK (Shin *et al.*, 2014). Whether the same mechanism is occurring in MB and GBM cell lines would require further exploration.

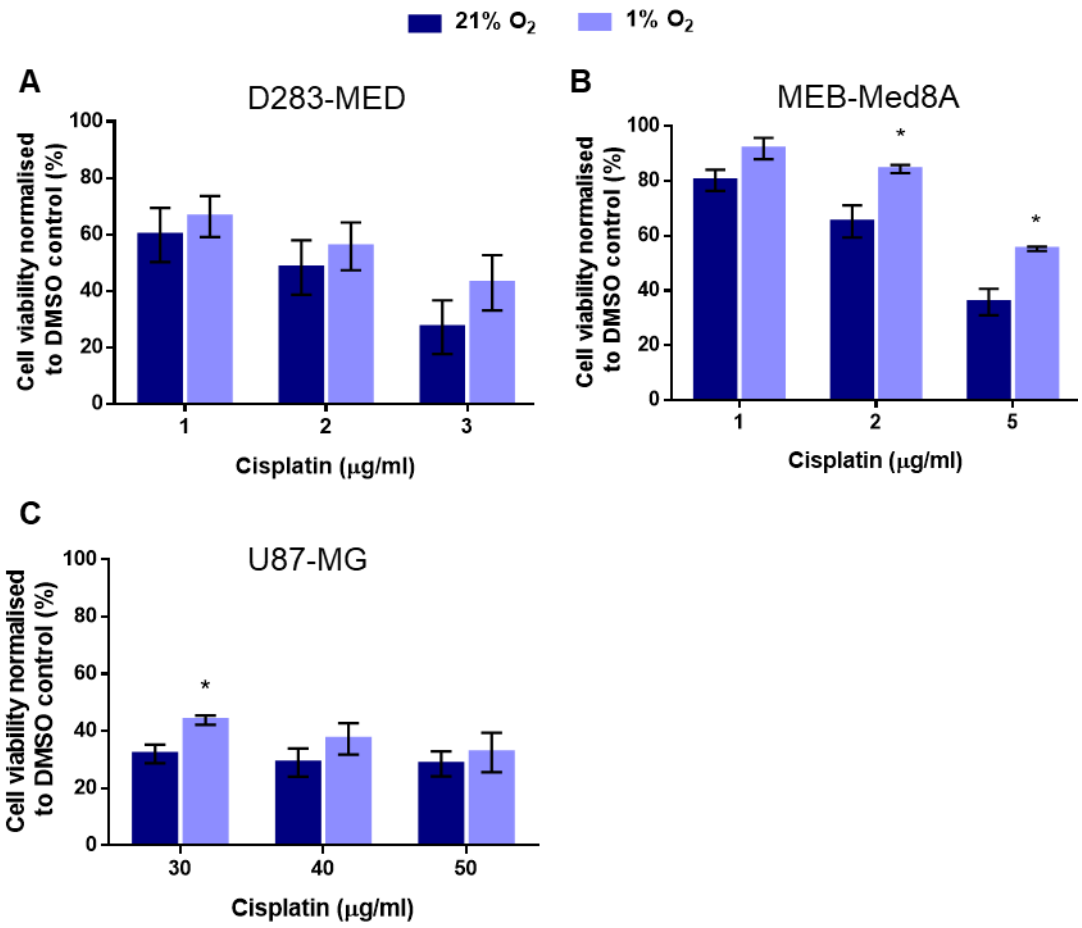

*Figure 3.4: Cisplatin sensitivity in hypoxia. (A) D283-MED, (B) MEB-Med8A and (C) U87-MG cells were pre-incubated in 1% or 21% O_2 for 5 days, before treatment with cisplatin. Cells were assayed for viability 48 h after treatment using MTS assays. Absorbance values were normalised to DMSO control and data is representative of the mean of three independent experiments. Error bars show S.E.M. * denotes significant data where $p<0.05$ indicated by student t-test.*

3.4.1.4 Hypoxia and phleomycin sensitivity

Phleomycin, a glycol-peptide antibiotic, can directly induce DNA double strand breaks (Sleigh., 1976). Phleomycin is not currently used clinically, yet the closely related compound, bleomycin is utilised for the treatment of testicular cancer and ovarian cancer. General resistance to bleomycin is thought to be attributed to a number of cellular adaptation such as the enhanced repair of bleomycin induced DNA damage (Tuimala *et al.*, 2002). Whether hypoxia-induced cellular adaptions contribute to bleomycin or phleomycin resistance has not yet been explored.

To determine whether hypoxia could affect sensitivity to phleomycin in GBM, U87-MG cells were pre-incubated in 21% or 1% O_2 prior to phleomycin treatment. The cells remained in their respective O_2 condition throughout the treatment duration before assaying viability, as previously done with etoposide and cisplatin (Figure 3.5 A, C). The U87-MG cells were sensitive to phleomycin treatment shown by the ~39% viability in normoxia. However, phleomycin was not effective in hypoxia (100% viability) (Figure 3.5 C). Molecular oxygen is required for the production of reactive oxygen species by phleomycin (Sleigh., 1976), which explains the lack of activity in hypoxia. To combat this, U87-MG cells and D283-MED cells were pre-incubated in 21% or 1% O_2 for 5 days but treated in 21% O_2 (Figure 3.5 B). Similar viability was observed U87-MG cells irrespective of pre-incubation in hypoxia (Figure 3.5 B). In contrast, for D283-MED reduced viability in hypoxic cells (48%) was observed in comparison to normoxia (58%) (Figure 3.5 C), yet this was not statistically significant ($p=0.20$).

In summary, for U87-MG and D283-MED cells, pre-incubation in hypoxia does not significantly reduce sensitivity to phleomycin. Due to the re-oxygenation step, any hypoxia-induced adaptions may be lost. From a clinical perspective, the use of phleomycin against hypoxic tumours would likely be ineffective due to a lack of activity.

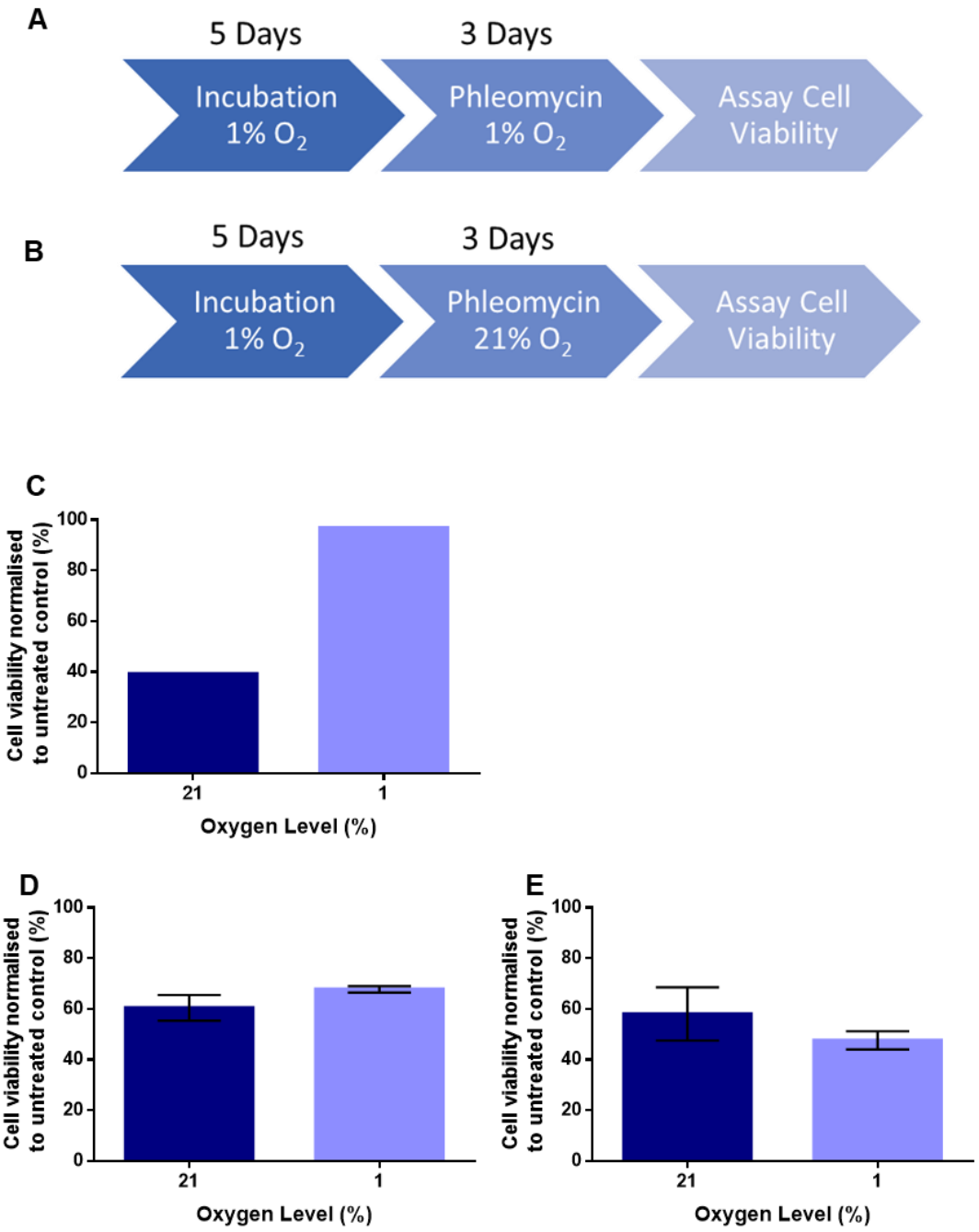

*Figure 3.5: Pre-incubation in hypoxia does not influence sensitivity to phleomycin. (A, B) Schematic of experimental procedure. (C, D) U87-MG and (E) D283-MED cells were pre-incubated in 1% or 21% O_2 for 5 days, before treatment with phleomycin either in (C) hypoxic conditions for U87-MG (50µg/ml) or (D, E) in normoxia for U87-MG (50 µg/ml) and D283-MED (40 µg/ml). Cell viability was determined after 72 h treatment using MTS assay, where absorbance values were normalised to untreated control. Data in (C) is a single experiment, (D, E) is representative of the mean for three independent experiments, with error bars indicating S.E.M. * denotes significant data where $p<0.05$ indicated by student t-test.*

3.4.1.5 X-ray irradiation sensitivity in hypoxic MB and GBM cells

Resistance to radiotherapy is a common characteristic of hypoxic tumours, shown by countless studies *in vitro* and in a clinical setting. Treatment of MB and GBM relies heavily on RT, therefore it is important to understand whether hypoxic MB and GBM present a resistance phenotype. To address this, GBM and MB cells were pre-incubated for 5 days in 21% or 1% O_2 before irradiating in a normoxic environment. Subsequently, cells were returned to their respective oxygen environment for 48 h before assaying cell viability (Figure 3.6 A). Irradiating in normoxia enables the examination of acquired resistance rather than resistance due to reduced effectiveness of radiotherapy in a low oxygen environment.

Preliminary experiments were preformed to establish the adequate dose of X-ray irradiation in order to induce cell death (data not shown). GBM cells were less sensitive to irradiation compared to MB cells, as they required a significantly higher doses (~80Gy), yet 30-40 Gy was sufficient for MB cells. This reduced sensitivity of GBM cells to anti-cancer treatments was previously observed with etoposide and correlates with the poor treatment response of GBM in the clinic.

Hypoxic D283-MED cells were less sensitive to X-ray irradiation, with 29% cell viability in normoxic cells compared to 38% in hypoxic cells (Figure 3.6 A). However, this was not statistically significant, likely due to the high variability in the data. In contrast, for MEB-Med8A cells, a reverse trend was observed with higher viability in normoxic cells (Figure 3.6 A). However, these cells were stressed during the irradiation procedure (cooling, transportation etc.), which caused highly variable data, thus the observed trends are hard to interpret. Similar to D283-MED cells, hypoxic U87-MG were less sensitive to X-ray irradiation, with 23% and 36% cell viability for hypoxia and normoxia respectively ($p=0.03$) (Figure 3.6 B). The same trend was also observed in

D566-MG cells, yet with no statistical significance. In contrast, hypoxia did not impact X-ray irradiation sensitivity in U251-MG (Figure 3.6 B).

In summary, pre-incubation in hypoxia resulted in reduced sensitivity to X-ray irradiation in D283-MED, U87-MG and D566-MG cells. However, hypoxic U251-MG cells responded similar to normoxic cells.

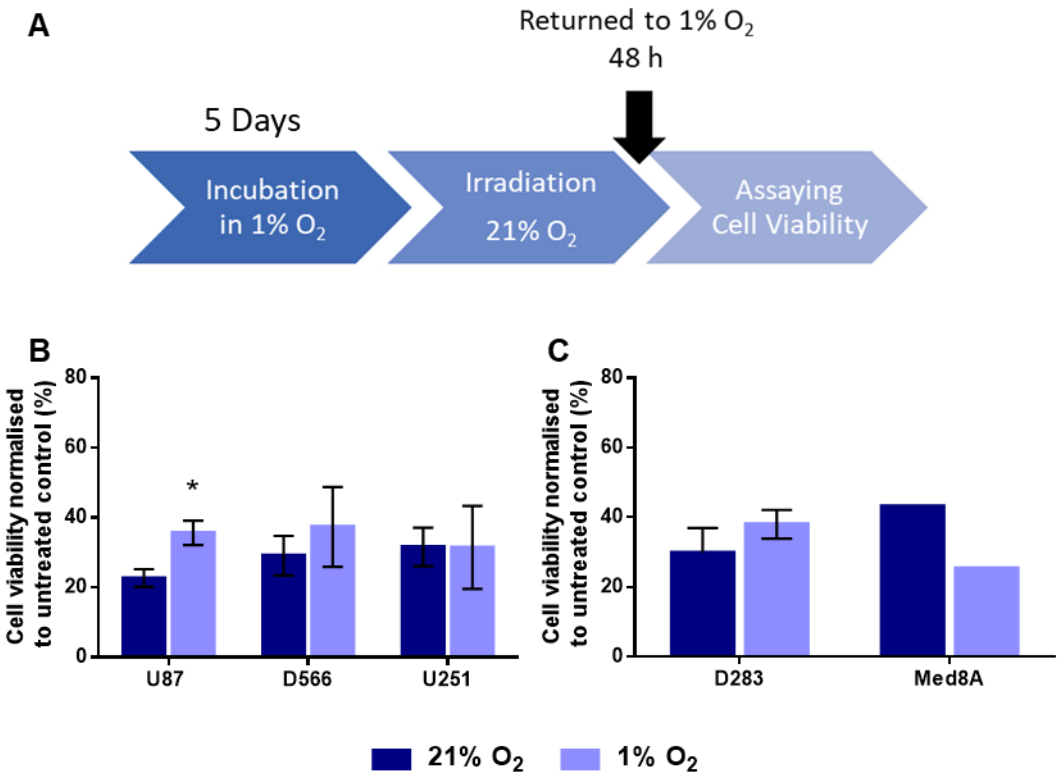

*Figure 3.6: Sensitivity to X-ray irradiation in chronic hypoxia. (A) schematic detailing the experimental procedure for hypoxic cells. (B) MB cells and (C) GBM cells were pre-incubated in 1% O_2 or 21% O_2 for 5 days before irradiation in 21% O_2 with 30 Gy D283-MED, 40 Gy MEB-Med8A, 80 Gy U251-MG and D566-MG, two doses 80 Gy U87-MG. Cells were assayed for viability with MTS assay 48 h after treatment, absorbance values were normalised to DMSO control. Data are the mean of at least three independent experiments, with exception of MEB-Med8A n = 2. Error bars represent S.E.M. * denotes significant data where $p<0.05$ indicated by student t-test.*

3.4.1.6 Exploration of alternative cell survival assays

The MTS/MTT assay is widely used for the determination of drug sensitivity. This method relies on metabolic activity of cells, resulting in the reduction of a tetrazolium compound to a coloured formazan product (Berridge and Tan, 1993), where the number of viable cells is proportional to absorbance. Benefits of this assay include ease of use, suitability for many cell lines and high-throughput drug testing. However, the MTS assay may not be a good indicator of cell survival, as senescent cells are measured as metabolically active even though these cells would not proliferate and generate future cell populations. Alternative methods to determine cell viability include crystal violet (CV) proliferation assays and clonogenic assays. For the classical GBM cell line, U87-MG, pre-incubation in hypoxia results in reduced sensitivity to etoposide (Figure 3.3 C), therefore to complement this study, U87-MG cells were used CV proliferation assays to compare with the MTS assay results. Additionally, preliminary experiments were conducted to test the suitability of U87-MG in the clonogenic assay; however, these cells formed overlapping colonies, which were difficult to count. Therefore, optimisation and investigation of analysis methods would be required if the clonogenic was used further.

The crystal violet (CV) proliferation assays is based on the proliferation rate of cells. In summary, cells are seeded at a low density followed by treatment with a cytotoxic agent. Cells are then left to grow for 5 -7 days in fresh medium before staining with crystal violet. Unlike the clonogenic assay, colonies are not counted, but instead the CV is solubilised and optical density measured. As colony formation is not a requirement, cells unsuitable for the clonogenic assay can be utilised in the CV proliferation assay. However, in comparison to the MTS assay, it can be time consuming (up to 7 days) and does not allow for the assessment of multiple cell lines and cytotoxic agents in parallel.

To determine whether reduced sensitivity to etoposide was observed in hypoxic U87-MG cells with the CV proliferation assay, cells were pre-

incubated in 1% or 21% O_2 before treating with etoposide (24 h) and measuring CV absorbance 5 days post-treatment. Similar to the clonogenic assay, low doses of etoposide were sufficient to induce cell death (Figure 3.7). Additionally, it appears that pre-incubation in hypoxia results in increased cell survival after etoposide treatment (Figure 3.7), a similar finding to the MTS assay. However, experimental data was highly variable shown by the large error bars, potentially due to variations in staining efficiency.

Overall, the proliferation assay confirmed the MTS data obtained in normoxic and hypoxic U87-MG cells treated with etoposide. However, given the low throughput and time consuming nature of this assay, a low number of biological repeats were obtained.

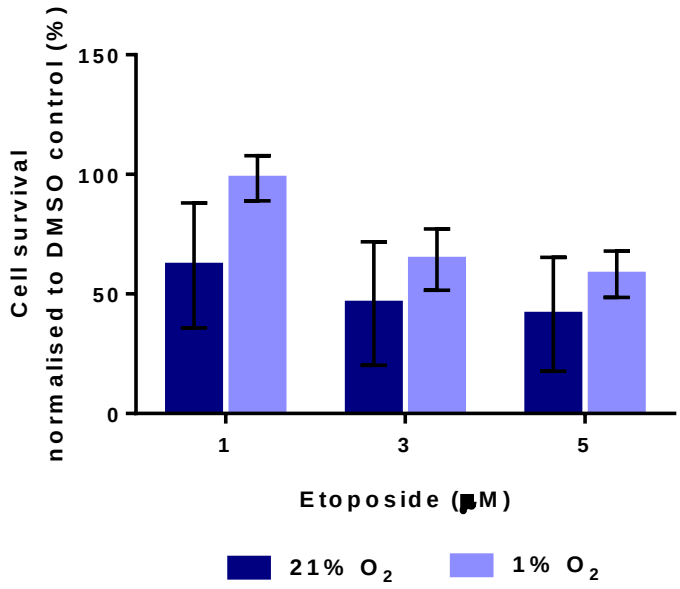

Figure 3.7: Sensitivity to etoposide in hypoxia shown by CV proliferation assay. Cells were pre-incubated in 21% or 1% O_2 prior to treatment with 1-5 μM etoposide for 24 h. Cells were then left to grow for 5 days before staining with crystal violet, which was then dissolved in 10% SDS. Absorbance was measured at 595 nm and normalised to untreated control. Data represent two independent experiments. Error bars represent S.E.M.

3.4.1.7 Summary of hypoxia and treatment sensitivity results

Hypoxia-induced treatment resistance is highly problematic from a clinical perspective. Here, the impact of hypoxia on the sensitivity to a number of common cancer treatments was explored for multiple MB and GBM cell lines (Table 3.1). Chronic exposure to 1% O_2 resulted in reduced sensitivity to etoposide, cisplatin and irradiation for a number of cell lines. In particular, D283-MED and U87-MG cells exhibited the greatest reduction in treatment sensitivity after hypoxic exposure.

The agents tested here caused different types of DNA damage. Nevertheless, DNA damage such as interstrand crosslinks for example, can lead to DSB, the most toxic damage type. Often, DSB arise due to the stalling and collapse of replication forks, which occurs when the replication machinery encounters damage such as a crosslink. Microarray analysis by Fan 2014, identified that the MRN complex, responsible for initial recognition of double strand breaks, was downregulated in hypoxic D283-MED cells. It was hypothesised that this could contribute to hypoxia-induced reduction in etoposide sensitivity. Therefore, to understand whether changes to MRN could induce the hypoxia-related resistance identified here, the level of MRN as well as other DNA damage response proteins were assessed.

Table 3.1: Summary of reduced sensitivities in hypoxia observations in MB and GBM cell lines. Light blue ticks denote statistically significant results.

	Reduced sensitivity in hypoxia?			
Cell Line	**Etoposide**	**Cisplatin**	**Phleomycin**	**X-ray Irradiation**
D283-MED	✔	✔	✘	✔
MEB-Med8A	✘	✔	N/A	✘
U87-MG	✔	✔	✘	✔
U251-MG	✔	N/A	N/A	✔
D566-MG	✘	N/A	N/A	✘

3.4.2 Downregulation of the double strand break recognition complex in hypoxic MB cells

The MRN complex composed of MRE11, RAD50, and NBN, is responsible for the recognition of double strand breaks. Previous studies determined that hypoxic exposure results in the downregulation of NBN (To *et al.*, 2006; Fan, 2014). Specifically, Fan 2014 observed reduced expression of both *NBN* and *MRE11* in hypoxic D283-MED cells. This observation was to be confirmed in D283-MED and explored in other MB and GBM cell lines.

3.4.2.1 *NBN* and *MRE11* gene expression in hypoxic MB and GBM cells

RT-PCR was utilised to determine the mRNA level of *MRE11, RAD50, NBN*, in MB and GBM cells incubated in 21% or 1% O_2 for 5 days. Similar to Fan 2014, hypoxia caused a 2.3-fold (-1.2 log_2) downregulation of *NBN* and *MRE11* in D283-MED (Figure 3.8 A), yet there was little impact on *RAD50*. In MEB-Med8A cells there was no significant change in expression of either *NBN, MRE11* or *RAD50*, indicating that downregulation of *NBN* and *MRE11* is not a general phenomenon across all MB cells. Additionally, there was no change in expression levels of the MRN components in U87-MG or U251-MG upon hypoxic exposure (Figure 3.8 B). Whilst the downregulation of NBN in D566-MG was statistically significant (Figure 3.8 B), the fold reduction was small (1.6-fold) with potentially little functional impact.

To understand whether the reduced levels in MRN are specific to chronic hypoxia (5 days), D283-MED cells were pre-incubated in 21% or 1% O_2 for 6-96 h. The chosen time points correlate with peaks of HIF accumulation in long-term hypoxia (Fan 2014). Short hypoxic exposure (6 h) had no impact on the expression of *NBN*, *MRE11* or *RAD50* yet from 24 h onwards significant downregulation of *NBN* and *MRE11* occurred. At later time points (>48 h) the strongest downregulation was observed (4.5-fold *NBN*, 3.2-fold *MRE11*)

(Figure 3.9 A). Interestingly, at 48 h hypoxic exposure *RAD50* was downregulated 2-fold (-1 log_2), yet this was not statistically significant.

Additionally, U87-MG cells were also subjected to 1% O_2 for 6-96 h and the levels of *NBN, MRE11* and *RAD50* assessed. Although no downregulation of the MRN complex was observed at 5 days hypoxic exposure (Figure 3.8 B), changes may occur at earlier time points, which could contribute to the hypoxia-induced reduction in sensitivity to DNA damaging agents previously identified. The expression level of all three components of the MRN complex was highly variable, and the observed changes did not reach the 2-fold threshold for RT-PCR sensitivity (Figure 3.9 B). Therefore, regardless exposure time, hypoxic incubation did not significantly affect gene expression of the MRN complex in U87-MG cells.

Taken together, this data corroborates data of Fan 2014, whereby the expression of *NBN* and *MRE11,* key components of the MRN complex are downregulated by hypoxia in D283-MED cells. This downregulation appears to require long hypoxic exposure (>48 h), which could explain why reduced etoposide sensitivity is not observed after 24 h of hypoxic exposure.

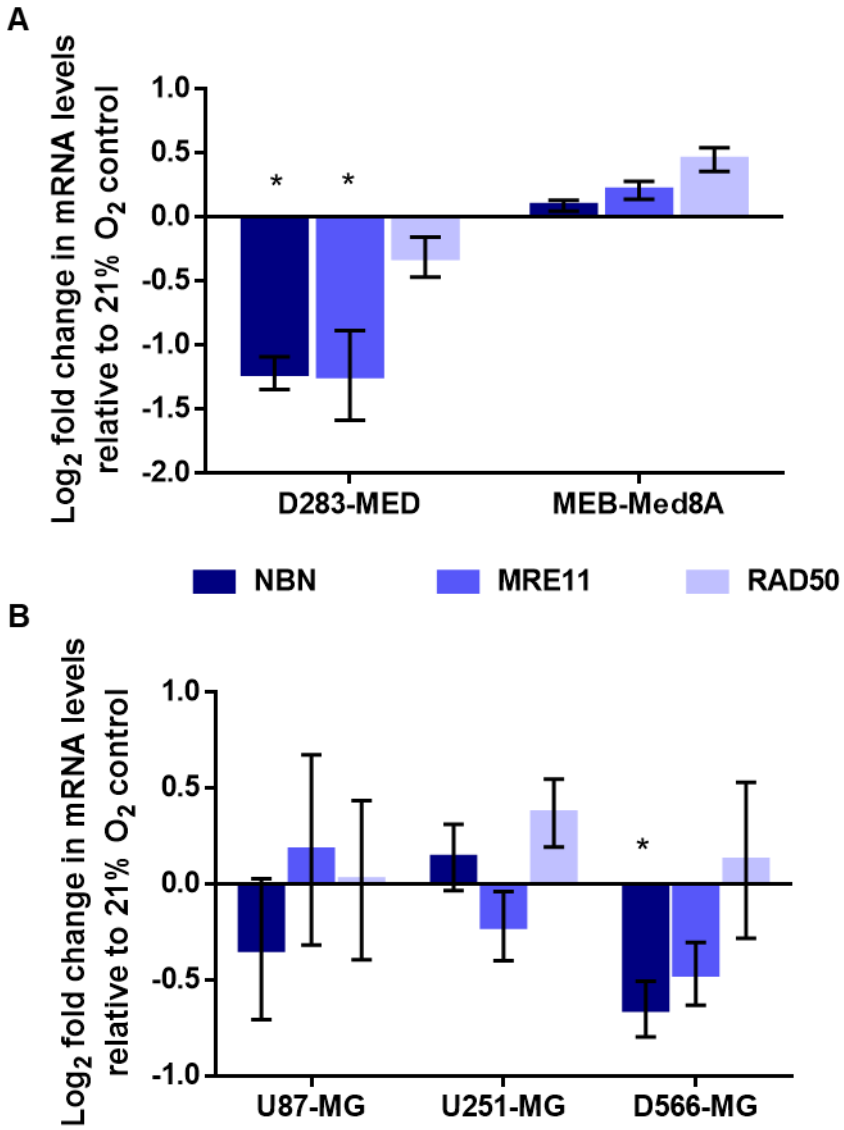

*Figure 3.8: NBN and MRE11 mRNA levels in chronic hypoxia. (A) MB cells and (B) GBM cells were incubated in 1% or 21% O_2 for 5 days. After incubation, RNA was extracted and converted to cDNA for RT-PCR experiments, probing for NBN, MRE11 and RAD50. Data is represented as log_2 fold change in mRNA levels with respect to level for 21% O_2 samples. Data are representative of the mean for at least three independent experiments, with error bars showing S.E.M. * denotes significant data where $p<0.05$ indicated by one-way student t-test.*

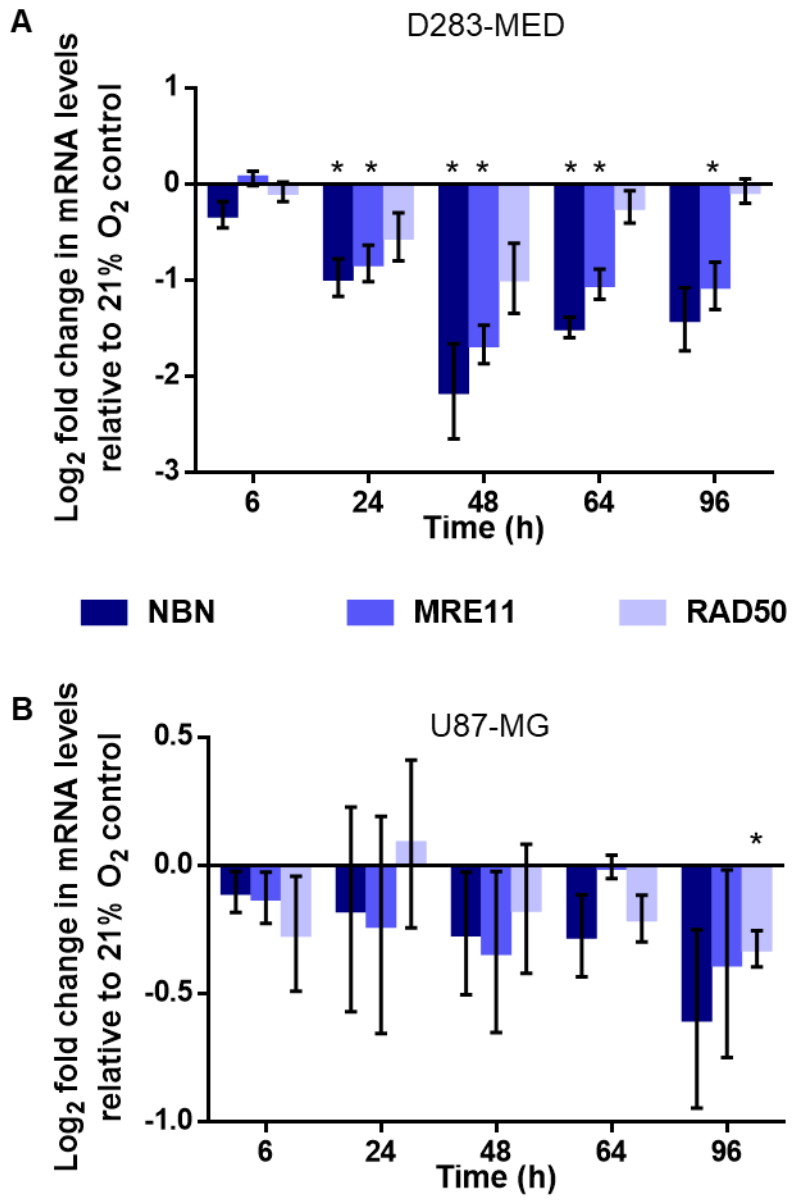

*Figure 3.9: NBN and MRE11 mRNA levels over time in hypoxia. (A) D283-MED and (B) U87-MG cells were incubated in 1% or 21% O_2 for 6-96 h. After incubation, RNA was extracted and converted to cDNA for RT-PCR experiments, probing for NBN, MRE11 and RAD50. Data is represented as log_2 fold change in mRNA levels with respect to level for 21% O_2 samples. Data are representative of the mean for at least three independent experiments, with error bars showing S.E.M. * denotes significant data where $p<0.05$ indicated by one-way student t-test.*

3.4.2.2 NBN and MRE11 protein levels in hypoxic MB and GBM cells

Chronic hypoxic exposure resulted in downregulation of *NBN* and *MRE11* mRNA in D283-MED cells. To confirm these hypoxia-induced changes translate to the protein level, western blotting was performed. Similar to the RT-PCR data, there was a ~2-fold downregulation of both MRE11 and NBN in hypoxic D283-MED cells (Figure 3.11 A, B). For each experimental condition, 25-30 μg of protein was loaded equally per sample as determined by BCA assay (see Figure 3.10 for example calculations for the BCA assay). Additionally, after protein transfer, membranes were stained with Ponceau to ensure the amount of protein from each sample was similar, and the transfer was even (data not shown). However, downregulation of β actin was observed, which is unlikely due to uneven loading. The level of other common housekeeping genes, cyclophilin A and Histone2B, were tested, and were all regulated by hypoxia similar to β actin (data not shown), specifically in the D283-MED cells. Therefore, for quantification, intensity was not normalised to the loading control in this cell line. Further explanation of housekeeping protein regulation by hypoxia can be found on p102.

Hypoxia can result in direct changes to DNA repair protein levels through regulation of translation (reviewed in Scanlon and Glazer, 2015), therefore both MEB-Med8A and GBM cells were included in western blotting experiments for NBN and MRE11. However, in line with the RT-PCR results, there was no significant downregulation in NBN or MRE11 in these cell lines (Figure 3.11, Figure 3.12), with the exception of a small change in MRE11 in hypoxic U251-MG (Figure 3.12 B).

Overall, significant downregulation of both NBN and MRE11 was observed in D283-MED cells, similar to the RT-PCR data. This correlates with the findings of Fan 2014, who determined that NBN (mRNA, protein) and MRE11 (mRNA) were downregulated by hypoxia (Fan, 2014).

A

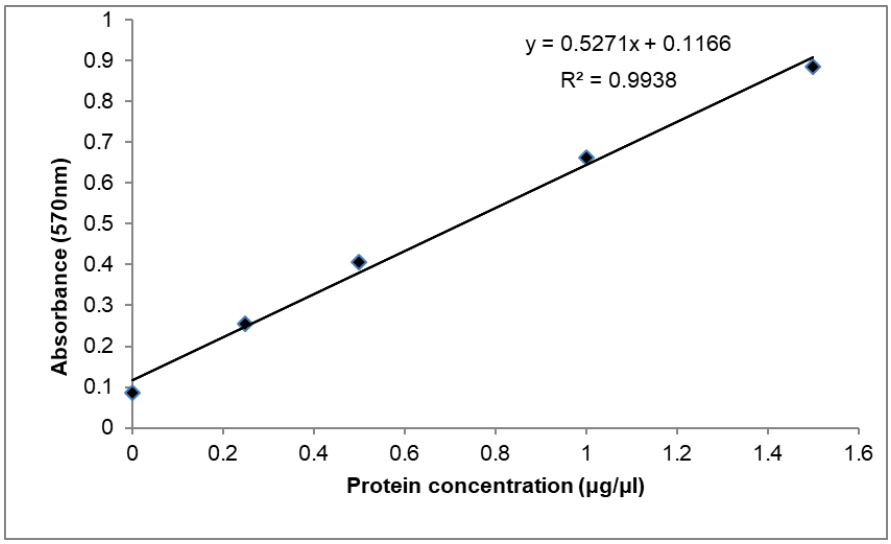

B

Sample	Stock Concentration (µg/µl)	Protein added (µl)	H_2O added (µl)	Total Protein Loaded (µg)
D283-MED 21% O_2	2.9	8.6	27.3	25
D283-MED 1% O_2	1.4	18.0	18.0	25

Figure 3.10: Example BCA assay of D283-MED cells. Protein was collected from D283-MED cells incubated in 21% or 1% O_2 for 5 days. (A) A standard curve was produced using a BCA assay and bovine serum albumin at 0-1.5 µg/µl. B) Using the standard curve, the stock concentration of D283-MED protein samples was determined, and the volume required for 25 µg was calculated. This ensured that an equal amount of protein was loaded into a western blot for each sample.

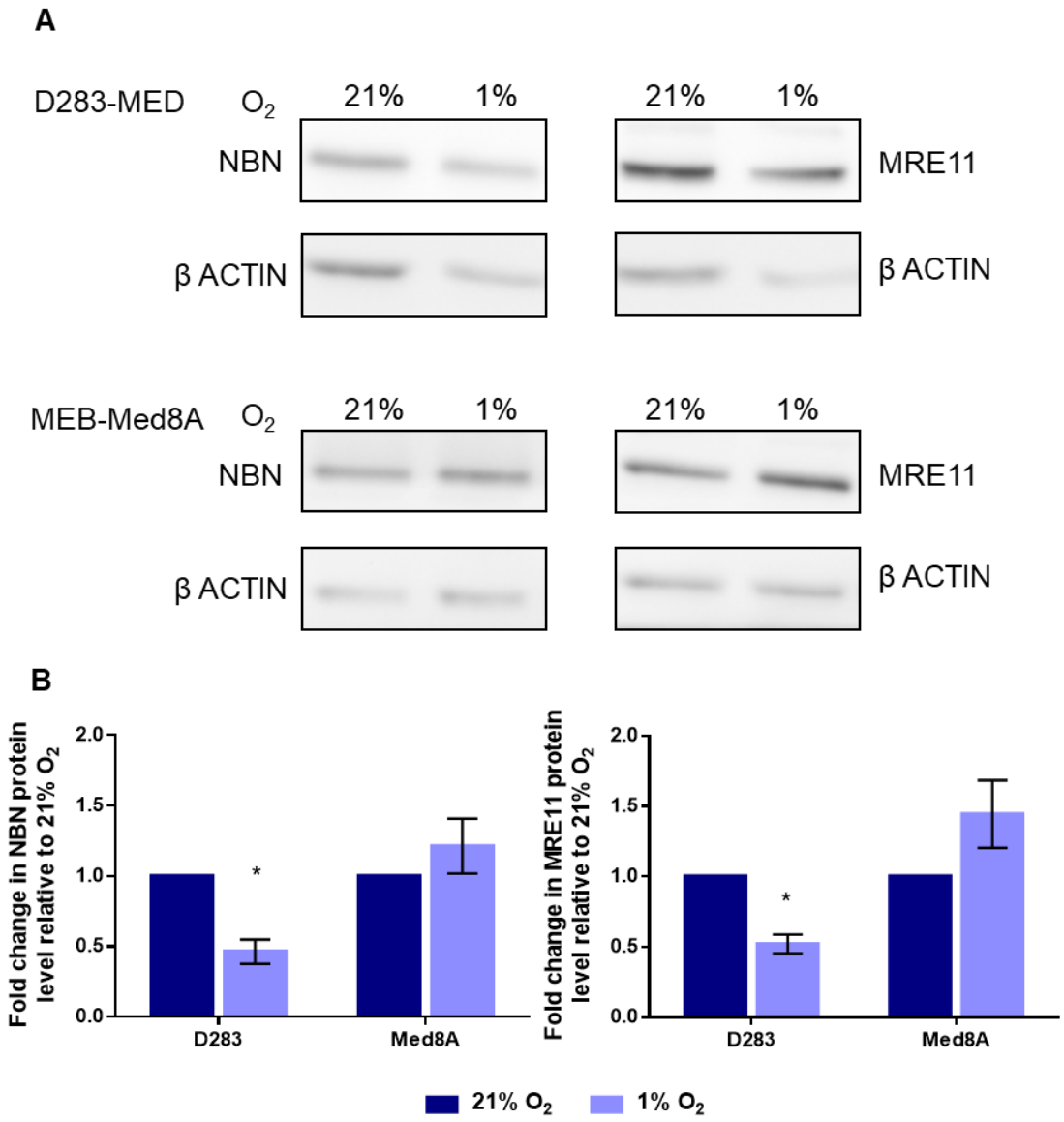

*Figure 3.11: NBN and MRE11 protein levels in hypoxic MB cells. D283-MED and MEB-Med8A cells were incubated in 1% or 21% O_2 for 5 days before protein extraction. (A) Levels of NBN and MRE11 were determined by western blotting. (B) Densitometry was measured using Image J. Data represent the mean of at least three independent experiments, with error bars indicating S.E.M. * denotes significant data where $p<0.05$ indicated by one way student t-test.*

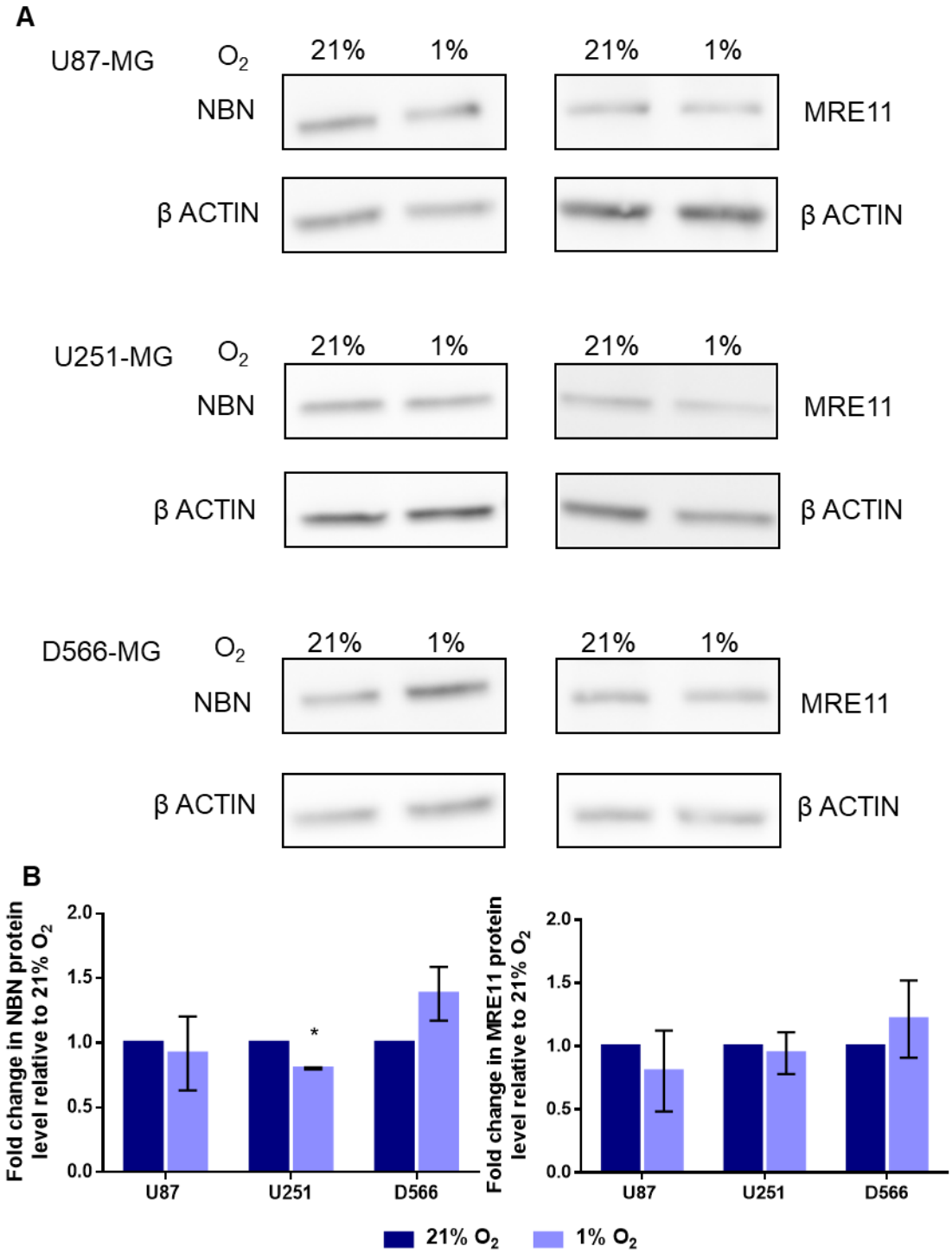

*Figure 3.12: NBN and MRE11 protein levels in hypoxic GBM cells. U87-MG, U251-MG and D566-MG cells were incubated in 1% or 21% O_2 for 5 days before protein extraction. (A) Levels of NBN and MRE11 were determined by western blotting. (B) Densitometry was measured using Image J. Data represent the mean of at least three independent experiments, with error bars indicating S.E.M. * denotes significant data where $p<0.05$ indicated by one way student t-test.*

3.4.3 Assessing DNA damage signal transduction in hypoxia

Upon double strand break recognition, ATM is recruited and activated at the damage site. The primary role of ATM is to transduce the damage signal via multiple targets including γH2AX, which can be used as an indicator of double strand breaks. To further understand how the DNA damage machinery is affected by hypoxia, the impact of the impact of hypoxia on both γH2AX and ATM was explored further.

3.4.3.1 Increased γH2AX in hypoxic U87-MG after long exposure to etoposide

Fan 2014 previously observed reduced γH2AX in hypoxic D283-MED cells (Figure 3.13). This could be explained by 1) etoposide being less effective in hypoxia resulting in reduced γH2AX signal. 2) downregulation of the MRN complex could reduce transduction of the damage signal leading to less H2AX phosphorylation. To explore these two possibilities further, the level of γH2AX after etoposide treatment was assessed in U87-MG cells, which did not exhibit reduced MRN expression in hypoxia.

U87-MG cells were pre-incubated in 21% or 1% O_2 for 5 days before treatment with etoposide and γH2AX levels were measured using immunocytochemistry. Interestingly, the γH2AX signal after etoposide treatment appeared somewhat pan nuclear with small foci. This unexpected patterning was not due to problematic antibody specificity, as with other cells (D283-MED, HeLa) classical foci formation was observed. Therefore, pan nuclear γH2AX is a feature specific to U87-MG, and could imply a high level of DSB. After 15-30 min of etoposide treatment, the levels of γH2AX were similar in hypoxic and normoxic U87-MG, suggesting that etoposide is able to induce DSB regardless the oxygen environment and preconditioning (Figure 3.14). At later time points, there was a general tendency for increased γH2AX in hypoxic etoposide-treated cells. For example, after 360 min, a 3.6-fold increase in

γH2AX was observed in normoxic cells, compared to 12.0-fold in hypoxic cells (Figure 3.14 C). Throughout the treatment period, DNA repair mechanisms will be actively repairing the DSB present resulting in loss γH2AX, therefore increased γH2AX in hypoxia could be due to reduced effectiveness of repair in hypoxia. Residual γH2AX in hypoxia after DNA damage has previously been reported (Kumareswaran *et al.*, 2012). The effectiveness of DSB repair in GBM cells will be explored further in Chapter 5. Interestingly, a number of reports suggest that hypoxia alone results in the phosphorylation of H2AX (Hammond, Dorie, *et al.*, 2003; Bencokova *et al.*, 2009; Harding *et al.*, 2011), however, this was not the case here, as there was minimal γH2AX staining in untreated hypoxic cells (Figure 3.14 B). A possible explanation for this is that previous studies utilised serve hypoxia (<0.1%), compared to the mild hypoxia (1%) used here.

Overall, residual γH2AX was observed in hypoxic U87-MG cells after long exposure to etoposide. This is in contrast to hypoxic D283-MED cells where γH2AX was reduced (Fan, 2014). The hypoxia-induced downregulation of the MRN complex in D283-MED may impact the DNA damage signalling cascade resulting in reduced γH2AX. To explore this concept further, the impact of hypoxia on ATM activation needed to be addressed.

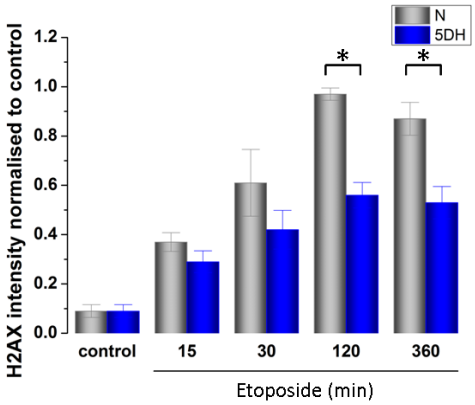

Figure 3.13: γH2AX levels in hypoxic and normoxic D283-MED after etoposide treatment observed by Fan 2014. D283-MED cells were pre-incubated in 21% O_2 and 1% O_2 for 5 days prior to etoposide treatment and staining for γH2AX. Signal intensity was measured for >350 cells. Data represent mean and S.E.M. Figure taken directly from Fan 2014.

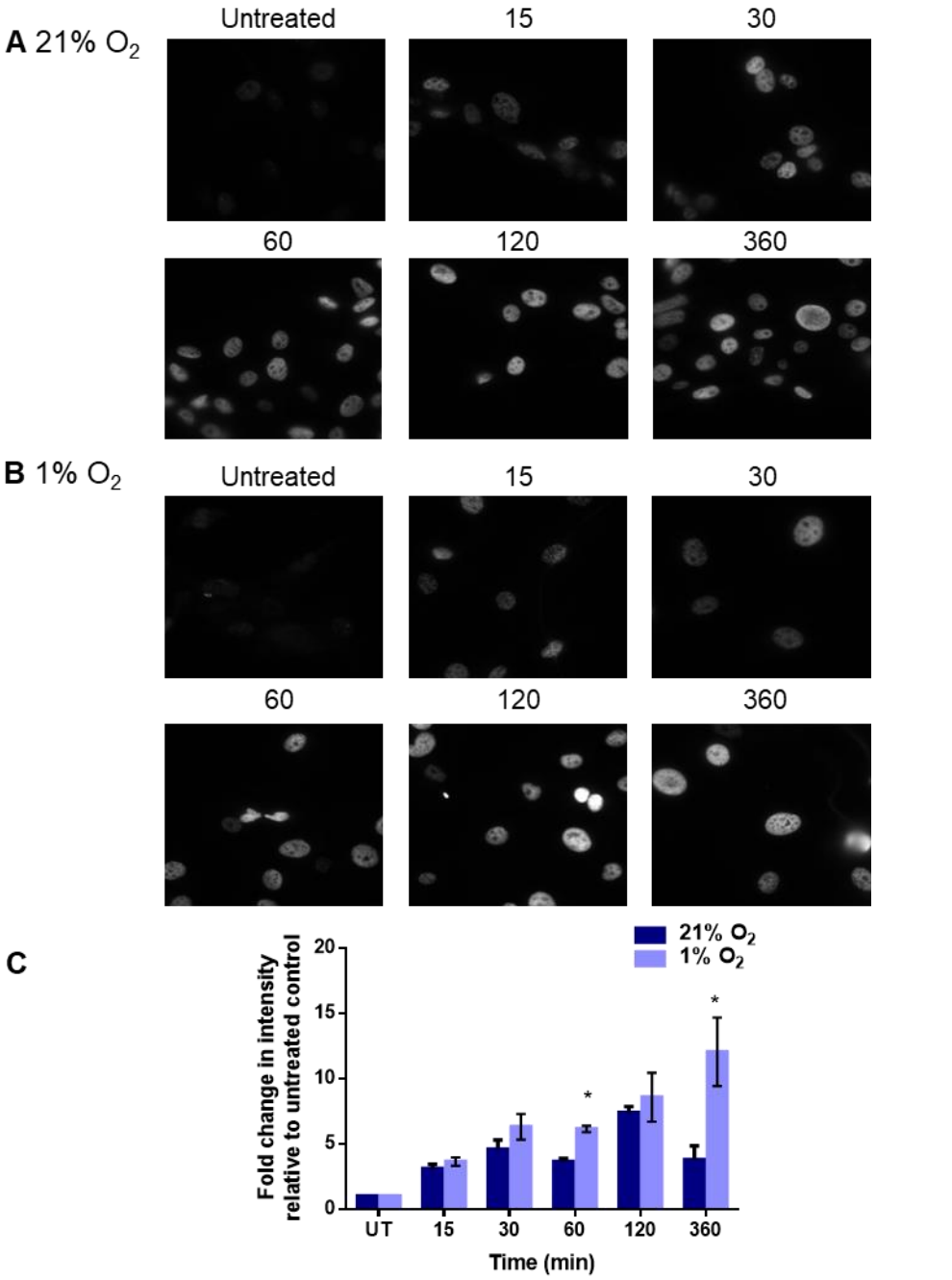

*Figure 3.14: γH2AX levels in hypoxic and normoxic U87-MG after etoposide treatment. U87-MG cells were incubated in (A) 21% O_2 or (B) 1% O_2 prior to treating with 100 μM etoposide for 0-360 min. Cells were fixed and subjected to immunocytochemistry for γH2AX. (C) Intensity measurements were taken using Image J. Data are represented as intensity fold change with respect to untreated control. Figure depicts mean of at least three independent experiments with error bars representing S.E.M. >200 cells were analysed per experimental condition. * denotes significant data where $p<0.05$ indicated by student t-test*

3.4.3.2 ATM activation in hypoxic MB and GBM cells

In order to determine the appropriate etoposide treatment duration to observe sufficient ATM activation, U87-MG cells were treated with 100 µM etoposide for 0 – 24 h, and the level of ATM and ATMSer1981 was assessed (Figure 3.15). U87-MG cells were utilised here as their culture requirements are less complex compared to D283-MED (faster growing, do not require large cell amounts of cells to obtain adequate protein), meaning that multiple samples for a range of time points could be readily produced. The level of ATM remained relatively stable regardless of treatment duration (Figure 3.15 A, C). 1 h of etoposide resulted in the accumulation of ATMSer1981, which plateaued after 2 h (Figure 3.15 B, C). For further experiments, a 4 h treatment duration was chosen to detect ATMSer1981 changes. Longer exposure may have negative effects on the health of the cells, yet accumulation at earlier time points was more variable, shown by repeated experiments.

The level of ATM and ATMSer1981 was determined for MB and GBM cell lines incubated in normoxia as well as moderate (1% O_2) and severe (0.1% O_2) hypoxia. Severe hypoxia was included here as others suggest that in extreme hypoxia, ATM can be activated without DNA damage induction. Treatment of cells pre-incubated in 0.1% O_2 was done in normoxia to ensure that severe hypoxia did not impact etoposide efficacy. However, a 'control' sample was included, which remained in 0.1% O_2, to determine whether severe hypoxic exposure could indeed induce ATM activation. For the D283-MED cells, there was a clear downregulation of ATM in 1% O_2 (Figure 3.16 A), which strengthened with increased hypoxia severity (Figure 3.17 A). In addition, the levels of ATMSer1981 was downregulated to a similar extent (Figure 3.16 A, Figure 3.17 B). Whether this downregulation of ATMSer1981 is due to reduced DNA damage signalling or reduced total ATM protein cannot be determined here. However, the reduced ATMSer1981 in hypoxia may explain the decrease in γH2AX signal in this cell line. In contrast, MEB-Med8A, cells had a small reduction in ATM protein at 0.1% O_2 (Figure 3.17 B), but not at 1%, nor was

there any impact of hypoxia on ATMSer1981 (Figure 3.16 B). Additionally, in all GBM cells examined both moderate and severe hypoxia did not affect the level of ATM or ATMSer1981 (Figure 3.18, appendix 1.5 & 1.6). Therefore, the signal transduction via ATM is unlikely to be affected by hypoxia in GBM cells.

In all the MB and GBM cell lines examined here, 0.1% O_2 alone did not induce ATM activation, nor did reoxygenation induce ATM activation (Figure 3.16 - 3.18). This contrasts previous reports which suggest that severe hypoxic exposure can result in ATM activation independent of DNA damage (Hammond, Dorie, *et al.*, 2003; Bencokova *et al.*, 2009).

To conclude, hypoxia results in a significant reduction of ATM and ATMSer1981 in D283-MED cells. This could have an impact on the DNA damage signalling within these cells, and could explain the reduced p53 phosphorylation in hypoxia observed by Fan 2014. It could be argued that D283-MED cells have an unspecific response to hypoxia as multiple proteins are regulated. However, Fan 2014 did not observe any change in p53 protein levels, nor was there any difference in γH2AX levels after short etoposide exposure, suggesting that H2AX protein level is likely to be similar in normoxia and hypoxia (Fan 2014). Regulation of common housekeeping genes by hypoxia, similar to the observations in D283-MED, has previously been reported. Caradeck *et al* found that hypoxia regulates a number of housekeeping genes as the mRNA level including *GAPDH* and *β Actin*. Yet, the direction and extent of regulation was dependant on cell type and hypoxia severity (Caradec *et al.*, 2010). Additionally, cell-type specific regulation of GAPDH protein in hypoxia, through post-translational mechanisms, has been observed (Graven *et al.*, 1994; Said *et al.*, 2009). As regulation of housekeeping genes is a common feature of hypoxic exposure, the response of D283-MED to hypoxia is likely specific, resulting in adaptations previously observed and discussed in the literature.

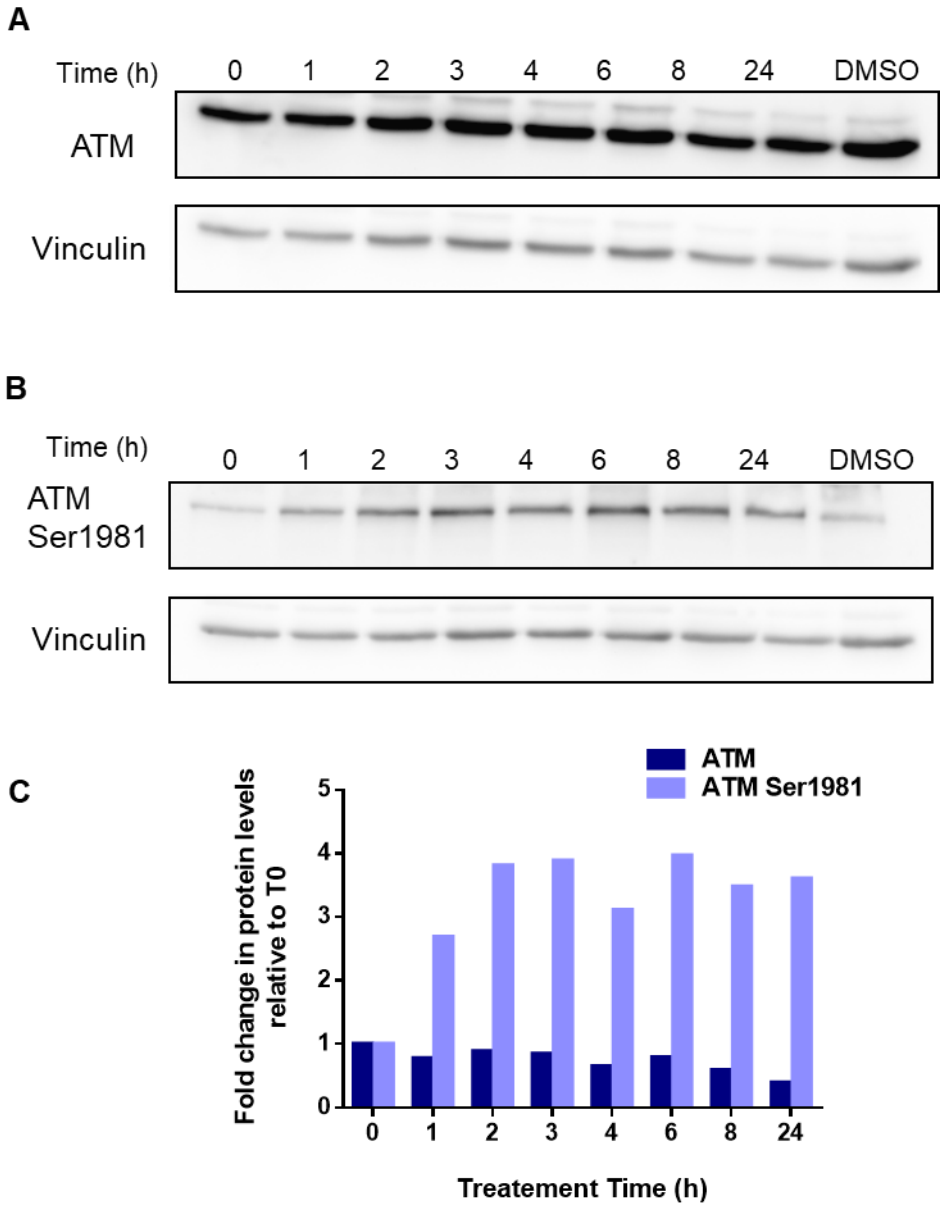

Figure 3.15: ATM activation by etoposide. U87-MG cells were treated with 100 µM etoposide for 0-24 h. Western blotting was conducted for (A) ATM and (B) ATMSer1981, for three independent experiments. (C) Densitometry of a representative blot was performed using Image J.

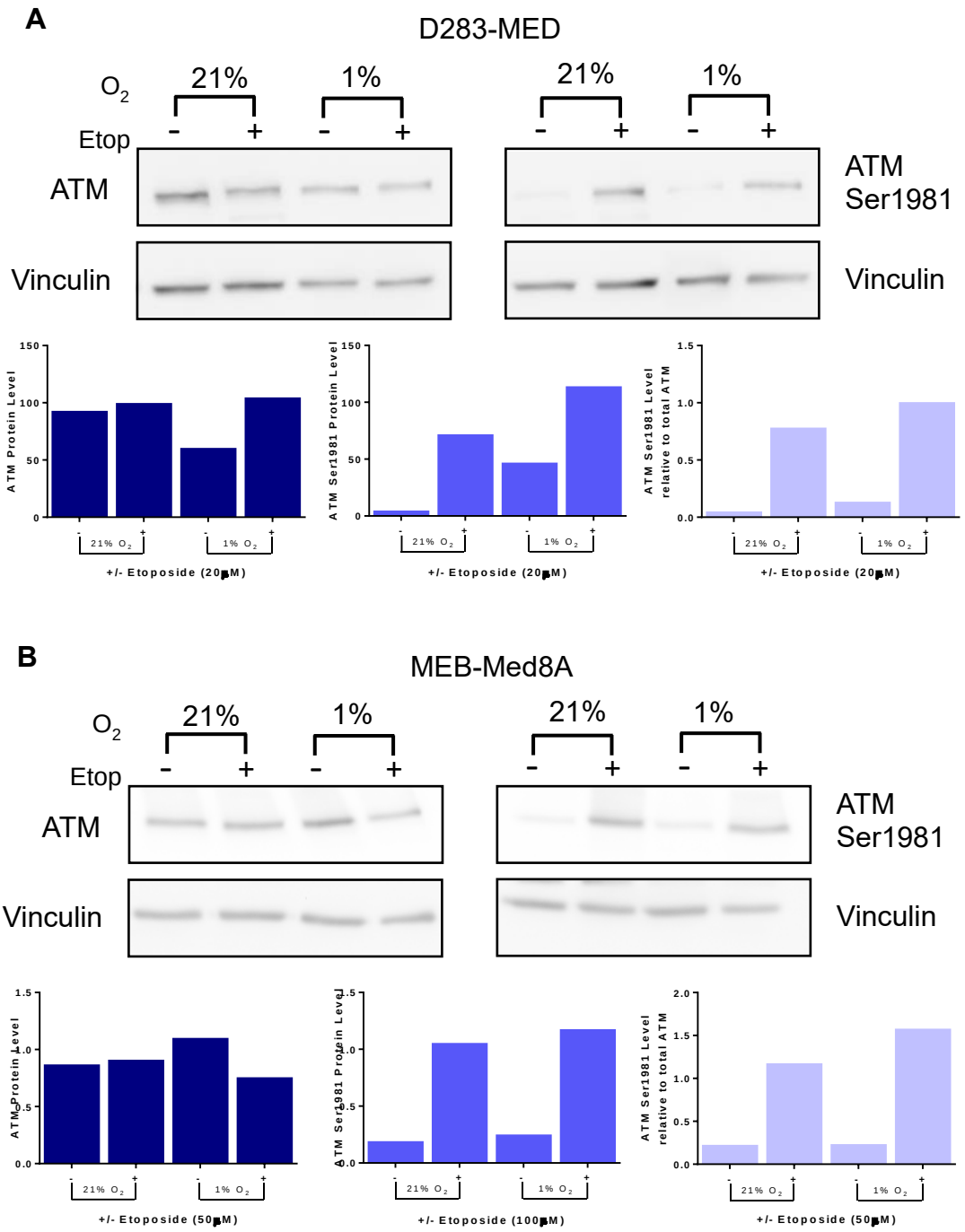

Figure 3.16: ATM and ATMSer1981 levels in MB cells exposed to moderate hypoxia. (A) D283-MED and (B) MEB-Med8A cells were incubated in in 1% or 21% O_2 for 5 days before treatment with either 20 μM (D283-MED) or 50 μM (MEB-Med8A) etoposide for 4 h. Protein was extracted and a western blot performed for ATM and ATMSer1981. At least three independent experiments were conducted. Densitometry was performed on a single representative blot using Image J.

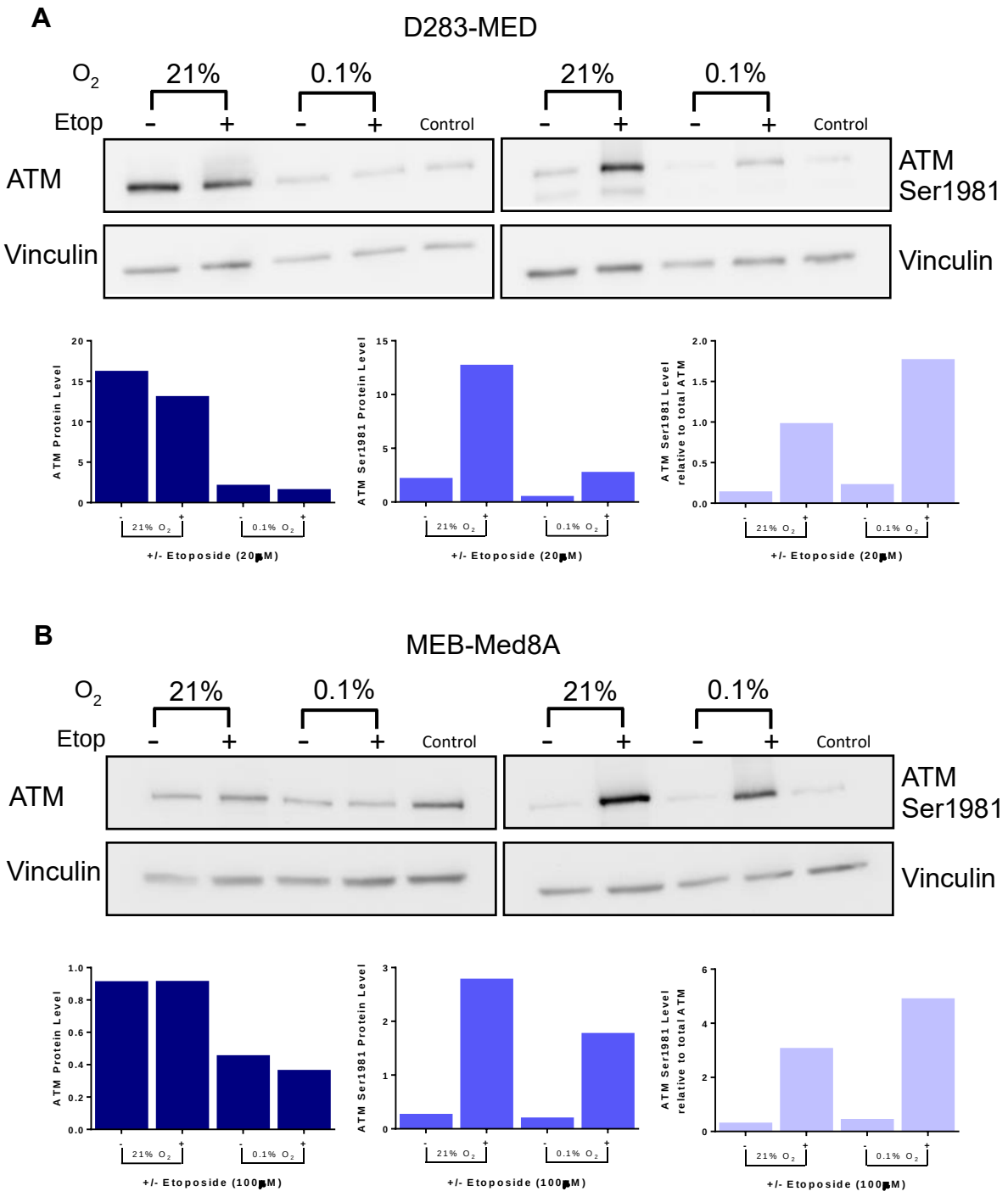

Figure 3.17: ATM and ATMSer1981 levels in MB cells exposed to severe hypoxia. (A) D283-MED and (B) MEB-Med8A cells were incubated in in 0.1% or 21% O_2 for 5 days before treatment with 20 µM (D283-MED) or 50 µM (MEB-Med8A) etoposide for 4 h in 21% O_2. Western blot was performed for ATM and ATMSer1981. Control represents cells remaining in 0.1% O_2 during treatment. At least three independent experiments were conducted. Densitometry was performed on a single representative blot using Image J.

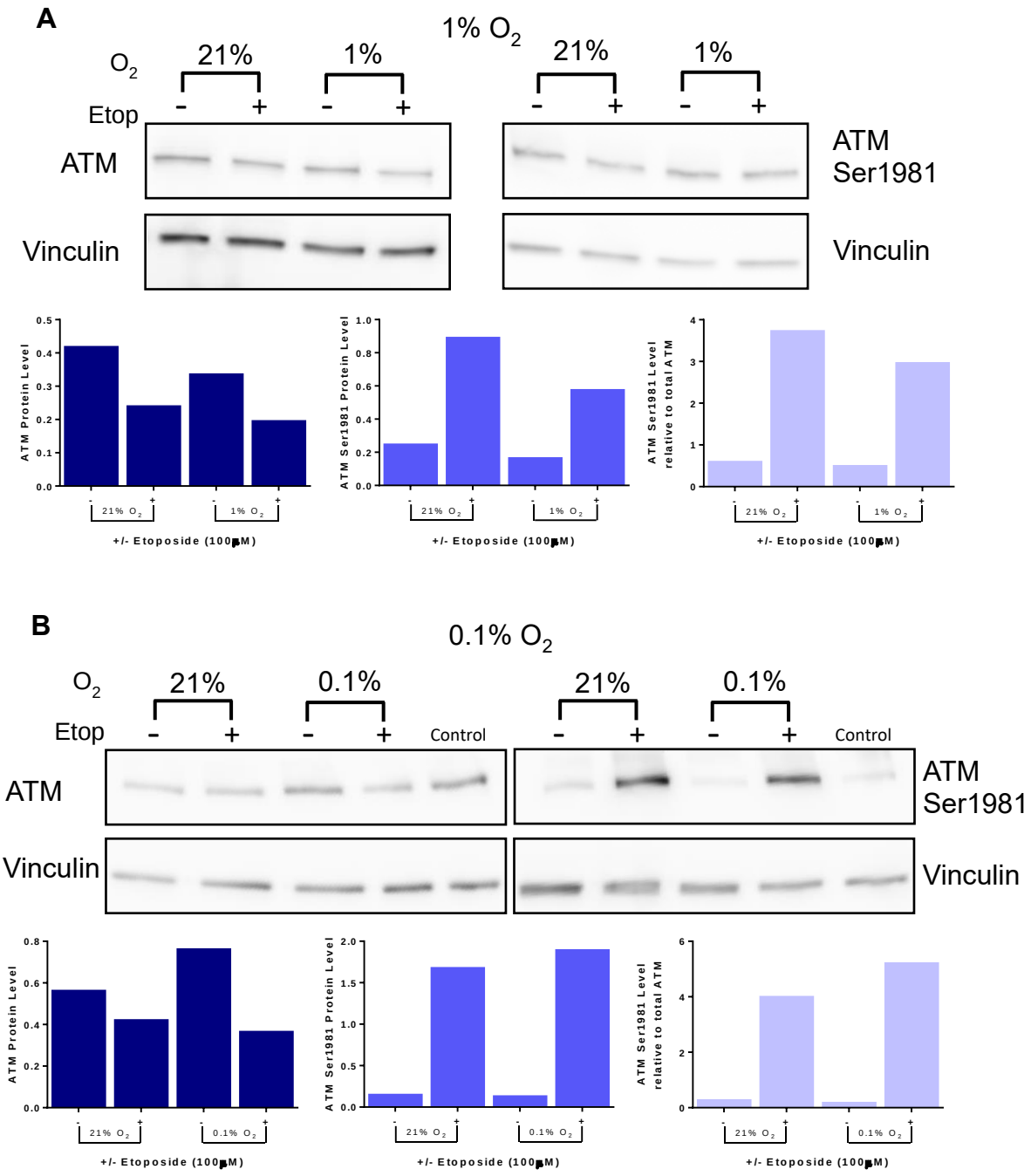

Figure 3.18: ATM and ATMSer1981 in hypoxic U87-MG cells. U87-MG were incubated in (A) 1% and (B) 0.1% as well as 21% O_2 for 5 days before treatment with 100 μM etoposide for 4 h (in 21% O_2 for 0.1% cells). Protein was extracted and a western blot performed for ATM and ATMSer1981. Control represents cells remaining in 0.1% O_2 during treatment. At least three independent experiments were conducted. Densitometry was performed on a single representative blot using Image J.

3.4.4 Summary of Results

This current chapter aimed to build on the work of Fan 2014, to explore the mechanism behind reduced etoposide sensitivity in hypoxic D283-MED cells. In addition to etoposide, D283-MED cells were resistant to cisplatin and X-ray irradiation, although to a lesser extent. Downregulation of NBN and MRE11 was confirmed at both the gene expression and protein level, which required chronic (>48 h) hypoxic exposure. Furthermore, both ATM and ATMSer1981 were downregulated in hypoxic D283-MED cells. These findings, along with observations of Fan 2014, suggest that DSB signalling is dampened by chronic hypoxia in D283-MED cells, which leads to reduced treatment sensitivity, as described in Figure 3.19. Overall, work in this chapter successfully supported and built on the previous findings. Table 3.2 highlights the confirmed and additional findings between Fan 2014 and the work presented here.

Table 3.2: Findings in Fan 2014 and Chapter 3.

Finding	Fan 2014 D283-MED cells	Chapter 3 Confirmation of finding?
Etoposide sensitivity in hypoxia	Chronic hypoxia reduces sensitvity	✔
Sensitivity to other agents in hypoxia	Not investigated	✔ Cisplatin, Irradiation
The MRN complex	NBN and MRE11 downregulated in hypoxia (mRNA)	✔ NBN and MRE11 downregulated in hypoxia (mRNA + Protein)
γH2AX	Decreased in hypoxia after long term treatment	✔ Lower γH2AX due to less signalling not reduced effectiveness of etoposide in hypoxia
ATM	Not investigated	✔ Hypoxia reduced total ATM and active ATM

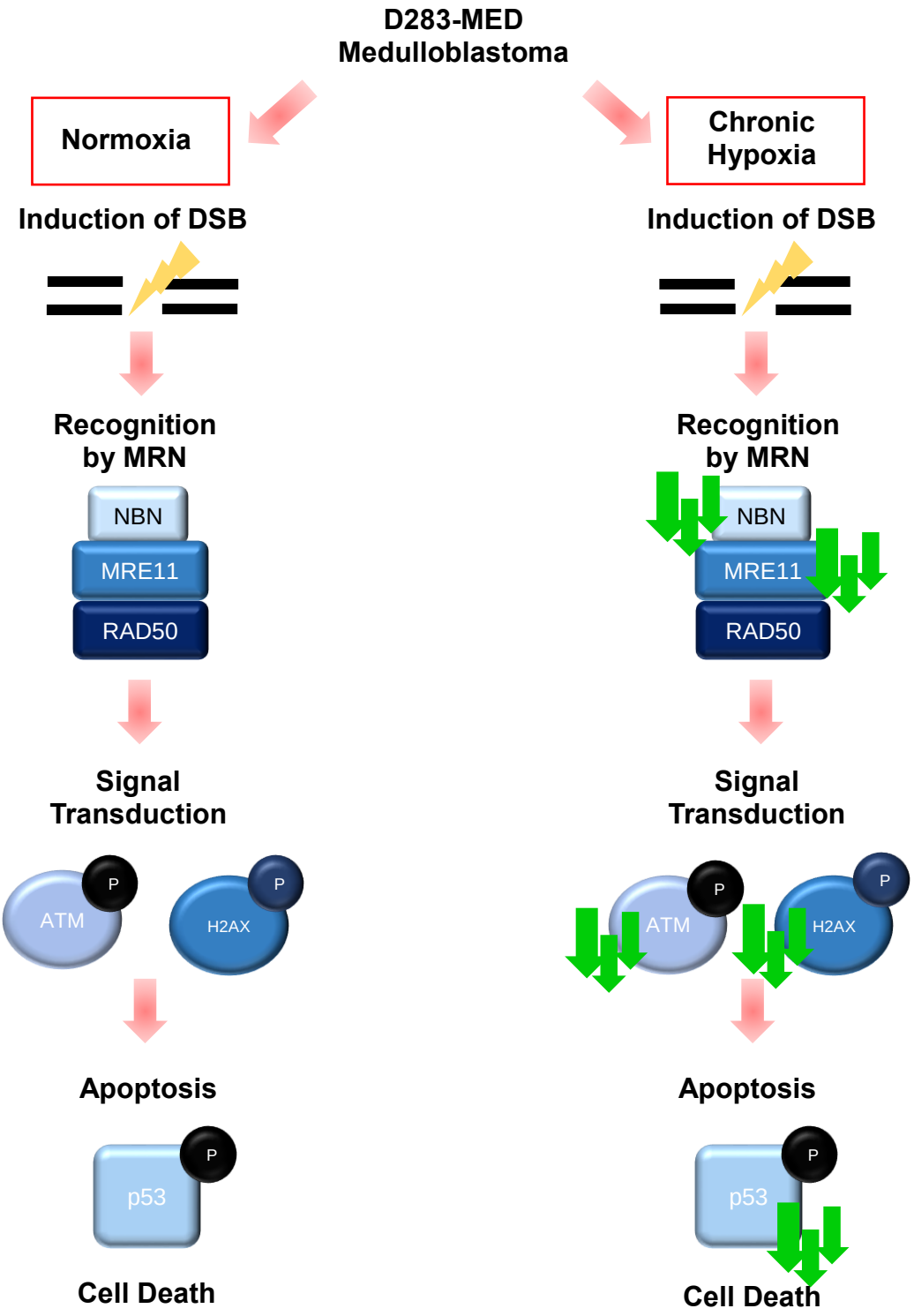

Figure 3.19: The impact of chronic hypoxia on D283-MED. Chronic hypoxia downregulates the MRN complex and ATM in D283-MED cells. This leads to reduced damage signalling to H2AX and p53 resulting in a decrease in cell death.

3.5 Discussion

Tumour hypoxia correlates with a poor patient outcome, in part due to the highly resistant nature of hypoxic cells. To combat this, identification of the molecular mechanism behind resistance is essential. The cellular response to DNA damage is the cornerstone of cancer therapy for MB and GBM, and the effect of hypoxia on the DNA damage response (DDR) has been well explored. However, discrepancies arise due to variations in hypoxic exposure and the diversity of cell lines.

3.5.1 DNA damage response and hypoxia

Treatment of MB and GBM relies heavily on the induction of DNA damage to initiate the DDR. Data presented here suggest that downregulation of the DSB recognition complex (MRN) and ATM in hypoxic D283-MED leads to dampened DNA damage signalling, resulting in reduced treatment sensitivity (Figure 3.19). Regulation of several DSB repair components by hypoxia has been identified in the literature, including downregulation of RAD51, RAD52, BRCA2 and BRCA1 leading to reduced repair of DSB in hypoxia (Bindra *et al.*, 2004, 2005; Meng *et al.*, 2005; Bindra and Glazer, 2007; Chan *et al.*, 2008). These changes are thought to cause enhanced sensitivity to DNA damaging agents. For example, hypoxia-induced decrease in HRR proteins increased sensitivity to mitomycin C, cisplatin and radiation (Chan *et al.*, 2008). However, alternatively, downregulation of the MRN complex, required for DSB recognition, results in reduced sensitivity to etoposide in MB cells. Previous studies observed downregulation of NBN and ATM in hypoxic cells (To *et al.*, 2006; Eren and Tabor, 2014), correlating with findings in D283-MED. Reduced ATM signalling will cause decreased p53 stabilisation, therefore reduced induction of pro-apoptotic genes, leading to survival after chemotherapeutic exposure. Low levels of p53, thus less p53 activity, has been attributed to chemoresistance in renal carcinoma (Roberts *et al.*, 2009). Overall, studies exploring the impact of hypoxia on DNA repair have gained

mixed results with many discrepancies. For example, reports suggest that hypoxia results in the activation of ATM, p53, and γH2AX independent of DNA damage (Hammond, Dorie, *et al.*, 2003; Bencokova *et al.*, 2009). However, no induction of ATMSer1981 or γH2AX was observed in hypoxic MB or GBM cells. Induction of ATM phosphorylation independent of DNA damage is likely due to replication stress caused by severe hypoxia (0.02%) (Hammond *et al.*, 2002; Hammond, Dorie, *et al.*, 2003; Bencokova *et al.*, 2009). Mild hypoxic exposure (1%), used here, is unlikely to induce sufficient replication arrest. Therefore, ATM and p53 are not activated. It is imperative to consider the specific protocol of hypoxic exposure when assessing hypoxia-induced cellular adaptations. Length and severity of exposure, as well as cell lines used, can influence the observed response to hypoxia.

3.5.2 Genetic and environmental heterogeneity

Heterogeneity of the cellular response to hypoxia has somewhat hindered the development of targeted treatment for hypoxic tumours. The differential response of MB and GBM cells to hypoxia is likely due to variations in the molecular signature of cell lines. For example, MEB-Med8A is a Group 3 MB due to classical characteristics of *MYC* amplification and *PTV1-MYC* fusion (Langdon *et al.*, 2006; Northcott *et al.*, 2012). In contrast, D283-MED does not have amplified MYC, and the sub-grouping is less clear (Sengupta *et al.*, 2014). The molecular signature of tumours can impact treatment response. Wnt MB tumours, for example, respond well to therapy, therefore, have the highest overall survival (Cho *et al.*, 2011; Northcott *et al.*, 2011; Kool *et al.*, 2012; Taylor *et al.*, 2012). Therefore, it is to be expected that brain tumour cell lines respond differently to hypoxia. Work by Cosse *et al.* found that acquired resistance to etoposide in hypoxia is cell line specific (Cosse *et al.*, 2007). Understanding the genetic background of tumours, and how this affects the response to the microenvironment, is essential in order to develop targeted treatments for a personalised medical approach.

Specifics of hypoxic exposure adds further complexity when studying the cellular response to hypoxia. In D283-MED and U87-MG cells, chronic hypoxia (5 days), not acute (1 day), was required to reduce etoposide sensitivity. The definition of chronic (1 day to several weeks) and acute hypoxia (1 h to 48 h), is not so clear-cut. However, acute hypoxia, not chronic, is thought to lead to a highly aggressive phenotype with increased metastatic potential. For example, acute hypoxic exposure enhanced lymph node metastasis in a murine model of human cervical carcinoma (Cairns and Hill, 2004). However, chronic hypoxia can have a direct impact on treatment response, as shown here. This is highlighted by the requirement of long hypoxic exposure (>48 h) to induce downregulation of the MRN complex. Few studies utilise hypoxic exposure over 72 h. Therefore the effects of long-term exposure may have been overlooked. Overall, chronic and acute hypoxia differentially affect cell biology, adding further complications when identifying the mechanism of hypoxia-induced resistance.

3.5.3 Alternative mechanisms leading to reduced treatment sensitivity

The resistance phenotype of hypoxic cells can be attributed to 1) acquired resistance 2) reduced treatment efficacy in hypoxia, contributing to a poor patient outcome. Teasing these two factors apart is challenging. Chemotherapeutic agents and irradiation may be less effective in a hypoxic environment. For example, studies suggest that etoposide requires oxygen for functionality (Wozniak and Ross, 1983; Wozniak *et al.*, 1984). Here etoposide was capable of inducing a comparable levels of cell death in moderate hypoxia (1%) and normoxia, as well as similar levels of DNA damage (comet assays, γH2AX), shown by Fan 2014. The effectiveness of anti-cancer therapy may be dependent on the hypoxia severity within pockets of a tumour. However, successful treatment can be thwarted by hypoxia-induced acquired resistance. Downregulation of DNA damage signalling in hypoxic D283-MED resulted in reduced sensitivity to etoposide, cisplatin and irradiation. Acquired resistance to etoposide and cisplatin has previously been observed in several studies

(Kalra *et al.*, 1993; Cosse *et al.*, 2007, 2009; Sermeus *et al.*, 2008; L. Chen *et al.*, 2009). No change in MRN or ATM was identified in hypoxic U87-MG cells, suggesting an alternative mechanism causing reduced drug sensitivity must be at play. In the glioma cell line, T98G, hypoxia-induced expression of MPR-1, a multidrug resistance gene, resulting in resistance to etoposide and doxorubicin (L. Chen *et al.*, 2009). Additionally, acquired resistance to etoposide has been attributed to reduced p53 protein levels and an increase in c-jun DNA binding in hypoxia (Cosse *et al.*, 2009). Hypoxic U87-MG were also less sensitive to irradiation. This could be explained by reduced proliferation in hypoxia, alterations to DNA damage response mechanisms, or increased levels of ROS scavengers. To explore this further, determination of U87-MG proliferative ability as well as further assessment of U87-MG DNA repair capacity in hypoxia would be ideal. With many potential causes of treatment resistance and reduced sensitivity in hypoxia, it is challenging to find a one-size-fits-all mechanism. Determination of a universal mechanism across multiple tumour types appears unlikely due to the significant variations in cellular genetic background, hypoxic environment and treatment choices, which add further complexity.

3.5.4 Direct targeting of the hypoxic response

Reversing the hypoxia-induced resistance phenotype is essential to improve treatment response. Targeting the hypoxic response poses a potential therapeutic option. Inhibition of HIF, the activator of hypoxia-related cellular changes, is becoming a popular strategy. For example, in the U251-MG cell line, camptothecins (CPTs) analogues can inhibit the accumulation of HIF-1α protein (Rapisarda *et al.*, 2004). Tumours that have reduced HIF-1 function have an enhanced response to radiotherapy (Williams *et al.*, 2005). NBN, a component of the resistance mechanism in D283-MED, is downregulated through HIF activity (To *et al.*, 2006). Inhibiting HIF may be useful to restore NBN to 'normoxic' levels, and resensitise cells to anti-cancer treatment. Interfering with HIF may have direct therapeutic benefits. However, this

requires the molecular mechanism of resistance to be HIF dependent, which may not be the case. Therefore, alternative molecular targets need to be identified. The involvement of HIF in hypoxia-induced DNA repair changes will be explored further in Chapter 5.

3.5.5 Concluding remarks and future work

Hypoxia-induced resistance to cancer treatment is a life-threatening issue in the clinic. In the current study, downregulation of components of the DSB repair pathway caused reduced treatment sensitivity hypoxic D283-MED cells. Whether hypoxia-induced changes to DNA repair mechanisms play a role in altered treatment response in GBM is yet unknown. The impact of hypoxia on DNA repair gene expression in both MB and GBM will be explored using an unbiased transcriptomic approach in Chapter 4. Additionally, future exploration of alternative mechanims of reduced treatment sensitivity in hypoxia as well as the adoption of clonogenic assays to examine cell survival would be advantageous. Development of targeted therapies against mechanism causing altered treatment sensitivity may reduce the requirement of high dose chemo- and radiotherapy, a desirable outcome for young MB patients.

Chapter 4: Global impact of hypoxia on DNA repair gene expression

4.1 Introduction

In the previous chapter, the impact of hypoxia on the double strand break recognition machinery was explored. In D283-MED, the MRN complex was downregulated in hypoxia, yet this was not universal across multiple cell lines. Therefore, a thorough investigation of multiple DNA repair genes is required to gain a comprehensive view of the effect of hypoxia on DNA repair gene expression.

Mild hypoxia itself is not capable of inducing DNA damage, as shown in Chapter 3 and by the work of others (Hammond *et al.*, 2002; Hammond, Dorie, *et al.*, 2003; Hammond, Green, *et al.*, 2003). However, hypoxia can lead to alterations to DNA repair through transcriptional, translational and post-translational modifications of the DNA repair machinery, resulting in an altered response to DNA damage. Often these changes to DNA repair mechanisms are highly dependent on the severity and duration of hypoxia.

Both chronic and acute hypoxic exposure can alter transcription of DNA repair proteins (reviewed in Scanlon and Glazer, 2015). The effect of hypoxia on the transcription of DNA repair genes has been reported to be primarily downregulation. For example, the expression of nucleotide excision repair gene, *ERCC1*, is downregulated by hypoxia even after periods of reoxygenation (Dudás *et al.*, 2014). Additionally, hypoxia downregulates *UBE2T*, an E2 conjugating enzyme involved in the repair of interstrand crosslinks in the Fanconi anaemia pathway (Ramaekers *et al.*, 2011).

One additional complication is the significant overlap between DNA repair pathways. For example, in the repair of double strand breaks, the MRN complex was initially thought to participate primarily in HRR, however roles of MRE11 in NHEJ, dependant and independent of XRCC4, have now been identified (Rass *et al.*, 2009; Anyong Xie& Amy Kwok, 2010). Additionally, loss

of functionality of a single DNA repair pathway, often found in cancer can, in some cases, be compensated for by the use of alternative pathways. For example, if base excision repair (BER) is defective and the single strand breaks formed cannot be repaired, these become DSBs, which are repaired by HRR or NHEJ. Also, nucleotide excision repair (NER) is thought to repair some oxidative lesions, suggesting that, in a BER deficient setting, NER may be used as a compensatory mechanism (Reardon *et al.*, 1997). In most studies focusing on the impact of hypoxia on DNA repair mechanisms, often only a single repair pathway is investigated, which can be limiting. Therefore a more global investigation into the effect of hypoxia on multiple DNA repair pathways is required.

4.1.1 NanoString technology

To assess the broad impact of chronic hypoxia on DNA repair gene expression, a NanoString approach was adopted. The NanoString nCounter gene expression system is a multiplexed assay, which enables the assessment of the expression of up to 800 genes in an individual reaction. In summary, the technology works through the use of a 'capture count system', whereby two specific probes bind to target mRNA. A 'capture' probe enables hybridisation to a cartridge, and a 'reporter' probe contains a colour-coded tag, which is unique to the mRNA in question. These tags, made up of ordered fluorophores, are detected by a CCD camera. The number of identified tags relate to the level of expression of each gene. This approach enables the examination of the expression of a number of DNA repair genes without the need for extensive RT-PCR experiments or costly microarrays. Additionally, the NanoString system is deemed as more sensitive than microarrays (Geiss *et al.*, 2008), and does not require complex analysis.

In order to understand the broader impact of hypoxia on DNA repair gene expression, four glioblastoma, two medulloblastoma and one neuroblastoma cell line was incubated in moderate (1% O_2) and severe hypoxia (0.1% O_2).

Experimental conditions are detailed in Table 4.1. Target genes from various DNA repair pathways as well as other key genes involved in the cellular response to DNA damage (Table 4.2) were analysed using the NanoString nCounter gene expression system, with a total of 180 genes, plus 12 housekeeping genes (appendix 1.2).

In brief, the experimental procedure of the NanoString study involved pre-incubation of cells for 5 days in 21%, 1% and 0.1% O_2, except D283-MED cells, which were cultured only in 21% and 1% O_2 due to poor RNA quality from cells cultured in 0.1% O_2. RNA was extracted and a portion converted to cDNA for RT-PCR to ensure that an increase in hypoxic markers (*GLUT1* or *VEGF*) was present for hypoxic samples. Only samples with an evident hypoxic effect were taken forth into the NanoString experiment. Total RNA was used in the experimental protocol (see methods 2.14). Analysis of NanoString data was conducted using the nSolver™ Analysis Software (3.0).

Table 4.1: Tumour type, cell lines and oxygen conditions assessed in the NanoString study.

Tumour Type	Cell Line	O_2 Conditions Tested
Glioblastoma	U87-MG	21%, 1%, 0.1%
	U251-MG	21%, 1%, 0.1%
	D566-MG	21%, 1%, 0.1%
	T98G	21%, 1%, 0.1%
Medulloblastoma	MEB-Med8A	21%, 1%, 0.1%
	D283-MED	21%, 1%
Neuroblastoma	SK-N-AS	21%, 1%, 0.1%

Table 4.2: Details of the gene annotation groups analysed with the NanoString nCounter system.

Annotation Group	Number of Genes
Base Excision Repair	29
Nucleotide Excision Repair	23
Homologous Recombination	21
Non-homologous End Joining	5
Fanconi Anemia	14
Mismatch Repair	13
Translesion Synthesis	7
Checkpoint Activation	12
Apoptosis	17
Cell Cycle and Signalling	44
Independent Repair Enzymes/Polymerases	25

4.2 Objectives

The experimental aims for this chapter were as follows:

1. Analyse the expression level of DNA repair genes under hypoxic and normoxic conditions in GBM and MB cell lines.

2. Determine the impact of moderate (1% O_2) versus severe (0.1% O_2) hypoxia on the expression of DNA repair genes.

3. Determine common hypoxia-induced changes in expression between cell lines.

4.3 NanoString results

4.3.1 Unsupervised clustering

Before data from the NanoString experiments could be analysed, several quality control (QC) steps had to be passed. These steps included an examination of probe binding density and image quality as described in methods 2.14.4.1. A common QC procedure in gene expression studies is the unsupervised clustering of the data. Clustering is a visual tool, which allows easy identification of samples with similar gene expression patterns. Therefore, if samples (i.e. biological replicates) from an experimental condition cluster together, this indicates their expression patterns are similar. Random clustering of replicates could be caused by several factors including uncontrolled elements during experimentation, or for biological reasons.

Expression data for each cell line was subjected to unsupervised clustering. For each experimental replicate, gene 'counts' were normalised to the selected housekeeping genes and scaled to give each expression value equal variance. From this, unsupervised clustering was performed and heat-maps produced (Figure 4.1 and Figure 4.2). Between biological replicates, for example, U87-MG 21% samples (Figure 4.1 A) there was significant variation in the data shown by the varied colour pattern (representing up and down regulated genes). This could imply that the NanoString platform is unreliable, as similar results are not being achieved for each biological replicate. However, in the D566-MG cell line, the samples at 0.1% O_2 show a very similar patterning suggesting that the NanoString assay is capable of producing robust data. Therefore, the sample variation in the remaining cell lines tested is likely due to unknown factors such as biological variation. Interestingly, only D566-MG appeared to show reproducible gene changes with respect to oxygen conditions. This could suggest that these cells are more sensitive to hypoxia, resulting in a more distinct and global impact of hypoxia on DNA repair gene expression.

When examining the clustering of experimental samples with respect to oxygen concentration, in the GBM cell lines, U87-MG and D566-MG, each experimental sample clustered with other samples from the same oxygen condition (Figure 4.1 A, C.) This suggests that the expression patterns are similar to one another. In contrast, whilst normoxic T98G samples clustered together, the hypoxic samples (1% and 0.1% O_2) clustered randomly (Figure 4.1 D), suggesting that changes in 1% and 0.1% O_2 cannot be differentiated. In U251-MG, D283-MED and MEB-Med8A, clustering of samples was random (Figure 4.1 B, Figure 4.2), indicating that the gene expression patterns in 21%, 1% and 0.1% O_2 are not discernible from each other. The cause of this 'random' clustering suggests that gene expression is not dramatically altered in hypoxia, resulting in clustering with less distinct separation.

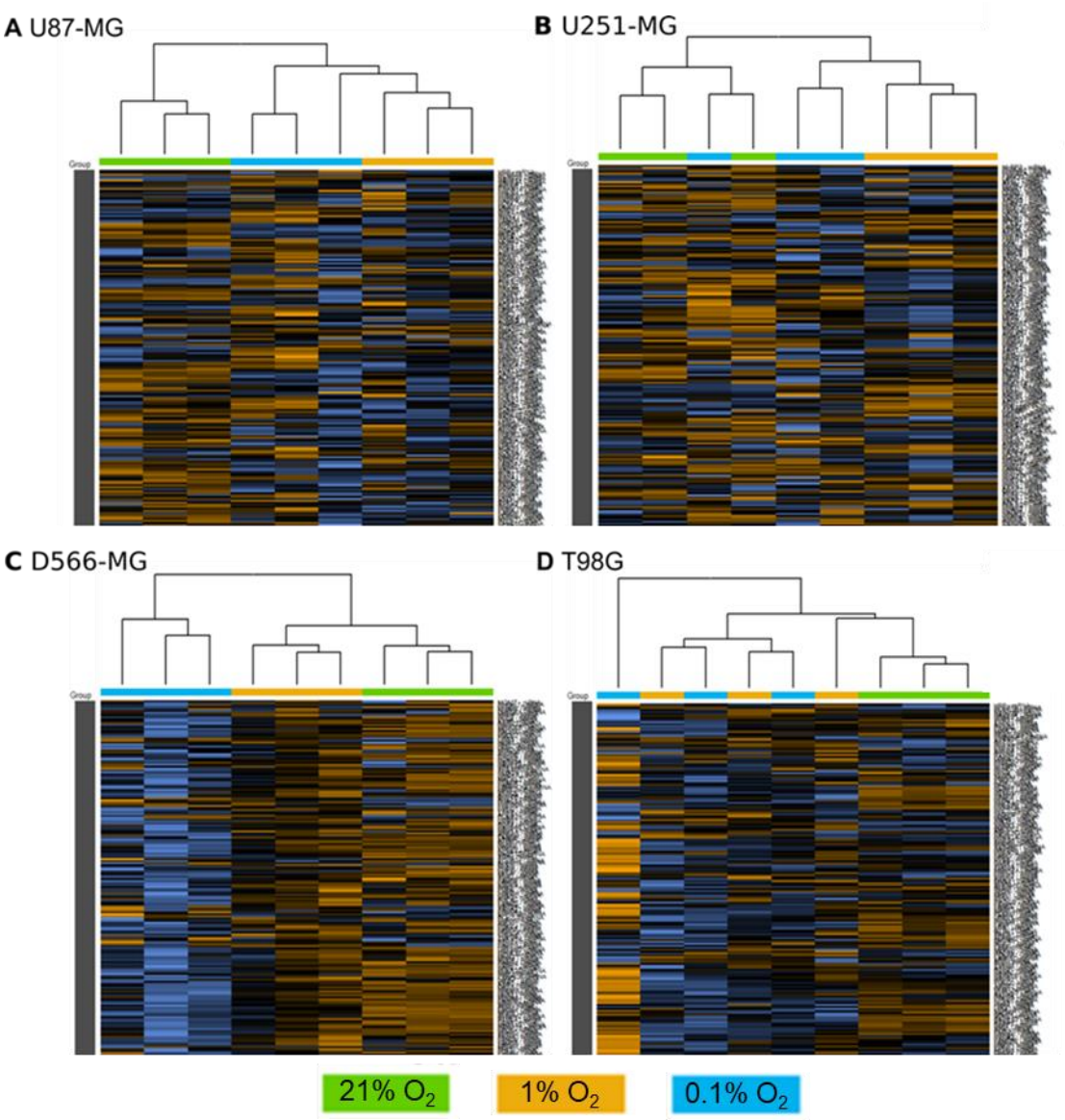

Figure 4.1: Heat-map with unsupervised clustering of gene expression data for GBM cell lines. The gene 'counts' of (A) U87-MG, (B) U251-MG, (C) D566-MG and (D) T98-MG were normalised to selected housekeeping genes, then scaled to ensure equal variance. Clustering of data was performed based solely on gene expression patterns. Orange indicates upregulation; blue indicates downregulation of gene expression.

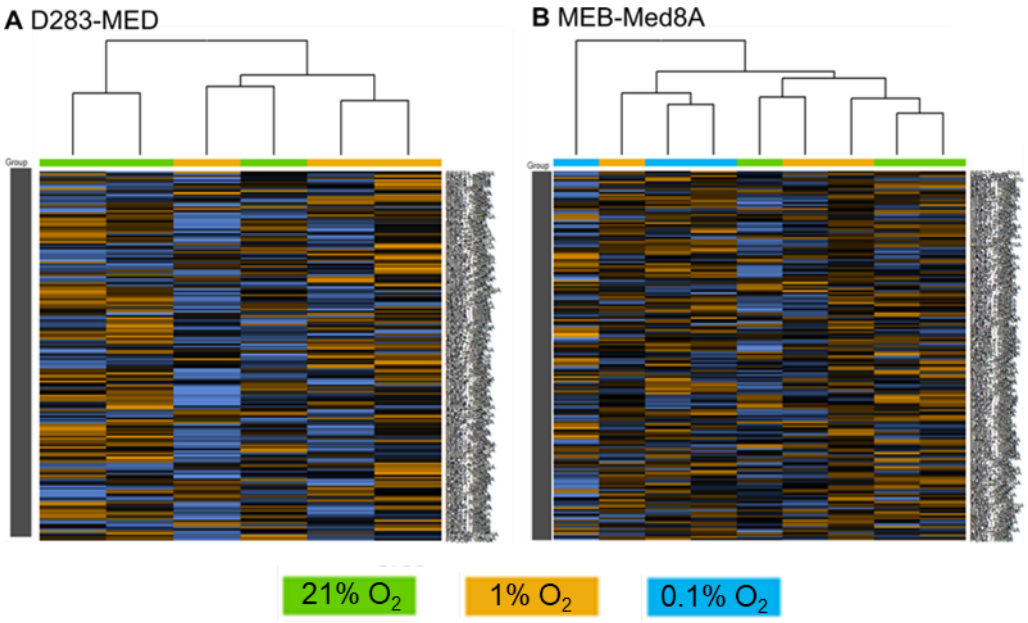

Figure 4.2: Heat-map with unsupervised clustering of gene expression data for MB cell lines. The gene 'counts' of (A) D283-MED and (B) MEB-Med8A were normalised to selected housekeeping genes, then scaled to ensure equal variance. Clustering of data was performed based solely on gene expression patterns. Orange indicates upregulation; blue indicates downregulation of gene expression

4.3.2 Differential gene expression analysis

Normoxia (21 % O_2) was used as the reference condition to compare hypoxic expression levels. Using multivariate linear regression, differentially expressed genes in 1% and 0.1% O_2 were identified, and the number of significantly regulated genes for each cell line and hypoxic condition was determined (Table 4.3). Here significantly regulated refers to genes whose $\log_2$ fold change in expression (hypoxia versus normoxia) is at least +/- 0.58 (representing a 1.5-fold change), as well as having a significance value of $p \leq 0.01$.

Overall, the MB lines, MEB-Med8A and D283-MED, had the fewest significantly regulated genes in hypoxia. Specifically, in D283-MED, only three genes met these significance criteria, whereas in MEB-Med8A one gene was regulated at 1% O_2, and eight genes in 0.1% O_2 (Table 4.3). In contrast, the GBM cell lines have a higher number of hypoxia-regulated genes. In particular, in U87-MG and D566-MG 16 and 12 genes respectively were regulated at

1% O_2, which increased to 37 and 59 genes respectively with increased severity of hypoxia (Table 4.3). Therefore, hypoxia has a greater influence on the gene expression of DNA repair genes in GBM than MB cell lines. Additionally, as a comparison, a single experiment of SK-NA-S cells (Neuroblastoma) was performed (data not shown). Similar to MB cell lines, there were few changes in gene expression (four genes in 1% O_2, six genes in 0.1% O_2), which might be characteristic of paediatric tumours. These data are based on a $\log_2$ fold change in expression of at least +/- 0.58 and a 'yes' DE call (see methods 2.14.4.4).

Table 4.3: Number of significantly regulated genes for each cell line and hypoxic condition. Significantly regulated represents genes which expression level (compared to 21% O_2) is at least +/- 0.58 $\log_2$ fold change (representing a 1.5-fold change), as well as having a significance of $p \leq 0.01$ based on multivariate linear regression.

Cell Line	O_2 Condition	Number of significantly regulated genes
U87-MG	1%	16
	0.1%	37
U251-MG	1%	17
	0.1%	8
D566-MG	1%	12
	0.1%	59
T98G	1%	13
	0.1%	18
MEB-Med8A	1%	1
	0.1%	8
D283-MED	1%	3

4.3.2.1 Volcano plots

A simple way to visualise the differential expression of genes in large datasets is with volcano plots. Volcano plots display a datum for each gene, where the log_2 fold change (mean of 3 biological replicates) is plotted against the p-value. This produces a 'volcano' shaped plot where any datum, which is high on the y-axis as well as either the far left or far right of the on the x-axis, is a highly differentially expressed and highly statistically significant gene. This enables the easy identification of greatly regulated and strongly significant genes.

Volcano plots were produced for GBM cells (Figure 4.3, Figure 4.4) and MB cells (Figure 4.5). In U87-MG cells, a number of genes in both 1% and 0.1% O_2 reached the critical significance value of $p \leq 0.01$, with 20 genes reaching the stricter statistical threshold of $p \leq 0.001$ in 0.1% O_2 (Figure 4.3 A). Also, the data appear to be spread equally across both left and right-hand-side of the x-axis, indicating that neither up or downregulation of gene expression is predominating in this cell line. In contrast, D566-MG shows a clear preference for downregulation. Particularly in the more serve hypoxic condition of 0.1% O_2 with 70/180 genes reaching high statistical significance (Figure 4.4 A). For U251-MG, there are more statistically significant genes in 1% O_2 compared to 0.1% O_2 yet the volcano is quite narrow suggesting the fold change in gene expression is small (Figure 4.3 B). In contrast, for T98G the volcano plots are spread across the x-axis. Therefore, there is strong regulation of many genes, yet neither up, or downregulation is predominating (Figure 4.4 B). In the MB cell lines, MEB-Med8A and D283-MED, similar to U251-MG the volcanos are very narrow implying only small and potentially negligible fold changes in expression (Figure 4.5).

In summary, hypoxia significantly influences gene expression in GBM cells lines compared to MB. Specifically, in U87-MG and D566-MG, a significant proportion of genes reach statistical significance (28% U87-MG, 38% D566-MG in 0.1%).

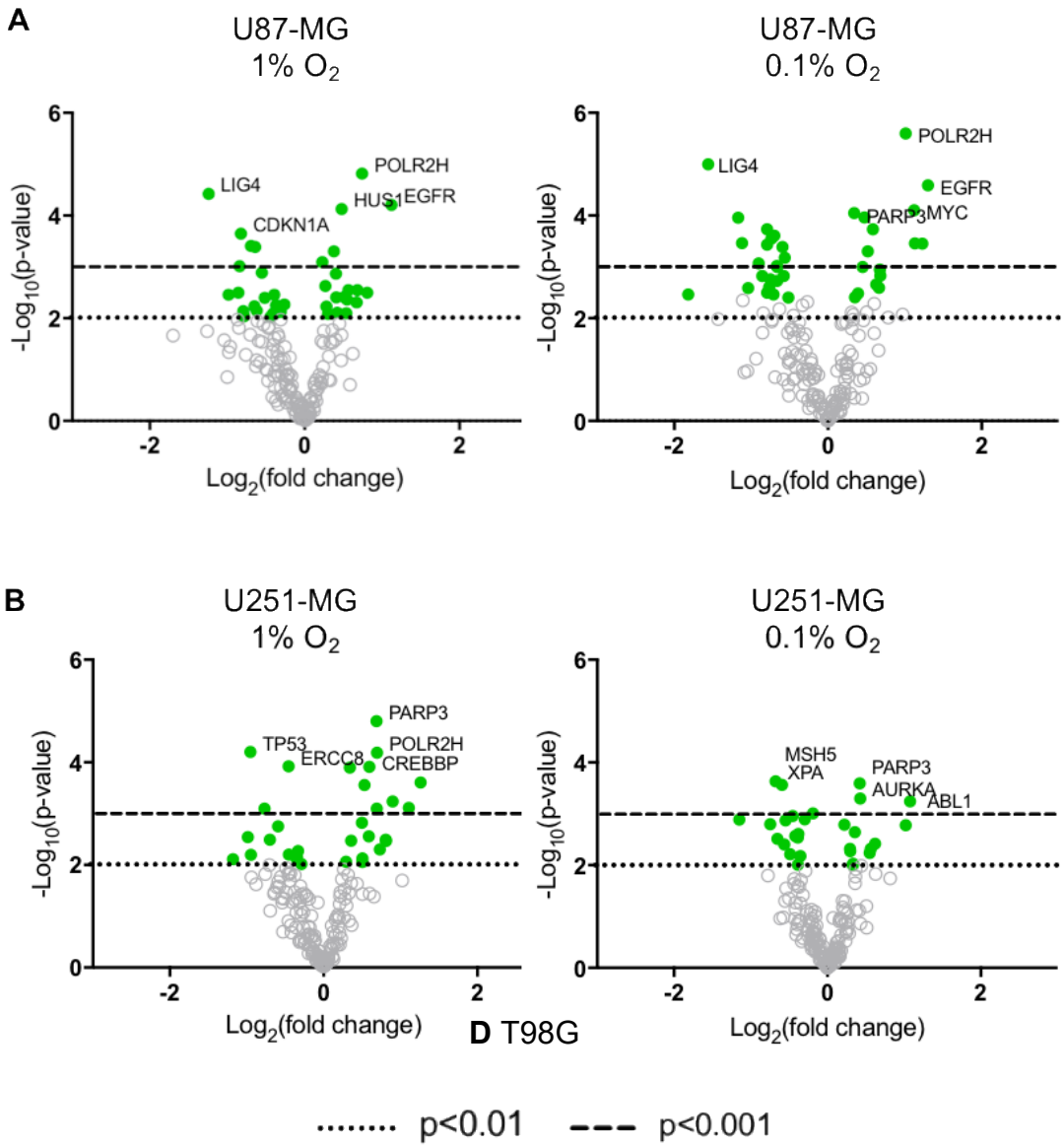

Figure 4.3: Gene expression volcano plots for U87-MG and U251-MG. Gene expression data for (A) U87-MG and (B) U251-MG is represented as log_2 fold change for each gene plotted with log_{10} p-value. Each point represents the average of three experimental replicates. Green filled circles signify genes that have a p-value above the p<0.01 threshold. Grey hollow circles represent non-statistically significant genes. The top 5 statistically significant genes are identified with the gene name.

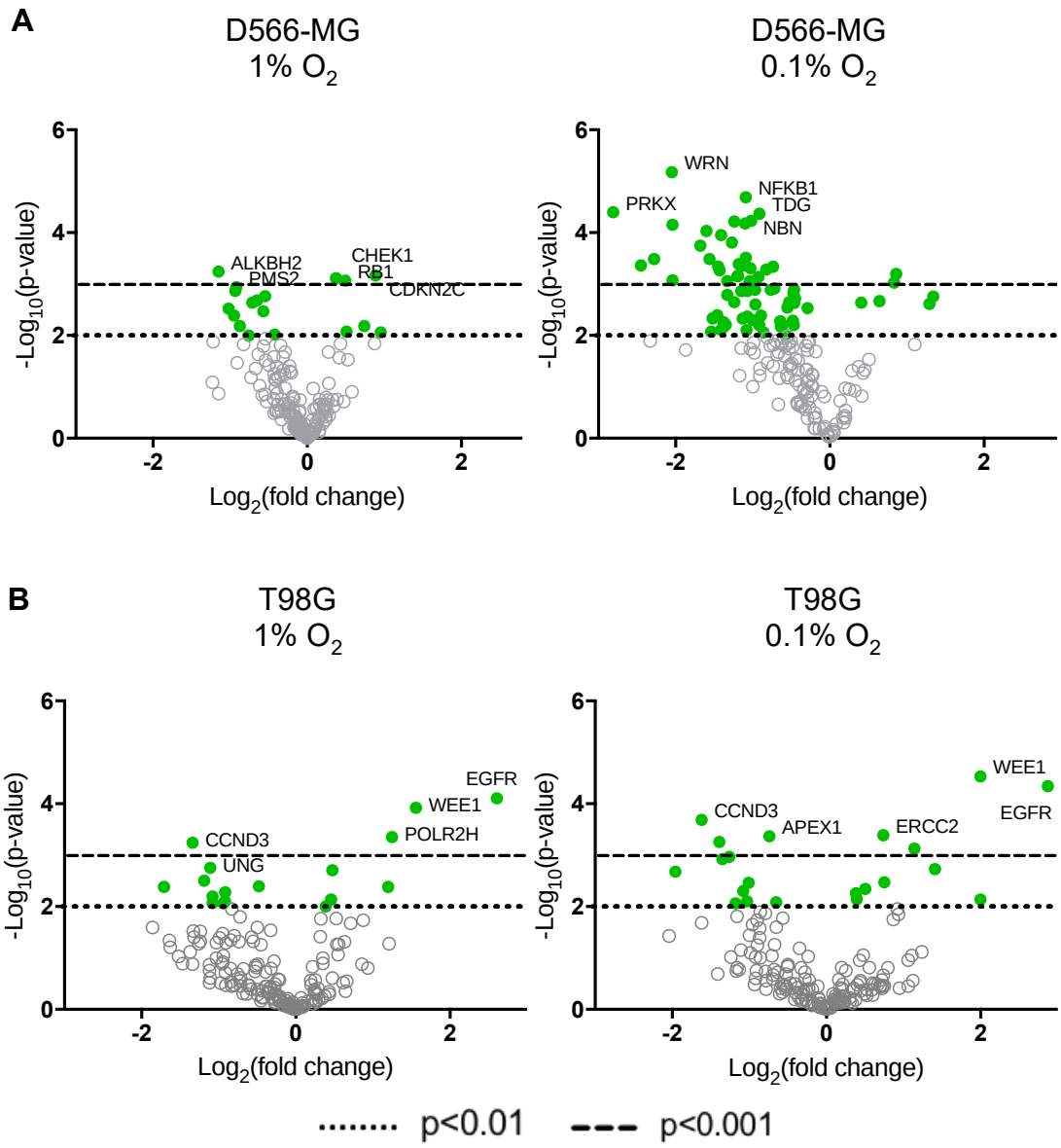

Figure 4.4: Gene expression volcano plots for D566-MG and T98G. Gene expression data for (A) D566-MG and (B) T98G is represented as log_2 fold change for each gene plotted with log_{10} p-value. Each point represents the average of three experimental replicates. Green filled circles signify genes that have a p-value above the p<0.01 threshold. Grey hollow circles represent non-statistically significant genes. The top 5 statistically significant genes are identified with the gene name.

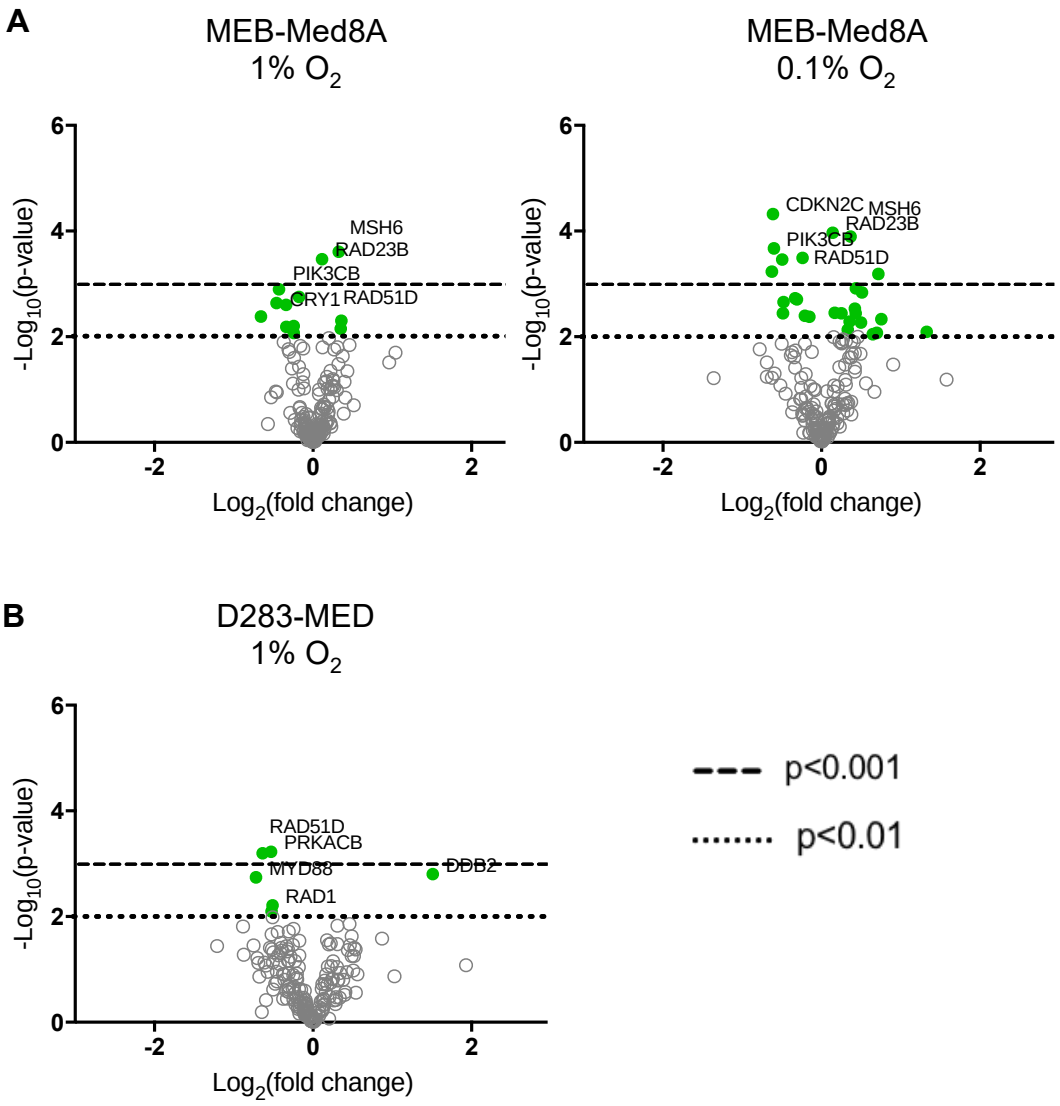

Figure 4.5: Gene expression volcano plots for MB cell lines. Gene expression data for (A) MEB-Med8A and (B) D283-MED is represented as log_2 fold change for each gene plotted with log_{10} p-value. Each point represents the average of three experimental replicates. Green filled circles signify genes that have a p-value above the p<0.01 threshold. Grey hollow circles represent non-statistically significant genes. The top 5 statistically significant genes are identified with the gene name.

4.3.3 Significance scoring

To understand the influence of hypoxia on the expression of genes within each annotation group (DNA repair pathway), global significance (GS) and directed global significance (DGS) scores were calculated and displayed as heat-maps (Figure 4.6, Figure 4.7). GS scores measure the overall differential regulation of a set of genes with respect to the reference condition (21% O_2); with DGS adding directionality (see methods 2.11.4.5). This enables the visualisation of gene regulation in each DNA repair pathway. Overall, the strongest gene regulation, shown by a high GS score (dark blue), was observed in D566-MG (Figure 4.6 C), correlating with the increased number of differentially regulated genes in this cell line (Table 4.3). At 0.1% O_2, apoptosis, homologous recombination repair and mismatch repair, are the top three annotation groups, which had the strongest gene regulation (Figure 4.6 C), with downregulation predominating for most pathways in this cell line (Figure 4.7 C).

For U87-MG and U251-MG, up and downregulation was observed across the annotation groups (Figure 4.7 A, B). However, in U87-MG the strongest regulation was observed in non-homologous end joining genes (Figure 4.6 B), which was identified as downregulation (Figure 4.7 A). Interestingly, the direction of expression in both U87-MG and U251-MG does not correlate with changes in hypoxia severity. For example, checkpoint activation in U87-MG is upregulated in 1% O_2 but downregulated in 0.1% O_2 (Figure 4.7 A). Although it could be assumed that changes in moderate hypoxia would be heightened in severe hypoxia, often altering the degree of hypoxia can result in activation of different signalling pathways. Therefore, in the case of U87-MG and U251-MG, the differing severities of hypoxia may cause alternative mechanisms of gene regulation, resulting in the switch from up to downregulation of a DNA repair pathway for example.

In MB cells, upregulation of gene expression predominates in MEB-Med8A, with nucleotide excision repair showing strongest overall regulation (Figure 4.6 E, Figure 4.7 E). In D283-MED the pathways are mostly downregulated, yet regulation of gene expression is very weak (Figure 4.6 F).

Overall, U87-MG and D566-MG showed the strongest level of gene regulation, with non-homologous end joining, mismatch repair and apoptosis having high rates of gene regulation. In contrast, for the MB cell lines, GS and DGS suggested low levels of regulation of gene expression, which correlates with the differential gene expression analysis.

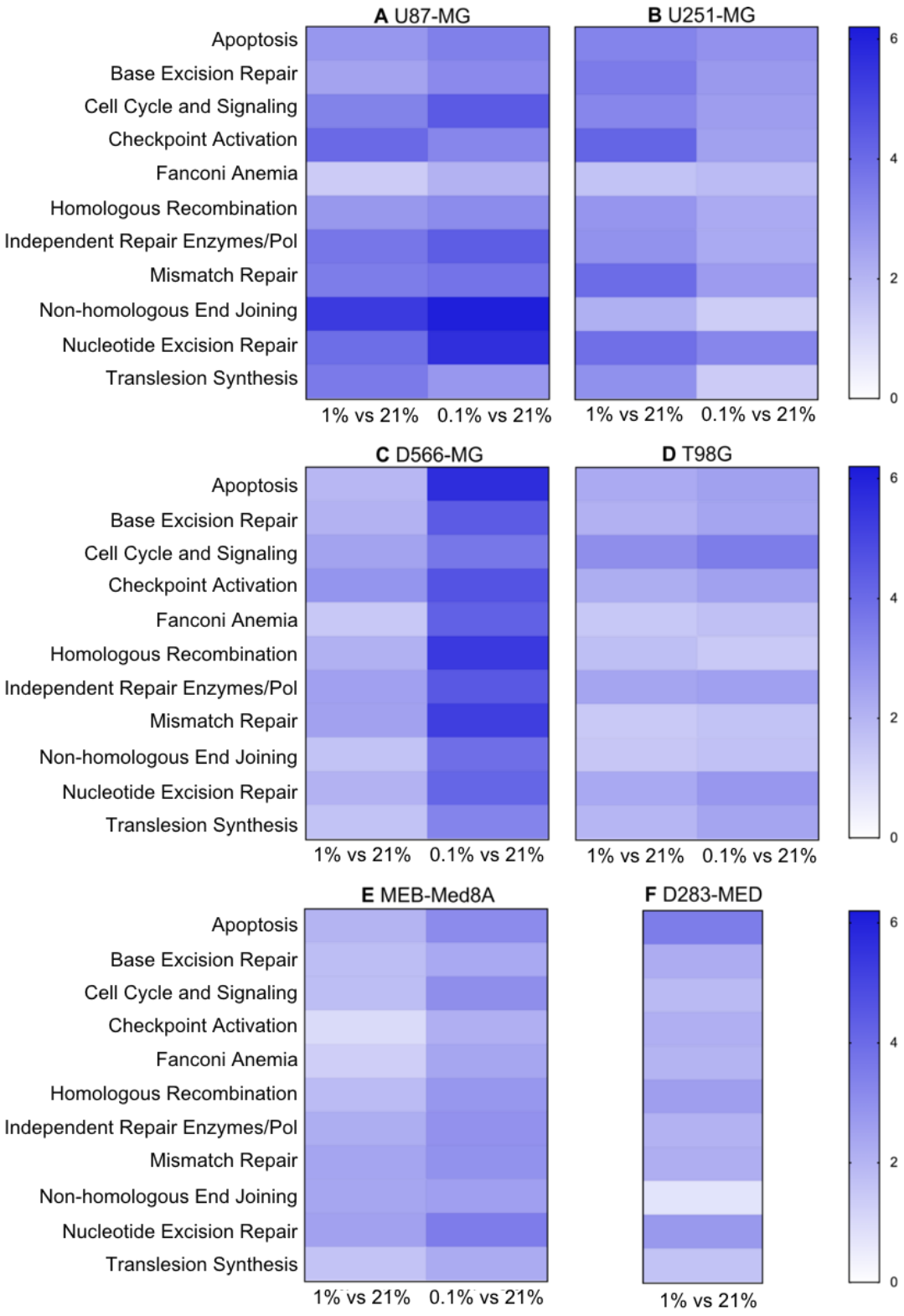

Figure 4.6: Global significance heat-maps. Global significance scores were calculated for each defined annotation group and cell line. Scores are represented in a heat map (white = weak regulation, dark blue = strong regulation). An individual plot was produced for each cell line and hypoxic condition. Data representative of three independent experiments.

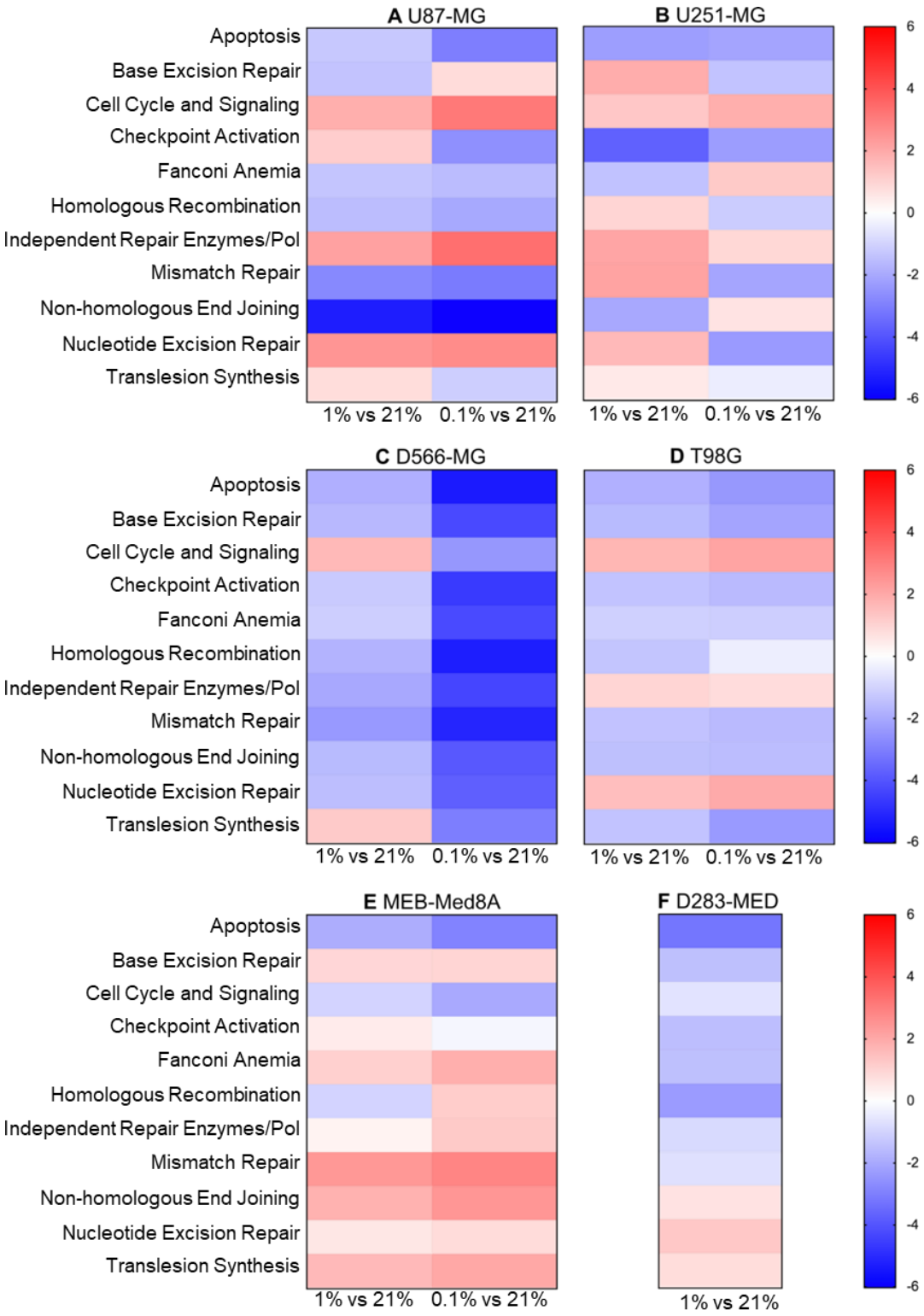

Figure 4.7: Directed global significance heat-maps. Directed global significance scores were calculated for each defined annotation group and cell line. Scores are represented in a heat map (blue = downregulation, red = upregulation). An individual plot was produced for each cell line and hypoxic condition. Data representative of three independent experiments.

4.3.4 Gene level analysis of DNA repair pathways

Both differential gene expression analysis (volcano plots) and global significance scoring indicate how hypoxia affects collective gene expression for several genes within a defined pathway. However, the individual gene level is key to fully comprehend how different DNA repair pathways are influenced by hypoxia. This is because the protein products of DNA repair genes can play varied roles within a pathway, with differing degrees of redundancy. Homologous recombination repair, non-homologous end joining, base excision repair and mismatch repair (Chapter 1, Figure 1.8) were the focus of further exploration. These pathways were selected based on their role in repair of many common DNA damage types induced by chemo- and radiotherapy.

4.3.4.1 Homologous recombination repair

HRR is responsible for the repair of double strand breaks. Repair steps involve recognition of the break and processing of DNA ends, followed by DNA strand invasion, DNA synthesis and resolution of complex structures. In the previous chapter, the impact of hypoxia on the expression of genes involved in damage recognition was examined, namely, *NBN*, *MRE11* and *RAD50*. The NanoString set-up enabled the measurement of expression of 21 genes involved in HRR. For each cell line, the $\log_2$ fold change in expression with respect to expression at 21% O_2 was determined (Figure 4.8).

Across all cell lines, very few genes reached the designated fold change threshold in both 1% and 0.1% O_2 (Figure 4.8), yet genes that did cross the threshold were primarily downregulated. In the T98G cell line, 8/21 genes were downregulated by at least -1 $\log_2$ fold in 1% O_2, but the majority did not reach statistical significance (Figure 4.8 A). Similarly, D566-MG had a number of strongly downregulated HRR genes, which were also statistically significant. Yet, this strong downregulation was only observed at 0.1% O_2, with 2/21 in 1% O_2 compared to 12/21 in 0.1% O_2.

For components of the MRN complex, there was little change in *MRE11* except -0.78 log_2 fold downregulation at 0.1% O_2 in D566-MG (Figure 4.8 B). Also, *RAD50* is predominantly unchanged across the cell lines tested. However, the expression levels of *NBN* were decreased in T98G at 1% O_2 (-0.95 log_2 fold) (Figure 4.8 A) and both T98G (-0.79 log_2 fold) and D566-MG (-1.0 log_2 fold) at 0.1% O_2 (Figure 4.8 B). Interestingly, in D283-MED, *MRE11* and *NBN* were not downregulated to the same extent as described in Chapter 3. Previously, in 1% O_2, *NBN* and *MRE11* were downregulated -1.20 and -1.10 log_2 fold respectively. However, in the NanoString study, *NBN* was downregulated -0.45 log_2 fold and *MRE11* -0.33 log_2 fold (Figure 4.8 A). A potential explanation for this could be that the RT-PCR primers may pick up different transcript variants to the NanoString probes, which could alter the fold changes observed. As discussed in Chapter 3, the downregulation of *NBN* in hypoxia has previously been documented and is thought to occur through the displacement of MYC by HIF on the *NBN* gene promoter (To *et al.*, 2006).

After damage recognition and end processing, RAD51 binds to DNA forming a nucleoprotein filament. There was no change in *RAD51* expression at 1% O_2 (Figure 4.8 A). However, at 0.1% O_2, there is a strong and statistically significant -1.7 log_2 and -1.0 log_2 fold downregulation in D566-MG cells and T98G respectively. This matches previous studies that found *RAD51* to be downregulated by 0.2% - 0.01% O_2 (Bindra *et al.*, 2004, 2005; Meng *et al.*, 2005), suggesting that a more severe hypoxic environment is required for these changes to occur.

In a severe hypoxic environment (0.01% O_2), *BRCA1* is reported to be downregulated after 48 h exposure (Bindra et al., 2005, 2004). *BRCA1* was downregulated in a number of GBM cell lines incubated in 1% O_2 (U251-MG, U87-MG, and T98G) (Figure 4.8 A). However, in more severe hypoxia (0.1% O_2) a -1.0 log_2 fold downregulation was observed only in D566-MG (Figure 4.8 B). In prostate cancer, exposure to 0.2% O_2 for 48 h resulted in the

downregulation of both *BRCA1* and *BRCA2* (Meng *et al.*, 2005). Similarly, *BRCA2* was downregulated by hypoxia in breast cancer (Fanale *et al.*, 2013). These studies very much contrast the NanoString observations as there was minimal change, particularly in *BRCA2*. Therefore, hypoxia-induced changes to *BRCA1* and *BRCA2* may be a cell type-specific phenomenon.

Finally, significant downregulation of *WRN*, involved in Holliday junction resolution (Constantinou *et al.*, 2000), was observed in U87-MG and D566-MG at 1% O_2, with -0.69 and -0.71 $\log_2$ fold change respectively (Figure 4.8 A). Both of these cell lines, plus T98G, showed clear downregulation of *WRN* in 0.1% O_2, with all changes being statistically significant (Figure 4.8 B). Interestingly, WRN has been implicated in HIF-1α repression, with depletion of WRN leading to accumulation of HIF-1α (Labbé *et al.*, 2012).

In summary, the expression of a number of HRR genes is impacted by hypoxia, specifically *WRN*, and *RAD51* were strongly downregulated in 0.1% O_2 in two or more GBM cell lines. However, several previously documented changes such as downregulation of *BRCA2*, *RAD52* and *RAD54* (Bindra *et al.*, 2005; Meng *et al.*, 2005; Bindra and Glazer, 2007) were not identified in the cell lines tested here. This supports the notion that hypoxia-induced changes can be subjective to the cell type as well as to the severity and duration of hypoxia used in each study.

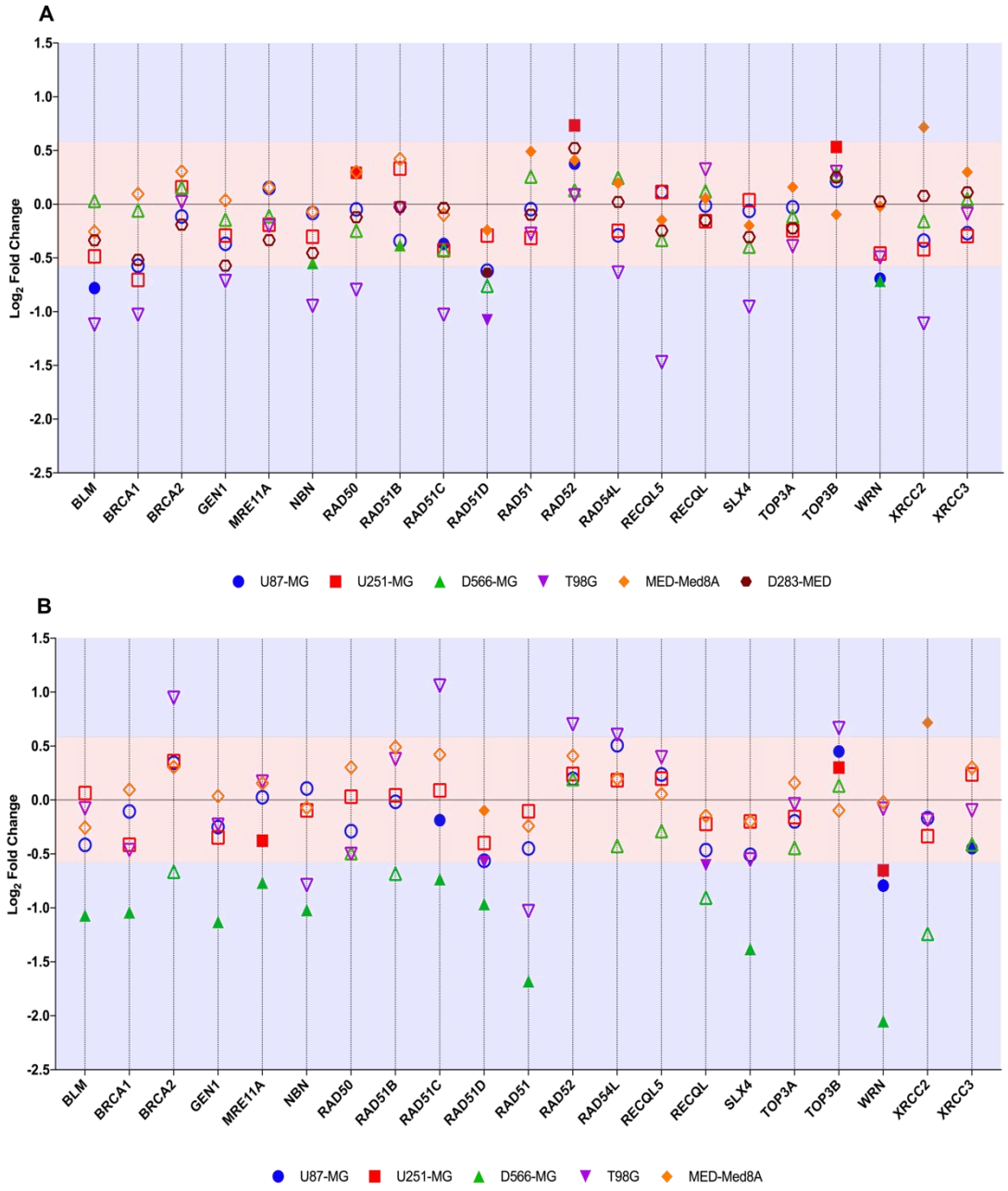

Figure 4.8: Differential expression of HRR genes in 1% and 0.1% O_2. Differential gene expression was calculated for each gene as log_2 fold change for (A) 1% O_2 and (B) 0.1% O_2 with respect to the expression level in 21% O_2. Red shaded area denotes fold change values below the +/-0.58 log_2 fold (+/-1.5-fold) threshold of change. Blue area denotes fold change values above the designated threshold. Filled shapes represent data which is statistically significant ($p<0.01$), whereas hollow shapes show no statistical significance. Data are represented as the mean of three independent experiments.

4.3.4.2 Non-homologous end joining

NHEJ is a second pathway responsible for the repair of DSB. Unlike HRR, NHEJ does not require the presence of homologous DNA. This simple process involves recognition of damage, end processing and ligation of DNA strands. Several studies have attempted to deduce the impact of hypoxia on NHEJ gene expression, yet little consensus has been achieved. In the NanoString study, the majority of genes did not cross the fold change threshold (Figure 4.9). However, in all GBM cell lines analysed, *LIGIV* (DNA Ligase IV) is at least -0.58 $\log_2$ fold (1.5 fold) downregulated by hypoxia (1% and 0.1% O_2.), although, this was only statistically significant in U87-MG. Interestingly, this downregulation appears to strengthen for T98G and D566-MG with increasing hypoxia severity. In contrast, the expression level of *XRCC4*, the binding partner of DNA Ligase IV, was not impacted by hypoxia. Work by Meng *et al* 2005, observed similar hypoxia-induced gene expression changes for *LIGIV*, also with no change in *XRCC4* (Meng *et al.*, 2005).

In 0.1% O_2, *PRKDC* (DNA-PKcs) was downregulated -0.86 and 0.63 $\log_2$ fold in T98G and D566-MG respectively (Figure 4.9 B). The gene expression of PRKDC in hypoxia has not previously been reported, however in breast cancer cells exposed to moderate hypoxia (1.8%) DNA-PKcs protein was upregulated (Madan *et al.*, 2012). Additionally, a large-scale proteomic analysis showed an increase in Ku70 and Ku80 protein under hypoxia (Ren *et al.*, 2013). However, the NanoString data does not indicate any change to Ku gene expression (XRCC5 and XRCC6) (Figure 4.9).

Taken together, it is clear that *LIGIV* is strongly downregulated by hypoxia, shown here and by the work of others (Meng *et al.*, 2005). However, very few changes were observed for the other genes involved in the NHEJ. Previously observed changes to DNA-PKcs, Ku70 and Ku80 protein might not be due to gene expression changes.

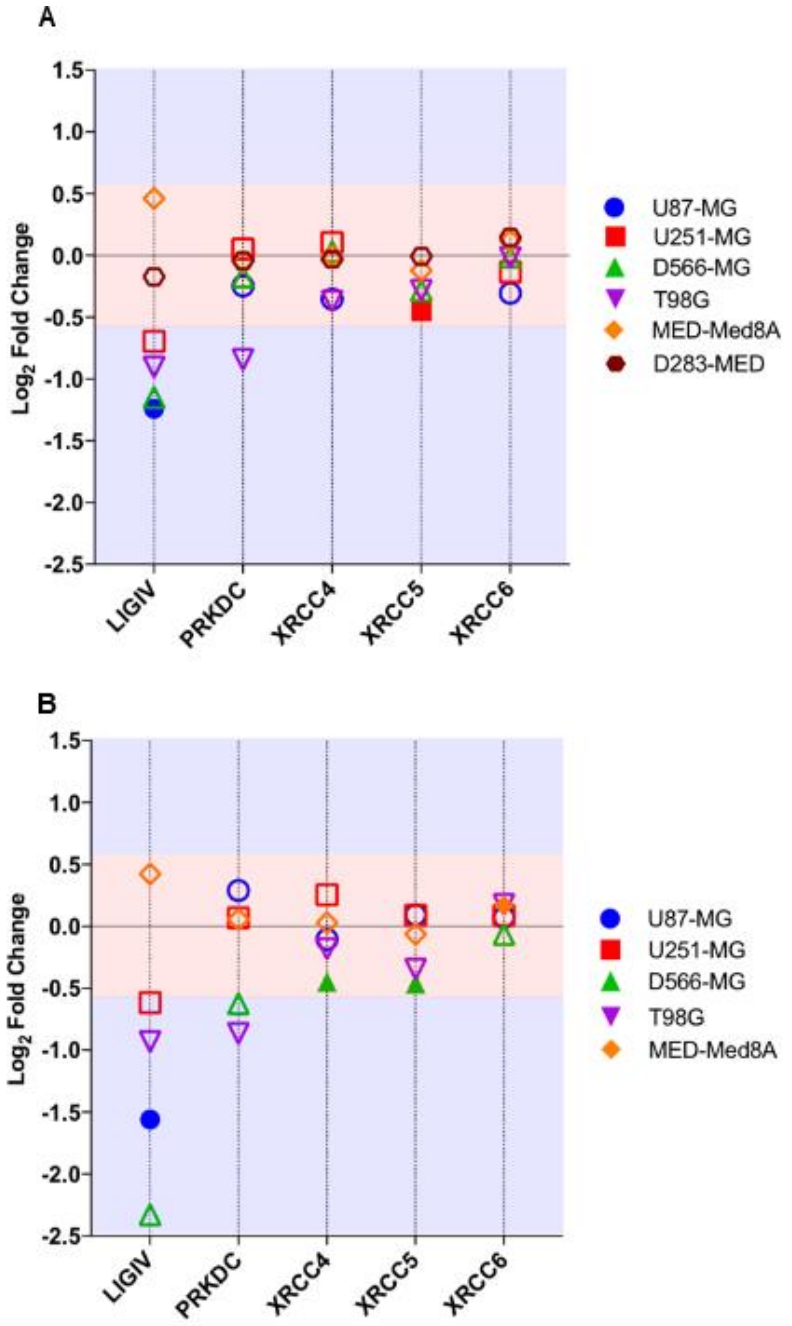

Figure 4.9: Differential expression of NHEJ genes in 1% and 0.1% O_2. Differential gene expression was calculated for each gene as log_2 fold change for (A) 1% O_2 and (B) 0.1% O_2 with respect to the expression level in 21% O_2. Red shaded area denotes fold change values below the +/-0.58 log_2 fold (+/-1.5-fold) threshold of change. Blue area denotes fold change values above the designated threshold. Filled shapes represent data which is statistically significant ($p<0.01$), whereas hollow shapes show no statistical significance. Data are represented as the mean of three independent experiments.

4.3.4.3 Base excision repair

BER is responsible for the removal of aberrant DNA bases. Specific glycosylases recognise the DNA base, which is removed. The DNA ends are then processed and ligated back together. Similar to NHEJ, the effect of hypoxia on BER gene expression is not well known. The expression of 27 BER-related genes were assessed in the NanoString experiment (Figure 4.10). For the DNA glycosylase, *NEIL1* a 1.11 $\log_2$ fold upregulation U251-MG and 0.96-fold in MEB-Med8A at 1% O_2 was observed (Figure 4.10 A). However, the data for *NEIL1* could be deemed unreliable due to low count numbers for these genes, which in some cases did not reach the noise threshold (data not shown). *UNG*, responsible for the removal of incorrectly inserted uracil, was downregulated in both T98G and D566-MG at 1% O_2 and 0.1% O_2, which was statistically significant (Figure 4.10). Additionally, *MUTYH* was downregulated in all the GBM cell lines tested at 0.1% O_2, and to a lesser extent in 1% O_2. Previous studies in colorectal cancer cells found OGG1 protein to be downregulated by hypoxia (Chan *et al.*, 2014). Altered OGG1 gene expression was only observed in D566-MG cells at 0.1% O_2 (Figure 4.10 B). However, the same study found MUTYH protein to be downregulated by hypoxia similar to the NanoString results (Chan *et al.*, 2014), suggesting that the decrease in protein may be attributed to reduced transcription.

For both *PARP1* and *PCNA*, critical facilitators of BER, at 0.1% O_2 downregulation in T98G, U87-MG and D566-MG were observed (Figure 4.10 B). Interestingly, PARP1 has been shown to interact with both HIF-1α and HIF-2α and aid in the expression of hypoxia-inducible genes (Elser *et al.*, 2008; Gonzalez-Flores *et al.*, 2014). The observed downregulation of *PARP1* gene expression in hypoxia, suggest that PARP-1 could be part of a negative feedback loop ensuring controlled expression of HIF target genes.

For the DNA polymerases involved in BER, *POLE2* was downregulated in 1% and 0.1% O_2 for U87-MG, T98G and D566-MG. For D566-MG cells incubated

in 0.1% O_2, the strongest downregulation of *POLE2* was observed (-2.28 log_2 fold, $p<0.000$; Figure 4.11 B). *POLB* was also downregulated in D566-MG cells. The downregulation of POLB protein by hypoxia been reported in previous studies (Chan *et al.*, 2014), yet less is known about the effects of hypoxia on gene expression. Finally, in T98G, U251-MG and U87-MG at 1% O_2, *FEN1* was downregulated, yet downregulation was observed in T98G and D566-MG only, at 0.1% O_2.

In summary, significant regulation of the DNA glycosylases *MUTYH* and *UNG* in hypoxia was observed, in addition to regulation of *POLE2, PARP1, PCNA* and *FEN1*. These changes could impact the functionality of BER, particularly in the removal of incorrectly inserted uracil and adenine. Also, long-patch BER will be affected by the downregulation of *FEN1*. Few studies explore the impact of hypoxia on BER. Therefore this NanoString based study provides further potentially valuable knowledge for this field.

Figure 4.10: Differential expression of BER genes in 1% and 0.1% O_2. Differential gene expression was calculated for each gene as log_2 fold change for (A) 1% O_2 and (B) 0.1% O_2 with respect to the expression level in 21% O_2. Red shaded area denotes fold change values below the +/-0.58 log_2 fold (+/-1.5-fold) threshold of change. Blue area denotes fold change values above the designated threshold. Filled shapes represent data which is statistically significant ($p<0.01$), whereas hollow shapes show no statistical significance. Data are represented as the mean of three independent experiments.

4.3.4.4 Mismatch repair

MMR removes incorrectly inserted nucleotides added during DNA replication. Search processes identify the incorrect nucleotide, which is excised and the gap is filled and sealed. As part of the NanoString study, the expression of 13 genes involved in mismatch repair was assessed (Figure 4.11). Overall, few genes are regulated by hypoxia, as they do not reach the fold change threshold. However, strong regulation was observed in some crucial players of MMR.

Initial steps of MMR involve the formation of the MutSα complex composed of MSH2 and MSH6. *MSH6* was not regulated by hypoxia. However, *MSH2* was strongly downregulated -1.18 $\log_2$ fold in D566-MG and -1.01 fold in T98G incubated in 0.1% O_2 (Figure 4.11 B). In a previous study by Koshiji *et al*, *MSH2* and *MSH6* were downregulated in 1% O_2 in a HIF-1 dependent manner (Koshiji *et al.*, 2005). In contrast, a second study found no significant downregulation of *MSH2* or *MSH6* after incubation in <0.001% (Mihaylova *et al.*, 2003), suggesting that anoxia causes a different response with regards to expression of MMR genes.

PMS2, a central component of the MutLα complex, was downregulated in T98G, D566-MG and U87-MG cell (Figure 4.11). Specifically, the expression of *PMS2* in D566-MG at 0.1% O_2 was -1.41 $\log_2$ fold change (Figure 4.11 B). Previous studies did not observe *PMS2* downregulation at the mRNA level, but at the protein level (Mihaylova *et al.,* 2003). The expression of PMS2's binding partner, *MLH1*, was found to be downregulated in hypoxic stem cells (Rodríguez-Jiménez *et al.*, 2008), which is thought to be via transcriptional repression (Nakamura *et al.*, 2008). However, there was no change to *MLH1* in GBM or MB cell lines tested here. Similarly, Koshiji *et al* determined that *MLH1* is unchanged by hypoxia (Koshiji *et al.*, 2005).

Further observed changes include the downregulation of *MSH5* in a number of cells lines in 1% O_2 and 0.1% O_2, with particularly strong downregulation in D566-MG (-2.04 log_2 fold) at 0.1% O_2 (Figure 4.11 B). Additionally, *MSH4* appears to be upregulated in U251-MG, MEB-Med8A and D283-MED in 1% O_2 but without reaching statistical significance (Figure 4.11 A). There is no data available for the expression of *MSH4* in other cell lines due to the gene being deemed as 'undetectable' early rounds of analysis (see methods for information on quality control of data). Both MSH5 and MSH4 are primarily involved in meiosis (Bocker *et al.*, 1999; Snowden *et al.*, 2004), therefore the impact of these hypoxia-induced changes in brain tumour cell lines is debatable. However, activation of meiotic genes is thought to aid in the initiation and maintenance of oncogenesis (McFarlane and Wakeman, 2017). Therefore hypoxia-induced changes in *MSH5* and *MSH4* may indeed play an unknown role in brain tumour cells.

Overall, hypoxia-induced gene expression changes have been observed for two key players in the initial steps of mismatch repair, namely *MSH2* and *PMS2*, which correlates with previous findings in the literature. As both genes are involved in critical steps of MMR, this reduction of gene expression may have a significant consequence for MMR capacity in hypoxia.

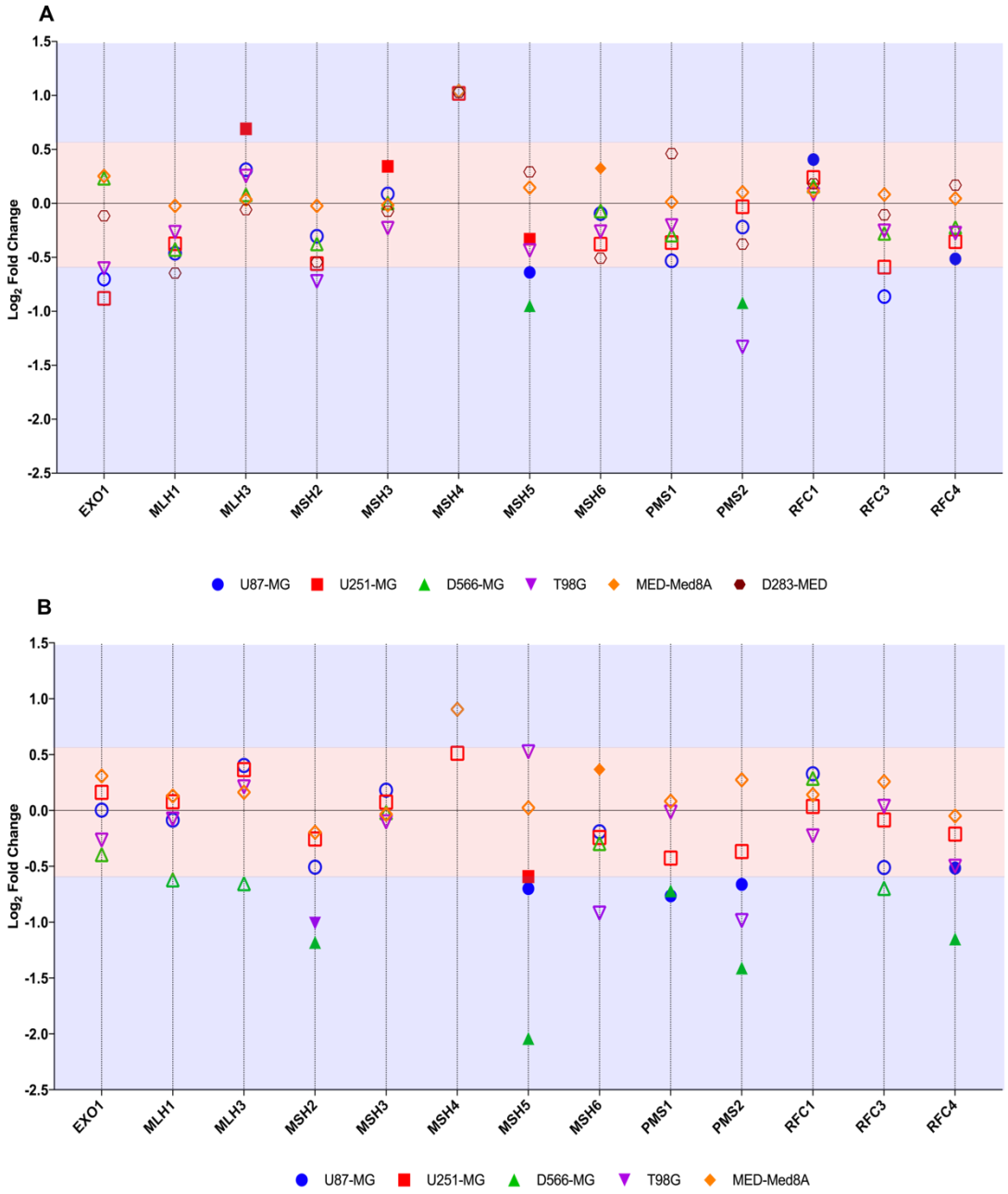

Figure 4.11: Differential expression of MMR genes in 1% and 0.1% O_2. Differential gene expression was calculated for each gene as log_2 fold change for (A) 1% O_2 and (B) 0.1% O_2 with respect to the expression level in 21% O_2. Red shaded area denotes fold change values below the +/-0.58 log_2 fold (+/-1.5-fold) threshold of change. Blue area denotes fold change values above the designated threshold. Filled shapes represent data which is statistically significant ($p<0.01$), whereas hollow shapes show no statistical significance. Data are represented as the mean of three independent experiments.

4.4 Validation

4.4.1 mRNA validation

Several studies comparing the NanoString gene expression platform and RT-PCR, deemed the NanoString platform to be a robust and reliable method for the determination of gene expression (Malkov *et al.*, 2009; Veldman-Jones *et al.*, 2015; Bentley-Hewitt *et al.*, 2016). However, to ensure this was the case for this current NanoString based study, several genes were subjected to further gene expression analysis by RT-PCR. Genes were selected on the basis that they were regulated in at least one cell line. In total, the expression of seven genes was confirmed by RT-PCR using cDNA from U87-MG, U251-MG and D566-MG RNA samples (Figure 4.12).

There is a strong correlation between the NanoString and RT-PCR expression data. For example, the extent of upregulation for *ABL* was similar between the RT-PCR and NanoString data (Figure 4.12). However, there were some exceptions. For example, *MSH5* in U251-MG showed opposite regulation in RT-PCR and NanoString, with 0.36 $\log_2$ and -0.59 $\log_2$ fold change respectively. Additionally, there was a notable fold change difference for *MSH5* in D566-MG at 1% O_2 (Figure 4.12 C). This is potentially due to the low overall expression of *MSH5* (data not shown), which would increase the likelihood of more substantial discrepancies in fold changes between the two analysis platforms. Overall, the NanoString platform is a reliable method to assess gene expression however further validation with other gene expression analysis platforms or assessment of the protein level is always valuable.

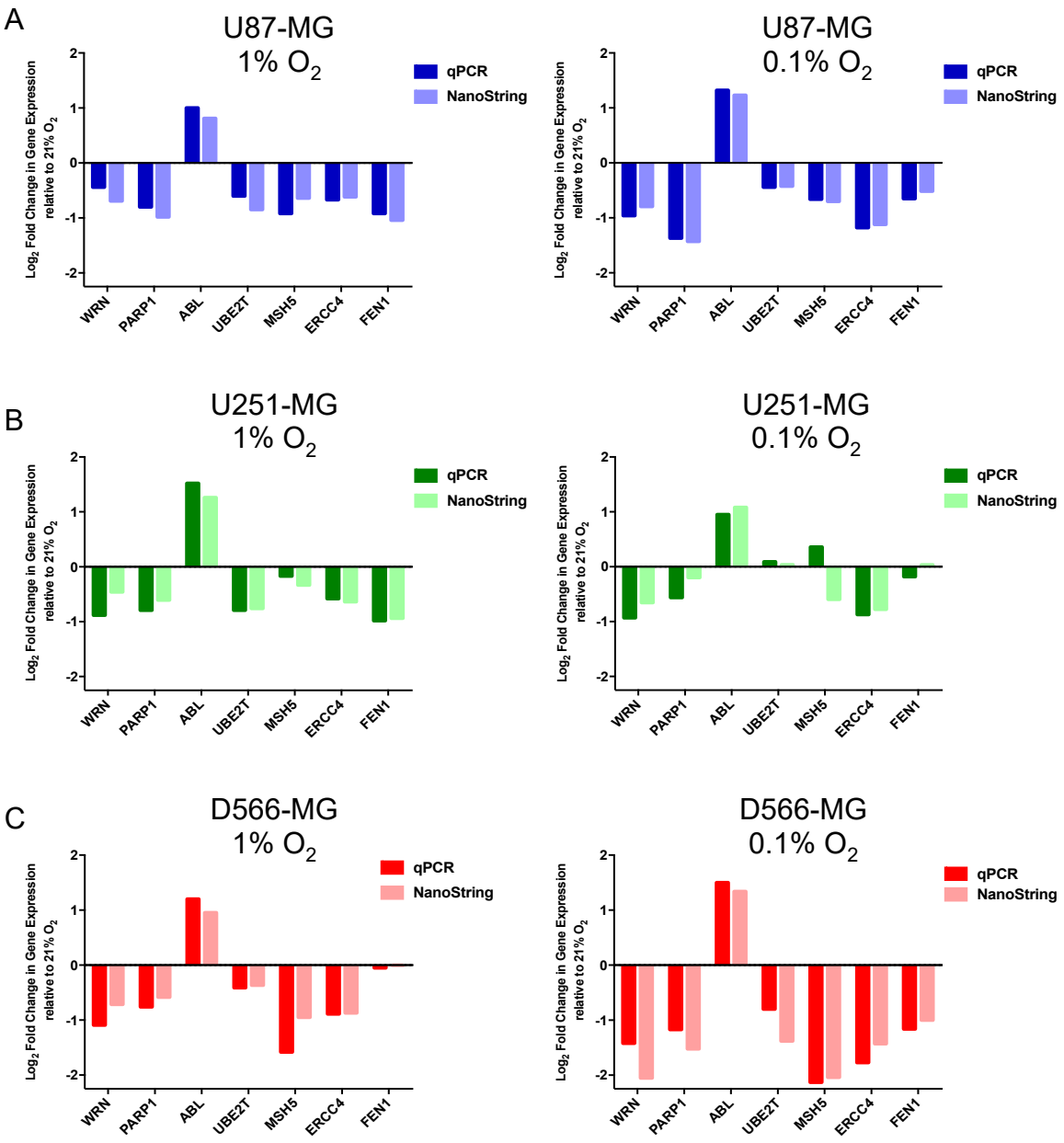

Figure 4.12: NanoString Validation by RT-PCR. Seven genes were selected from the NanoString panel for validation by RT-PCR. cDNA samples for (A) U87-MG, (B) U251-MG and (C) D566-MG was utilised in RT-PCR experiments to assess the expression levels of selected genes. Data are expressed as log_2 fold change with respect to expression at 21% O_2. Data from NanoString is included for direct comparison. RT-PCR data is represented as the mean of three independent experiments.

4.4.2 Protein level validation

In order for hypoxia-induced gene expression changes to directly impact DNA repair functionality, the protein levels must be affected. Previous reports suggest this is not always the case. For example, hypoxia-induced downregulation of Ku70 mRNA in prostate cancer cells did not impact the Ku70 protein levels (Meng *et al.*, 2005). To determine whether the hypoxia-induced gene expression changes observed in the NanoString assay translated to the protein level, three proteins (PARP1, PCNA, PMS2) were selected for analysis by western blotting. These three proteins were chosen due to the availability of suitable antibodies. Protein levels were examined in D566-MG and U87-MG cells, which displayed downregulation of *PARP1, PCNA* and *PMS2* gene expression in hypoxia. Cells were pre-incubated in 21%, 1% or 0.1% O_2 for 5 days before western blotting. Actin or Vinculin was used as a loading control, and densitometry measurements were performed to determine the fold change in protein with respect to the level at 21% O_2 (Figure 4.13).

PARP1 and PCNA protein levels were relatively similar in hypoxia and normoxia for both cell lines (Figure 4.13 A, B), yet a decrease (0.58 fold) in PARP1 was observed in U87-MG pre-incubated in 1% O_2. In contrast, the gene expression data suggested a 1.49 (-0.58 $\log_2$) and 1.97 (-0.98 $\log_2$) fold change at 1% O_2 for D566-MG and U87-MG respectively (Figure 4.10 A). PMS2, a component of mismatch repair, was strongly downregulated in hypoxic D566-MG and U87-MG, particularly at 0.1% O_2, where a 0.55 fold and 0.72 fold change was observed (Figure 4.13 C). Similarly, a 2.66 (D566-MG) and 1.58 (U87-MG) mRNA fold change was identified in the NanoString assay.

Overall, not all proteins tested were downregulated by hypoxia. However, the mismatch repair protein, PMS2, was strongly downregulated in both GBM cell lines at the mRNA and protein level. This suggests that some of the hypoxia-induced changes to gene expression are likely to impact the amount of protein available to repair mechanisms.

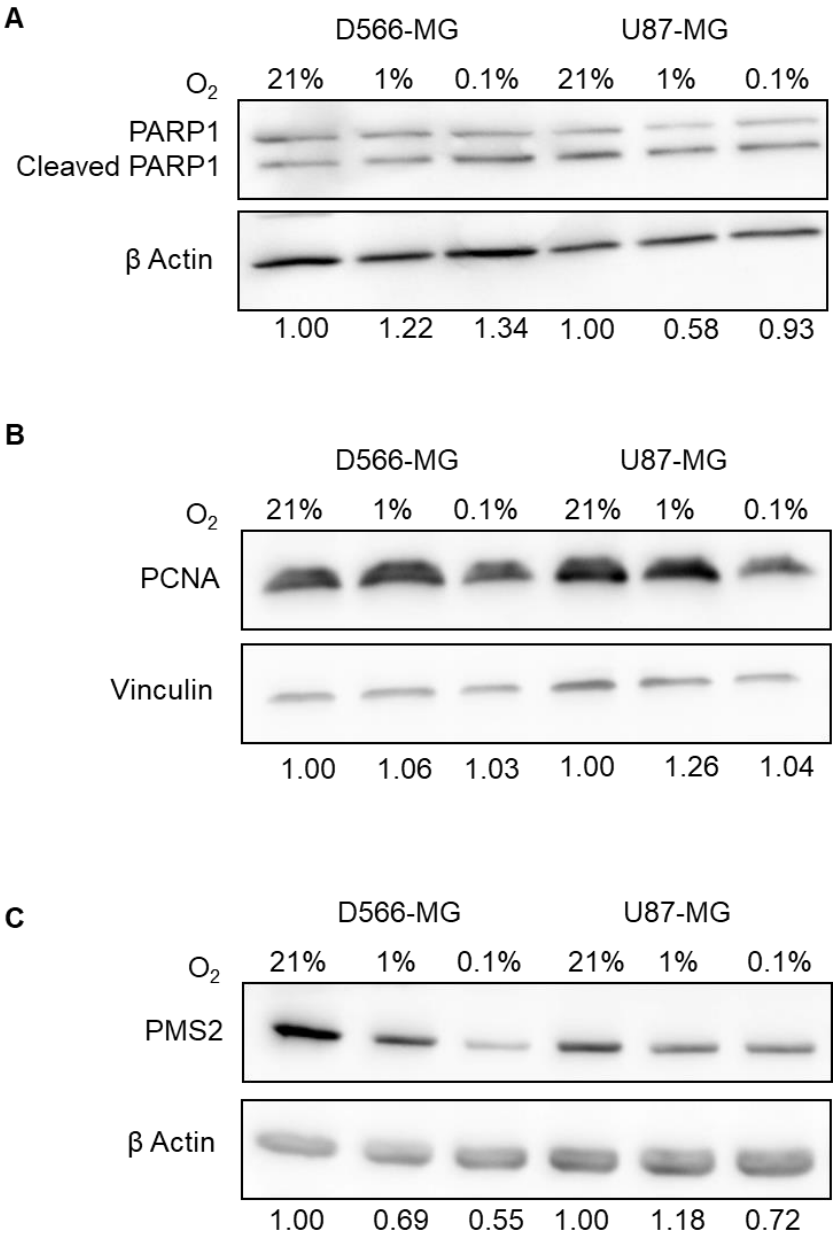

Figure 4.13: The impact of hypoxia on PARP1, PCNA, PMS2 protein levels. D566-MG and U87-MG cells were pre-incubated in 21%, 1% or 0.1% O_2 for 5 days before western blotting for (A) PARP1 (B) PCNA and (C) PMS2. Image J was used for blot quantification, with the mean fold change in protein levels with respect to 21% O_2 for three independent experiments, shown below bands. PARP1 and PCNA blots were repeated twice. PMS2 blots conducted at least three times. Figure shows representative blots.

4.5 Discussion

Hypoxic exposure can alter the expression of essential DNA repair genes, yet this had not yet been explored in GBM and MB. Using a NanoString based approach, multiple changes to gene expression were identified across several cell lines, with a variable impact of increasing hypoxia severity. Understanding the functional consequences and the molecular mechanism driving these changes will enable an improved understanding of the impact of hypoxia in GBM and MB.

4.5.1 Moderate versus severe hypoxic exposure

Within a brain tumour, the median oxygen concentration is ~1.7%, yet this can vary from close to anoxia (0%) to more moderate hypoxia (~3%) (Rampling *et al.*, 1994). These extremes in the microenvironment can have a varied impact on cell biology. However, the effect of moderate and severe hypoxia on DNA repair gene expression was not so clear-cut, in the current study. Previous work exploring hypoxia and DNA repair primarily utilise severe hypoxic exposure (0.0 – 0.2%) over short time periods. For example, the hypoxia-induced downregulation of *RAD51*, *BRCA1*, *DNA-PKcs*, *Ku70* and *LIGIV*, was determined after exposure to <0.2% O_2 (Bindra *et al.*, 2004, 2005; Meng *et al.*, 2005). Within brain tumours, the proportion of cells exposed to such extreme hypoxia is low, with most cells experiencing ~0.5% O_2 (Evans *et al.*, 2004). Therefore, using such severe hypoxia in DNA repair studies may be less valuable. Such extreme hypoxic exposure can have devastating consequences for many cellular processes resulting in cell death. In 0.02% O_2, cell cycle arrest is induced, and p53 protein accumulates (Amellem and Pettersen, 1991; Graeber *et al.*, 1994). This could directly influence the response of cells to DNA damaging agents, in part, due to the requirement of cycling cells for damage induction. Additionally, in severely hypoxic cells, replication arrest occurs leading to the activation of ATR, ATM, H2AX, Chk2 and p53, independent of DNA damage (Hammond *et al.*, 2002; Bencokova *et al.*, 2009), and further

issues can arise upon reoxygenation. Within the tumour microenvironment, fluctuations in tumour oxygenation is common due to the hectic architecture of the vasculature. Cellular reoxygenation can lead to replication restart and the induction of excessive DNA damage (Pires *et al.*, 2010). Overall, severe hypoxia (close to anoxia), causes multiple cellular events that can lead to the induction of apoptosis. Therefore, it is unlikely that these cells would affect the tumour population as a whole, and may have little relevance clinically. To enable a consensus between findings related to hypoxia and DNA repair, standardising the definitions of hypoxia would be ideal. This is challenging due to cell line variations, primarily impacted by the physioxia of the originating tissue.

4.5.2 PMS2 and the mismatch repair pathway

The findings of the NanoString assay were not so clear-cut, with multiple changes in different cell lines. However, some common gene expression changes dominate, particularly in GBM cells. Specifically, downregulation of *PMS2* and *LIGIV* was found in nearly all GBM cell lines tested. The functional consequence of *LIGIV* downregulation is to be explored in Chapter 5. Therefore, only the potential impact of *PMS2* downregulation will be discussed here.

During DNA replication, polymerase errors can occur leading to the insertion of incorrect nucleotides. These mismatched base pairs are removed and replaced by MMR. PMS2 is essential for this process, and alterations to *PMS2* expression may impact MMR activity. Defects in any of the critical MMR repair proteins (PMS2, MLH1, MSH2, MSH6), can lead to hypermutation and microsatellite instability, due to the increased number of point mutations (Kim *et al.*, 1999). Point mutations drive tumorigenesis and cancer progression. For example, in a brain tumour based multicellular tumour spheroid cultures, downregulation of *PMS2* and *MLH1* promoted the initiation of tumour cell formation and growth (Collins *et al.*, 2011). Therefore, it is likely

that the downregulation of *PMS2* in hypoxic GBM will increase the mutation rate and drive further tumour progression.

In addition to an increased mutation rate, MMR deficiencies have been implicated in treatment resistance. In 1996, the link between MMR and cisplatin resistance was established, when cisplatin-resistant human ovarian adenocarcinoma cells were found to have reduced MLH1 protein (Aebi *et al.*, 1996). In the same year, both MLH1 and MLH2 downregulation was found to induce both cisplatin and carboplatin resistance (Fink *et al.*, 1998), although this was only a low-level resistance. Similarly, in U87-MG cells, which display *PMS2* downregulation, a low level of cisplatin resistance was observed (Chapter 3). MMR defects can have further clinical impact for GBM, due to the requirement of MMR for temozolomide sensitivity. In 1997, the necessity of functional MMR for apoptosis induced by temozolomide was determined (D'Atri *et al.*, 1998). Further work established that loss of MSH6 was associated with increased tumour progression during temozolomide treatment in GBM (Cahill *et al.*, 2007), and alterations of *MSH2* expression could predict patient response to TMZ therapy, with reduced expression correlating with decreased overall patient survival (McFaline-Figueroa *et al.*, 2015). Downregulation of *PMS2* in hypoxia could have a significant clinical impact for GBM. Increased mutation rate driving tumorigenesis and reduced sensitivity to temozolomide would be disastrous for the successful treatment of GBM, potentially reducing overall survival rates. Identifying the mechanism behind MMR gene regulation would be essential in order to develop targeted molecular-based therapies.

4.5.3 Mechanisms of hypoxia-induced gene regulation

Regulation of gene expression in hypoxia can arise due to a number of mechanisms. Epigenetic modifications can lead to long-term alterations to gene expression. For example, alterations to histone methylation and acetylation at the promoters of *BRCA1* and *RAD51* can lead to reduced gene

expression (Lu *et al.*, 2011). However, transient changes to DNA repair gene expression are more common, with both HIF dependent and independent mechanisms described in the literature. HIF can directly modulate the transcription of genes through binding at the hypoxia response elements within promoters of DNA repair genes. In the *MLH1* promoter, HREs have been identified (Mihaylova *et al.*, 2003). The presence of HREs does not necessarily suggest that regulation is entirely through HIF binding, as hypoxia-induced downregulation of *MLH1* was found also to be independent of HIF (Mihaylova *et al.*, 2003). However, contradicting mechanisms of *MLH1* regulation with regards to the requirement of HIF, are reported due to differences in hypoxia severity and duration (Koshiji *et al.*, 2005; Rodríguez-Jiménez *et al.*, 2008).

A well characterised HIF independent mechanism affecting DNA repair gene expression is an alteration of E2F transcription binding. In normoxia, the expression of *BRCA1* is mediated through the binding of the activating factor E2F1 as well as the E2F4/P130 suppressor. However, under hypoxic conditions, p130 binding to E2F4 is enhanced, due to alterations to p130 post-translational modifications. This results in an increase in E2F4/p130 transcriptional suppressor binding at the *BRCA1* promotor, reducing the rate of transcription (Bindra *et al.*, 2005). Regulation of *RAD51* and *FANCD2* are thought to occur by a similar E2F related mechanism (Bindra and Glazer, 2007; Scanlon and Glazer, 2014). Overall, the direct mechanism of hypoxia-induced expression of DNA repair genes has only been determined in a limited number of cases, however in order to further understand how hypoxia influences DNA repair within a tumour setting, defining the molecular mechanism behind the observed changes is essential.

4.5.4 Concluding remarks and future work

To conclude, changes to DNA repair gene expression by hypoxia is not so clear-cut, with the specifics of hypoxic exposure and cell lines creating a high level of variation. However, several genes were found to be downregulated in multiple GBM cell lines, such as *PMS2* and *LIGIV*. A reduction in crucial MMR components could reduce repair efficiency, having a significant clinical consequence for GBM, due to the increased mutation rate and treatment resistance of MMR deficient cells. The consequences of hypoxia on NHEJ efficiency through examination of XRCC4 kinetics is to be explored in Chapter 5. Beneficial future work includes the examination of DNA repair gene expression in cells with knocked down HIF to aid in further identifying the drivers of the observed gene changes. Understanding the molecular mechanism behind gene expression changes in hypoxia is required in order to develop targeted therapies to tackle these highly resistant tumours.

Chapter 5: Exploring the impact of hypoxia on *LIGIV* expression and XRCC4 kinetics

5.1 Introduction

In Chapter 4, several genes were downregulated by hypoxia in multiple cell lines. In particular, *LIGIV*, encoding DNA ligase IV, was downregulated in all GBM cell lines. Similarly, Meng *et al*, observed *LIGIV* downregulation in hypoxic prostate cancer cells (Meng *et al.*, 2005). DNA ligase IV (named ligase IV from here) is an essential component of the canonical NHEJ, responsible for the repair of DSB. Therefore, downregulation of *LIGIV* may lead to reduced functionality of NHEJ.

NHEJ is the primary pathway for repair of DSB. To summarise, when a DSB is present Ku70/80 and DNA-PKcs are initially recruited to stabilise the DNA ends (Gottlieb and Jackson, 1993; Kurimasa et al., 1999). The exposed ends are processed by Artemis, PNK, WRN or DNA polymerases (Mahaney *et al.*, 2009), followed by the recruitment of XRCC4 : ligase IV, triggered by the interaction of XLF and XRCC4 (Yano *et al.*, 2009). XLF can stimulate ligase activity, yet this is cell line dependent (Roy *et al.*, 2015). Additionally, the presence of Ku70/80 is essential for XRCC4 and ligase IV recruitment (Nick McElhinny *et al.*, 2000; Mari *et al.*, 2006). Ligase IV is responsible for ligation of the DNA ends, the final step of NHEJ (Chapter 1, Figure 1.8).

In 1997, Grawunder *et al* and Critchlow *et al* observed the dimerisation of XRCC4 and ligase IV, an essential step for ligase IV activity (Critchlow *et al.*, 1997; Grawunder *et al.*, 1997). XRCC4 binds to ligase IV via the XRCC4 interacting region (XIR) between the BRCT domains (Grawunder *et al.*, 1998). During DNA ligation, AMP bound to ligase IV is transferred to the 5' phosphate end of DNA, which is then displaced by the 3'OH, resulting in the covalent bonding of DNA strands (Ellenberger and Tomkinson, 2008). Afterwards, ligase IV requires re-adenylation, which is stimulated by XRCC4, leading to protein stabilisation (Modesti *et al.*, 1999). The C-terminal region of ligase IV, containing the XIR and BRCT domains, is essential for nuclear localisation of XRCC4 (Fonslow *et al.*, 2015). In ligase IV-deficient cells,

XRCC4 localisation was dysregulated, and reduced XRCC4 protein levels were observed with *LIGIV* mutations (Fonslow *et al.*, 2015). Therefore, ligase IV plays a fundamental role in XRCC4 localisation and stabilisation. This dynamic relationship between XRCC4 and ligase IV is crucial for efficient NHEJ. Disruption of this relationship through ligase IV downregulation may be catastrophic for NHEJ functionality.

Traditionally, assessment of DNA repair efficiency and function was conducted using cell-free biochemical assays, which have provided great insight into the role of essential repair proteins. For example, Ku80 was found to be essential for precise NHEJ in cell-free assays (Feldmann *et al.*, 2000). However, measuring repair mechanisms directly within the cellular environment is critical for an accurate understanding of these complex interdependent mechanisms. Methods that address this include ionising radiation-induced focus formation (IRIF) and laser microirradiation studies. IRIF is a popular method, which has been highly valuable for the identification of recruited proteins and understanding their modification. For example, IRIF experiments led to the observation that γH2AX is essential for BRCA1, RAD50 and RAD51 recruitment (Paull *et al.*, 2000). However, not all repair proteins can recruit to IRIF, which limits its use. Therefore, laser microirradiation methods have been developed.

In 1999, Rogakou *et al* first described the use of a UVA laser with bromodeoxyuridine (BrdU) to induce DNA damage in specific sites of the nucleus, triggering DSB repair protein recruitment (Rogakou *et al.*, 1999). Since these initial studies, several groups commonly use UVA lasers (337-405 nm), to study DNA repair protein recruitment. However, as well as DSB, irradiation with a UVA laser leads to other damage types including cyclobutane-pyrimidine dimers (CPDs), which is not ideal. Also, sensitisers (BrdU, Hoechst) are required for DNA breaks to form, which can have unwanted side effects (Dinant *et al.*, 2007). Therefore, UVA lasers may not be

the most suitable choice for DNA damage induction. Alternatively, irradiating with a near-infrared laser (near-IR) (≥780 nm) removes the requirement for sensitisation, and may reduce the unwanted DNA damage products (i.e. CPDs). Work by Träutlein *et al* compared the specificity of DNA damage induced by an infrared multiphoton femtosecond laser, tuned to wavelengths 775 nm and 1050 nm. Using a 1050 nm laser increased the specificity for DSB, with a marked reduction in unwanted DNA damage. However, 775 nm resulted in CPD formation (Träutlein *et al.*, 2009). Similarly, irradiation with an 800 nm femtosecond laser causes CPD formation and recruitment of nucleotide excision repair proteins (Dinant *et al.*, 2007). The specifics of laser tuning can significantly affect the resultant DNA damage induced. However, in comparison to UVA lasers, near-IR pulsed femtosecond lasers enable high spatial resolution of DNA damage, with 3D confinement and a reduction of overall photo-toxicity (Meldrum and Botchway, 2003), making them a better choice. Overall, laser microirradiation can provide valuable insight into DNA repair protein dynamics in live cells. Therefore, to induce DNA breaks and assess the functional impact of *LIGIV* downregulation, a near-IR pulsed laser was used.

5.2 Objectives

The experimental aims for this chapter were as follows:

1. Explore the impact of hypoxia on *LIGIV* expression.

2. Develop a multiphoton laser microirradiation protocol to assess DNA repair protein recruitment.

3. Compare the kinetics of XRCC4 recruitment in hypoxic and normoxic GBM cells.

5.3 Results

5.3.1 Further investigation of *LIGIV* regulation in hypoxia

In Chapter 4, hypoxia-induced *LIGIV* downregulation was identified in the GBM cell lines, U87-MG, D566-MG, U251-MG and T98G. These changes were observed in both 1% and 0.1% O_2, albeit to a lesser extent in 1%. Here, the hypoxia-induced regulation of *LIGIV* was explored further, to understand how the length of hypoxic exposure, reoxygenation and HIF inhibition can affect *LIGIV* expression.

5.3.1.1 Assessment of *LIGIV* expression across multiple cell types

To validate the NanoString data, RT-PCR experiments were performed to assess the *LIGIV* mRNA levels of cells pre-incubated in 21%, 1% or 0.1% O_2 for 5 days. Hypoxia-induced downregulation of *LIGIV* was observed in U87-MG, D566-MG, U251-MG, and T98G, yet data for T98G were highly variable and not statistically significant (Figure 5.1). In D566-MG, pre-incubation in 1% and 0.1% O_2 resulted in 2.0-fold (-1.0 $\log_2$) and 3.9-fold (-1.9 $\log_2$) decrease in *LIGIV* expression respectively, yet without statistical significance. In U87-MG, statistically significant downregulation of *LIGIV* was observed for cells incubated in both 1% ($p=0.0191$) and 0.1% O_2 ($p=0.0135$) (Figure 5.1). In MB cells, D283-MED and MEB-Med8A, there was little change in *LIGIV* expression in hypoxia, which correlates with the NanoString data. Additionally, HeLa cells were included in RT-PCR experiments. If HeLa cells displayed hypoxia-induced *LIGIV* downregulation, they could be used in later studies as they are easier to manipulate and transfect. However, *LIGIV* mRNA levels were highly variable, suggesting there is no clear impact of hypoxia on *LIGIV* expression in these cells (Figure 5.1).

Overall, *LIGIV* is downregulated by hypoxia in U87-MG, U251-MG and D566-MG, which correlates with the NanoString data. Ideally, assessment of

the protein levels would further validate these findings. However, a specific and good quality DNA ligase IV antibody could not be sourced despite several trial experiments (appendix 1.7).

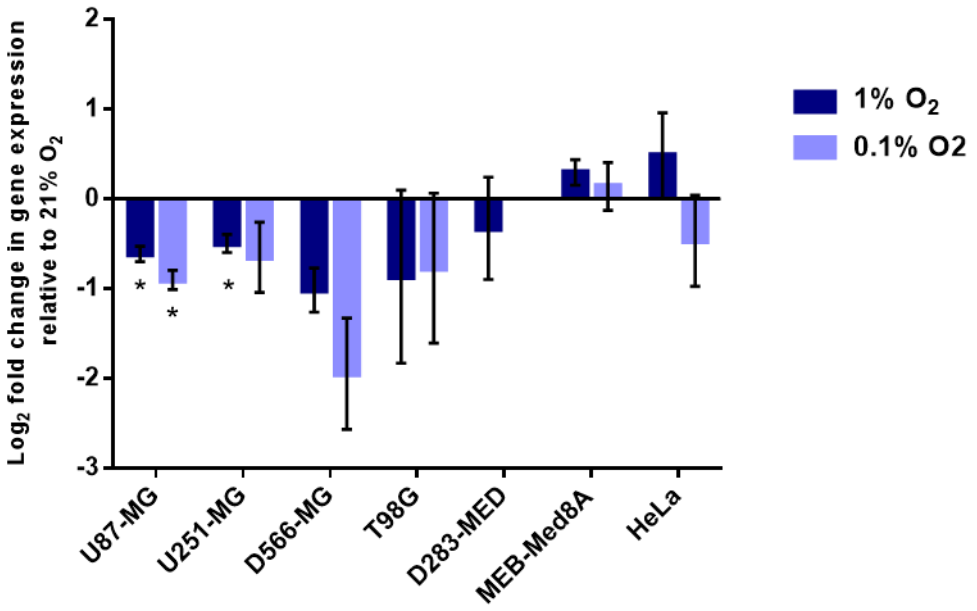

*Figure 5.1: LIGIV expression in multiple cell lines pre-incubated in hypoxia. Cells were incubated in 21%, 1% or 0.1% O_2 for 5 days. After incubation, RNA was extracted and converted to cDNA for RT-PCR experiments, probing for LIGIV. Data is represented as log_2 fold change in mRNA levels with respect to level for the 21% O_2 samples. Data are the mean for at least three independent experiments, with error bars showing S.E.M. * denotes significant data where $p<0.05$ indicated by one-way student t-test.*

5.3.2 *LIGIV* expression in chronic and acute hypoxia

In Chapter 3, chronic hypoxia was necessary to reduce sensitivity to chemo and radio-therapy. This, in part, was linked to the downregulation of the MRN complex after chronic hypoxic exposure (>48 h). Also, Fan 2014 observed a high level of DNA repair gene regulation in chronic hypoxia (96 h) (Fan, 2014). With this in mind, for the NanoString study, chronic hypoxic exposure (5 days) was used, however, the timing for *LIGIV* downregulation needs to be

established. Therefore, D566-MG cells, which displayed the strongest hypoxia-induced downregulation of *LIGIV*, were exposed to 21% and 1% O_2 for 1-5 days, before performing RT-PCR experiments to assess *LIGIV* and *GLUT1* expression. *GLUT1*, a common hypoxic marker, was elevated as expected throughout the time course (Figure 5.2). Overall, *LIGIV* was downregulated at all-time points (1-5 days). The strongest regulation was observed after only 1-day hypoxic exposure, with 3.0-fold downregulation (-1.6 log_2, p=0.002) (Figure 5.2). Therefore, both acute and chronic hypoxic exposure can induce *LIGIV* regulation. Similarly, *PARP1* and *PMS2* expression was also reduced in both chronic and acute hypoxia (appendix 1.8).

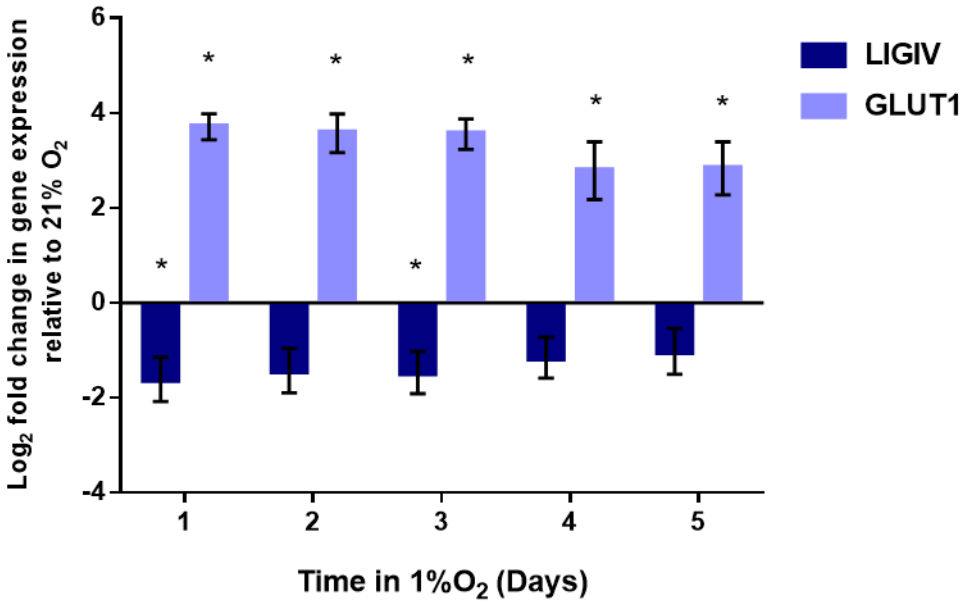

*Figure 5.2: LIGIV is downregulated after chronic and acute hypoxic exposure. D566-MG cells were incubated in 1% O_2 for 1-5 days, as well as 21% O_2. After incubation, RNA was extracted and converted to cDNA for RT-PCR experiments, probing for LIGIV and GLUT1. Data is represented as log_2 fold change in mRNA levels with respect to level for the 21% O_2 samples. Data are the mean of at least three independent experiments, with error bars showing S.E.M. * denotes significant data where p<0.05 indicated by one-way student t-test.*

5.3.3 Restoration of *LIGIV* expression upon reoxygenation

Within the tumour microenvironment, oxygen levels fluctuate due to the dynamic nature of tumour blood vessel formation. Therefore, tumour cells can experience periods of hypoxia and reoxygenation events. In previous studies, Bindra *et al* observed hypoxia-induced downregulation of RAD51, which persisted up to 48 h after reoxygenation (Bindra *et al.*, 2004), suggesting that alterations to repair protein expression may continue. To understand whether this was true for hypoxia-induced *LIGIV* downregulation, D566-MG cells were pre-incubated in 21% and 1% O_2 before reoxygenating for 24-72 h. The levels of *LIGIV* and *GLUT1* (hypoxic marker) mRNA was determined using RT-PCR. During hypoxic exposure, *GLUT1* mRNA increased in cells incubated in 1% O_2 (control), yet decreased upon reoxygenation as expected (Figure 5.3). For cells incubated in 1% O_2, there was a 3.9-fold (-1.9 log_2) reduction in *LIGIV* mRNA levels, and after 24 h reoxygenation, the level of *LIGIV* mRNA was restored to the normoxic levels (1.13-fold), which was maintained up to 72 h (Figure 5.3). Therefore, hypoxia-induced *LIGIV* downregulation does not persist upon reoxygenation in D566-MG cells.

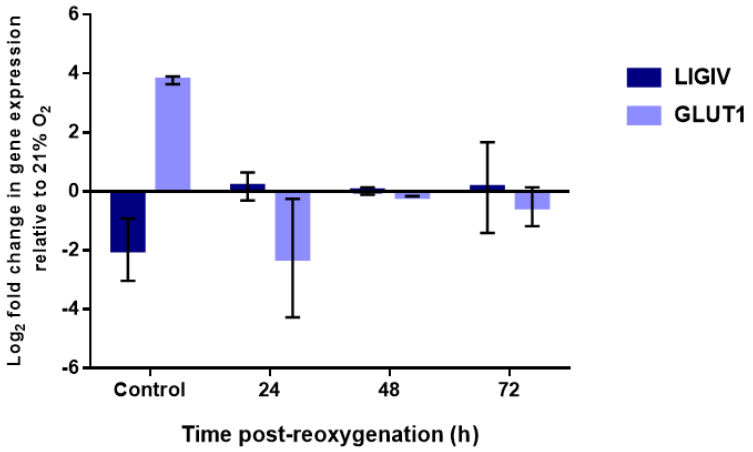

Figure 5.3: Reoxygenation restores LIGIV mRNA levels. D566-MG cells were incubated in 21% and 1% O_2 for 5 days before reoxygenation for 24-72 h. After incubation, RT-PCR experiments were performed for LIGIV and GLUT1. Control represents samples from 5 days 1% O_2 incubation. Data is represented as log_2 fold change with respect to 21% O_2. Data are the mean of two independent experiments, with error bars showing S.E.M.

5.3.4 Acriflavin treatment restores *LIGIV* mRNA levels

The hypoxia-inducible factor, HIF, is the master regulator of the hypoxic response. HIF can influence the expression of many genes including *GLUT1*, *VEGF* and *EPO*, as well as DNA repair genes. The HIF pathway forms a negative feedback loop, which results in the downregulation of HIF after long periods of hypoxia. However, in D566-MG and U87-MG cells, after 5 days of hypoxic exposure, HIF-1α remained high, with similar levels to 6 h and 24 h exposure (Figure 5.4). Therefore, it is feasible that hypoxic downregulation of *LIGIV* is dependent on HIF activity. To explore this further, an inhibitor of HIF was used to block HIF activity.

Several commercially available inhibitors of HIF have been developed, which result in the reduction of HIF activity through various mechanisms. Acriflavin (AF) can inhibit HIF-1 and HIF-2 through binding to the PAS-B subdomain in the α subunit, preventing dimerisation of the α and β subunits, and reducing HIFs transcriptional activity (Lee *et al.*, 2009). However, AF can also significantly impact other signalling pathways therefore is not a specific and 'clean' HIF inhibitor. In order to determine whether hypoxia-induced downregulation of *LIGIV* is dependent on HIF transcriptional activity, D566-MG and U87-MG cells were treated with 5 μM AF and incubated in 21%, 1% and 0.1% O_2 for 24 h before assessing *LIGIV* mRNA levels (Figure 5.6). Preliminary experiments, assessing *GLUT1* expression after 1 - 10 μM AF treatment, determined that 5 μM of AF was sufficient to reduce *GLUT1* expression in hypoxia (Figure 5.5). However, due to the toxicity of AF, cells could be treated for 24 h only. In both D566-MG and U87-MG, downregulation of *LIGIV* was observed in control untreated hypoxic cells (Figure 5.6). With AF treatment, *LIGIV* mRNA levels remained similar to normoxic conditions. For example, in U87-MG cells incubated in 0.1% O_2, a 1.8 fold (-0.87 $\log_2$ fold) reduction of *LIGIV* was observed, yet with AF, there was no downregulation of *LIGIV* mRNA (Figure 5.6). However, the expression levels of *LIGIV* with AF were highly variable.

Overall, treatment with the HIF inhibitor, acriflavin, inhibits the hypoxia-induced downregulation of *LIGIV* in D566-MG and U87-MG, suggesting *LIGIV* regulation may be HIF dependent. Additionally, in D566-MG cells treatment with DMOG results in *LIGIV* downregulation (Figure 5.7). DMOG is a competitive inhibitor of PHDs, which causes the accumulation of HIF in normoxia. This finding strengthens the notion that HIF is involved in *LIGIV* downregulation.

Interestingly, *PARP1*, *PMS2* and *WRN*, which were downregulated in the NanoString assay, were not restored by acriflavin addition (appendix 1.9), suggesting that the regulation of some DNA repair genes may not be through the canonical HIF pathway. Yet, this does not rule out the indirect involvement of HIF. To explore this further, knockdown of HIF using siRNA would be ideal. However, this requires 2-3 days transfection, which would trigger stress to D566-MG and U87-MG as they are highly sensitive to the transfection reagents. As an alternative, digoxin, a cardiac glycoside, inhibiting the translation of HIF (Zhang *et al.*, 2008) and thereby reducing HIF protein levels was used. However, with dioxin treatment, no change to HIF protein levels was observed at non-lethal doses, nor was there any reduction in hypoxia-induced *GLUT1* expression (appendix 1.10).

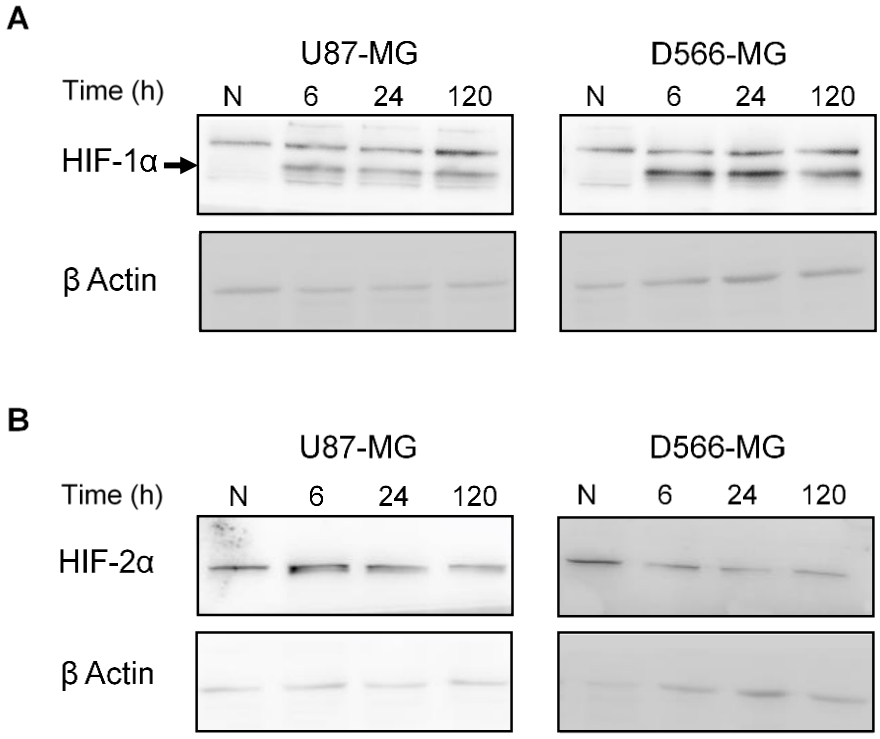

Figure 5.4: HIF-1α and HIF-2α is upregulated in chronic hypoxia. U87-MG and D566-MG cells were incubated in 1% O_2 and 21% O_2 for 0-120 h. Protein was extracted and the levels of HIF-1α and HIF-2α determined by western blotting for two independent experiments

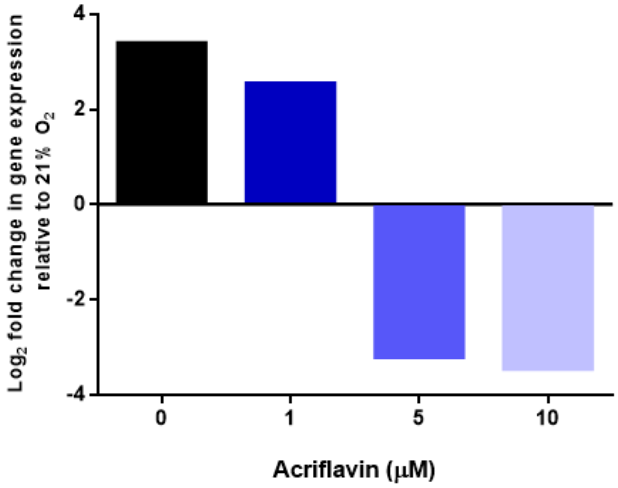

Figure 5.5: Hypoxia-induced GLUT1 upregulation is eliminated with acriflavin treatment. D566-MG cells were incubated in 0.1% O_2 with treated with 0-10 μM Acriflavin for 24 h. Control cells remained in 21% O_2. RT-PCR experiments were performed to assess GLUT1 expression levels. Data represents the fold change in GLUT1 expression relative to 21% O_2. Data are from a single experiment.

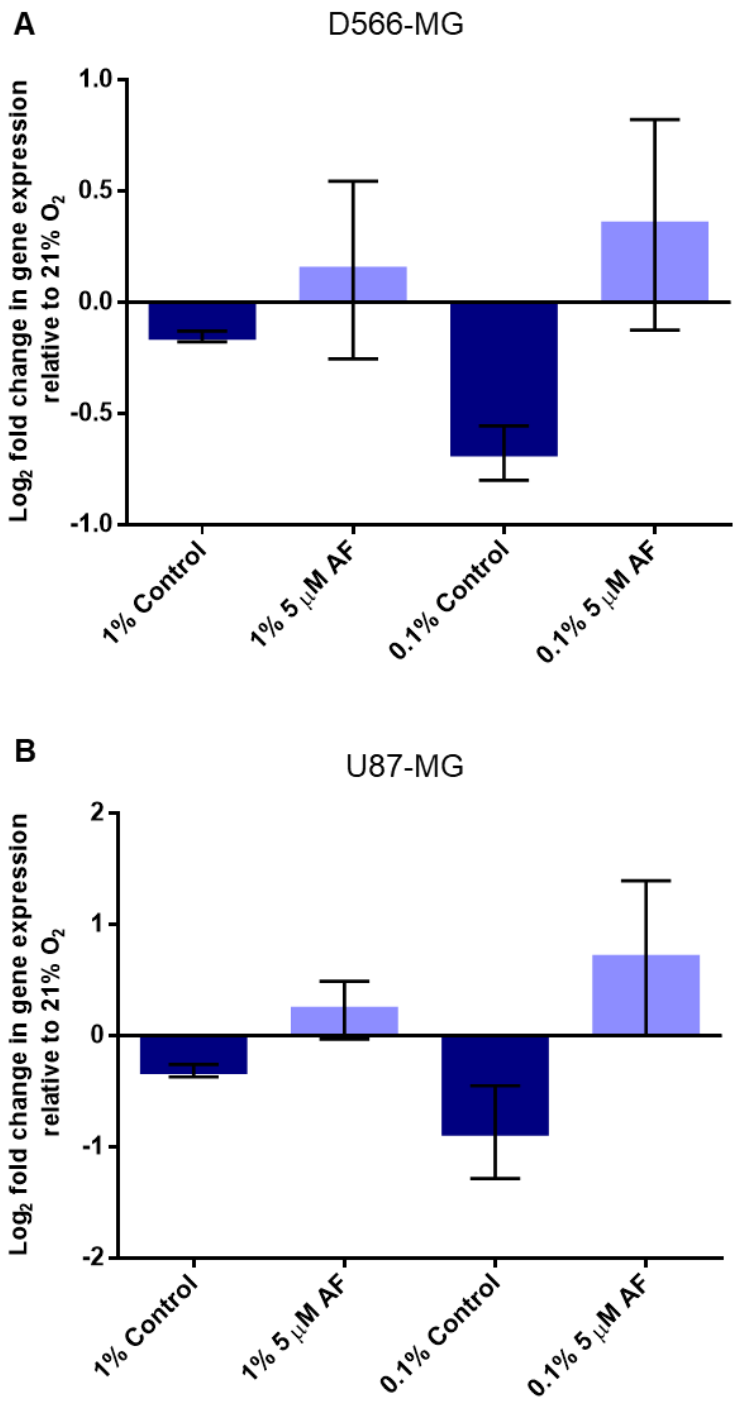

Figure 5.6: Acriflavin treatment restores LIGIV mRNA levels in hypoxia. (A) D566-MG and (B) U87-MG cells were incubated in 21% and 1% O_2 for 24 h with and without 5 μM Acriflavin. After incubation, RNA was extracted and converted to cDNA for RT-PCR experiments, probing for LIGIV. Data is represented as log_2 fold change in mRNA levels with respect to level for the 21% O_2 samples. Data are the mean of at least three independent experiments, with error bars showing S.E.M. Data not significant indicated by one-way student t-test.

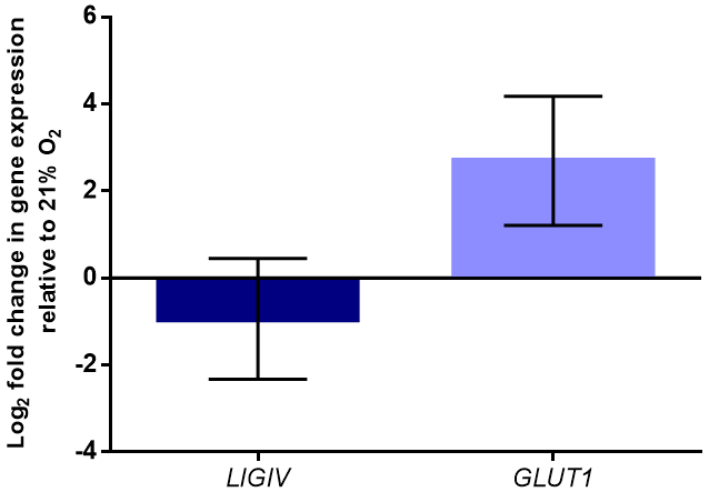

Figure 5.7: DMOG treatment induces LIGIV downregulation. D566-MG cells were treated with 0.5 mM DMOG for 24 h. RT-PCR was performed to examine the mRNA levels of LIGIV and GLUT1. Data are relative to the mRNA levels in the 21% O_2 control. Data represent the mean of three independent experiments, with error bars showing S.E.M. Data not significant indicated by one-way student t-test.

5.3.5 Development of a multiphoton laser microirradiation protocol

Assessment of the recruitment of DNA repair factors to the nucleus has traditionally been accomplished with IRIF and laser microirradiation studies. IRIF has provided a wealth of data, specifically for DSB repair, and is commonly favoured due to the simplistic protocols and opportunities for high throughput assessment. However, use of an ionising radiation source is essential to induce foci formation. Etoposide and phleomycin were investigated to determine whether they could induce foci of NBN and MRE11, yet no foci was observed (appendix 1.11). Therefore, without an ionising irradiation source, these foci formation assays are challenging. Alternatively, laser microirradiation can be employed.

Ligase IV and XRCC4 form a heterodimer, which is recruited to double strand breaks as part of the NHEJ pathway. A reduction of ligase IV may therefore impact the behaviour of XRCC4, and alter the effectiveness of NHEJ. To explore the impact of hypoxia on XRCC4 kinetics, a multiphoton laser microirradiation protocol was developed

5.3.5.1 Optimisation of multiphoton laser to induce DNA damage

Within the Centre for Cell Imaging at the University of Liverpool, laser microirradiation for DNA damage studies had not yet been attempted. Therefore, optimisation was required in order to ensure that 1) recruitment of EGFP-XRCC4 was identifiable and 2) cells were not excessively damaged during experimentation. The initial optimisation was conducted in HeLa cells, due to ease of transfection and suitability for live cell imaging.

Work by Träutlein *et al* determined that irradiating with long wavelengths (1050 nm) could selectively induce DNA breaks, with a reduction in unwanted cyclobutane-pyrimidine dimers (Träutlein *et al.*, 2009). Therefore, irradiation with the Ti:Sapphire multiphoton laser, was done using various wavelengths

to determine whether EGFP-XRCC4 recruitment to the damage site could be observed. Irradiation with long wavelengths (900 nm and above) resulted in no observable recruitment of EGFP-XRCC4, even with increased power (Figure 5.8). A common characteristic of the multiphoton laser is a decreasing power output with increasing wavelength, therefore observing reduced or no visible EGFP-XRCC4 recruitment is not surprising. Increasing the laser iterations (number of times laser hits the sample) can result in higher energy delivery. However, a high number of iterations increases the time required to irradiate the cell. Therefore, increasing the iterations further (over 100) for longer wavelengths is not ideal. Previous publications successfully induced DNA damage at high wavelengths (1050 nm) (Träutlein *et al.*, 2009). However, lasers can vary, with differences in pulse length and overall energy output.

Irradiating with shorter wavelengths (700-850 nm) successfully induced EGFP-XRCC4 recruitment (Figure 5.8). After irradiating with the 700 nm laser, in some cases, recruitment was very rapid and not localised specifically to the damage region. This could suggest that proteins are aggregating rather than recruiting, likely due to the high-power output with shorter wavelengths. Therefore, an 800 nm laser was chosen for future experiments (Figure 5.9), as irradiating with this wavelength created distinct regions of the recruited protein.

Further optimisation of irradiation with the 800 nm laser was conducted to determine the minimum laser power and iterations required to observe EGFP-XRCC4 protein recruitment reliably. Ideally, fewer iterations are preferable to reduce the time taken to irradiate, therefore 20 iterations were chosen. Over time, the efficiency of a laser can alter due to several variables such as alignment, age, usage etc. therefore, it was necessary to directly measure the laser power output with a laser power meter rather than relying on the arbitrary percentages of the acquisition software. The optimal power

output required to induce EGFP-XRCC4 recruitment was 10 mW. Due to the high-powered nature of a multiphoton laser, it is possible to create direct structural damage to cells and tissue. However, this was not the case with the optimised settings. The transmitted light images obtained showed no alterations to the nucleus at the site of irradiation (Figure 5.9). Additionally, after irradiation cells were left for 1-2 hours to recover, before observing their general appearance. The irradiation protocol did not appear to kill cells, nor did it have a negative impact on the overall observed cell morphology.

After several optimisation steps, a laser microirradiation protocol with a multiphoton laser was successfully developed. Using the optimised parameters (800 nm, 10 mW, 20 iterations), EGFP-XRCC4 recruitment was observed with no direct impact on the structural integrity of the cell or induction of cell death. Ideally, a longer wavelength is desirable due to the reduction in unwanted DNA damage types (Träutlein *et al.*, 2009), yet this was not possible with this specific laser. However, using a multiphoton laser is beneficial due to no requirement for sensitisers and an overall reduced photo-toxicity, making this method favourable compared to traditional UVA lasers.

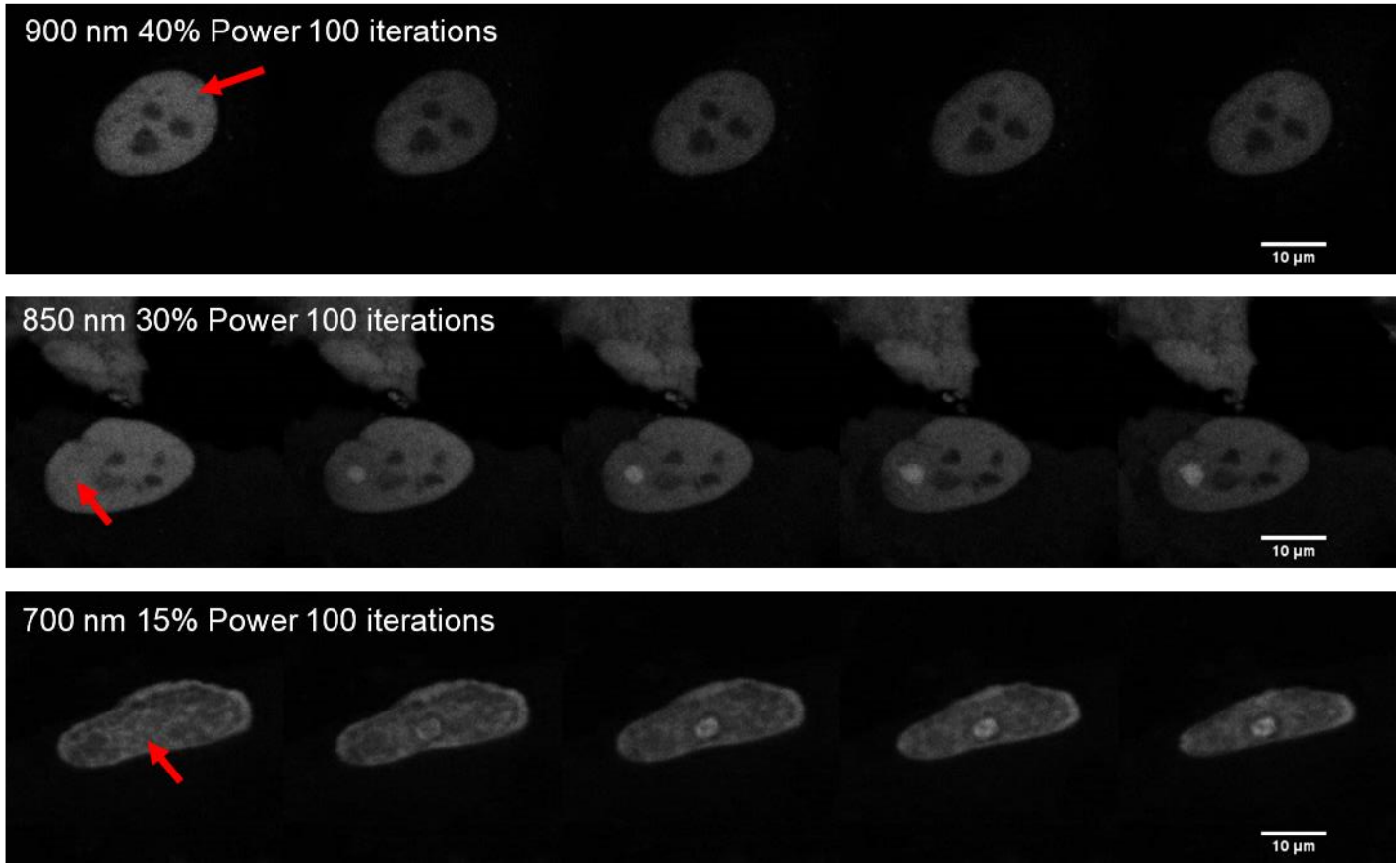

Figure 5.8: Optimisation of multiphoton DNA damage induction. HeLa cells were transfected with EGFP-XRCC4. EGFP signal was excited with a 488 nm laser and imaged using a 40x objective and 5x zoom. A specified region of interest was irradiated with a multiphoton laser (700 nm – 900 nm), with variable powers and iterations. Subsequent to irradiation, cells were images in 15-second intervals. Red arrow signals region of irradiation.

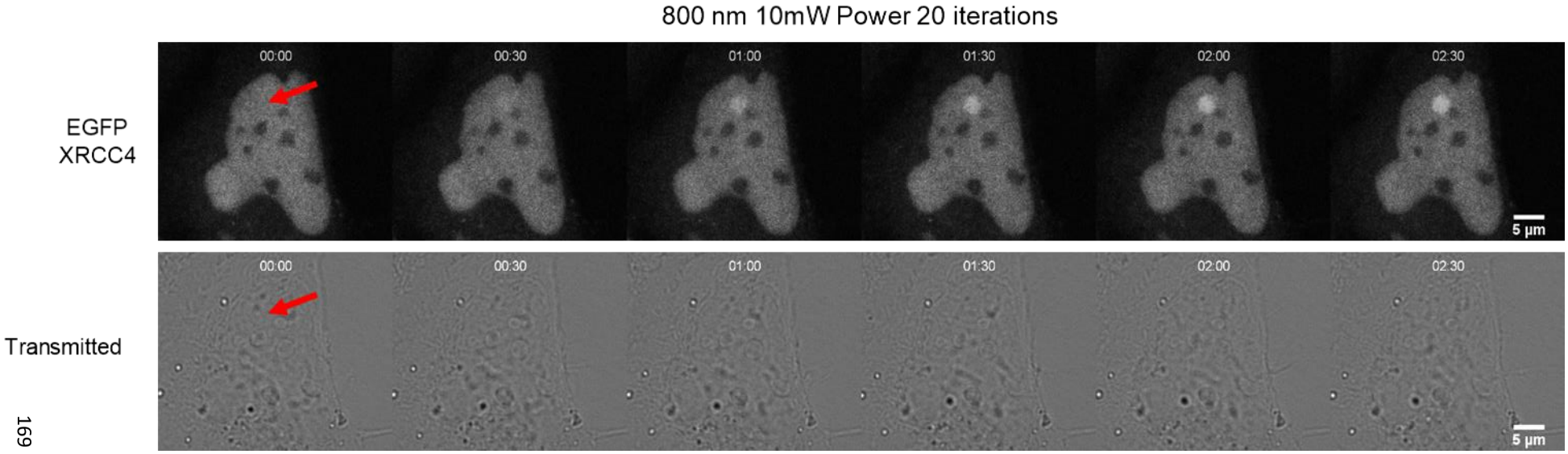

Figure 5.9: Irradiation with an 800 nm laser has minimal impact on cellular structural integrity. HeLa cells were transfected with EGFP-XRCC4. EGFP signal was excited with a 488 nm laser and imaged using a 40x objective and 5x zoom. A specified region of interest was irradiated with an 800 nm multiphoton laser at 10 mW power with 20 iterations. Fluorescent and transmitted images were acquired at 30-second intervals post-irradiation. Red arrow signals region of irradiation.

5.3.6 Comparing XRCC4 kinetics in normoxic and hypoxic GBM cells

D566-MG cells displayed the highest number of hypoxia-induced changes to DNA repair gene expression. Therefore, these cells were used in the laser microirradiation experiments to assess XRCC4 recruitment. In preliminary testing, D566-MG responded similarly to HeLa with the optimised laser settings. However, using D566-MG resulted in several challenges. Firstly, in comparison to HeLa cells, D566-MG transfected poorly. Therefore, transfection was optimised to ensure a sufficient number of cells were transfected with EGFP-XRCC4 without negatively affecting cell health. In addition, imaging D566-MG was difficult as the cells moved excessively, causing them to travel out of the field of view after a short period. Therefore, the length of image acquisition had to be limited to 20 minutes. However, this was sufficient to observe the recruitment of EGFP-XRCC4 (Figure 5.10 A).

In order to determine the impact of hypoxia on XRCC4 kinetics, D566-MG cells were pre-incubated in 21% or 1% O_2 for 5 days, before transfecting with EGFP-XRCC4. An 800 nm laser (10 mW, 20 iterations) was used to create DNA damage in a 2 µm region of the nucleus, and images acquired (488 nm laser) in 15 s intervals over 20 minutes (Figure 5.10 A). Imaging and laser microirradiation was conducted in 21% O_2, to ensure the oxygen environment did not influence the extent of DNA damage induced by the laser. For each cell imaged, signal intensity of the damaged spot was measured for each frame and normalised to the background and to non-irradiated sections of the nucleus (see methods 2.15.1 for details), using Matlab scripts for batch processing (appendix 1.4 & 1.5). The normalised intensity at each time point was determined for each cell, defined here on out as a 'trace' (Figure 5.10 C, B). As expected, there is significant variation between each trace within datasets, in part due to imaging noise as well as cell-to-cell variability. However, when the average of each trace is determined, the variation (standard error of the mean) was similar between hypoxic and normoxic cells (Figure 5.11).

Overall, in normoxic and hypoxic cells, EGFP-XRCC4 was recruited within 480 – 600 s (8 – 10 minutes). This is significantly slower than other components of the NHEJ, such as Ku70/80, which reached maximal accumulation after ~3 minutes (Mari *et al.*, 2006). However, recruitment of XRCC4 first requires the recruitment of Ku70/80 and DNA-Pkcs, followed by DNA end processing. Therefore, a delay in XRCC4 recruitment compared to Ku70/80 was expected. Interestingly, normoxic cells (Figure 5.11 A) reached a higher peak intensity (i.e. recruit more protein) than hypoxic cells (Figure 5.11 B). This is unlikely due to differences in protein levels within the cells, as the fluorescent signal does not fully deplete from the surrounding un-damaged nucleus. In general, DNA repair proteins are in excess to ensure rapid recruitment of proteins when DNA damage occurs. Therefore, it is possible that some of the XRCC4 recruited to the DNA damage site might not be complexed with ligase IV. During experimentation, cells were preferentially selected for low GFP signal, to reduce the pool of un-complexed XRCC4. However, it is not possible to completely separate the recruitment of complexed and un-complexed XRCC4 experimentally. Therefore, it is important to note that the recruitment of un-complexed XRCC4 may dampen any impact of hypoxia on complexed XRCC4 kinetics.

After the initial accumulation of EGFP-XRCC4, rapid loss of protein occurs. This is thought to be indicative of DSB repair (Mari *et al.*, 2006). In normoxia, dissociation of EGFP-XRCC4 appears to be quicker (steeper slope) than hypoxia, suggesting that DSB repair may be delayed in hypoxic cells. However, in order to fully assess and compare the recruitment/dissociation of EGFP-XRCC4, parameters representing EGFP-XRCC4 kinetics need to be measured for each trace individually, rather than examining the population as a whole. Each trace was divided into two features, protein recruitment and protein dissociation (Figure 5.12), which was the focus of further analysis.

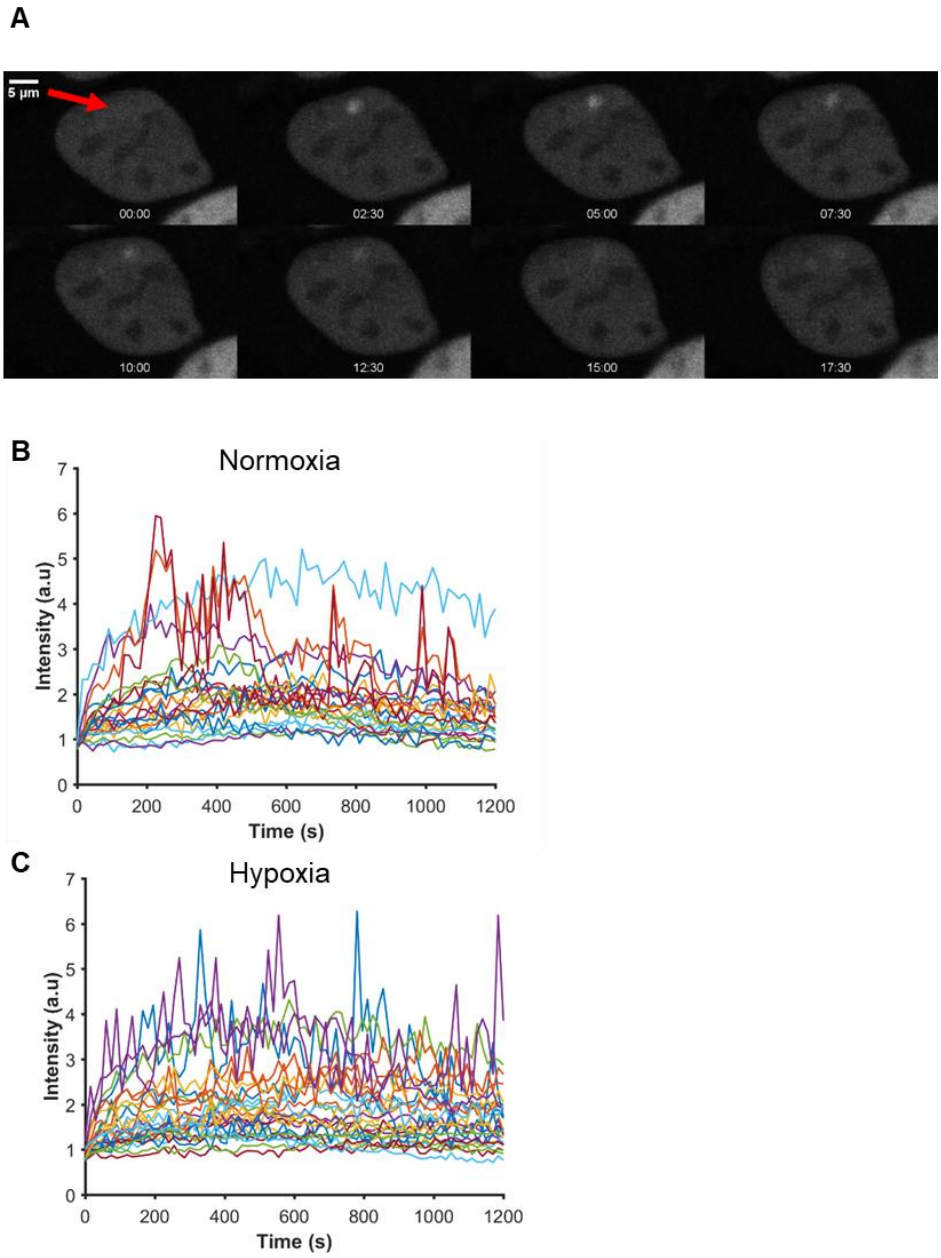

Figure 5.10: XRCC4 protein dynamics in GBM cells. D566-MG cells were pre-incubated in 21% or 1% O_2 for 5 days before EGFP-XRCC4 transfection. EGFP signal was excited with a 488 nm laser and imaged using a 40x objective and 5x zoom. A 2 µm region was irradiated with the nucleus with an 800 nm multiphoton laser (10 mW, 20 iterations). Images were acquired at 15-second intervals for 20 min post-irradiation. (A) Representative images of an irradiated cell. The red arrow indicates the irradiated region. (B, C) Intensity of the irradiated region was measured using Image J. Measured signal was background subtracted and normalised to the pre-damage intensity (see methods). Normalised intensity for B) normoxic (n = 22) and (C) hypoxic cells (n =27) were plotted.

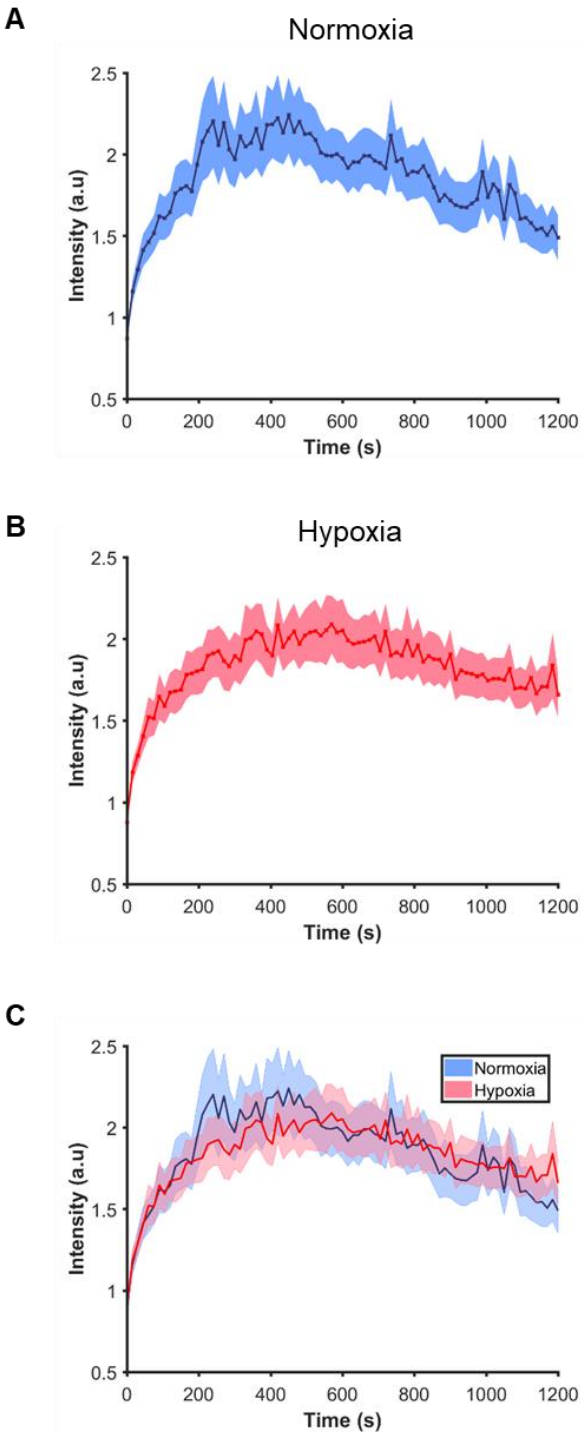

Figure 5.11: Mean normalised intensity of all irradiated cells. D566-MG cells transfected with EGFP-XRCC4 were subjected to laser microirradiation. Signal intensity was measured for each cell and normalised to several parameters (see methods). The mean signal intensity was calculated for all (A) normoxic (n = 22) and (B) hypoxic cells (n = 27), which was plotted (solid line). The shaded region represents the standard error of the mean. (C) An overlay of the hypoxic and normoxic data.

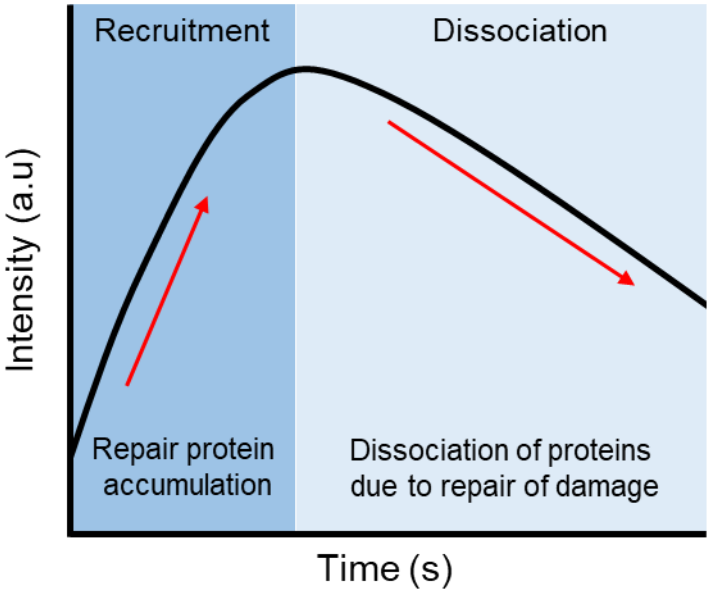

Figure 5.12: Schematic of the features of the intensity plots. After laser microirradiation, signal intensity rapidly increases due to protein recruitment, followed by a steady dissociation of protein from the irradiated site.

5.3.6.1 Assessment of XRCC4 recruitment

To determine whether pre-incubation in hypoxia influences XRCC4 recruitment, D566-MG cells were pre-incubated for 5 days in 21% or 1% O_2 and subjected to the laser microirradiation protocol (Figure 5.13). Recruitment of protein can be described by a first order response to a step change, whereby XRCC4 recruitment is a function of the time-dependent generation of double strand breaks. This enables the fitting of a first order differential equation (see methods 2.15.1), from which parameters can be derived. Specifically, the time to 50% accumulation was determined for each trace (Figure 5.13 A). A similar time to 50% accumulation was obtained for hypoxic and normoxic cells, with 125 s and 167 s and respectively (Figure 5.13 B). This difference was not statistically significant and relatively small (42 s) with respect to the total 8-10 minutes required for recruitment. This is exemplified by the fact that both

normoxic and hypoxic datasets have a similar overall distribution (Figure 5.13 C), with the majority of data points below 200 s. Additionally, the time to time to maximal recruitment (intensity) was also determined for the normoxic and hypoxic dataset, which showed a similar results for both conditions (appendix 1.12).

By fitting a first order differential equation, the recruitment time constant (τ) can be determined, which provides insight into the recruitment kinetics of XRCC4. In hypoxic cells, the recruitment of XRCC4 is similar to normoxia, with recruitment constants of 180.3 s and 204.9 s respectively (Table 5.1). This correlates with the time required to reach 50% intensity, supporting the notion that recruitment of XRCC4 to DSB is similar regardless of pre-incubation conditions. Therefore, hypoxia does not significantly impact XRCC4 recruitment.

Table 5.1: EGFP-XRCC4 recruitment constant in D566-MG

Condition	Mean τ (s)	S.E.M	Significant?
Normoxia	240.9	60.14	N/A
Hypoxia	180.3	35.65	No; p=0.3913

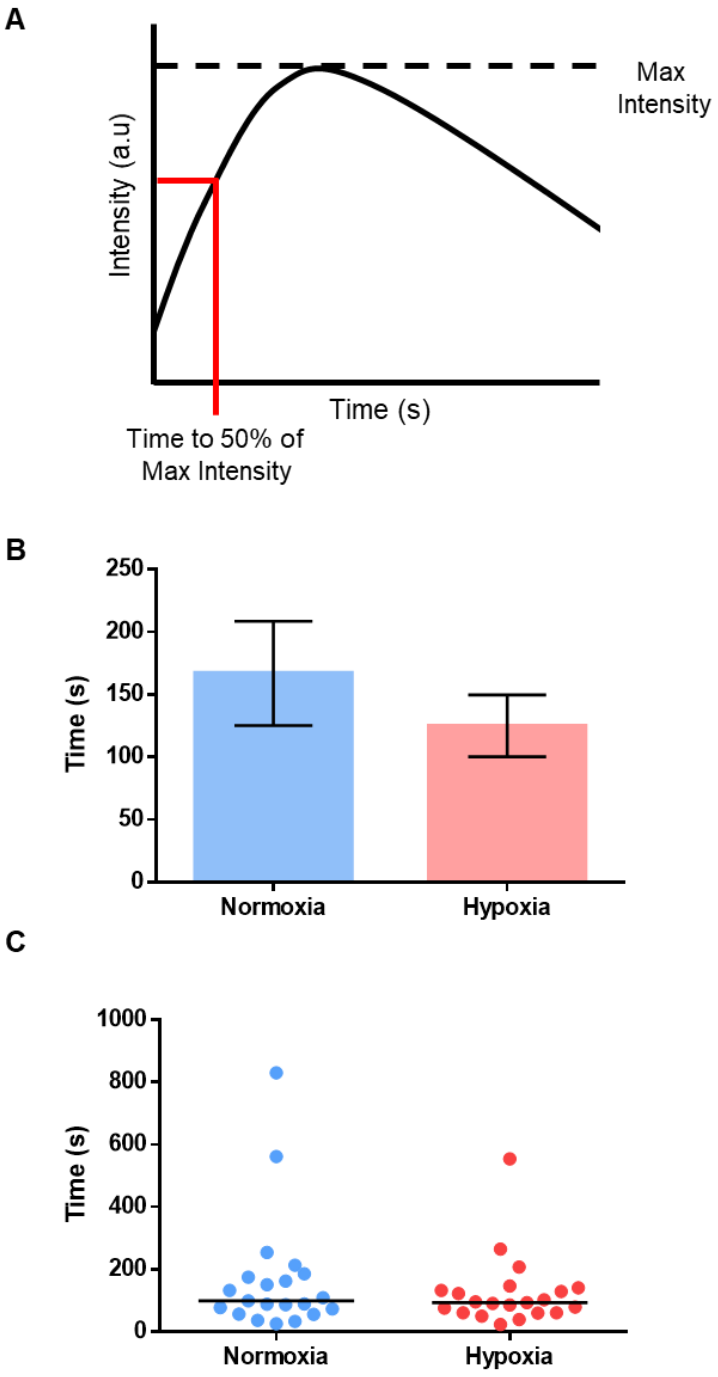

Figure 5.13: Time to 50% of maximum intensity. D566-MG cells transfected with EGFP-XRCC4 were subjected to laser microirradiation. Signal intensity was measured for each cell. A first-order differential equation was fitted to normalised signal intensity, to determine the time to 50% of maximum intensity, as depicted by the schematic (A). (B) The mean time to 50% intensity for normoxic (n = 21) and hypoxic (n = 21) cells was determined, with error bars representing S.E.M. (C) The distribution of time to 50% intensity for each hypoxic and normoxic cell. The line represents the median. Data not significant indicated by student t-test.

5.3.6.2 Assessment of XRCC4 dissociation

Once repair of a DSB by NHEJ is complete, repair proteins dissociate from the damage site. Little is known regarding the signals that initiate dissociation. Hypoxia my impact XRCC4 dissociation, potentially due reduced ligation events as a result of Ligase IV downregulation. To explore this, D566-MG cells were pre-incubated in 21% or 1% O_2 for 5 days before laser microirradiation. For each normalised trace produced, an exponential decay curve (see methods 5.15.1) was fitted after the peak intensity, and the time taken for 50% of the total protein to dissociate determined (Figure 5.14). In hypoxic cells, the mean time to 50% dissociation was higher than normoxia, with 813 s and 582 s respectively (Figure 5.14 B). However, the data was not statistically significant. A similar distribution of data was observed for both conditions, with a higher median for hypoxia, correlating with the increased mean (Figure 5.14 C). The rate of EGFP-XRCC4 loss from the irradiated site can be determined by the slope of the exponential decay curve, expressed as a.u s^{-1} (Figure 5.15 A). In hypoxic D566-MG, the rate of protein dissociation was less (slower protein dissociation) than normoxia, with a mean rate of 4.66 x 10^{-4} a.u s^{-1} and 7.96 x 10^{-4} a.u s^{-1} respectively (Figure 5.15 B). This correlates with the longer time taken for hypoxic cells to have 50% of recruited protein dissociated.

Overall, in hypoxia, it takes longer to achieve dissociation of 50% of the protein from the irradiation site. This is exemplified by the reduced rate of signal loss in hypoxic cells compared to normoxic cells. These results suggest that NHEJ may be less efficient in hypoxia.

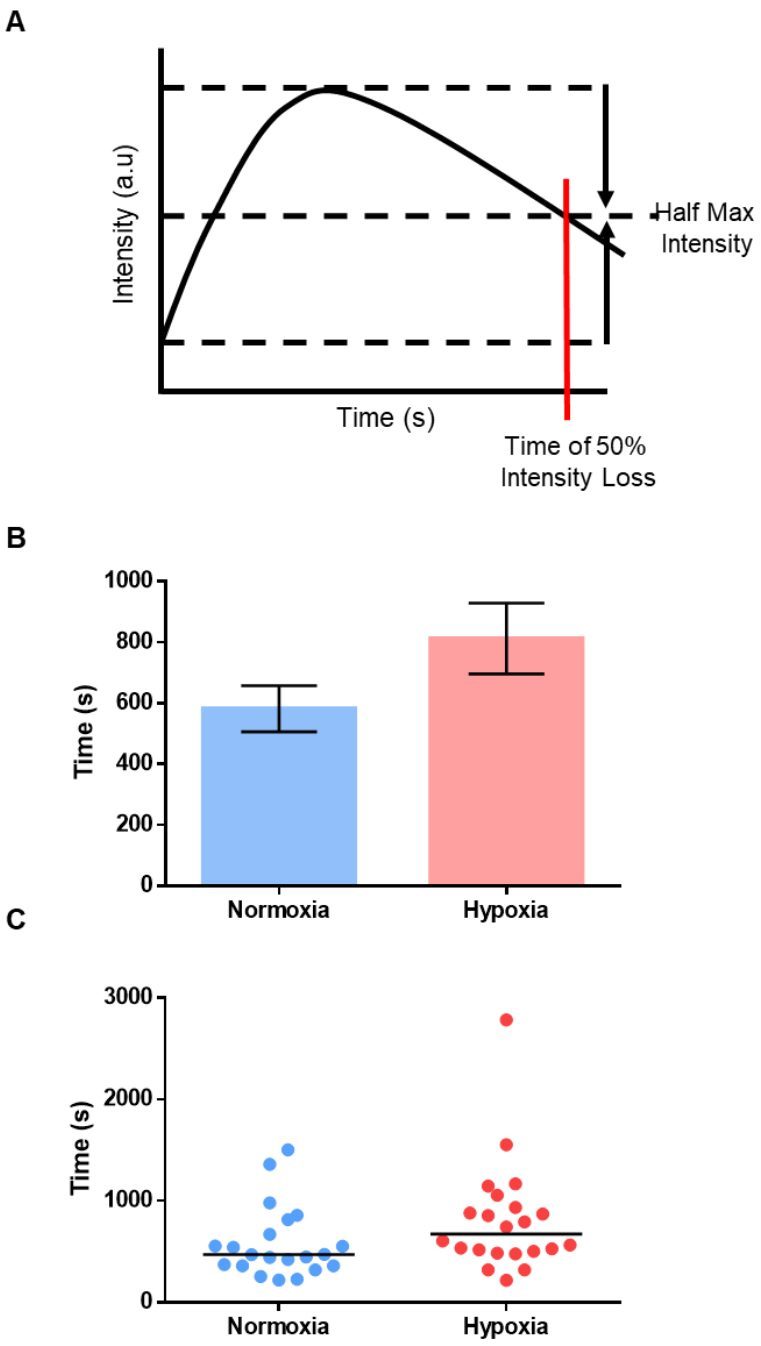

Figure 5.14: Time to 50% intensity loss. D566-MG cells transfected with EGFP-XRCC4 were subjected to laser microirradiation. Signal intensity was measured for each cell. Normalised signal intensity was used to determine the time at which half of the maximal intensity is lost as depicted by the schematic in (A). (B) The mean time to half maximum intensity for normoxic (n = 21) and hypoxic (n = 22) cells was determined, with error bars representing S.E.M. (C) The distribution of time to half-maximal intensity for each hypoxic and normoxic cell. The line represents the median. Data not significant (with and without outliers) indicated by student t-test.

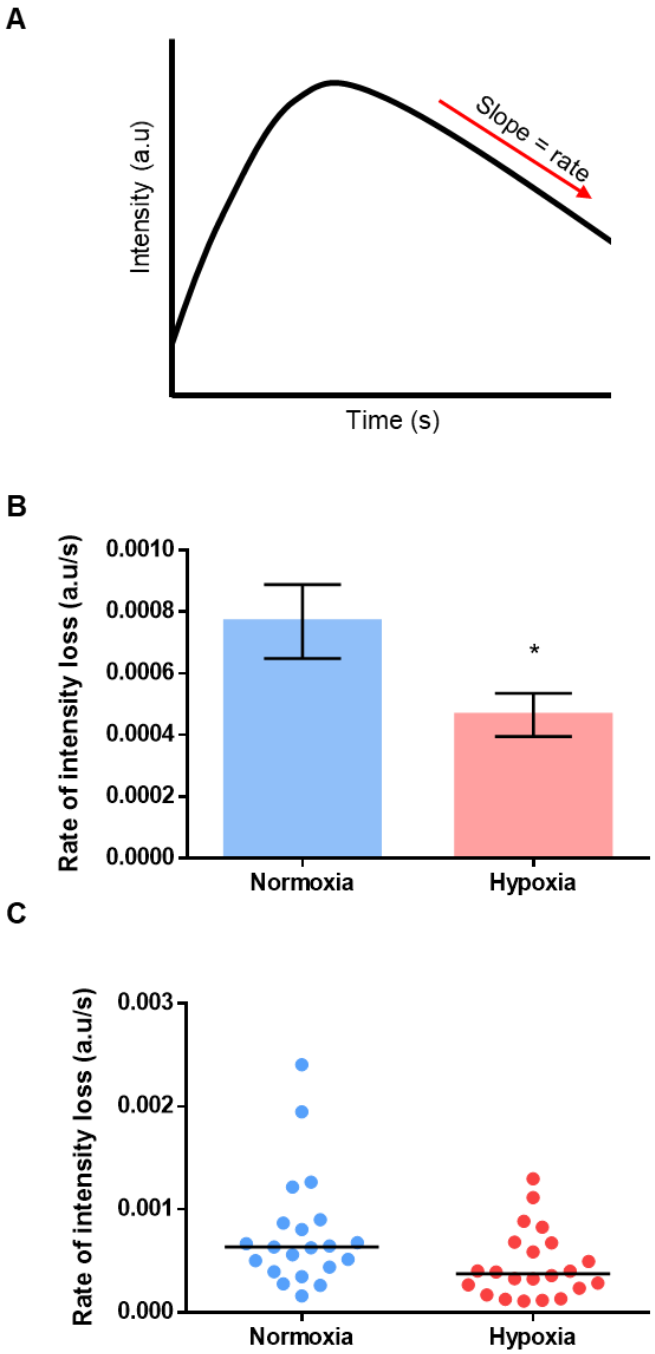

*Figure 5.15: The rate of protein dissociation. D566-MG cells transfected with EGFP-XRCC4 were subjected to laser microirradiation. Signal intensity was measured for each cell. Normalised signal intensity was used to determine the rate of protein dissociation as depicted by the schematic in (A). (B) The rate for normoxic (n = 21) and hypoxic (n = 22) cells was determined, with error bars representing S.E.M. (C) The distribution of the rate of dissociation for each hypoxic and normoxic cell. The line represents the median. * denotes significant data where p<0.05 indicated by student t-test. Data remains significant after outliers removed.*

Development of a multiphoton laser irradiation protocol has enabled the successful assessment of XRCC4 behaviour in hypoxic and normoxic cells. Overall, hypoxic D566-MG have a similar rate of EGFP-XRCC4 recruitment, yet a slower dissociation of the protein away from the damage site, suggesting a reduced efficiency of repair. Ideally, to examine this further, a longer acquisition period would be required to better measure the characteristics of XRCC4 dissociation. For example, Mari *et al* determined that 20% of recruited Ku protein remain 2 h post damage, which was similar to the level of damage remaining 2 h after ionising radiation (Mari *et al.*, 2006). However, extending imaging periods was challenging due to cell movement out of the field of view. Significant time and effort was given to optimisation and this challenge was solved by using tile scanning and image stitching, to obtain a larger field of view, without losing magnification. However, unfortunately, due to multiple technical issues with equipment (loss of laser power, laser misalignment and other optical problems), this work had to cease, as it was becoming too time consuming in terms of troubleshooting. The laser irradiation protocol is a highly sensitive procedure; therefore, small changes in the instrument can significantly influence the extend of DNA damage and subsequent recruitment.

Further experiments that were planned included the knockdown of ligase IV to determine whether hypoxia-induced ligase IV downregulation could be causing the altered XRCC4 kinetics. Also, fluorescence recovery after photobleaching (FRAP) of the recruited EGFP-XRCC4 would have given an interesting insight into the movement of XRCC4 within the nuclear compartment, and the extent of immobilisation. As further experimentation with the laser microirradiation protocol was not possible, an end joining assay was employed as an alternative assay for NHEJ activity.

5.3.7 The impact of hypoxia on DNA end joining

Experimental techniques to directly assess cellular end joining capabilities are limited. However, plasmid end joining assays have recently been developed. For example, Nagel *et al* engineered a florescent constructs, which enabled the assessment of NHEJ (Nagel *et al.*, 2014). Bindra *et al*, utilised a luciferase-based 'end joining' (religation) assay to compare NHEJ capacity in normoxic and hypoxic cells (Bindra *et al.*, 2005). Therefore, to assess the impact of hypoxia on end joining a similar approach was adopted.

A luciferase expressing plasmid (CMV-pGL4.16) was linearised using a HindIII restriction enzyme (Figure 5.16 A). The HindIII restriction site lies between the CMV promoter and the start of the luciferase gene; therefore in order for the luciferase gene to be expressed, the plasmid requires ligation. Thus, end joining activity can be measured by the assessment of luciferase activity. To determine the impact of hypoxia on end joining activity, D566-MG cells and U87-MG cells were pre-incubated in 21%, 1% or 0.1% O_2 for 1 day or 5 days, with transient transfection of the undigested and digested plasmid 24 h before assaying activity. Experimental workflow is described in Figure 5.14 B. In D566-MG cells, 1-day hypoxic incubation (1% and 0.1% O_2) resulted in a significant increase in luciferase activity, thus end joining was enhanced (Figure 5.16 A). For example, in cells incubated in 0.1% O_2, there was a 1.9 fold increase in luciferase activity compared to normoxia (Figure 5.17 A). Similarly, for D566-MG cells incubated for 5 days in hypoxia, higher luciferase activity was observed with 3.0 and 2.7 fold change for 1% and 0.1% O_2 respectively (Figure 5.18 A). In contrast, U87-MG displayed no significant change in end joining activity after acute hypoxic exposure (Figure 5.17 B). However, after chronic exposure (5 days), cells pre-incubated in 0.1% O_2 had a 1.5 fold increase in end joining activity, which was statistically significant ($p = 0.0134$) (Figure 5.18 B).

Overall, both acute and chronic exposure results in increased end joining in D566-MG, whereas, U87-MG cells required chronic severe hypoxia (5 days 0.1% O_2) for a similar trend to be observed. Although the end joining assay has been used in previous publications to examine NHEJ efficiency (Bindra *et al.*, 2005), the specificity of this assay for NHEJ is questionable. Firstly, the the DNA repair mechanims are acting upon plasmid DNA which is not consricted in nucleosomes, as with endogenous DNA. Thus the end joining activities may be different. Additionally, multiple DNA ligase enzymes exist within the cell, which would have the ability to religate the digested plasmid. Therefore, there is no direct specificity for ligase IV. Hypoxia could enhance the activity or levels of other DNA ligases, which may cause the increase in ligation activity. In order to determine the specificity of the end joining assay, inhibition of the NHEJ pathway or knockdown of *LIGIV* would be ideal. In 2012, SCR7, a potential chemical inhibitor of NHEJ was identified, which was thought to selectively inhibit DNA ligase IV (Srivastava *et al.*, 2012). However, in 2016 SCR7 was found not to be ligase IV specific, nor did it significantly inhibit NHEJ (Greco *et al.*, 2016). Similarly, when SCR7 was applied to the luciferase end joining assay, no difference in luciferase activity was observed (data not shown). Therefore, there is currently no commercially available inhibitor of NHEJ.

Since the specificity of the end joining assay for NHEJ is debatable, significant conclusions on the impact of hypoxia on NHEJ cannot be drawn. In contrast, the laser microirradiation assay specifically examined NHEJ proteins, and suggested that NHEJ may be less effective in hypoxic GBM as hypothesised.

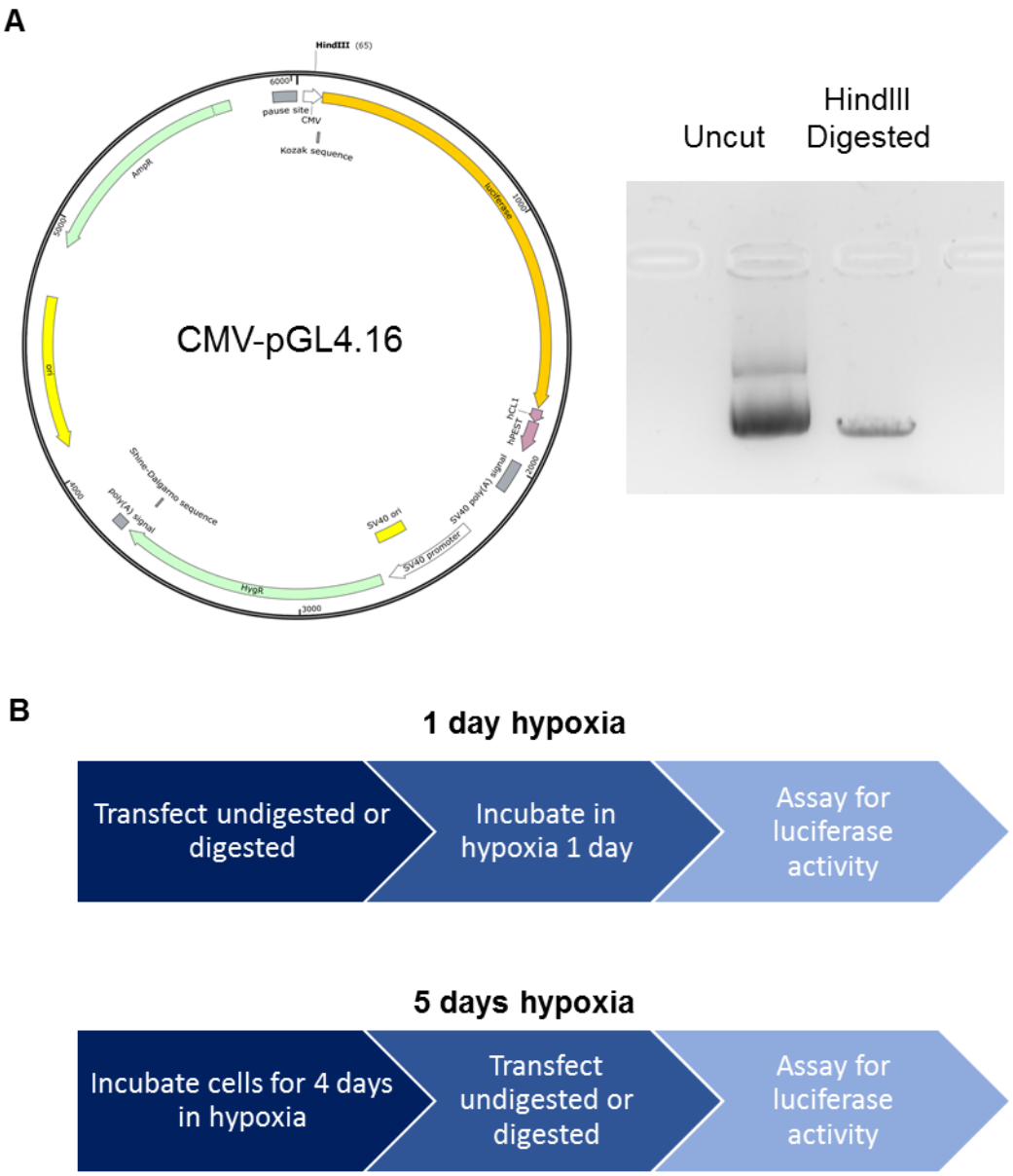

Figure 5.16: The end joining assay protocol. (A) Schematic of the CMV-pGL4.16 plasmid encoding a luciferase gene used in the end joining assay. HindIII was used to digest the plasmid, with successful digest tested by DNA gel electrophoresis. (B) Schematic detailing the protocol for cells incubated for 1 day or 5 days in hypoxia, whereby transient transfection of the undigested and digested plasmid was done 24 h before assaying luciferase activity.

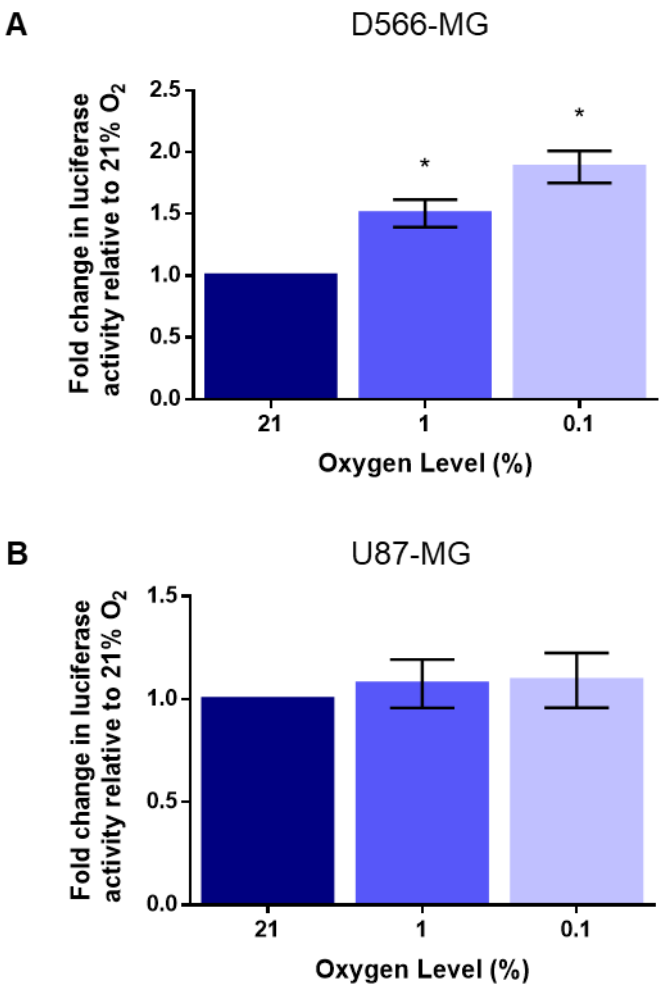

*Figure 5.17: End joining activity in acute hypoxia. (A) D566-MG and (B) U87-MG cells were transfected with HindIII digested CMV-pGL4.16, before incubation in 21%, 1% and 0.1% O_2. After 24 h, cells were lysed and subjected to a luciferase assay. Data were normalised to signal from un-digested CMV-pGL4.16, before calculating fold changes relative to 21% O_2 samples. Data are representative of the mean for at least three independent experiments, with error bars showing S.E.M. * denotes significant data where $p<0.05$ indicated by one-way student t-test.*

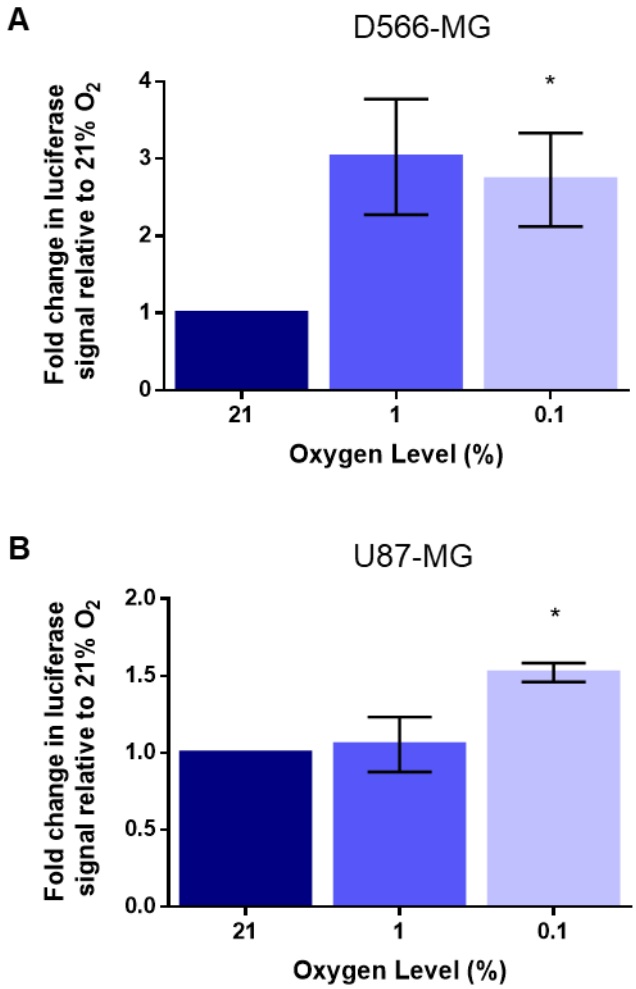

*Figure 5.18: End joining activity in chronic hypoxia. (A) D566-MG and (B) U87-MG cells were pre-incubated in 21%, 1% and 0.1% O_2 for 4 days followed by transfection of HindIII digested CMV-pGL4.16 for 24 h. Cells were then lysed and subjected to a luciferase assay. Data were normalised to signal from un-digested CMV-pGL4.16, before calculating fold changes relative to 21% O_2 samples. Data are representative of the mean for at least three independent experiments, with error bars showing S.E.M. * denotes significant data where $p<0.05$ indicated by one-way student t-test.*

5.4 Discussion

A rapid response to DNA damage is essential to maintain genome integrity. Small alteration to repair mechanisms, through a reduction in available repair proteins can be catastrophic, leading to reduced repair efficacy and the accumulation of DNA damage. Genetic and environmental factors can affect DNA repair proteins, such as tumour hypoxia, which can cause changes to transcription, translation and post-translational modifications of essential repair proteins. The expression of the *LIGIV* gene, encoding DNA ligase IV, a critical component of NHEJ, is reduced in hypoxic GBM. This resulted in an altered response to DNA damage, which might have significant clinical consequences. However, examining the impact of reduced levels of DNA repair proteins can be challenging.

5.4.1 Laser microirradiation for DNA repair studies

Laser microirradiation during live cell imaging is a popular technique in DNA repair studies enabling the assessment of DNA repair protein recruitment in live cells. To some degree, the classical technique of irradiation-induced foci formation, has been overtaken by laser microirradiation, in part due to the limited repertoire of factors that can be explored with IRIF (Kong *et al.*, 2009). Mari *et al* first described the use of laser microirradiation for examination of NHEJ. Using a multiphoton laser to induce DNA damage, the group observed recruitment of Ku80, DNA-Pkcs, ligase IV and XRCC4, which co-localised with γH2AX, an indicator of DSB. Additionally, the Ku80 dissociation kinetics were established, which signified repair of the DSB, and Ku70/80 was found to be essential for XRCC4 recruitment (Mari *et al.*, 2006). Using a similar laser-based approach, in the current study, reduced levels of ligase IV were found to impact XRCC4 dissociation.

Whilst laser microirradiation studies have provided valuable insight into the NHEJ repair pathway, many limitations remain. Specifically, UVC lasers

require sensitizers, which can alter chromatin structure, impact cell metabolism, and result in DNA damage after illumination with visible light (Turner and Denny, 1996; Wojcik and Dobrucki, 2008; Solarczyk *et al.*, 2012). Lasers absorption also occurs along the whole irritated path, not just the focal plane, causing further nuclear damage above and below the area of interest (Ferrando-May *et al.*, 2013). These issues can be avoided to some extent by using tuneable near-IR lasers (multiphoton), which have increased spatial resolution and reduced toxicity, without the need for sensitisers (Meldrum and Botchway, 2003). IRIF remains a popular experimental choice, due to extensive characterisation of ionising irradiation induced DNA damage, examination of endogenous protein and the ability to perform high-throughput experiments. In contrast, laser microirradiation coupled with fluorescence confocal microscopy provides dynamic measurement of recruitment, dissociation and immobilisation (by using FRAP) of DNA repair proteins in live cells.

5.4.2 Measuring DNA repair - challenges

Although a number of techniques are available to assess DNA repair, such as laser microirradiation or IRIF, these are often limited and pose significant experimental challenges. For IRIF, antibodies are required to detect repair proteins, yet a large number of repair components do not have specific commercially available antibodies. Additionally, tools such as the homologous recombination assays require the transfection of multiple constructs with a high transfection efficiency (Nakanishi *et al.*, 2011), yet this is not always possible for all cell types. For some DNA repair pathways, such as DSB repair, several tools are available to explore repair capacity. However, fewer options are available for other pathways such as mismatch repair (MMR). In Chapter 4, PMS2, a key component of MMR was shown to be downregulated in hypoxic GBM cells. Exploring the functional impact of this change is challenging with limited assays available. Plasmid-based MMR assays have been reported in the literature, yet these require complex and time-consuming

molecular biology, as well as highly efficient transient transfection (Lei *et al.*, 2004). Further development of DNA repair assays is required to enable rapid high-throughput analysis of DNA repair capacity of multiple DNA repair pathways. Nagel *et al*, has come somewhat close to making this a reality, by engineering several reporter constructs with varying DNA damage types, which activate different repair pathways including MMR, BER, HRR and NHEJ. Using these constructs, Negal *et al* were able to measure DNA repair capacity of multiple DNA repair pathways in primary GBM cells. Technology like this brings us one step closer to high-throughput assessment of DNA repair. This would enable further understanding of the impact of hypoxia-induced changes to DNA repair proteins, such as *LIGIV* downregulation, and the potential influence on cancer treatment.

5.4.3 Consequences of *LIGIV* downregulation for NHEJ

DNA ligase IV is essential for efficient re-ligation of DNA strands during NHEJ. Reduced ligase IV activity can lead to the accumulation of DNA damage, genomic instability, and the induction of apoptosis. In the current study, *LIGIV* was downregulated in hypoxic GBM cells. Similarly, hypoxia-induced *LIGIV* downregulation has previously been identified in prostate cancer cells (Meng *et al.*, 2005), yet the molecular mechanism behind this reduction has not yet been identified. Here, it was determined that *LIGIV* downregulation was likely to be HIF dependent and potentially caused reduced NHEJ activity, as shown by the slow dissociation upon laser microirradiation-induced damage. This could lead to the accumulation of DSB after DNA damage. Sharpless *et al* observed that loss of a single copy of *LIGIV* resulted in the formation of chromosomal aberrations, arising from DSB (Sharpless *et al.*, 2001). Additionally, with reduced ligase IV levels the fidelity of NHEJ is compromised, as ligase IV plays an important role in end protection, preventing nucleotide loss (Smith *et al.*, 2003). In the absence of efficient NHEJ, microhomology-mediated end joining (MHEJ) is utilised to repair breaks. MHEJ is highly mutagenic, as sequence deletions arise due to this

repair mechanism (Liang *et al.*, 2008), which could further contribute to genome instability. Overall, a reduction in ligase IV will negatively affect NHEJ, resulting in increased chromosomal aberrations, genome instability and mutagenesis. These consequences will drive tumorigenesis and can have a significant clinical impact.

5.4.4 Clinical implications of *LIGIV* downregulation

Mutations in the *LIGIV* gene give rise to DNA ligase IV syndrome, a rare autosomal recessive disorder. Common characteristics include microcephaly, immunodeficiency and increased sensitivity to ionising radiation (Altmann and Gennery, 2016). Loss of function mutations are the primary cause, such as missense mutations which reduce ligase IV functionality by ~90% (Buck *et al.*, 2006). Downregulation of *LIGIV* in tumour cells is likely to result in a similar radiosensitive phenotype observed in DNA ligase IV syndrome, which would be ideal particularly for GBM. Increased sensitivity to DNA damaging agents as a result of ligase IV knockdown has previously been explored. For example, siRNA knockdown of ligase IV sensitised A172 glioblastoma cells to temozolomide, with a 3-fold reduction in colony formation (Kondo *et al.*, 2009). Also, sensitivity to nimustine (ACNU), a chemotherapeutic agent used for recurrent GBM, increased with ligase IV knockdown (Kondo *et al.*, 2010). This could have significant implications for GBM treatment, suggesting that hypoxic GBM cells with *LIGIV* downregulation should display increased sensitivity to treatment. However, this was not the case (Chapter 3), suggesting that alternative resistance mechanisms may be masking the impact of reduced NHEJ functionality. *LIGIV* downregulation is likely causing the build-up of DSB, yet the residual damage may not be sufficient to trigger apoptosis. Alternatively, this low-level damage may lead to chromosomal aberrations, thereby driving tumour progression. To induce the radiosensitivity often associated with defects in NHEJ, knockdown or inhibition of ligase IV, may be required. This could be a potential therapeutic

option for GBM and would reduce the amount of high dose chemo- and radiotherapy required for effective treatment.

5.4.5 Concluding remarks and future work

To conclude, the laser microirradiation protocol was an invaluable and exciting tool for assessing DNA repair through observations of XRCC4 kinetics. Future development of imaging modalities, allowing for a high throughput approach will likely make this method a popular choice for DNA repair studies. *LIGIV* downregulation in hypoxia may be responsible for the reduced XRCC4 dissociation, yet further experiments would be required to confirm this. Additionally, optimisation of the comet assay would enable a thorough examination of DSB repair kinetics and would undoubtedly give deeper insight into the impact of hypoxia on repair mechanism. Although the data presented here suggests reduced NHEJ capacity, increased sensitivity to DNA damaging agents was not observed. Therefore, it is likely that the residual DSB are low level and are not inducing apoptosis.

Chapter 6: Discussion

6.1 Project overview

Work in this thesis aimed to explore the impact of hypoxia on DNA repair. A mechanism of hypoxia-induced reduction in treatment sensitivity involving double strand break recognition was proposed for some MB cells, yet found not to be universal. Alternatively, a broad exploration of DNA repair gene expression was undertaken, and the functional impact of the hypoxia-induced changes was investigated. Few DNA repair genes were regulated by hypoxia, with little commonality between cell lines. This suggests that clear-cut hypoxia-induced regulation of DNA repair may not be as prevalent as others suggest. Further development of tools for DNA repair studies as well as the use of 3D tumour spheroid models will enable additional exploration of the impact of hypoxia on DNA repair for MB and GBM. This will bridge the gap between *in vitro* 2D and *in vivo* based studies. Improving the understanding of brain tumour cell biology will aid in the development of new treatment methods, to increase overall survival rates.

6.2 The future of DNA repair studies

DNA repair is essential for maintenance of genome integrity. Dysregulation of repair leads to the build-up of mutations and genomic instability, promoting cancer progression. Assessment of the efficiency of DNA repair can be challenging, with limited experimental options suitable for varied cell types, as discussed in Chapter 5. The repertoire of tools for DNA repair studies have remained similar in the last 20 years, yet further technological advancements have enabled the recent improvement of classical techniques as well as the development of novel methods. Primarily, DNA repair is assessed through monitoring levels of DNA damage. With advancing technologies, further opportunities for highly accurate and high-throughput assessment of DNA damage is becoming a reality.

A classical technique for DNA damage assessment is the comet assay, known for high rates of variation (Collins, 2004; Azqueta and Collins, 2013), which was experienced in this thesis. Recently this commonly used technique has had a makeover. The CometChip, developed by Sykora *et al.*, increases comet assay throughput enabling the analysis of thousands of comets within a single experiment (96 well, 400-500 microwells per well). This upgraded method reduces inter- and intra- assay variability compared to slide-based methods (Sykora *et al.*, 2018). Using this technique, the authors successfully screened compound libraries for DNA damaging capabilities, highlighting its potential value in drug development studies (Sykora *et al.*, 2018). Such a technique would be useful for hypoxia and DNA repair studies, particularly when using multiple cell lines, as in this thesis. However, the comet assay assesses global DNA damage with little understanding of the genomic location. Alternatively, PCR based assays can provide insight into damage position. For example, long run real-time PCR quantifies DNA damage within specific nucleotide sequences (Lehle *et al.*, 2014). Also, mass spectrometry can identify altered DNA sequences arising due to polymerase errors (Su *et al.*, 2018). However, these methods are still limited to specific pre-selected regions of the DNA, without high nucleotide resolution.

Arguably, the gold star of DNA damage detection is DNA sequencing. Since completion of the human genome project in 2003 (Lander *et al.*, 2001; Collins *et al.*, 2004), sequencing technologies have boomed, with faster, cheaper and more precise methods available. Adoption of sequencing for DNA repair studies was inevitable. However, sequencing techniques are not without limitations. Illumina 'short read' sequencing has a high rate of incorrect nucleotide incorporation, due to the necessity of sequence amplification (Sloan *et al.*, 2018). This high noise threshold makes the detection of single base mutations challenging. Therefore, Illumina-based sequencing methods have been adapted to increase fidelity through redundant sequencing, whereby multiple sequence reads are produced for a single DNA fragment (Ahn *et al.*, 2015; Schmitt *et al.*, 2015; Hoang *et al.*, 2016). This enables the

reliable assessment of single nucleotide changes. Detection of chemical DNA damage using sequencing relies on the blocking of the polymerase by bulky adducts. Using this principle Hu *et al* developed a novel protocol for DNA damage sequencing, 'Damage-seq', which was used to map cisplatin and UV induced DNA damage and repair (Hu *et al.*, 2016, 2017) Overall, sequencing-based methods for the detection of DNA damage and repair enables high nucleotide resolution without bias for specific regions of the genome. Therefore, it is likely that such methods will be adopted for future DNA repair studies. These techniques will be particularly useful for investigations using patient-derived tumour samples, as no cell culture is required. Potential applications include the optimisation of chemotherapy regimens and exploration into why treatment sometimes fails, such as in the case of hypoxia-induced drug resistance.

High-throughput comet assays and sequencing based methods will undoubtedly be adopted in the next few years. However, associated cost is likely to be a barrier. The current toolbox available to researchers, such as plasmid based assays, IRIF, laser microirradiation etc. have significant limitations, making selection of the perfect tool somewhat impossible. Most DNA repair studies are conducted in model cell lines (HeLa, U2OS), which are easily manipulated, making the DNA repair 'toolkit' appear sufficient. However, these cell lines no longer truly recapitulate the essence of physiological cell biology, making the relevance of any findings questionable. To take DNA repair studies one-step further, the development of techniques, which are easily applicable to multiple cell types, with a high-throughput and cost effective application, is required. However, whether this is possible is yet unknown. Likely, in the near future, techniques to examined DNA repair in 3D cell culture based studies will be developed as an alternative to 2D models, yet this may add further technical complexity.

6.3 Moving towards 3D and *in vivo* investigations

In this thesis, MB and GBM cell lines provided valuable insight into the effect of hypoxia on DNA repair mechanisms. However, the extent to which 2D monolayer recaptures the tumour microenvironment is questionable. Alternatively, 3D tumour spheroids are a possibility. GBM and MB cells can successfully form tumour spheroids, which can replicate features such as oxygen, nutrient and pH gradients as well as cell-matrix interactions (Baker and Chen, 2012). Tumour spheroids have already been employed for DNA repair studies. For example, Mondesert *et al* developed a DNA damage response reporter consisting of a p21 promotor linked to an RFP gene. This construct enabled the visualisation of the activation of the DNA damage response in spheroids, using confocal microscopy (Mondesert *et al.*, 2015). Further advances in live cell imaging technologies, such as the development of light sheet microscopy has taken spheroid imaging a step further enabling 3D live cell imaging. For example, the Sée group successfully used tumour spheroids with light sheet microscopy to assess invasion of U87-MG spheroids (Richards *et al* in preparation). Light sheet microscopy enables deeper yet less toxic imaging of samples in comparison to conventional confocal microscopy, with the added benefit of 3D imaging capabilities (Reynaud *et al.*, 2008). This technology could be applied to DNA repair studies, and would enable the assessment of DNA repair in a 3D setting, where cells are exposed to varying oxygen tensions and nutrient gradients. However, the current resolution of commercial light sheet microscopy may not be sufficient to obtain single cell observations within the 3D environment (Santi, 2011). Combining light sheet microscopy with super resolution imaging would circumvent this issue but may not be a reality for many years to come.

3D spheroid models to some extent can recreate the tumour microenvironment. However, often these do not represent the mixed cell types found within a tumour. Therefore, xenografts and tissue samples are undoubtedly one-step closer to true *in vivo* patient studies. Previous work

examining the impact of hypoxia on DNA repair proteins, found significant correlation between *in vitro* and *in vivo* observations using xenografts. For example, hypoxia is thought to induce ATM phosphorylation *in vitro*. Assessment of tumour xenografts showed that CAIX, a common hypoxic marker, co-localised with phosphoATM, correlating with the *in vitro* observations (Olcina *et al.*, 2013). Additionally, hypoxia-induced downregulation of RAD51 was identified *in vitro* and in cervical and prostate cancer xenografts (Bindra *et al.*, 2004). However, within the DNA repair field it is rare to find extensive DNA repair studies that heavily utilise xenografts or patient samples. Often these are additional experiments, potentially added to improve the impact factor of the publication. Does this highlight potential lack of applicability of DNA repair findings to actual human samples? Likely this is true for model cell line (HeLa, U2OS etc.) based work. However, due to the heterogeneous nature of patient samples and xenografts, variations in findings involving DNA repair or hypoxia are expected. Yet, in order to generate translational data, using patient samples or xenografts is essential and needs to be more commonplace in DNA repair and hypoxia studies. However, obtaining patient samples in particular can be difficult for rare cancers, such as MB. Therefore, a cheap and high-throughput animal model is desirable.

Several genetically engineered mouse models exist for MB and GBM, however working with mice can be costly and requires extensive licencing. Recently, the chick embryo has been shown to be an effective model for cancer research, allowing for high-throughput experimentation (Herrmann *et al.*, 2015). The use of this model in hypoxic studies has been exemplified by Herrmann *et al*. Authors showed that hypoxic neuroblastoma tumours grown within the chick embryo had metastasised to other organs, whereas normoxic tumours did not (Herrmann *et al.*, 2015). Using this model, tumours of different cancer types can be grown, which are fully vascularised. Measurements of oxygen tension within these tumour have been taken in real time, and an average of ~1% O_2 was found (Al-Mutawa *et al.*, 2018), which is physiologically relevant and

correlates with the oxygen levels in brain tumours (Evans *et al.*, 2004). Currently, there are only a handful of publications using the chick embryo model for cancer studies, yet this would be an invaluable low cost resource GBM and MB studies. Exploration of DNA repair mechanism would also be possible, such as examining the impact of reduced levels of repair proteins on the response to DNA damaging agents. Tumours grown on the chick embryo model can be taken for further lab based *in vitro* experiments, such as the assessment of DNA repair capacity. This has previously been done with tissue samples, for example Slyskova *et al.* used colorectal cancer biopsies to extract DNA repair proteins, which were used in a comet assay (Slyskova *et al.*, 2014). Development of the chick embryo model for cancer research is currently underway, and its adoption as a primary model is likely.

6.4 Prospects for brain tumour treatment

There have been little change to treatment protocols for brain tumours over the past few decades, with no new drugs having been developed. Tumour hypoxia can cause resistance to common treatment methods, however as exemplified in this thesis, the mechanism behind this resistance is not so clear-cut. Therefore, the extent to which tumour hypoxia and treatment resistance should influence brain tumour drug development currently is small. However, as the majority of MB and GBM treatments are based on the generation of DNA damage, understanding the DNA damage response within these tumours is essential, particularly for the generation of new and emerging therapies.

Proton beam therapy is an emerging irradiation-based treatment protocol for brain tumours. Already, several clinical trials have provided evidence of the usefulness of proton beam therapy for GBM and MB (Mizumoto *et al.*, 2014; Yock *et al.*, 2016). Until recently, little was known regarding the type of DNA damage induced by this technique. However, extensive research by Carter *et al*, has provided further understanding of the complex DNA damage created

and the cellular response initiated (Carter *et al.*, 2017). Studies like this will aid in assessment of the cancer killing power of proton beam therapy, and will provide further evidence for its usefulness in a clinical setting. However, this leads to the question, how does hypoxia influence the repair of proton beam induced DNA damage? Will hypoxia-induced resistance to proton beam therapy occur and will this be a significant clinical barrier? Further research conducted by teams at the University of Liverpool, will undoubtedly aid in answering these important questions. The UK government has provided £250 million to proton beam therapy centres, suggesting that adoption of this technique by the NHS is likely.

Drug-based precision medicine is becoming a fashionable trend within cancer research. Already this approach is being explored for MB treatment, with the use of GLI inhibitors for SHH MB (Kim *et al.*, 2010, 2013). This is partly attributed to the successful evaluation of the molecular architecture of MB. However, attempts to generate targeted GBM therapies have been largely unsuccessful. Determination of potential mechanisms of hypoxia-induced resistance in these tumour may aid in development of targeted therapies, however as described in this thesis, there was no clear-cut mechanism of hypoxia-induced treatment resistance, nor were there any strong changes to DNA repair genes across multiple cells lines. Therefore, it is unlikely that this research will directly contribute to the generation of targeted treatments in the near future. However, brain tumour patients are still dying and a rapid short-term solution is desperately needed. Likely, this will come in the form of drug repositioning. Dissemination of GBM tumours can disrupt the blood-brain barrier. However delivery of effective drug doses can still be challenging (Sarkaria *et al.*, 2018). Repositioning of non-oncology based drugs, which already show high CNS activity, is becoming a popular strategy for brain tumour treatment. For example, the antidepressant, fluoxetine, has been shown to suppress GBM tumour growth in preclinical models (Liu *et al.*, 2015). Additionally, Disulfiram used to manage alcoholism, can increase sensitivity to temozolomide through inhibition of MGMT (Triscott *et al.*, 2012; Paranjpe *et*

al., 2014). Two clinical trials using Disulfiram in combination with standard GBM therapy are currently underway (ClinicalTrials.gov Identifier: NCT01907165, NCT03363659). Due to the wealth of safety information already available on these drugs, the initiation of clinical trials is accelerated. Therefore, repositioning of drugs is likely a viable short-term option for improving GBM treatment.

6.5 Final remarks

Both MB and GBM are complex diseases with devastating consequences. Due to the biological and environmental complexity of these tumours, creating advanced personalised treatments is challenging. Thus far, little research has been conducted exploring hypoxia and DNA repair in these brain tumours. Work in this thesis provides novel insight into the complex response of GBM and MB to hypoxia and the implications for DNA repair mechanisms. Investigating these findings in a 3D tumour spheroid models of would support the 2D culture work, yet further technical issues may arise in a 3D system. Hypoxia has not yet been shown to be a causative factor in the generation of pro-tumorigenic mutations. However, alteration to DNA repair mechanisms may drive further genome instability leading to cancer progression. It is hoped that exploration of the fundamental cell biology of these complex tumours will lead to the development of new treatment protocols to overcome the low rate of patient survival. The main findings of this thesis are as follows:

1. Hypoxia can downregulate key components of the DSB recognition machinery leading to reduced treatment sensitivity in D283-MED cells. Yet this is not a universal mechanism.
2. The impact of hypoxia on DNA repair gene expression is not clear-cut, and relies heavily on the severity of hypoxia and is cell line dependent.
3. Hypoxia results in altered dissociation of XRCC4 from sites of DNA damage suggesting that NHEJ may be impaired in hypoxia.

References

Abraham, J., Salama, N. N. and Azab, A. K. (2015) 'The role of P-glycoprotein in drug resistance in multiple myeloma', *Leukemia & Lymphoma*, 56(1), pp. 26–33.

Aebi, S., Kurdi-haidar, B., Gordon, R., Cenni, B., Zheng, H., Fink, D., Christen, R. D., Boland, C. R., Koi, M., Fishel, R. and Howell, S. B. (1996) 'Loss of DNA Mismatch Repair in Acquired Resistance to Cisplatin Loss of DNA Mismatch Repair in Acquired Resistance to Cisplatin', *Cancer Research*, 2(619), pp. 3087–3090.

Ahn, E. H., Prindle, M. J., Kuong, K. J. and Shen, J. (2015) 'Detecting ultralow-frequency mutations by Duplex Sequencing', *Nature Protocols*, 9(11), pp. 2586–2606.

Akbarnejad, Z., Eskandary, H., Dini, L., Vergallo, C., Nematollahi-Mahani, S. N., Farsinejad, A., Abadi, M. F. S. and Ahmadi, M. (2017) 'Cytotoxicity of temozolomide on human glioblastoma cells is enhanced by the concomitant exposure to an extremely low-frequency electromagnetic field (100 Hz, 100 G)', *Biomedicine and Pharmacotherapy*, 92, pp. 254–264.

Al-Mutawa, Y., Herrmann, A., Corbishley, C., Losty, P. D., Phelan, M. and Sée, V. (2018) 'Effects of hypoxic preconditioning on neuroblastoma tumour oxygenation and metabolic signature in a chick embryo model.', *Bioscience Reports*, 38(4).

Alcantara Llaguno, S. R., Wang, Z., Sun, D., Chen, J., Xu, J., Kim, E., Hatanpaa, K. J., Raisanen, J. M., Burns, D. K., Johnson, J. E. and Parada, L. F. (2015) 'Adult Lineage-Restricted CNS Progenitors Specify Distinct Glioblastoma Subtypes', *Cancer Cell*. Elsevier Inc., 28(4), pp. 429–440.

Altmann, T. and Gennery, A. R. (2016) 'DNA ligase IV syndrome; a review', *Orphanet Journal of Rare Diseases*, 11(1), pp. 1–7.

Amellem and Pettersen, E. O. (1991) 'Cell inactivation and cell cycle inhibition as induced by extreme hypoxia: the possible role of cell cycle arrest as a protection against hypoxia-induced lethal damage', *Cell Proliferation*, 24(2), pp. 127–141.

Ansell, W. and Shamash, J. (2008) 'Testicular cancer before and after cisplatin: A 30-year view',

International Journal of Urological Nursing, 2(3), pp. 103–112.

Anyong Xie, Amy Kwok, and R. S. (2010) 'Role of mammalian Mre11 in classical and alternative non- homologous end joining', *Nature Structural & Molecular Biology*, 16(8), pp. 814–818.

Arany, Z. and Huang, L. (1996) 'An essential role for p300/CBP in the cellular response to hypoxia', *Proceedings of the National Academy of Sciences of the United States of America*, 93, pp. 12969–12973.

Athanassiou, H., Synodinou, M., Maragoudakis, E., Paraskevaidis, M., Verigos, C., Misailidou, D., Antonadou, D., Saris, G., Beroukas, K. and Karageorgis, P. (2005) 'Randomized phase II study of temozolomide and radiotherapy compared with radiotherapy alone in newly diagnosed glioblastoma multiforme', *Journal of Clinical Oncology*, 23(10), pp. 2372–2377.

Azab, A. K., Hu, J., Quang, P., Azab, F., Pitsillides, C., Thompson, B., Maiso, P., Roccaro, A. M., Sacco, A., Ngo, H. T., Issa, G. C., Lin, C., Kung, A. L., Vanderkerken, K. and Ghobrial, I. M. (2011) 'Hypoxia promotes dissemination of multiple myeloma through acquisition of Endothelial to Mesenchymal Transition (EMT) features', *Blood*, 118(21), pp. 5782–5795.

Azqueta, A. and Collins, A. R. (2013) 'The essential comet assay: A comprehensive guide to measuring DNA damage and repair', *Archives of Toxicology*, 87(6), pp. 949–968.

Azqueta, A., Gutzkow, K. B., Brunborg, G. and Collins, A. R. (2011) 'Towards a more reliable comet assay: Optimising agarose concentration, unwinding time and electrophoresis conditions', *Mutation Research*, 724(1–2), pp. 41–45.

Baker, B. M. and Chen, C. S. (2012) 'Deconstructing the third dimension – how 3D culture microenvironments alter cellular cues', *Journal of Cell Science*, 125(13), pp. 3015–3024.

Balkwill, F. R., Capasso, M. and Hagemann, T. (2012) 'The tumor microenvironment at a glance', *Journal of Cell Science*, 125(23), pp. 5591–5596.

Banin, S., Moyal, L., Shieh, S.-Y., Taya, Y., Anderson, C. W., Chessa, L., Smorodinsky, N. I., Prives, C., Reiss, Y., Shiloh, Y. and Ziv, Y. (1998) 'Enhanced Phosphorytation of p53 by ATM in Response to DNA Damage', *Science*, 281(5383), pp. 1674–1677.

Bao, P., Zheng, Y., Wang, C., Gu, K., Jin, F. and Lu, W. (2009) 'Time Trends and Characteristics of Childhood Cancer Among Children Age 0 – 14 in Shanghai', *Pediatric Blood Cancer*, 53(December 2008), pp. 13–16.

Barry, M. A., Behnke, C. A. and Eastman, A. (1990) 'Activation of programmed cell death (apoptosis) by cisplatin, other anticancer drugs, toxins and hyperthermia', *Biochemical Pharmacology*, 40(10), pp. 2353–2362.

Bellot, G., Garcia-Medina, R., Gounon, P., Chiche, J., Roux, D., Pouyssegur, J. and Mazure, N. M. (2009) 'Hypoxia-Induced Autophagy Is Mediated through Hypoxia-Inducible Factor Induction of BNIP3 and BNIP3L via Their BH3 Domains', *Molecular and Cellular Biology*, 29(10), pp. 2570–2581.

Ben-Yosef, Y., Lahat, N., Shapiro, S., Bitterman, H. and Miller, A. (2002) 'Regulation of endothelial matrix metalloproteinase-2 by hypoxia/reoxygenation', *Circulation Research*, 90(7), pp. 784–791.

Bencokova, Z., Kaufmann, M. R., Pires, I. M., Lecane, P. S., Giaccia, A. J. and Hammond, E. M. (2009) 'ATM activation and signaling under hypoxic conditions.', *Molecular and Cellular Biology*, 29(2), pp. 526–37.

Bennett, C. B., Lewis, A. L., Baldwin, K. K. and Resnick, M. A. (1993) 'Lethality induced by a single site-specific double-strand break in a dispensable yeast plasmid.', *Proceedings of the National Academy of Sciences*, 90(12), pp. 5613–5617.

Bentley-Hewitt, K. L., Hedderley, D. I., Monro, J., Martell, S., Smith, H. and Mishra, S. (2016) 'Comparison of quantitative real-time polymerase chain reaction with NanoString®methodology using adipose and liver tissues from rats fed seaweed', *New Biotechnology*, 33(3), pp. 380–386.

Berger, J. M., Gamblin, S. J., Harrison, S. C. and Wang, J. C. (1996) 'Structure and mechanism of DNA topoisomerase II.', *Nature*, pp. 225–232.

Berridge, M. V. and Tan, A. S. (1993) 'Characterization of the Cellular Reduction of 3-(4,5-dimethylthiazol-2-yl)-2,5-diphenyltetrazolium bromide (MTT): Subcellular Localization,

Substrate Dependence, and Involvement of Mitochondrial Electron Transport in MTT Reduction', *Archives of Biochemistry and Biophysics*, 303(2), pp. 474–482.

Binaschi, M., Zunino, F. and Capranico, G. (1995) 'Mechanism of action of DNA topoisomerase inhibitors.', *Stem cells*, 13(4), pp. 369–379.

Bindra, R. S., Crosby, M. E. and Glazer, P. M. (2007) 'Regulation of DNA repair in hypoxic cancer cells', *Cancer and Metastasis Reviews*, 26(2), pp. 249–260.

Bindra, R. S., Gibson, S. L., Meng, A., Westermark, U., Jasin, M., Pierce, A. J., Bristow, R. G., Classon, M. K. and Glazer, P. M. (2005) 'Hypoxia-induced down-regulation of BRCA1 expression by E2Fs', *Cancer Research*, 65(24), pp. 11597–11604.

Bindra, R. S. and Glazer, P. M. (2007) 'Repression of RAD51 gene expression by E2F4/p130 complexes in hypoxia', *Oncogene*, 26(14), pp. 2048–2057.

Bindra, R. S., Schaffer, P. J., Meng, A., Woo, J., Måseide, K., Roth, M. E., Lizardi, P., David, W., Bristow, R. G., Glazer, P. M. and Hedley, D. W. (2004) 'Down-Regulation of Rad51 and Decreased Homologous Recombination in Hypoxic Cancer Cells', *Molecular and Cellular Biology*, 24(19), pp. 8504–8518.

Blackwell, L. J., Martik, D., Bjornson, K. P., Bjornson, E. S. and Modrich, P. (1999) 'Nucleotide-promoted release of hMutSα from heteroduplex DNA is consistent with an ATP-dependent translocation mechanism', *Journal of Biological Chemistry*, 273(48), pp. 32055–32062.

Bocker, T., Barusevicius, A., Snowden, T., Rasio, D., Guerrette, S., Robbins, D., Schmidt, C., Burczak, J., Croce, C. M., Copeland, T., Kovatich, A. J. and Fishel, R. (1999) 'hMSH5: A human MutS homologue that forms a novel heterodimer with hMSH4 and is expressed during spermatogenesis', *Cancer Research*, 59(4), pp. 816–822.

Borhani, S., Mozdarani, H., Babalui, S., Bakhshandeh, M. and Nosrati, H. (2017) 'In vitro radiosensitizing effects of temozolomide on U87MG cell lines of human glioblastoma multiforme', *Iranian Journal of Medical Sciences*, 42(3), pp. 258–265.

Brada, M., Judson, I., Beale, P., Moore, S., Reidenberg, P., Statkevich, P., Dugan, M., Batra, V.

and Cutler, D. (1999) 'Phase I dose-escalation and pharmacokinetic study of temozolomide (SCH 52365) for refractory or relapsing malignancies.', *British Journal of Cancer*, 81(6), pp. 1022–30.

De Braganca, K. C. and Packer, R. J. (2013) 'Treatment Options for Medulloblastoma and CNS Primitive Neuroectodermal Tumor (PNET).', *Current Treatment Options In Neurology*, 15(5), pp. 593–606.

Braithwaite, E. K., Kedar, P. S., Lan, L., Polosina, Y. Y., Asagoshi, K., Poltoratsky, V. P., Horton, J. K., Miller, H., Teebor, G. W., Yasui, A. and Wilson, S. H. (2005) 'DNA polymerase λ protects mouse fibroblasts against oxidative DNA damage and is recruited to sites of DNA damage/repair', *Journal of Biological Chemistry*, 280(36), pp. 31641–31647.

Brennan, C. W., Verhaak, R. G. W., McKenna, A., Campos, B., Noushmehr, H., Salama, S. R., Zheng, S., Chakravarty, D., Sanborn, J. Z., Berman, S. H., Beroukhim, R., Bernard, B., Wu, C. J., Genovese, G., Shmulevich, I., *et al.* (2013) 'The somatic genomic landscape of glioblastoma', *Cell*, 155(2), pp. 462–477.

Brodbelt, A., Greenberg, D., Winters, T., Williams, M., Vernon, S. and Collins, V. P. (2015) 'Glioblastoma in England: 2007-2011', *European Journal of Cancer*, 51(4), pp. 533–542.

Brown, J. M. and Wilson, W. R. (2004) 'Exploiting tumour hypoxia in cancer treatment', *Nature Reviews Cancer*, 4(6), pp. 437–447.

Bruick, R. K. and McKnight, S. L. (2001) 'A conserved family of prolyl-4-hydroxylases that modify HIF.', *Science*, 294(5545), pp. 1337–1340.

Buck, D., Moshous, D., de Chasseval, R., Ma, Y., le Deist, F., Cavazzana-Calvo, M., Fischer, A., Casanova, J. L., Lieber, M. R. and de Villartay, J. P. (2006) 'Severe combined immunodeficiency and microcephaly in siblings with hypomorphic mutations in DNA ligase IV', *European Journal of Immunology*, 36(1), pp. 224–235.

Burden, D. A. and Osheroff, N. (1998) 'Mechanism of action of eukaryotic topoisomerase II and drugs targeted to the enzyme', *Biochimica et Biophysica Acta*, 1400(1–3), pp. 139–154.

Cahill, D. P., Levine, K. K., Betensky, R. A., Codd, P. J., Romany, C. A., Reavie, L. B., Batchelor, T. T., Futreal, P. A., Stratton, M. R., Curry, W. T., Lafrate, A. J. and Louis, D. N. (2007) 'Loss of the mismatch repair protein MSH6 in human glioblastomas is associated with tumor progression during temozolomide treatment', *Clinical Cancer Research*, 13(7), pp. 2038–2045.

Cairns, R. A. and Hill, R. P. (2004) 'Acute Hypoxia Enhances Spontaneous Lymph Node Metastasis in an Orthotopic Murine Model of Human Cervical Carcinoma', *Cancer Research*, 64(6), pp. 2054–2061.

Caldecott, K. W., McKeown, C. K., Tucker, J. D., Ljungquist, S. and Thompsonl, L. H. (1994) 'An Interaction between the Mammalian DNA Repair Protein XRCC1 and DNA Ligase III', *Molecular and Cellular Biology*, 14(1), pp. 68–76.

Câmara-Costa, H., Resch, A., Kieffer, V., Lalande, C., Poggi, G., Kennedy, C., Bull, K., Calaminus, G., Grill, J., Doz, F., Rutkowski, S., Massimino, M., Kortman, R.-D., Lannering, B., Dellatolas, G., *et al.* (2015) 'Neuropsychological outcome of children treated for standard risk medulloblastoma in the PNET4 European randomised controlled trial of hyperfractionated (HFRT) versus standard radiotherapy (STRT) and maintenance chemotherapy', *International Journal of Radiation Oncology Biology Physics*, 92(5), pp. 978–985.

Canman, C. E., Lim, D. S., Cimprich, K. A., Taya, Y., Tamai, K., Sakaguchi, K., Appella, E., Kastan, M. B. and Siliciano, J. D. (1998) 'Activation of the ATM kinase by ionizing radiation and phosphorylation of p53', *Science*, 281(5383), pp. 1677–1679.

Caradec, J., Sirab, N., Keumeugni, C., Moutereau, S., Chimingqi, M., Matar, C., Revaud, D., Bah, M., Manivet, P., Conti, M. and Loric, S. (2010) 'Desperate house genes: The dramatic example of hypoxia', *British Journal of Cancer*, 102(6), pp. 1037–1043.

Carmichael, J., Degraff, W. G., Gazdar, A. F., Minna, J. D. and Mitchell, J. B. (1987) 'Evaluation of a Tetrazolium-based Semiautomated Colorimetric Assay: Assessment of Chemosensitivity Testing Evaluation of a Tetrazolium-based Semiautomated Colorimetrie Assay', *American Association for Cancer Research*, 47, pp. 936–942.

Carter, R. J., Nickson, C. M., Thompson, J. M., Kacperek, A., Hill, M. A. and Parsons, J. L. (2017) 'Complex DNA Damage Induced by High Linear Energy Transfer Alpha-Particles and Protons Triggers a Specific Cellular DNA Damage Response', *International Journal of Radiation*

Oncology Biology Physics, 100(3), pp. 776–784.

Castro, G. N., Cayado-Gutiérrez, N., Zoppino, F. C. M., Fanelli, M. A., Cuello-Carrión, F. D., Sottile, M., Nadin, S. B. and Ciocca, D. R. (2015) 'Effects of temozolomide (TMZ) on the expression and interaction of heat shock proteins (HSPs) and DNA repair proteins in human malignant glioma cells', *Cell Stress and Chaperones*, 20(2), pp. 253–265.

Cavalli, F. M. G., Remke, M., Rampasek, L., Peacock, J., Shih, D. J. H., Luu, B., Garzia, L., Torchia, J., Nor, C., Morrissy, A. S., Agnihotri, S., Thompson, Y. Y., Kuzan-Fischer, C. M., Farooq, H., Isaev, K., *et al.* (2017) 'Intertumoral Heterogeneity within Medulloblastoma Subgroups', *Cancer Cell*, 31(6), p. 737–754.e6.

Ceccarelli, M., Barthel, F. P., Malta, T. M., Sabedot, T. S., Salama, S. R., Murray, B. A., Morozova, O., Newton, Y., Radenbaugh, A., Pagnotta, S. M., Anjum, S., Wang, J., Manyam, G., Zoppoli, P., Ling, S., *et al.* (2016) 'Molecular Profiling Reveals Biologically Discrete Subsets and Pathways of Progression in Diffuse Glioma', *Cell*, 164(3), pp. 550–563.

Chan, D. and Less-Miller, S. (1996) 'The DNA-dependent protein kinase is inactivates by autophosphorylation of the catalytic subunit', *The Journal of Biological Chemistry*, 271(15), pp. 8936–8941.

Chan, N., Ali, M., McCallum, G. P., Kumareswaran, R., Koritzinsky, M., Wouters, B. G., Wells, P. G., Gallinger, S. and Bristow, R. G. (2014) 'Hypoxia Provokes Base Excision Repair Changes and a Repair-Deficient, Mutator Phenotype in Colorectal Cancer Cells', *Molecular Cancer Research*, 12(10), pp. 1407–1415.

Chan, N., Koritzinsky, M., Zhao, H., Bindra, R., Glazer, P. M., Powell, S., Belmaaza, A., Wouters, B. and Bristow, R. G. (2008) 'Chronic hypoxia decreases synthesis of homologous recombination proteins to offset chemoresistance and radioresistance', *Cancer Research*, 68(2), pp. 605–614.

Chang, C. H., Horton, J., Schoenfeld, D., Salazer, O., Perez-Tamayo, R., Kramer, S., Weinstein, a, Nelson, J. S. and Tsukada, Y. (1983) 'Comparison of postoperative radiotherapy and combined postoperative radiotherapy and chemotherapy in the multidisciplinary management of malignant gliomas. A joint Radiation Therapy Oncology Group and Eastern Cooperative Oncology Group study.', *Cancer*, 52(6), pp. 997–1007.

Chapman, J. D., Reuvers, a P., Borsa, J. and Greenstock, C. L. (1973) 'Chemical radioprotection and radiosensitization of mammalian cells growing in vitro.', *Radiation Research*, 56(2), pp. 291–306.

Chen, J., Kobayashi, M., Darmanin, S., Qiao, Y., Gully, C., Zhao, R., Yeung, S. C. and Lee, M. H. (2009) 'Pim-1 plays a pivotal role in hypoxia-induced chemoresistance', *Oncogene*, 28(28), pp. 2581–2592.

Chen, L., Feng, P., Li, S., Long, D., Cheng, J., Lu, Y. and Zhou, D. (2009) 'Effect of hypoxia-inducible factor-1α silencing on the sensitivity of human brain glioma cells to doxorubicin and etoposide', *Neurochemical Research*, 34(5), pp. 984–990.

Cheng, C. L., Johnson, S. P., Keir, S. T., Quinn, J. a, Ali-Osman, F., Szabo, C., Li, H., Salzman, A. L., Dolan, M. E., Modrich, P., Bigner, D. D. and Friedman, H. S. (2005) 'Poly(ADP-ribose) polymerase-1 inhibition reverses temozolomide resistance in a DNA mismatch repair-deficient malignant glioma xenograft.', *Molecular Cancer Therapeutics*, 4(9), pp. 1364–1368.

Chinot, O. L., Wick, W., Mason, W., Henriksson, R., Saran, F., Nishikawa, R., Carpentier, A. F., Hoang-Xuan, K., Kavan, P., Cernea, D., Brandes, A. A., Hilton, M., Abrey, L. and Cloughesy, T. (2014) 'Bevacizumab plus Radiotherapy–Temozolomide for Newly Diagnosed Glioblastoma', *New England Journal of Medicine*, 370(8), pp. 709–722.

Cho, Y. J., Tsherniak, A., Tamayo, P., Santagata, S., Ligon, A., Greulich, H., Berhoukim, R., Amani, V., Goumnerova, L., Eberhart, C. G., Lau, C. C., Olson, J. M., Gilbertson, R. J., Gajjar, A., Delattre, O., *et al.* (2011) 'Integrative genomic analysis of medulloblastoma identifies a molecular subgroup that drives poor clinical outcome', *Journal of Clinical Oncology*, 29(11), pp. 1424–1430.

Choi, B. J., Park, S. A., Lee, S. Y., Cha, Y. N. and Surh, Y. J. (2017) 'Hypoxia induces epithelial-mesenchymal transition in colorectal cancer cells through ubiquitin-specific protease 47-mediated stabilization of Snail: A potential role of Sox9', *Scientific Reports*. Springer US, 7(1), pp. 1–15.

Choi, J. Y., Jang, Y. S., Min, S. Y. and Song, J. Y. (2011) 'Overexpression of MMP-9 and hif-1?? in breast cancer cells under hypoxic conditions', *Journal of Breast Cancer*, 14(2), pp. 88–95.

Chou, C. W., Wang, C. C., Wu, C. P., Lin, Y. J., Lee, Y. C., Cheng, Y. W. and Hsieh, C. H. (2012) 'Tumor cycling hypoxia induces chemoresistance in glioblastoma multiforme by upregulating the expression and function of ABCB1', *Neuro-Oncology*, 14(10), pp. 1227–1238.

Ciccia, A. and Elledge, S. J. (2010) 'The DNA Damage Response: Making It Safe to Play with Knives', *Molecular Cell*, 40(2), pp. 179–204.

Clarke, K., Smith, K., Gullick, W. J. and Harris, A. L. (2001) 'Mutant epidermal growth factor receptor enhances induction of vascular endothelial growth factor by hypoxia and insulin-like growth factor-1 via a PI3 kinase dependent pathway.', *British Journal of Cancer*, 84(10), pp. 1322–9.

Clifford, S. C., Lusher, M. E., Lindsey, J. C., Langdon, J. A., Gilbertson, R. J., Straughton, D. and Ellison, D. W. (2006) 'Wnt/Wingless pathway activation and chromosome 6 loss characterize a distinct molecular sub-group of medulloblastomas associated with a favorable prognosis.', *Cell Cycle*, 5(22), pp. 2666–2670.

Cohen, M. H., Shen, Y. L., Keegan, P. and Pazdur, R. (2009) 'FDA Drug Approval Summary: Bevacizumab (Avastin(R)) as Treatment of Recurrent Glioblastoma Multiforme', *The Oncologist*, 14(11), pp. 1131–1138.

Collins, A. R. (2004) 'The comet assay for DNA damage and repair: principles, applications, and limitations', *Molecular Biotechnology*, 26(3), pp. 249–261.

Collins, F. S., Lander, E. S., Rogers, J. and Waterson, R. H. (2004) 'Finishing the euchromatic sequence of the human genome', *Nature*, 431(7011), pp. 931–945.

Collins, S. L., Hervé, R., Keevil, C. W., Blaydes, J. P. and Webb, J. S. (2011) 'Down-regulation of DNA mismatch repair enhances initiation and growth of neuroblastoma and brain tumour multicellular spheroids', *PLoS ONE*, 6(12), pp. 1–8.

Comerford, K. M., Wallace, T. J., Karhausen, J., Louis, N. A., Montalto, M. C. and Colgan, S. P. (2002) 'Hypoxia-inducible factor-1-dependent regulation of the multidrug resistance (MDR1) gene', *Cancer Research*, 62(12), pp. 3387–3394.

Constantinou, A., Tarsounas, M., Karow, J. K., Brosh, R. M., Bohr, V. A., Hickson, I. D. and West, S. C. (2000) 'Werner's syndrome protein (WRN) migrates Holliday junctions and co-localizes with RPA upon replication arrest', *EMBO Reports*, 1(1), pp. 80–84.

Cornago, M., Garcia-Alberich, C., Blasco-Angulo, N., Vall-llaura, N., Nager, M., Herreros, J., Comella, J. X., Sanchis, D. and Llovera, M. (2014) 'Histone deacetylase inhibitors promote glioma cell death by G2 checkpoint abrogation leading to mitotic catastrophe', *Cell Death and Disease*, 5(10), pp. 1435–13.

Cosse, J.-P., Ronvaux, M., Ninane, N., Raes, M. J. and Michiels, C. (2009) 'Hypoxia-Induced Decrease in p53 Protein Level and Increase in c-jun DNA Binding Activity Results in Cancer Cell Resistance to Etoposide', *Neoplasia*, 11(10), pp. 976–986.

Cosse, J.-P., Sermeus, A., Vannuvel, K., Ninane, N., Raes, M. and Michiels, C. (2007) 'Differential effects of hypoxia on etoposide-induced apoptosis according to the cancer cell lines.', *Molecular Cancer*, 6(61), pp. 1–16.

Critchlow, S. E., Bowater, R. P. and Jackson, S. P. (1997) 'Mammalian DNA double-strand break repair protein XRCC4 interacts with DNA ligase IV.', *Current Biology*, 7(8), pp. 588–598.

Crosby, M. E., Kulshreshtha, R., Ivan, M. and Glazer, P. M. (2010) 'MicroRNA regulation of DNA repair gene expression in hypoxic stress', *Cancer*, 69(3), pp. 1221–1229.

Cruzeiro, G., dos Reis, M., Silveira, V., Lira, R., Jr, C., Neder, L., Oliveira, R., Yunes, J., Brandalise, S., Aguiar, S., Eterovic, A., Tone, L., Scrideli, C. and Valera, E. (2017) 'HIF1A is overexpressed in medulloblastoma and its inhibition reduces proliferation and increases EPAS1 and ATG16L1 methylation', *Current Cancer Drug Targets*, 17(999), pp. 1–1.

Cunningham, M. L., Ringrose, P. S. and Lokesh, B. R. (1984) 'Inhibition of the genotoxicity of bleomycin by superoxide dismutase.', *Mutation Research*, 135(3), pp. 199–202.

D'Atri, S., Tentori, L., Lacal, P. M., Graziani, G., Pagani, E., Benincasa, E., Zambruno, G., Bonmassar, E. and Jiricny, J. (1998) 'Involvement of the mismatch repair system in temozolomide-induced apoptosis.', *Molecular Pharmacology*, 54(2), pp. 334–341.

Dahmen, R. P., Koch, A., Denkhaus, D., Wiestler, O. D., Pietsch, T., Tonn, J. C., Sörensen, N., Berthold, F., Behrens, J. and Birchmeier, W. (2001) 'Deletions of AXIN1, a component of the WNT/wingless pathway, in sporadic medulloblastomas', *Cancer Research*, 61(19), pp. 7039–7043.

Demple, B., Herman, T. and Chen, D. S. (1991) 'Cloning and expression of APE, the cDNA encoding the major human apurinic endonuclease: definition of a family of DNA repair enzymes.', *Proceedings of the National Academy of Sciences of the United States of America*, 88, pp. 11450–4.

Desai-mehta, A., Cerosaletti, K. M. and Concannon, P. (2001) 'Distinct Functional Domains of Nibrin Mediate Mre11 Binding , Focus Formation , and Nuclear Localization Distinct Functional Domains of Nibrin Mediate Mre11 Binding , Focus Formation , and Nuclear Localization', *Molecular and Cellular Biology*, 21(6), pp. 2184–2191.

Deschner, E. E. and Gray, L. H. (1959) 'Influence of oxygen tension on x-ray-induced chromosomal damage in Ehrlich ascites tumor cells irradiated in vitro and in vivo.', *Radiation Research*, 11(1), pp. 115–146.

Deshmukh, H., Yeh, T. H., Yu, J., Sharma, M. K., Perry, A., Leonard, J. R., Watson, M. A., Gutmann, D. H. and Nagarajan, R. (2008) 'High-resolution, dual-platform aCGH analysis reveals frequent HIPK2 amplification and increased expression in pilocytic astrocytomas', *Oncogene*, 27(34), pp. 4745–4751.

Desjardins, A., Reardon, D. A., Coan, A., Marcello, J., Herndon, J. E., Bailey, L., Peters, K. B., Friedman, H. S. and Vredenburgh, J. J. (2012) 'Bevacizumab and daily temozolomide for recurrent glioblastoma', *Cancer*, 118(5), pp. 1302–1312.

Dinant, C., de Jager, M., Essers, J., van Cappellen, W. A., Kanaar, R., Houtsmuller, A. B. and Vermeulen, W. (2007) 'Activation of multiple DNA repair pathways by sub-nuclear damage induction methods', *Journal of Cell Science*, 120(15), pp. 2731–2740.

Dolecek, T. A., Propp, J. M., Stroup, N. E. and Kruchko, C. (2012) 'CBTRUS statistical report: Primary brain and central nervous system tumors diagnosed in the United States in 2005-2009', *Neuro-Oncology*, 14(SUPPL_5), pp. v1–v88.

Dudás, J., Schartinger, V. H., Romani, A., Schweigl, G., Kordsmeyer, K., Marta, P. I., Url, C., Kral, F. and Riechelmann, H. (2014) 'Cell cycle association and hypoxia regulation of excision repair cross complementation group 1 protein (ERCC1) in tumor cells of head and neck cancer', *Tumor Biology*, 35(8), pp. 7807–7819.

Dzantiev, L., Constantin, N., Genschel, J., Iyer, R. R., Burgers, P. M. and Modrich, P. (2004) 'A defined human system that supports bidirectional mismatch-provoked excision', *Molecular Cell*, 15(1), pp. 31–41.

Ellenberger, T. and Tomkinson, A. E. (2008) 'Eukaryotic DNA Ligases: Structural and Functional Insights', *Annual Review of Biochemistry*, 77(1), pp. 313–338.

Ellison, D. W., Onilude, O. E., Lindsey, J. C., Lusher, M. E., Weston, C. L., Taylor, R. E., Pearson, A. D. and Clifford, S. C. (2005) ??'-catenin status predicts a favorable outcome in childhood medulloblastoma: The United Kingdom Children's Cancer Study Group Brain Tumour Committee', *Journal of Clinical Oncology*, 23(31), pp. 7951–7957.

Elser, M., Borsig, L., Hassa, P. O., Erener, S., Messner, S., Valovka, T., Keller, S., Gassmann, M. and Hottiger, M. O. (2008) 'Poly(ADP-Ribose) Polymerase 1 Promotes Tumor Cell Survival by Coactivating Hypoxia-Inducible Factor-1-Dependent Gene Expression', *Molecular Cancer Research*, 6(2), pp. 282–290.

Epstein, A. C. R., Gleadle, J. M., Mcneill, L. A., Hewitson, K. S., Rourke, J. O., Mole, D. R., Mukherji, M., Metzen, E., Wilson, M. I., Dhanda, A., Tian, Y., Masson, N., Hamilton, D. L., Jaakkola, P., Barstead, R., *et al.* (2001) 'C. elegans EGL-9 and mammalian homologs define a family of dioxygenases that regulate HIF by prolyl hydroxylation', *Cell*, 107, pp. 43–54.

Eren, M. K. and Tabor, V. (2014) 'The role of hypoxia inducible factor-1 alpha in bypassing oncogene-induced senescence', *PLoS ONE*, 9(7), pp. 1–10.

Eriksson, P. S., Perfilieva, E., Bjork-Eriksson, T., Alborn, A. M., Nordborg, C., Peterson, D. A. and Gage, F. H. (1998) 'Neurogenesis in the adult human hippocampus', *Nature Medicine*, 4(11), pp. 1313–1317.

Erler, J. T., Cawthorne, C. J., Williams, K. J., Koritzinsky, M., Wouters, B. G., Wilson, C., Miller,

C., Demonacos, C., Stratford, I. J. and Dive, C. (2004) 'Hypoxia-mediated down-regulation of Bid and Bax in tumors occurs via hypoxia-inducible factor 1-dependent and -independent mechanisms and contributes to drug resistance.', *Molecular and Cellular Biology*, 24(7), pp. 2875–2889.

Esteller, M., Garcia-Foncillas, J. and Andion, E. (2000) 'Inactivation of The DNA Repair Gene MGMT And The Clinical Response of Gliomas to Alkylating Agents', *New England Journal of Medicine*, 343(19), pp. 4–8.

Evans, S. M., Judy, K. D., Dunphy, I., Jenkins, W. T., Nelson, P. T., Collins, R., Wileyto, E. P., Jenkins, K., Hahn, S. M., Stevens, C. W., Judkins, A. R., Phillips, P., Geoerger, B. and Koch, C. J. (2004) 'Comparative Measurements of Hypoxia in Human Brain Tumors Using Needle Electrodes and EF5 Binding', *Cancer Research*, 64, pp. 1886–1892.

Falanga, V., Su Wen Qian, Danielpour, D., Katz, M. H., Roberts, A. B. and Sporn, M. B. (1991) 'Hypoxia upregulates the synthesis of TGF-β1 by human dermal fibroblasts', *Journal of Investigative Dermatology*, pp. 634–637.

Falck, J., Coates, J. and Jackson, S. P. (2005) 'Conserved modes of recruitment of ATM, ATR and DNA-PKcs to sites of DNA damage.', *Nature*, 434(7033), pp. 605–611.

Fan, Y. (2014) 'The Role of Genetic Background and Hypoxia in the Chemotherapeutic Efficiency in Paediatric Brain Tumours', *PhD Thesis*.

Fanale, D., Bazan, V., Caruso, S., Castiglia, M., Bronte, G., Rolfo, C., Cicero, G. and Russo, A. (2013) 'Hypoxia and human genome stability: Downregulation of BRCA2 expression in breast cancer cell lines', *BioMed Research International*, 2013.

Feldmann, E., Schmiemann, V., Goedecke, W., Reichenberger, S. and Pfeiffer, P. (2000) 'DNA double-strand break repair in cell-free extracts from Ku80-deficient cells: implications for Ku serving as an alignment factor in non-homologous DNA end joining', *Nucleic Acids Research*, 28(13), pp. 2585–2596.

Ferrando-May, E., Tomas, M., Blumhardt, P., St??ckl, M., Fuchs, M. and Leitenstorfer, A. (2013) 'Highlighting the DNA damage response with ultrashort laser pulses in the near infrared and

kinetic modeling', *Frontiers in Genetics*, 4, pp. 1–8.

Field, K. M., Simes, J., Nowak, A. K., Cher, L., Wheeler, H., Hovey, E. J., Brown, C. S. B., Barnes, E. H., Sawkins, K., Livingstone, A., Freilich, R., Phal, P. M., Fitt, G., Rosenthal, M. A., Arzhintar, I., *et al.* (2015) 'Randomized phase 2 study of carboplatin and bevacizumab in recurrent glioblastoma', *Neuro-Oncology*, 17(11), pp. 1504–1513.

Fink, D., Aebi, S. and Howell, S. B. (1998) 'The role of DNA mismatch repair in drug resistance.', *Clinical Cancer Research*, 4, pp. 1–6.

Fonslow, B. R., Stein, B. D., Webb, K. J., Xu, T., Choi, J., Kyu, S. and Iii, J. R. Y. (2015) 'DNA Ligase IV regulates XRCC4 nuclear localisation', *DNA Repair*, 21, pp. 36–42.

Fortini, P. and Dogliotti, E. (2007) 'Base damage and single-strand break repair: Mechanisms and functional significance of short- and long-patch repair subpathways', *DNA Repair*, 6(4), pp. 398–409.

Fortini, P., Fortini, P., Rossi, O., Carrozzino, F., Raspaglio, G., Cox, L. S., Lane, D. P., Abbondandolo, A. and Dogliotti, E. (1996) 'Two Pathways for Base Excision Repair in Mammalian Cells', *Journal of Biological Chemistry*, 271(16), pp. 9573–9578.

Frederick, L., Wang, X. Y., Eley, G. and James, C. D. (2000) 'Diversity and frequency of epidermal growth factor receptor mutations in human glioblastomas.', *Cancer research*, 60(5), pp. 1383–1387.

Friedman, J. I. and Stivers, J. T. (2010) 'Detection of damaged DNA bases by DNA glycosylase enzymes', *Biochemistry*, 49(24), pp. 4957–4967.

Gardner, L. B., Li, Q., Park, M. S., Flanagan, W. M., Semenza, G. L. and Dang, C. V. (2001) 'Hypoxia Inhibits G1/S Transition through Regulation of p27 Expression', *Journal of Biological Chemistry*, 276(11), pp. 7919–7926.

Geiss, G. K., Bumgarner, R. E., Birditt, B., Dahl, T., Dowidar, N., Dunaway, D. L., Fell, H. P., Ferree, S., George, R. D., Grogan, T., James, J. J., Maysuria, M., Mitton, J. D., Oliveri, P., Osborn, J. L., *et al.* (2008) 'Direct multiplexed measurement of gene expression with color-

coded probe pairs', *Nature Biotechnology*, 26(3), pp. 317–325.

Gibson, P., Tong, Y., Robinson, G., Thompson, M. C., Currle, D. S., Eden, C., Kranenburg, T. A., Hogg, T., Poppleton, H., Martin, J., Finkelstein, D., Pounds, S., Weiss, A., Patay, Z. and Scoggins, M. (2011) 'Subtypes of medulloblastoma have distinct developmental origins', *Nature*, 468(7327), pp. 1095–1099.

Glassner, B. J., Weeda, G., Allan, J. M., Broekhof, J. L. M., Carls, N. H. E., Donker, I., Engelward, B. P., Hampson, R. J., Hersmus, R., Hickman, M. J., Roth, R. B., Warren, H. B., Wu, M. M., Hoeijmakers, J. H. J. and Samson, L. D. (1999) 'DNA repair methyltransferase (Mgmt) knockout mice are sensitive to the lethal effects of chemotherapeutic alkylating agents', *Mutagenesis*, 14(3), pp. 339–347.

Goda, N., Ryan, H. E., Khadivi, B., McNulty, W., Rickert, R. C. and Johnson, R. S. (2003) 'Hypoxia-inducible factor 1alpha is essential for cell cycle arrest during hypoxia.', *Molecular and Cellular Biology*, 23(1), pp. 359–69.

Gold, D. R., Packer, R. J. and Cohen, B. H. (1999) 'Treatment strategies for medulloblastoma and primitive neuroectodermal tumors.', *Neurosurgical Focus*, 7(2), pp. 1–12.

Gonzalez-Flores, A., Aguilar-Quesada, R., Siles, E., Pozo, S., Rodríguez-Lara, M. I., López-Jiménez, L., López-Rodríguez, M., Peralta-Leal, A., Villar, D., Martín-Oliva, D., Del Peso, L., Berra, E. and Oliver, F. J. (2014) 'Interaction between PARP-1 and HIF-2 in the hypoxic response', *Oncogene*, 33(7), pp. 891–898.

Goodman, L., Wintrobe, M., Dameshek, W., Goodman, M., Gilman, A. and Mclennan, M. (1946) 'Nitrogen mustard therapy. Use of methyl-bis(beta-chloroethyl)amine hydrochloride and tris(beta-chloroethyl)amine hydrochloride for Hodgkin's disease, lymphoscarcoma, leukemia and certain allied and miscellanous disorders', *JAMA*, 132(3), pp. 126–132.

Gottlieb, T. M. and Jackson, P. (1993) 'The DNA-Dependent Protein Kinase: Requirement for DNA ends and Association with Ku Antigen', *Cell*, 72, pp. 131–142.

Gradia, S., Acharya, S. and Fishel, R. (1997) 'The human mismatch recognition complex hMSH2-hMSH6 functions as a novel molecular switch', *Cell*, 91(7), pp. 995–1005.

Gradia, S., Subramanian, D., Wilson, T., Acharya, S., Makhov, A., Griffith, J. and Fishel, R. (1999) 'hMSH2-hMSH6 forms a hydrolysis-independent sliding clamp on mismatched DNA', *Molecular Cell*, 3(2), pp. 255–261.

Graeber, T. G., Peterson, J. F., Tsai, M., Monica, K., Fornace, A. J. and Giaccia, A. J. (1994) 'Hypoxia induces accumulation of p53 protein, but activation of a G1-phase checkpoint by low-oxygen conditions is independent of p53 status.', *Molecular and Cellular Biology*, 14(9), pp. 6264–6277.

Graven, K. K., Troxler, R. F., Kornfeld, H., Panchenko, M. V and Farber, H. W. (1994) 'Regulation of endothelial cell glyceraldehyde-3-phosphate dehydrogenase expression by hypoxia', *Journal of Biological Chemistry*, 269(39), pp. 24446–24453.

Grawunder, U., Wilm, M., Wu, X., Kulesza, P., Wilson, T. E., Mann, M. and Lieber, M. R. (1997) 'Activity of DNA ligase IV stimulated by complex formation with XRCC4 protein in mammalian cells', *Nature*, 388(6641), pp. 492–495.

Grawunder, U., Zimmer, D. and Lieber, M. R. (1998) 'DNA ligase IV binds to XRCC4 via a motif located between rather than within its BRCT domains', *Current Biology*, 8, pp. 873–876.

Greco, G. E., Matsumoto, Y., Brooks, R. C., Lu, Z., Lieber, M. R. and Tomkinson, A. E. (2016) 'SCR7 is neither a selective nor a potent inhibitor of human DNA ligase IV', *DNA Repair*, 43, pp. 18–23.

Guerra, C. A., Noor, A. M., Myint, H. Y., Hay, S. I., Marois, E., Levashina, E. A., Host, C., Christophides, G. K., Kafatos, F. C., Lambrechts, L., Koella, J. C., Bourgouin, C., Dimopoulos, G., Povelones, M., Blagborough, A. M., *et al.* (2009) 'Glioma-derived mutations in IDH1 dominantly inhibit IDH1 catalytic activity and induce HIF-1a', *Science*, 324, pp. 261–265.

Guo, Z., Kumagai, A., Wang, S. X. and Dunphy, W. G. (2000) 'regulation in response to DNA replication blocks and UV-damaged DNA in Xenopus egg extracts Requirement for Atr in phosphorylation of Chk1 and cell cycle regulation in response to DNA replication blocks and UV-damaged DNA in Xenopus egg extracts', *Genes & Development*, pp. 2745–2756.

Gupta, R., Chetty, C., Bhoopathi, P., Lakka, S., Mohanam, S., Rao, J. S. and Dinh, D. H. (2011)

'Downregulation of uPA/uPAR inhibits intermittent hypoxia-induced epithelial-mesenchymal transition (EMT) in DAOY and D283 medulloblastoma cells', *International Journal of Oncology*, 38(3), pp. 733–744.

Hammond, E. M., Denko, N. C., Dorie, M. J., Abraham, R. T. and Giaccia, A. J. (2002) 'Hypoxia Links ATR and p53 through Replication Arrest', *Molecular and Cellular Biology*, 22(6), pp. 1834–1843.

Hammond, E. M., Dorie, M. J. and Giaccia, A. J. (2003) 'ATR/ATM targets are phosphorylated by ATR in response to hypoxia and ATM in response to reoxygenation', *Journal of Biological Chemistry*, 278(14), pp. 12207–12213.

Hammond, E. M., Green, S. L. and Giaccia, A. J. (2003) 'Comparison of hypoxia-induced replication arrest with hydroxyurea and aphidicolin-induced arrest', *Mutation Research*, 532(1–2), pp. 205–213.

Hanahan, D. and Weinberg, R. A. (2000) 'The Hallmarks of Cancer', *Cell*, 100, pp. 57–70.

Hanahan, D. and Weinberg, R. A. (2011) 'Hallmarks of cancer: the next generation.', *Cell*, 144(5), pp. 646–674.

Harding, S. M., Coackley, C. and Bristow, R. G. (2011) 'ATM-dependent phosphorylation of 53BP1 in response to genomic stress in oxic and hypoxic cells', *Radiotherapy and Oncology*, 99(3), pp. 307–312.

Hargrave, D. R. and Zacharoulis, S. (2007) 'Pediatric CNS tumors: current treatment and future directions.', *Expert Review of Neurotherapeutics*, 7(8), pp. 1029–42.

Harrington, J. J. and Lieber, M. R. (1994) 'The characterization of a mammalian DNA structure-specific endonuclease.', *The EMBO journal*, 13(5), pp. 1235–1246.

Hegi., Marie-france, Tribolet, N. De, Weller, M., Kros, J. M., Hainfellner, J. A., Mason, W., Mariani, L., Bromberg, J. E. C., Hau, P. and Stupp, R. (2005) 'Gene Silencing and Benefit from Temozolomide in Glioblastoma', *New England Journal of Medicine*, 352(10), pp. 997–1003.

Hernández-Jiménez, M., Ayuso, M. I., Pérez-Morgado, M. I., García-Recio, E. M., Alcázar, A., Martín, M. E. and González, V. M. (2012) 'EIF4F complex disruption causes protein synthesis inhibition during hypoxia in nerve growth factor (NGF)-differentiated PC12 cells', *Biochimica et Biophysica Acta*, 1823(2), pp. 430–438.

Herrmann, Rice, M., Levy, R., Pizer, B., Losty, P., Moss, D. and See, V. (2015) 'Cellular memory of hypoxia elicits neuroblastoma metastasis and enables invasion by non-aggressive neighbouring cells', *Oncogenesis*, 4(2), pp. 1–11.

Hewitson, K. S., McNeill, L. a., Riordan, M. V., Tian, Y. M., Bullock, A. N., Welford, R. W., Elkins, J. M., Oldham, N. J., Bhattacharya, S., Gleadle, J. M., Ratcliffe, P. J., Pugh, C. W. and Schofield, C. J. (2002) 'Hypoxia-inducible factor (HIF) asparagine hydroxylase is identical to factor inhibiting HIF (FIH) and is related to the cupin structural family', *Journal of Biological Chemistry*, 277(29), pp. 26351–26355.

Hoang, M. L., Kinde, I., Tomasetti, C., McMahon, K. W., Rosenquist, T. A., Grollman, A. P., Kinzler, K. W., Vogelstein, B. and Papadopoulos, N. (2016) 'Genome-wide quantification of rare somatic mutations in normal human tissues using massively parallel sequencing', *Proceedings of the National Academy of Sciences*, 113(35), pp. 9846–9851.

Hoeijmakers, J. H. J. (2009) 'DNA Damage, Aging, and Cancer', *New England Journal of Medicine*, 361(15), pp. 1475–1485.

Hu, J., Adebali, O., Adar, S. and Sancar, A. (2017) 'Dynamic maps of UV damage formation and repair for the human genome', *Proceedings of the National Academy of Sciences*, 114(26), pp. 6758–6763.

Hu, J., Lieb, J. D., Sancar, A. and Adar, S. (2016) 'Cisplatin DNA damage and repair maps of the human genome at single-nucleotide resolution', *Proceedings of the National Academy of Sciences*, 113(41), pp. 11507–11512.

Hu, Y., DeLay, M., Jahangiri, A., Molinaro, A., Rose, S., Carbonell, S. and Aghi, M. (2009) 'Hypoxia-induced autophagy promotes tumor cell survival and adaptation to anti-angiogenic treatment in glioblastoma', *Cancer Research*, 19(5–6), pp. 389–399.

Huang, E., Teh, B. S., Strother, D. R., Davis, Q. G., Chiu, J. K., Lu, H. H., Carpenter, L. S., Mai, W. Y., Chintagumpala, M. M., South, M., Grant, W. H., Butler, E. B. and Woo, S. Y. (2002) 'Intensity-modulated radiation therapy for pediatric medulloblastoma: Early report on the reduction of ototoxicity', *International Journal of Radiation Oncology Biology Physics*, 52(3), pp. 599–605.

Hubscher, U., Jonsson, Z. O. and Hindges, R. (1998) 'Regulation of DNA replication and repair proteins through interaction with the front side of proliferating cell nuclear antigen', *Embo Journal*, 17(8), pp. 2412–2425.

Iaccarino, I., Marra, G., Dufner, P. and Jiricny, J. (2000) 'Mutation in the magnesium binding site of hMSH6 disables the hMutSα sliding clamp from translocating along DNA', *Journal of Biological Chemistry*, 275(3), pp. 2080–2086.

Ishida, J., Onishi, M., Kurozumi, K., Ichikawa, T., Fujii, K., Shimazu, Y., Oka, T. and Date, I. (2014) 'Integrin inhibitor suppresses bevacizumab-induced glioma invasion', *Translational Oncology*, 7(2), pp. 292–302.

Ivan, M., Kondo, K., Yang, H., Valiando, J., Ohh, M., Salic, A., Asara, J. M., Lane, W. S. and Kaelin, W. G. (2001) 'HIF alpha Targeted for VHL-mediated destruction by proline hydroxylation: implications for 02 sensing', *Science*, 292, pp. 464–468.

De Jager, M., Van Noort, J., Van Gent, D. C., Dekker, C., Kanaar, R. and Wyman, C. (2001) 'Human Rad50/Mre11 is a flexible complex that can tether DNA ends', *Molecular Cell*, 8(5), pp. 1129–1135.

Jakacki, R. I., Burger, P. C., Zhou, T., Holmes, E. J., Kocak, M., Onar, A., Goldwein, J., Mehta, M., Packer, R. J., Tarbell, N., Fitz, C., Vezina, G., Hilden, J. and Pollack, I. F. (2012) 'Outcome of children with metastatic medulloblastoma treated with carboplatin during craniospinal radiotherapy: A children's oncology group phase I/II study', *Journal of Clinical Oncology*, 30(21), pp. 2648–2653.

Johnson, A. B., Denko, N. and Barton, M. C. (2008) 'Hypoxia induces a novel signature of chromatin modifications and global repression of transcription', *Mutation Research*, 640(713), pp. 174–179.

Jones, D. T. W., Jäger, N., Kool, M., Zichner, T., Hutter, B., Sultan, M., Cho, Y. J., Pugh, T. J., Hovestadt, V., Stütz, A. M., Rausch, T., Warnatz, H. J., Ryzhova, M., Bender, S., Sturm, D., *et al.* (2012) 'Dissecting the genomic complexity underlying medulloblastoma', *Nature*, 488(7409), pp. 100–105.

Joseph, J. V., Conroy, S., Pavlov, K., Sontakke, P., Tomar, T., Eggens-Meijer, E., Balasubramaniyan, V., Wagemakers, M., den Dunnen, W. F. A. and Kruyt, F. A. E. (2015) 'Hypoxia enhances migration and invasion in glioblastoma by promoting a mesenchymal shift mediated by the HIF1α-ZEB1 axis', *Cancer Letters*, 359(1), pp. 107–116.

Kalra, R., Jones, A.-M., Kirk, J., Adams, G. E. and Stratford, I. J. (1993) 'The effect of hypoxia on acquired drug resistance and response to epidermal growth factor in Chinese hamster lung fibroblasts and human breast-cancer cells in vitro', *International Journal of Cancer*, 54(4), pp. 650–655.

Kawabata, M., Kawabata, T. and Nishibori, M. (2005) 'Role of recA/RAD51 family proteins in mammals', *Acta Medica Okayama*, 59(1), pp. 1–9.

Kawada, K., Yonei, T., Ueoka, H., Kiura, K., Tabata, M., Takigawa, M., Harada, M. and Tanimoto, M. (2002) 'Comparison of Chemisensitivity Tests: Clonogentic Assays versus MTT Assay', *Acta Medica Okayama*, pp. 129–134.

Kawauchi, D., Robinson, G., Uziel, T., Gibson, P., Rehg, J., Gao, C., Finkelstein, D., Qu, C., Pounds, S., Ellison, D. W., Gilbertson, R. J. and Roussel, M. F. (2012) 'A Mouse Model of the Most Aggressive Subgroup of Human Medulloblastoma', *Cancer Cell*, 21(2), pp. 168–180.

Keunen, O., Johansson, M., Oudin, A., Sanzey, M., Rahim, S. A. A., Fack, F., Thorsen, F., Taxt, T., Bartos, M., Jirik, R., Miletic, H., Wang, J., Stieber, D., Stuhr, L., Moen, I., *et al.* (2011) 'Anti-VEGF treatment reduces blood supply and increases tumor cell invasion in glioblastoma', *Proceedings of the National Academy of Sciences*, 108(9), pp. 3749–3754.

Kim, J., Aftab, B. T., Tang, J. Y., Kim, D., Lee, A. H., Rezaee, M., Kim, J., Chen, B., King, E. M., Borodovsky, A., Riggins, G. J., Epstein, E. H., Beachy, P. A. and Rudin, C. M. (2013) 'Itraconazole and Arsenic Trioxide Inhibit Hedgehog Pathway Activation and Tumor Growth Associated with Acquired Resistance to Smoothened Antagonists', *Cancer Cell*, 23(1), pp. 23–34.

Kim, J., Lee, J. J., Kim, J., Gardner, D. and Beachy, P. A. (2010) 'Arsenic antagonizes the Hedgehog pathway by preventing ciliary accumulation and reducing stability of the Gli2 transcriptional effector', *Proceedings of the National Academy of Sciences*, 107(30), pp. 13432–13437.

Kim, N., Bozek, G., Lo, J. C. and Storb, U. (1999) 'Different mismatch repair deficiencies all have the same effects on somatic hypermutation: intact primary mechanism accompanied by secondary modifications', *Journal of Experimental Medicine*, 190(1), pp. 21–30.

Kohn, K. W., Spears, C. L. and Doty, P. (1966) 'Inter-strand crosslinking of DNA by nitrogen mustard', *Journal of Molecular Biology*, 19(2), pp. 266–288.

Kondo, N., Takahashi, A., Mori, E., Noda, T., Su, X., Ohnishi, K., McKinnon, P. J., Sakaki, T., Nakase, H., Ono, K. and Ohnishi, T. (2010) 'DNA ligase IV is a potential molecular target in ACNU sensitivity', *Cancer Science*, 101(8), pp. 1881–1885.

Kondo, N., Takahashi, A., Mori, E., Ohnishi, K., McKinnon, P. J., Sakaki, T., Nakase, H. and Ohnishi, T. (2009) 'DNA ligase IV as a new molecular target for temozolomide', *Biochemical and Biophysical Research Communications*, 387(4), pp. 656–660.

Kong, X., Mohanty, S. K., Stephens, J., Heale, J. T., Gomez-Godinez, V., Shi, L. Z., Kim, J. S., Yokomori, K. and Berns, M. W. (2009) 'Comparative analysis of different laser systems to study cellular responses to DNA damage in mammalian cells', *Nucleic Acids Research*, 37(9).

Kool, M., Korshunov, A., Remke, M., Jones, D. T. W., Schlanstein, M., Northcott, P. A., Cho, Y. J., Koster, J., Schouten-Van Meeteren, A., Van Vuurden, D., Clifford, S. C., Pietsch, T., Von Bueren, A. O., Rutkowski, S., McCabe, M., *et al.* (2012) 'Molecular subgroups of medulloblastoma: An international meta-analysis of transcriptome, genetic aberrations, and clinical data of WNT, SHH, Group 3, and Group 4 medulloblastomas', *Acta Neuropathologica*, 123(4), pp. 473–484.

Koritzinsky, M., Rouschop, K. M. A., van den Beucken, T., Magagnin, M. G., Savelkouls, K., Lambin, P. and Wouters, B. G. (2007) 'Phosphorylation of eIF2α is required for mRNA translation inhibition and survival during moderate hypoxia', *Radiotherapy and Oncology*, 83(3), pp. 353–361.

Koshiji, M., To, K. K. W., Hammer, S., Kumamoto, K., Harris, A. L., Modrich, P. and Huang, L. E. (2005) 'HIF-1α induces genetic instability by transcriptionally downregulating MutSα expression', *Molecular Cell*, 17(6), pp. 793–803.

Krieg, A. J., Rankin, E. B., Chan, D., Razorenova, O., Fernandez, S. and Giaccia, A. J. (2010) 'Regulation of the Histone Demethylase JMJD1A by Hypoxia-Inducible Factor 1 Enhances Hypoxic Gene Expression and Tumor Growth', *Molecular and Cellular Biology*, 30(1), pp. 344–353.

Krock, B. L., Skuli, N. and Simon, M. C. (2011) 'Hypoxia-Induced Angiogenesis: Good and Evil', *Genes and Cancer*, 2(12), pp. 1117–1133.

Kulshreshtha, R., Ferracin, M., Wojcik, S. E., Garzon, R., Alder, H., Agosto-Perez, F. J., Davuluri, R., Liu, C.-G., Croce, C. M., Negrini, M., Calin, G. A. and Ivan, M. (2007) 'A MicroRNA Signature of Hypoxia', *Molecular and Cellular Biology*, 27(5), pp. 1859–1867.

Kumareswaran, R., Ludkovski, O., Meng, A., Sykes, J., Pintilie, M. and Bristow, R. G. (2012) 'Chronic hypoxia compromises repair of DNA double-strand breaks to drive genetic instability.', *Journal of Cell Science*, 125(Pt 1), pp. 189–99.

Kurimasa, A., Kumano, S., Boubnov, N. V, Story, M. D., Tung, C. S., Peterson, S. R. and Chen, D. J. (1999) 'Requirement for the kinase activity of human DNA-dependent protein kinase catalytic subunit in DNA strand break rejoining.', *Molecular and Cellular Biology*, 19(5), pp. 3877–84.

Labbé, A., Lafleur, V. N., Patten, D. A., Robitaille, G. A., Garand, C., Lamalice, L., Lebel, M. and Richard, D. E. (2012) 'The Werner syndrome gene product (WRN): A repressor of hypoxia-inducible factor-1 activity', *Experimental Cell Research*, 318(14), pp. 1620–1632.

Lander, E. S., Linton, L. M., Birren, B., Nusbaum, C., Zody, M. C., Baldwin, J., Devon, K., Dewar, K., Doyle, M., FitzHugh, W., Funke, R., Gage, D., Harris, K., Heaford, A., Howland, J., *et al.* (2001) 'Initial sequencing and analysis of the human genome', *Nature*, 409(6822), pp. 860–921.

Lando, D., Peet, D. J., Gorman, J. J., Whelan, D. a., Whitelaw, M. L. and Bruick, R. K. (2002)

'FIH-1 is an asparaginyl hydroxylase enzyme that regulates the transcriptional activity of hypoxia-inducible factor', *Genes and Development*, 16(12), pp. 1466–1471.

Langdon, J. A., Lamont, J. M., Scott, D. K., Dyer, S., Prebble, E., Bown, N., Grundy, R. G., Ellison, D. W. and Clifford, S. C. (2006) 'Combined genome-wide allelotyping and copy number analysis identify frequent genetic losses without copy number reduction in medulloblastoma', *Genes Chromosomes and Cancer*, 45(1), pp. 47–60.

Lee, K., Zhang, H., Qian, D. Z., Rey, S., Liu, J. O. and Semenza, G. L. (2009) 'Acriflavine inhibits HIF-1 dimerization, tumor growth, and vascularization', *Proceedings of the National Academy of Sciences*, 106(42), pp. 17910–17915.

Lehle, S., Hildebrand, D. G., Merz, B., Malak, P. N., Becker, M. S., Schmezer, P., Essmann, F., Schulze-Osthoff, K. and Rothfuss, O. (2014) 'LORD-Q: A long-run real-time PCR-based DNA-damage quantification method for nuclear and mitochondrial genome analysis', *Nucleic Acids Research*, 42(6).

Lei, X., Zhu, Y., Tomkinson, A. and Sun, L. (2004) 'Measurement of DNA mismatch repair activity in live cells', *Nucleic Acids Research*, 32(12), p. 100.

Leland, A. M. D., Jef, H. M. D., Paul, M. M. D., D, J. M. P., Lucy, B. M. D. and Philip, M. D. (1996) 'Effects of Medulloblastoma Resections on Outcome in Children : A Report from the Children 's Cancer Group', *Neurosurgery*, 38(2), pp. 265–271.

Lendahl, U., Zimmerman, L. and Mckay, R. (1990) 'CNS stem cells express a new class of intermediate filament protein', *Cell*, 60(4), pp. 585–595.

Leszczynska, K. B., Foskolou, I. P., Abraham, A. G., Anbalagan, S., Tellier, C., Haider, S., Span, P. N., O'Neill, E. E., Buffa, F. M. and Hammond, E. M. (2015) 'Hypoxia-induced p53 modulates both apoptosis and radiosensitivity via AKT', *Journal of Clinical Investigation*, 125(6), pp. 2385–2398.

Li, G. M. and Modrich, P. (1995) 'Restoration of mismatch repair to nuclear extracts of H6 colorectal tumor cells by a heterodimer of human MutL homologs.', *Proceedings of the National Academy of Sciences of the United States of America*, 92(6), pp. 1950–1954.

Li, J., Hou, N., Faried, A., Tsutsumi, S. and Kuwano, H. (2010) 'Inhibition of autophagy augments 5-fluorouracil chemotherapy in human colon cancer in vitro and in vivo model', *European Journal of Cancer*, 46(10), pp. 1900–1909.

Liang, L., Deng, L., Nguyen, S. C., Zhao, X., Maulion, C. D., Shao, C. and Tischfield, J. A. (2008) 'Human DNA ligases I and III, but not ligase IV, are required for microhomology-mediated end joining of DNA double-strand breaks', *Nucleic Acids Research*, 36(10), pp. 3297–3310.

Liau, L. M., Ashkan, K., Tran, D. D., Campian, J. L., Trusheim, J. E., Cobbs, C. S., Heth, J. A., Salacz, M., Taylor, S., D'Andre, S. D., Iwamoto, F. M., Dropcho, E. J., Moshel, Y. A., Walter, K. A., Pillainayagam, C. P., *et al.* (2018) 'First results on survival from a large Phase 3 clinical trial of an autologous dendritic cell vaccine in newly diagnosed glioblastoma', *Journal of Translational Medicine*, 16(142), pp. 1–9.

Lin, C. Y., Erkek, S., Tong, Y., Yin, L., Federation, A. J., Zapatka, M., Haldipur, P., Kawauchi, D., Risch, T., Warnatz, H. J., Worst, B. C., Ju, B., Orr, B. A., Zeid, R., Polaski, D. R., *et al.* (2016) 'Active medulloblastoma enhancers reveal subgroup-specific cellular origins', *Nature*, 530(7588), pp. 57–62.

Lindahl, T. (1993) 'Instability and decay of the primary structure of DNA', *Nature*, 362(6422), pp. 709–715.

Liu, D., Yang, Y., Liu, Q. and Wang, J. (2011) 'Inhibition of autophagy by 3-MA potentiates cisplatin-induced apoptosis in esophageal squamous cell carcinoma cells', *Medical Oncology*, 28(1), pp. 105–111.

Liu, K., Yang, S., Lin, Y.-K., Lin, J.-W., Lee, Y., Wang, J.-Y., Hu, C., Lin, E., Chen, S., Then, C. and Shen, S. (2015) 'Fluoxetine, an antidepressant, suppresses glioblastoma by evoking AMPAR-mediated calcium-dependent apoptosis.', *Oncotarget*, 6(7), pp. 5088–101.

Liu, L., Ning, X., Sun, L., Zhang, H., Shi, Y., Guo, C., Han, S., Liu, J., Sun, S., Han, Z., Wu, K. and Fan, D. (2008) 'Hypoxia-inducible factor-1α contributes to hypoxia-induced chemoresistance in gastric cancer', *Cancer Science*, 99(1), pp. 121–128.

Liu, Q., Guntuku, S., Cui, X. S., Matsuoka, S., Cortez, D., Tamai, K., Luo, G., Carattini-Rivera,

S., DeMayo, F., Bradley, A., Donehower, L. A. and Elledge, S. J. (2000) 'Chk1 is an essential kinase that is regulated by Atr and required for the G2/M DNA damage checkpoint', *Genes and Development*, 14(12), pp. 1448–1459.

Liu, X. W., Su, Y., Zhu, H., Cao, J., Ding, W. J., Zhao, Y. C., He, Q. J. and Yang, B. (2010) 'HIF-1α-dependent autophagy protects HeLa cells from fenretinide (4-HPR)-induced apoptosis in hypoxia', *Pharmacological Research*, 62(5), pp. 416–425.

Llaguno, S. A., Chen, J., Kwon, C., Jackson, E. L., Li, Y., Burns, D. K., Alvarez-buylla, A. and Parada, L. F. (2010) 'Malignant astrocytomas originate from nueral stem/projenitor cells in a somatic tumour suppressor mouse model', *Cancer*, 15(1), pp. 45–56.

Longley, M. J., Pierce, A. J. and Modrich, P. (1997) 'DNA polymerase δ is required for human mismatch repair in vitro', *Journal of Biological Chemistry*, 272(16), pp. 10917–10921.

Louis, D. N., Ohgaki, H., Wiestler, O. D., Cavenee, W. K., Burger, P. C., Jouvet, A., Scheithauer, B. W. and Kleihues, P. (2007) 'The 2007 WHO classification of tumours of the central nervous system', *Acta Neuropathologica*, 114(2), pp. 97–109.

Louis, D. N., Perry, A., Reifenberger, G., von Deimling, A., Figarella-Branger, D., Cavenee, W. K., Ohgaki, H., Wiestler, O. D., Kleihues, P. and Ellison, D. W. (2016) 'The 2016 World Health Organization Classification of Tumors of the Central Nervous System: a summary', *Acta Neuropathologica*, 131(6), pp. 803–820.

Lu, Y., Chu, A., Turker, M. S. and Glazer, P. M. (2011) 'Hypoxia-Induced Epigenetic Regulation and Silencing of the BRCA1 Promoter', *Molecular and Cellular Biology*, 31(16), pp. 3339–3350.

Lu, Y., Wajapeyee, N., Turker, M. S. and Glazer, P. M. (2014) 'Silencing of the DNA Mismatch Repair Gene MLH1 Induced by Hypoxic Stress in a Pathway Dependent on the Histone Demethylase LSD1', *Cell Reports*, 8(2), pp. 501–513.

Lukas, C., Falck, J., Bartkova, J., Bartek, J. and Lukas, J. (2003) 'Distinct spatiotemporal dynamics of mammalian checkpoint regulators induced by DNA damage.', *Nature Cell Biology*, 5(3), pp. 255–260.

Lum, J. J., DeBerardinis, R. J. and Thompson, C. B. (2005) 'Autophagy in metazoans: Cell survival in the land of plenty', *Nature Reviews Molecular Cell Biology*, 6(6), pp. 439–448.

Lundin, C., Erixon, K., Arnaudeau, C., Jenssen, D., Meuth, M., Helleday, T. and Schultz, N. (2002) 'Different Roles for Nonhomologous End Joining and Homologous Recombination following Replication Arrest in Mammalian Cells Different Roles for Nonhomologous End Joining and Homologous Recombination following Replication Arrest in Mammalian Cells', *Molecular and Cellular Biology*, 22(16), pp. 5869–5878.

Lv, Y., Zhao, S., Han, J., Zheng, L., Yang, Z. and Zhao, L. (2015) 'Hypoxia-inducible factor-1α induces multidrug resistance protein in colon cancer', *OncoTargets and Therapy*, 8, pp. 1941–1948.

Madan, E., Gogna, R. and Pati, U. (2012) 'p53 Ser ^{15} phosphorylation disrupts the p53–RPA70 complex and induces RPA70-mediated DNA repair in hypoxia', *Biochemical Journal*, 443(3), pp. 811–820.

Mahaney, B. L., Meek, K. and Lees-Miller, S. P. (2009) 'Repair of ionizing radiation-induced DNA double-strand breaks by non-homologous end-joining', *Biochemical Journal*, 417(3), pp. 639–650.

Malbari, F., Quinlan, A., Hanson, D., Levy, A. and Atlas, M. (2012) 'Tolerability of temozolomide in conjunction with craniospinal irradiation for the treatment of pediatric cns embryonal tumors', *Neuro-Oncology*, 1(1:8), pp. 1–4.

Malkov, V. A., Serikawa, K. A., Balantac, N., Watters, J., Geiss, G., Mashadi-Hossein, A. and Fare, T. (2009) 'Multiplexed measurements of gene signatures in different analytes using the Nanostring nCounterTM assay system', *BMC Research Notes*, 2, pp. 1–9.

Mari, P.-O., Florea, B. I., Persengiev, S. P., Verkaik, N. S., Bruggenwirth, H. T., Modesti, M., Giglia-Mari, G., Bezstarosti, K., Demmers, J. A. A., Luider, T. M., Houtsmuller, A. B. and van Gent, D. C. (2006) 'Dynamic assembly of end-joining complexes requires interaction between Ku70/80 and XRCC4', *Proceedings of the National Academy of Sciences*, 103(49), pp. 18597–18602.

Matsuoka, S., Rotman, G., Ogawa, A., Shiloh, Y., Tamai, K. and Elledge, S. J. (2000) 'Ataxia telangiectasia-mutated phosphorylates Chk2 in vivo and in vitro.', *Proceedings of the National Academy of Sciences of the United States of America*, 97(19), pp. 10389–94.

McFaline-Figueroa, J. L., Braun, C. J., Stanciu, M., Nagel, Z. D., Mazzucato, P., Sangaraju, D., Cerniauskas, E., Barford, K., Vargas, A., Chen, Y., Tretyakova, N., Lees, J. A., Hemann, M. T., White, F. M. and Samson, L. D. (2015) 'Minor changes in expression of the mismatch repair protein MSH2 exert a major impact on glioblastoma response to temozolomide', *Cancer Research*, 75(15), pp. 3127–3138.

McFarlane, R. J. and Wakeman, J. A. (2017) 'Meiosis-like functions in oncogenesis: A new view of cancer', *Cancer Research*, 77(21), pp. 5712–5716.

McLendon, R., Friedman, A., Bigner, D., Van Meir, E. G., Brat, D. J., Mastrogianakis, G. M., Olson, J. J., Mikkelsen, T., Lehman, N., Aldape, K., Yung, W. K. A., Bogler, O., Weinstein, J. N., VandenBerg, S., Berger, M., *et al.* (2008) 'Comprehensive genomic characterization defines human glioblastoma genes and core pathways', *Nature*, 455(7216), pp. 1061–1068.

McNeill, L. a, Hewitson, K. S., Claridge, T. D., Seibel, J. F., Horsfall, L. E. and Schofield, C. J. (2002) 'Hypoxia-inducible factor asparaginyl hydroxylase (FIH-1) catalyses hydroxylation at the beta-carbon of asparagine-803.', *The Biochemical Journal*, 367(Pt 3), pp. 571–575.

Meldrum, R. A. and Botchway, S. W. (2003) 'Nanoscale spatial induction of ultraviolet photoproducts in cellular DNA by three-photon near-infrared absorption', *EMBO Reports*, 4(12), pp. 1144–1149.

Meley, D., Spiller, D. G., White, M. R. H., McDowell, H., Pizer, B. and Sée, V. (2010) 'p53-mediated delayed NF-κB activity enhances etoposide-induced cell death in medulloblastoma.', *Cell Death & Disease*, 1, p. e41.

Meng, A. X., Jalali, F., Cuddihy, A., Chan, N., Bindra, R. S., Glazer, P. M. and Bristow, R. G. (2005) 'Hypoxia down-regulates DNA double strand break repair gene expression in prostate cancer cells', *Radiotherapy and Oncology*, 76(2), pp. 168–176.

Merkle, D., Douglas, P., Moorhead, G. B. G., Leonenko, Z., Yu, Y., Cramb, D., Bazett-Jones, D.

P. and Lees-Miller, S. P. (2002) 'The DNA-dependent protein kinase interacts with DNA to form a protein - DNA complex that is disrupted by phosphorylation', *Biochemistry*, 41(42), pp. 12706–12714.

Mihaylova, V. T., Bindra, R. S., Yuan, J., Campisi, D., Narayanan, L., Jensen, R., Giordano, F., Johnson, R. S., Rockwell, S. and Glazer, P. M. (2003) 'Decreased Expression of the DNA Mismatch Repair Gene Mlh1 under Hypoxic Stress in Mammalian Cells', *Molecular and Cellular Biology*, 23(9), pp. 3265–3273.

Mizumoto, M., Yamamoto, T., Takano, S., Ishikawa, E., Matsumura, A., Ishikawa, H., Okumura, T., Sakurai, H., Miyatake, S. I. and Tsuboi, K. (2014) 'Long-term survival after treatment of glioblastoma multiforme with hyperfractionated concomitant boost proton beam therapy', *Practical Radiation Oncology*. American Society for Radiation Oncology, 5(1), pp. e9–e16.

Modesti, M., Hesse, J. E. and Gellert, M. (1999) 'DNA binding of Xrcc4 protein is associated with V(D)J recombination but not with stimulation of DNA ligase IV activity.', *The EMBO journal*, 18(7), pp. 2008–2018.

Mondesert, O., Frongia, C., Clayton, O., Boizeau, M. L., Lobjois, V. and Ducommun, B. (2015) 'Monitoring the activation of the DNA damage response pathway in a 3D spheroid model', *PLoS ONE*, 10(7), pp. 1–12.

Moynahan, M. E., Chiu, J. W., Koller, B. H. and Jasint, M. (1999) 'Brca1 controls homology-directed DNA repair', *Molecular Cell*, 4(4), pp. 511–518.

Murphy, M. F. G., Bithell, J. F., Stiller, C. A., Kendall, G. M. and O'Neill, K. A. (2013) 'Childhood and adult cancers: Contrasts and commonalities', *Maturitas*, 76(1), pp. 95–98.

Muz, B., de la Puente, P., Azab, F., Ghobrial, I. M. and Azab, a. K. (2015) 'Hypoxia Promotes Dissemination and Colonization in New Bone Marrow Niches in Waldenstrom Macroglobulinemia', *Molecular Cancer Research*, 13(2), pp. 263–272.

Muz, B., Puente, P. de la, Azab, F. and Azab, A. K. (2015) 'The role of hypoxia in cancer progression angiogenesis metastasis and resistane to therapy', *Hypoxia*, 3, pp. 83–92.

Nagel, Z. D., Margulies, C. M., Chaim, I. A., McRee, S. K., Mazzucato, P., Ahmad, A., Abo, R. P., Butty, V. L., Forget, A. L. and Samson, L. D. (2014) 'Multiplexed DNA repair assays for multiple lesions and multiple doses via transcription inhibition and transcriptional mutagenesis', *Proceedings of the National Academy of Sciences*, 111(18), pp. E1823–E1832.

Nakamura, H., Tanimoto, K., Hiyama, K., Yunokawa, M., Kawamoto, T., Kato, Y., Yoshiga, K., Poellinger, L., Hiyama, E. and Nishiyama, M. (2008) 'Human mismatch repair gene, MLH1, is transcriptionally repressed by the hypoxia-inducible transcription factors, DEC1 and DEC2', *Oncogene*, 27(30), pp. 4200–4209.

Nakanishi, K., Cavallo, F., Brunet, E. and Jasin, M. (2011) 'Homologous recombination assay for interstrand crosslink repair', 745(12), pp. 1–8.

Nicholson, H. S., Kretschmar, C. S., Krailo, M., Bernstein, M., Kadota, R., Fort, D., Friedman, H., Harris, M. B., Tedeschi-Blok, N., Mazewski, C., Sato, J. and Reaman, G. H. (2007) 'Phase 2 study of temozolomide in children and adolescents with recurrent central nervous system tumors: A report from the Children's Oncology Group', *Cancer*, 110(7), pp. 1542–1550.

Nick McElhinny, S. A., Snowden, C. M., McCarville, J. and Ramsden, D. A. (2000) 'Ku recruits the XRCC4-ligase IV complex to DNA ends', *Molecular and Cellular Biology*, 20(9), pp. 2996–3003.

Northcott, P. A., Buchhalter, I., Morrissy, A. S., Hovestadt, V., Weischenfeldt, J., Ehrenberger, T., Gröbner, S., Segura-Wang, M., Zichner, T., Rudneva, V. A., Warnatz, H. J., Sidiropoulos, N., Phillips, A. H., Schumacher, S., Kleinheinz, K., *et al.* (2017) 'The whole-genome landscape of medulloblastoma subtypes', *Nature*, 547(7663), pp. 311–317.

Northcott, P. A., Korshunov, A., Witt, H., Hielscher, T., Eberhart, C. G., Mack, S., Bouffet, E., Clifford, S. C., Hawkins, C. E., French, P., Rutka, J. T., Pfister, S. and Taylor, M. D. (2011) 'Medulloblastoma comprises four distinct molecular variants', *Journal of Clinical Oncology*, 29(11), pp. 1408–1414.

Northcott, P. A., Shih, D. J. H., Peacock, J., Garzia, L., Sorana Morrissy, A., Zichner, T., Stütz, A. M., Korshunov, A., Reimand, J., Schumacher, S. E., Beroukhim, R., Ellison, D. W., Marshall, C. R., Lionel, A. C., Mack, S., *et al.* (2012) 'Subgroup-specific structural variation across 1,000 medulloblastoma genomes', *Nature*, 488(7409), pp. 49–56.

Noushmehr, H., Weisenberger, D. J., Diefes, K., Phillips, H. S., Pujara, K., Berman, B. P., Pan, F., Pelloski, C. E., Sulman, E. P., Bhat, K. P., Verhaak, R. G. W., Hoadley, K. A., Hayes, D. N., Perou, C. M., Schmidt, H. K., *et al.* (2010) 'Identification of a CpG Island Methylator Phenotype that Defines a Distinct Subgroup of Glioma', *Cancer Cell*, 17(5), pp. 510–522.

Ohgaki, H. and Kleihues, P. (2013) 'The definition of primary and secondary glioblastoma', *Clinical Cancer Research*, 19(4), pp. 764–772.

Ojalvo, L. S., King, W., Cox, D. and Pollard, J. W. (2009) 'High-density gene expression analysis of tumor-associated macrophages from mouse mammary tumors', *American Journal of Pathology*, 174(3), pp. 1048–1064.

Olcina, M. M., Foskolou, I. P., Anbalagan, S., Senra, J. M., Pires, I. M., Jiang, Y., Ryan, A. J. and Hammond, E. M. (2013) 'Replication stress and chromatin context link ATM activation to a role in DNA replication', *Molecular Cell*. The Authors, 52(5), pp. 758–766.

Olivier, M., Hollstein, M. and Hainaut, P. (2010) 'TP53 mutations in human cancers: origins, consequences, and clinical use.', *Cold Spring Harbor Perspectives in Biology*, 2(1), pp. 1–17.

Omuro, A. and DeAngelis, L. M. (2013) 'Glioblastoma and Other Malignant Gliomas', *Jama*, 310(17), p. 1842.

Packer, R. J., Gajjar, A., Vezina, G., Rorke-Adams, L., Burger, P. C., Robertson, P. L., Bayer, L., LaFond, D., Donahue, B. R., Marymont, M. H., Muraszko, K., Langston, J. and Sposto, R. (2006) 'Phase III study of craniospinal radiation therapy followed by adjuvant chemotherapy for newly diagnosed average-risk medulloblastoma', *Journal of Clinical Oncology*, 24(25), pp. 4202–4208.

Palanichamy, K., Kanji, S., Gordon, N., Thirumoorthy, K., Jacob, J. R., Litzenberg, K. T., Patel, Di. and Chakravarti, A. (2017) 'NNMT silencing activates tumor suppressor PP2A, inactivates oncogenic STKs, and inhibits tumor forming ability', *Clinical Cancer Research*, 23(9), pp. 2325–2334.

Pâques, F. and Haber, J. E. (1999) 'Multiple pathways of recombination induced by double-strand breaks in Saccharomyces cerevisiae.', *Microbiology and Molecular Biology Reviews*,

63(2), pp. 349–404.

Paranjpe, A., Zhang, R., Ali-Osman, F., Bobustuc, G. C. and Srivenugopal, K. S. (2014) 'Disulfiram is a direct and potent inhibitor of human O6-methylguanine-DNA methyltransferase (MGMT) in brain tumor cells and mouse brain and markedly increases the alkylating DNA damage', *Carcinogenesis*, 35(3), pp. 692–702.

Parsons, J. L., Dianova, I. I., Allinson, S. L. and Dianov, G. L. (2005) 'Poly(ADP-ribose) polymerase-1 protects excessive DNA strand breaks from deterioration during repair in human cell extracts', *FEBS Journal*, 272(8), pp. 2012–2021.

Paull, T. T. and Gellert, M. (1998) 'The 3′ to 5′ exonuclease activity of Mre11 facilitates repair of DNA double-strand breaks', *Molecular Cell*, 1(7), pp. 969–979.

Paull, T. T., Rogakou, E. P., Yamazaki, V., Kirchgessner, C. U., Gellert, M. and Bonner, W. M. (2000) 'A critical role for histone H2AX in recruitment of repair factors to nuclear foci after DNA damage', *Current Biology*, 10(15), pp. 886–895.

Pawlik, T. M. and Keyomarsi, K. (2004) 'Role of cell cycle in mediating sensitivity to radiotherapy', *International Journal of Radiation Oncology Biology Physics*, 59(4), pp. 928–942.

Pei, Y., Moore, C. E., Wang, J., Tewari, A. K., Eroshkin, A., Cho, Y. J., Witt, H., Korshunov, A., Read, T. A., Sun, J. L., Schmitt, E. M., Miller, C. R., Buckley, A. F., McLendon, R. E., Westbrook, T. F., *et al.* (2012) 'An Animal Model of MYC-Driven Medulloblastoma', *Cancer Cell*, 21(2), pp. 155–167.

Perreault, S., Ramaswamy, V., Achrol, A. S., Chao, K., Liu, T. T., Shih, D., Remke, M., Schubert, S., Bouffet, E., Fisher, P. G., Partap, S., Vogel, H., Taylor, M. D., Cho, Y. J. and Yeom, K. W. (2014) 'MRI surrogates for molecular subgroups of medulloblastoma', *American Journal of Neuroradiology*, 35(7), pp. 1263–1269.

Petr, C., Plank, J., Dombrowski, C. and Kowalczykowski, S. (2012) 'Decatenation of DNA by the S. cerevisiae Sgs1–Top3–Rmi1 and RPA complex: A mechanism for disentangling chromosomes', *Molecular Cell*, 47(6), pp. 886–896.

Phillips, H. S., Kharbanda, S., Chen, R., Forrest, W. F., Soriano, R. H., Wu, T. D., Misra, A., Nigro, J. M., Colman, H., Soroceanu, L., Williams, P. M., Modrusan, Z., Feuerstein, B. G. and Aldape, K. (2006) 'Molecular subclasses of high-grade glioma predict prognosis, delineate a pattern of disease progression, and resemble stages in neurogenesis', *Cancer Cell*, 9(3), pp. 157–173.

Pires, I. M., Bencokova, Z., Milani, M., Folkes, L. K., Li, J. A., Stratford, M. R., Harris, A. L. and Hammond, E. M. (2010) 'Effects of acute versus chronic hypoxia on DNA damage responses and genomic instability', *Cancer Research*, 70(3), pp. 925–935.

Pizer, B. and Clifford, S. (2008) 'Medulloblastoma: new insights into biology and treatment.', *Archives of Disease in Childhood. Education and Practice Edition*, 93(5), pp. 137–44.

Polkinghorn, W. R., Dunkel, I. J., Souweidane, M. M., Khakoo, Y., Lyden, D. C., Gilheeney, S. W., Becher, O. J., Budnick, A. S. and Wolden, S. L. (2011) 'Disease control and ototoxicity using intensity-modulated radiation therapy tumor-bed boost for medulloblastoma', *International Journal of Radiation Oncology Biology Physics*, 81(3), pp. 15–20.

Pugh, T. J., Weeraratne, S. D., Archer, T. C., Pomeranz Krummel, D. A., Auclair, D., Bochicchio, J., Carneiro, M. O., Carter, S. L., Cibulskis, K., Erlich, R. L., Greulich, H., Greulich, H., Lennon, N. J., Mc Kenna, A., Meldrim, J., *et al.* (2012) 'Medulloblastoma exome sequencing uncovers subtype-specific somatic mutations', *Nature*, 488(7409), pp. 106–110.

Qiu, Z. K., Shen, D., Chen, Y. S., Yang, Q. Y., Guo, C. C., Feng, B. H. and Chen, Z. P. (2014) 'Enhanced MGMT expression contributes to temozolomide resistance in glioma stem-like cells', *Chinese Journal of Cancer*, 33(2), pp. 115–122.

Ramaekers, C. H. M. a, Van Den Beucken, T., Meng, A., Kassam, S., Thoms, J., Bristow, R. G. and Wouters, B. G. (2011) 'Hypoxia disrupts the Fanconi anemia pathway and sensitizes cells to chemotherapy through regulation of UBE2T', *Radiotherapy and Oncology*, 101(1), pp. 190–197.

Rampling, R., Cruickshank, G., Lewis, A. D., Fitzsimmons, S. A. and Workman, P. (1994) 'Direct measurement of pO2 distribution and bioreductive enzymes in human malignant brain tumors', *International Journal of Radiation Oncology*Biology*Physics*, 29(3), pp. 427–431.

Ranjha, L., Howard, S. M. and Cejka, P. (2018) 'Main steps in DNA double-strand break repair: an introduction to homologous recombination and related processes', *Chromosoma*, pp. 1–28.

Rapisarda, A., Uranchimeg, B., Sordet, O., Pommier, Y., Shoemaker, R. H. and Melillo, G. (2004) 'Topoisomerase I-Mediated Inhibition of Hypoxia-Inducible Factor 1 : Mechanism and Therapeutic Implications Topoisomerase I-Mediated Inhibition of Hypoxia-Inducible Factor 1 : Mechanism and Therapeutic Implications', *Cancer Research*, 64, pp. 1475–1482.

Rass, E., Grabarz, A., Plo, I., Gautier, J., Bertrand, P. and Lopez, B. S. (2009) 'Role of Mre11 in chromosomal nonhomologous end joining in mammalian cells', *Nature Structural and Molecular Biology*, 16(8), pp. 819–824.

Ravi, R., Mookerjee, B., Bhujwalla, Z. M., Sutter, C. H., Artemov, D., Zeng, Q., Dillehay, L. E., Madan, A., Semenza, G. L. and Bedi, A. (2000) 'Regulation of tumor angiogenesis by p53-induced degradation of hypoxia-inducible factor 1α', *Genes & development*, 14(1), pp. 34–44.

Reardon, D. A., Peters, K. B., Desjardins, A., Gururangan, S., Sampson, J. H., McLendon, R. E., Herdon II, J., Bulusu, A., Threatt, S., Freidman, A. H., Vredenburgh, J. J. and Freidman, H. S. (2012) 'Phase II study of carboplatin irinotecan and bevacizumab for becacizumab naive recurrent glioblastoma', *Journal of Neuro-Oncology*, 107(1), pp. 155–164.

Reardon, J. T., Bessho, T., Kung, H. C., Bolton, P. H. and Sancar, A. (1997) 'In vitro repair of oxidative DNA damage by human nucleotide excision repair system: possible explanation for neurodegeneration in xeroderma pigmentosum patients', *Proceedings of the National Academy of Sciences of the United States of America*, 94(17), pp. 9463–9468.

Ren, Y., Hao, P., Dutta, B., Cheow, E. S. H., Sim, K. H., Gan, C. S., Lim, S. K. and Sze, S. K. (2013) 'Hypoxia Modulates A431 Cellular Pathways Association to Tumor Radioresistance and Enhanced Migration Revealed by Comprehensive Proteomic and Functional Studies', *Molecular & Cellular Proteomics*, 12(2), pp. 485–498.

Reynaud, E. G., Kržič, U., Greger, K. and Stelzer, E. H. K. (2008) 'Light sheet-based fluorescence microscopy: More dimensions, more photons, and less photodamage', *HFSP Journal*, 2(5), pp. 266–275.

Richards, R., Jenkinson, M. D., Haylock, B. J. and See, V. (2016) 'Cell cycle progression in glioblastoma cells is unaffected by pathophysiological levels of hypoxia.', *PeerJ*, 4, p. e1755.

Roberts, A. M., Watson, I. R., Evans, A. J., Foster, D. A., Irwin, M. S. and Ohh, M. (2009) 'Suppression of hypoxia-inducible factor 2α restores p53 activity via Hdm2 and reverses chemoresistance of renal carcinoma cells', *Cancer Research*, 69(23), pp. 9056–9064.

Robinson, G., Parker, M., Kranenburg, T. A., Lu, C., Chen, X., Ding, L., Phoenix, T. N., Hedlund, E., Wei, L., Zhu, X., Chalhoub, N., Baker, S. J., Huether, R., Kriwacki, R., Curley, N., *et al.* (2012) 'Novel mutations target distinct subgroups of medulloblastoma', *Nature*, 488(7409), pp. 43–48.

Robles, A. I. and Harris, C. C. (2009) 'Clinical Outcomes and Correlates of TP53 Mutations and Cancer', *Cold Spring Harbor Perspectives in Biology*, 2(3), pp. 1–15.

Rodríguez-Jiménez, F. J., Moreno-Manzano, V., Lucas-Dominguez, R. and Sánchez-Puelles, J.-M. (2008) 'Hypoxia Causes Downregulation of Mismatch Repair System and Genomic Instability in Stem Cells', *Stem Cells*, 26(8), pp. 2052–2062.

Rogakou, E. P., Boon, C., Redon, C. and Bonner, W. M. (1999) 'Megabase Chromatin Domains Involved in DNA Double-Strand Breaks in Vivo', *The Journal of Cell Biology*, 146(5), pp. 905–916.

Roos, W. P., Batista, L. F. Z., Naumann, S. C., Wick, W., Weller, M., Menck, C. F. M. and Kaina, B. (2007) 'Apoptosis in malignant glioma cells triggered by the temozolomide-induced DNA lesion O6-methylguanine.', *Oncogene*, 26(2), pp. 186–97.

Roos, W. P. and Kaina, B. (2006) 'DNA damage-induced cell death by apoptosis', *Trends in Molecular Medicine*, 12(9), pp. 440–450.

Rosenberg, B., Van Camp, L. and Krigas, T. (1965) 'Inhibition of cell division in Escherichia coli by electrolysis products from a platinum electrode', *Nature*, 205(4972), pp. 698–699.

Roy, S., de Melo, A. J., Xu, Y., Tadi, S. K., Négrel, A., Hendrickson, E., Modesti, M. and Meek, K. (2015) 'XRCC4/XLF Interaction Is Variably Required for DNA Repair and Is Not Required

for Ligase IV Stimulation', *Molecular and Cellular Biology*, 35(17), pp. 3017–3028.

Rutkowski, S., Gerber, N. U., von Hoff, K., Gnekow, A., Bode, U., Graf, N., Berthold, F., Henze, G., Wolff, J. E. A., Warmuth-Metz, M., Soerensen, N., Emser, A., Ottensmeier, H., Deinlein, F., Schlegel, P.-G., *et al.* (2008) 'Treatment of early childhood medulloblastoma by postoperative chemotherapy and deferred radiotherapy', *Neuro-Oncology*, 11(2), pp. 201–210.

Said, H. M., Polat, B., Hagemann, C., Anacker, J., Flentje, M. and Vordermark, D. (2009) 'Absence of GAPDH regulation in tumor-cells of different origin under hypoxic conditions in -Vitro', *BMC Research Notes*, 2, pp. 1–9.

Saito, S. N. I., Goodarzi, A. A., Higashimoto, Y., Noda, Y., Lees-Miller, S. P., Appella, E. and Anderson, C. W. (2002) 'ATM mediates phosphorylation at multiple p53 sites, including Ser46, in response to ionizing radiation', *Journal of Biological Chemistry*, 277(15), pp. 12491–12494.

Sanai, N., Alvarez-Buylla, A. and Berger, M. S. (2005) 'Neural Stem Cells and the Origin of Gliomas', *New England Journal of Medicine*, 353(8), pp. 811–822.

Santi, P. A. (2011) 'Light sheet fluorescence microscopy: A review', *Journal of Histochemistry and Cytochemistry*, 59(2), pp. 129–138.

Sarkaria, J. N., Hu, L. S., Parney, I. F., Pafundi, D. H., Brinkmann, D. H., Laack, N. N., Giannini, C., Burns, T. C., Kizilbash, S. H., Laramy, J. K., Swanson, K. R., Kaufmann, T. J., Brown, P. D., Agar, N. Y. R., Galanis, E., *et al.* (2018) 'Is the blood-brain barrier really disrupted in all glioblastomas? A critical assessment of existing clinical data', *Neuro-Oncology*, 20(2), pp. 184–191.

Scanlon, S. E. and Glazer, P. M. (2014) 'Hypoxic Stress Facilitates Acute Activation and Chronic Downregulation of Fanconi Anemia Proteins', *Molecular Cancer Research*, 12(7), pp. 1016–1028.

Scanlon, S. E. and Glazer, P. M. (2015) 'Multifaceted control of DNA repair pathways by the hypoxic tumor microenvironment', *DNA Repair*, 32, pp. 180–189.

Schietinger, A., Philip, M., Liu, R. B., Schreiber, K. and Schreiber, H. (2010) 'Bystander killing of cancer requires the cooperation of $CD4^+$ and $CD8^+$ T cells during the effector phase', *The*

Journal of Experimental Medicine, 207(11), pp. 2469–2477.

Schindelin, J., Arganda-carreras, I., Frise, E., Kaynig, V., Longair, M., Pietzsch, T., Preibisch, S., Rueden, C., Saalfeld, S., Schmid, B., Tinevez, J., White, D. J., Hartenstein, V., Eliceiri, K., Tomancak, P., *et al.* (2012) 'Fiji : an open-source platform for biological-image analysis', *Nature methods*, 9(7).

Schmitt, M., True, D., Radich, J. P. and Loeb, L. A. (2015) 'Sequencing small genomic targets with high efficicency and extreme accuracy', *Nature Methods*, 12(5), pp. 423–425.

Schüller, U., Heine, V. M., Mao, J., Kho, A. T., Dillon, A. K., Han, Y. G., Huillard, E., Sun, T., Ligon, A. H., Qian, Y., Ma, Q., Alvarez-Buylla, A., McMahon, A. P., Rowitch, D. H. and Ligon, K. L. (2008) 'Acquisition of Granule Neuron Precursor Identity Is a Critical Determinant of Progenitor Cell Competence to Form Shh-Induced Medulloblastoma', *Cancer Cell*, 14(2), pp. 123–134.

Semenza, G. L. and Wang, G. L. (1992) 'A nuclear factor induced by hypoxia via de novo protein synthesis binds to the human erythropoietin gene enhancer at a site required for transcriptional activation.', *Molecular and Cellular Biology*, 12(12), pp. 5447–5454.

Sengupta, S., Weeraratne, S. D., Sun, H., Phallen, J., Rallapalli, S. K., Teider, N., Kosaras, B., Amani, V., Pierre-Francois, J., Tang, Y., Nguyen, B., Yu, F., Schubert, S., Balansay, B., Mathios, D., *et al.* (2014) 'alpha5-GABAA receptors negatively regulate MYC-amplified medulloblastoma growth', *Acta Neuropathologica*, 127(4), pp. 593–603.

Sermeus, A., Cosse, J.-P., Crespin, M., Mainfroid, V., de Longueville, F., Ninane, N., Raes, M., Remacle, J. and Michiels, C. (2008) 'Hypoxia induces protection against etoposide-induced apoptosis: molecular profiling of changes in gene expression and transcription factor activity.', *Molecular Cancer*, 7, p. 27.

Sharan, S. K., Morimatsu, M., Albrecht, U., Lim, D.-S., Regel, E., Dinh, C., Sands, A., Eichele, G., Hasty, P. and Bradley, A. (1997) 'Embryonic lethality and radiation hypersensitivity mediated by Rad51 in mice lacking Brca2', *Nature*, 386(6627), pp. 804–810.

Sharpless, N. E., Ferguson, D. O., O'hagan, R. C., Castrillon, D. H., Lee, C., Farazi, P. A., Alson,

S., Fleming, J., Morton, C. C., Frank, K., Chin, L., Alt, F. W. and DePinho, R. A. (2001) 'Impaired nonhomologous end-joining provokes soft tissue sarcomas harboring chromosomal translocations, amplifications, and deletions', *Molecular Cell*, 8(6), pp. 1187–1196.

Shieh, S. Y., Ikeda, M., Taya, Y. and Prives, C. (1997) 'DNA damage-induced phosphorylation of p53 alleviates inhibition by MDM2', *Cell*, 91(3), pp. 325–334.

Shih, D. J. H., Northcott, P. A., Remke, M., Korshunov, A., Ramaswamy, V., Kool, M., Luu, B., Yao, Y., Wang, X., Dubuc, A. M., Garzia, L., Peacock, J., Mack, S. C., Wu, X., Rolider, A., *et al.* (2014) 'Cytogenetic prognostication within medulloblastoma subgroups', *Journal of Clinical Oncology*, 32(9), pp. 886–896.

Shin, D. H., Choi, Y. J. and Park, J. W. (2014) 'SIRT1 and AMPK mediate hypoxia-induced resistance of non-small cell lung cancers to cisplatin and doxorubicin', *Cancer Research*, 74(1), pp. 298–308.

Shiraishi, S., Tada, K., Nakamura, H., Makino, K., Kochi, M., Saya, H., Kuratsu, J. I. and Ushio, Y. (2002) 'Influence of p53 mutations on prognosis of patients with glioblastoma', *Cancer*, 95(2), pp. 249–257.

Skowron, P., Ramaswamy, V. and Taylor, M. D. (2015) 'Genetic and molecular alterations across medulloblastoma subgroups', *Journal of Molecular Medicine*, 93(10), pp. 1075–1084.

Sleigh., M. . (1976) 'The mechanism of DNA breakage by phleomycin in vitro', *Nucleic Acids Research*, 3(4), pp. 891–901.

Sloan, D. B., Broz, A. K., Sharbrough, J. and Wu, Z. (2018) 'Detecting Rare Mutations and DNA Damage with Sequencing-Based Methods', *Trends in Biotechnology*, 36(7), pp. 729–740.

Slyskova, J., Langie, S. A. S., Collins, A. R. and Vodicka, P. (2014) 'Functional evaluation of DNA repair in human biopsies and their relation to other cellular biomarkers', *Frontiers in Genetics*, 5(116), pp. 1–1.

Smith, J., Riballo, E., Kysela, B., Baldeyron, C., Manolis, K., Masson, C., Lieber, M. R., Papadopoulo, D. and Jeggo, P. (2003) 'Impact of DNA ligase IV on the fidelity of end joining in

human cells', *Nucleic Acids Research*, 31(8), pp. 2157–2167.

Snowden, T., Acharya, S., Butz, C., Berardini, M. and Fishel, R. (2004) 'hMSH4-hMSH5 recognizes holliday junctions and forms a meiosis-specific sliding clamp that embraces homologous chromosomes', *Molecular Cell*, 15(3), pp. 437–451.

Sobol, R. W., Horton, J. K., Kühn, R., Gu, H., Singhal, R. K., Prasad, R., Rajewsky, K. and Wilson, S. H. (1996) 'Requirement of mammalian DNA polymerase-β in base-excision repair', *Nature*, 379(6561), pp. 183–186.

Solarczyk, K. J., Zarębski, M. and Dobrucki, J. W. (2012) 'Inducing local DNA damage by visible light to study chromatin repair.', *DNA Repair*, 11(12), pp. 996–1002.

Song, X., Liu, X., Chi, W., Liu, Y., Wei, L., Wang, X. and Yu, J. (2006) 'Hypoxia-induced resistance to cisplatin and doxorubicin in non-small cell lung cancer is inhibited by silencing of HIF-1?? gene', *Cancer Chemotherapy and Pharmacology*, 58(6), pp. 776–784.

Srivastava, M., Nambiar, M., Sharma, S., Karki, S. S., Goldsmith, G., Hegde, M., Kumar, S., Pandey, M., Singh, R. K., Ray, P., Natarajan, R., Kelkar, M., De, A., Choudhary, B. and Raghavan, S. C. (2012) 'An inhibitor of nonhomologous end-joining abrogates double-strand break repair and impedes cancer progression', *Cell*, 151(7), pp. 1474–1487.

Stevens, M. F. G., Hickman, J. A., Langdon, S. P., Chubb, D., Vickers, L., Stone, R., Baig, G., Goddard, C., Gibson, N. W., Slack, J. A., Newton, C., Lunt, E. and Fizames, C. (1987) 'Antitumor Activity and Pharmacokinetics in Mice of (CCRG 81045 ; M & B 39831), a Novel Drug with Potential as an Alternative to Dacarbazine', *Cancer Research*, 4, pp. 5846–5852.

Stivers, J. T. and Jiang, Y. L. (2003) 'A mechanistic perspective on the chemistry of DNA repair glycosylases', *Chemical Reviews*, 103(7), pp. 2729–2759.

Su, K. Y., Lai, H. M., Goodman, S. D., Hu, W. Y., Cheng, W. C., Lin, L. I., Yang, Y. C. and Fang, W. horng (2018) 'Application of single nucleotide extension and MALDI-TOF mass spectrometry in proofreading and DNA repair assay', *DNA Repair*, 61, pp. 63–75.

Sung, P. (1994) 'Catalysis of ATP-dependent homologous DNA pairing and strand exchange by

yeast RAD51 protein', *Science*, 265(5176), pp. 1241–1243.

Sykora, P., Witt, K. L., Revanna, P., Smith-Roe, S. L., Dismukes, J., Lloyd, D. G., Engelward, B. P. and Sobol, R. W. (2018) 'Next generation high throughput DNA damage detection platform for genotoxic compound screening', *Scientific Reports*, 8(1), p. 2771.

Takata, M., Sasaki, M. S., Sonoda, E., Morrison, C., Hashimoto, M., Utsumi, H., Yamaguchi-Iwai, Y., Shinohara, A. and Takeda, S. (1998) 'Homologous recombination and non-homologous end-joining pathways of DNA double-strand break repair have overlapping roles in the maintenance of chromosomal integrity in vertebrate cells', *EMBO Journal*, 17(18), pp. 5497–5508.

Talks, K. L., Turley, H., Gatter, K. C., Maxwell, P. H., Pugh, C. W., Ratcliffe, P. J. and Harris, A. L. (2000) 'The expression and distribution of the hypoxia-inducible factors HIF-1alpha and HIF-2alpha in normal human tissues, cancers, and tumor-associated macrophages.', *The American journal of pathology*, 157(2), pp. 411–21.

Tanimoto, K. and Makino, Y. (2000) 'Mechanism of regulation of the hypoxia-inducible factor-1α by the von Hippel-Lindau tumor suppressor protein', *The EMBO Journal*, 19(16), pp. 4298–4309.

Taylor, M. D., Northcott, P. a., Korshunov, A., Remke, M., Cho, Y. J., Clifford, S. C., Eberhart, C. G., Parsons, D. W., Rutkowski, S., Gajjar, A., Ellison, D. W., Lichter, P., Gilbertson, R. J., Pomeroy, S. L., Kool, M., *et al.* (2012) 'Molecular subgroups of medulloblastoma: The current consensus', *Acta Neuropathologica*, 123, pp. 465–472.

Teicher, B. A., Holden, S. A. and Jacobs, J. L. (1987) 'Approaches to Defining the Mechanism of Enhancement by Fluosol-DA 20% with carbogen of Melphalan Antitumor Activity', *Cancer Research*, 47(2), pp. 513–518.

Thévenaz, P., Ruttimann, U. E. and Unser, M. (1998) 'A pyramid approach to subpixel registration based on intensity', *IEEE Transactions on Image Processing*, 7(1), pp. 27–41.

Thompson, E. M., Hielscher, T., Bouffet, E., Remke, M., Luu, B., Gururangan, S., McLendon, R. E., Bigner, D. D., Lipp, E. S., Perreault, S., Cho, Y. J., Grant, G., Kim, S. K., Lee, J. Y., Rao, A. A.

N., *et al.* (2016) 'Prognostic value of medulloblastoma extent of resection after accounting for molecular subgroup: a retrospective integrated clinical and molecular analysis', *The Lancet Oncology*.

Tiraby, J. G. and Fox, M. S. (1973) 'Marker discrimination in transformation and mutation of pneumococcus.', *Proceedings of the National Academy of Sciences of the United States of America*, 70(12), pp. 3541–5.

To, K. K.-W., Sedelnikova, O. a, Samons, M., Bonner, W. M. and Huang, L. E. (2006) 'The phosphorylation status of PAS-B distinguishes HIF-1alpha from HIF-2alpha in NBS1 repression.', *The EMBO Journal*, 25(20), pp. 4784–94.

Träutlein, D., Deibler, M., Leitenstorfer, A. and Ferrando-May, E. (2009) 'Specific local induction of DNA strand breaks by infrared multi-photon absorption', *Nucleic Acids Research*, 38(3).

Triscott, J., Lee, C., Hu, K., Fotovati, A., Berns, R., Pambid, M., Luk, M., Kast, R. E., Kong, E., Toyota, E., Yip, S., Toyota, B. and Dunn, S. E. (2012) 'Disulfiram, a drug widely used to control alcoholism, suppresses the self-renewal of glioblastoma and over-rides resistance to temozolomide', *Oncotarget*, 3(10), pp. 1112–1123.

Tuimala, J., Szekely, G., Gundy, S., Hirvonen, A. and Norppa, H. (2002) 'Genetic polymorphisms of DNA repair and xenobiotic- metabolizing enzymes : role in mutagen sensitivity increased risk of various human cancers . Sensitivity to bleomycin appears to have high heritability and is usually considered to reflect individual cap', *Carcinogenesis*, 23(6), pp. 1003–1008.

Turenne, G. A., Paul, P., Laflair, L. and Price, B. D. (2001) 'Activation of p53 transcriptional activity requires ATM's kinase domain and multiple N-terminal serine residues of p53', *Oncogene*, 20(37), pp. 5100–5110.

Turner, P. R. and Denny, W. A. (1996) 'The mutagenic properties of DNA minor-groove binding ligands', *Mutation Research - Fundamental and Molecular Mechanisms of Mutagenesis*, 355(1–2), pp. 141–169.

Uematsu, N., Weterings, E., Yano, K. I., Morotomi-Yano, K., Jakob, B., Taucher-Scholz, G., Mari, P. O., Van Gent, D. C., Chen, B. P. C. and Chen, D. J. (2007) 'Autophosphorylation of DNA-PKCS regulates its dynamics at DNA double-strand breaks', *Journal of Cell Biology*, 177(2), pp. 219–229.

Vaupel, P. and Harrison, L. (2004) 'Tumor hypoxia: causative factors, compensatory mechanisms, and cellular response', *The Oncologist*, 9(5), pp. 4–9.

Vaupel, P., Rallinoâ, F. and Okunieff, P. (1989) 'Blood Flow, Oxygen and Nutrient Supply, and Metabolic Microenvironment Human Tumors: A Review', *Cancer Research*, 49(23), pp. 6449–6465.

Veldman-Jones, M. H., Brant, R., Rooney, C., Geh, C., Emery, H., Harbron, C. G., Wappett, M., Sharpe, A., Dymond, M., Barrett, J. C., Harrington, E. A. and Marshall, G. (2015) 'Evaluating robustness and sensitivity of the nanostring technologies ncounter platform to enable multiplexed gene expression analysis of clinical samples', *Cancer Research*, 75(13), pp. 2587–2593.

Verhaak, R. G. W., Hoadley, K. A., Purdom, E., Wang, V., Qi, Y., Wilkerson, M. D., Miller, C. R., Ding, L., Golub, T., Mesirov, J. P., Alexe, G., Lawrence, M., O'Kelly, M., Tamayo, P., Weir, B. A., *et al.* (2010) 'Integrated Genomic Analysis Identifies Clinically Relevant Subtypes of Glioblastoma Characterized by Abnormalities in PDGFRA, IDH1, EGFR, and NF1', *Cancer Cell*, 17(1), pp. 98–110.

Verhoeff, J. J. C., Lavini, C., van Linde, M. E., Stalpers, L. J. A., Majoie, C. B. L. M., Reijneveld, J. C., van Furth, W. R. and Richel, D. J. (2010) 'Bevacizumab and dose-intense temozolomide in recurrent high-grade glioma', *Annals of Oncology*, 21(8), pp. 1723–1727.

Walker, J. R., Corpina, R. A. and Goldberg, J. (2001) 'Structure of the Ku heterodimer bound to dna and its implications for double-strand break repair', *Nature*, 412(6847), pp. 607–614.

Wang, G. L., Jiang, B. H., Rue, E. a and Semenza, G. L. (1995) 'Hypoxia-inducible factor 1 is a basic-helix-loop-helix-PAS heterodimer regulated by cellular O2 tension.', *Proceedings of the National Academy of Sciences of the United States of America*, 92(12), pp. 5510–5514.

Wang, Q., Hu, B., Hu, X., Kim, H., Squatrito, M., Scarpace, L., DeCarvalho, A., Lyu, S., Li, P., Li, Y., Barthe, F., Cho, H., Lin, Y., Satani, N., Martinez-Ledesma, E., *et al.* (2017) 'Tumor Evolution of Glioma-Intrinsic Gene Expression Subtypes Associates with Immunological Changes in the Microenvironment', *Cancer Cell*, 32(1), pp. 42–56.

Wang, X., Chen, J. X., Liu, J. P., You, C., Liu, Y. H. and Mao, Q. (2014) 'Gain of function of mutant TP53 in glioblastoma: Prognosis and response to temozolomide', *Annals of Surgical Oncology*, 21(4), pp. 1337–1344.

Wartenbert, M., Ling, F. C., Müschen, M., Klein, F. and Acker, H. (2003) 'Regulation of the multidrug resistance transporter P-Glycoprotein in multicellular tumor spheroids by hypoxia-inductible factor -1 and reactive oxygen species', *The FASEB Journal*, 240, pp. 1–22.

Wenger, R. H. (2002) 'Cellular adaptation to hypoxia: O2-sensing protein hydroxylases, hypoxia-inducible transcription factors, and O2-regulated gene expression.', *The FASEB Journal*, 16(10), pp. 1151–1162.

Wenger, R. H., Stiehl, D. P. and Camenisch, G. (2005) 'Integration of oxygen signaling at the consensus HRE.', *Science Signalling*, 2005(306), pp. 1–13.

Wheate, N. J., Walker, S., Craig, G. E. and Oun, R. (2010) 'The status of platinum anticancer drugs in the clinic and in clinical trials', *Dalton Transactions*, 39(35), pp. 8113–8127.

Willett, C. G., Boucher, Y., Di Tomaso, E., Duda, D. G., Munn, L. L., Tong, R. T., Chung, D. C., Sahani, D. V., Kalva, S. P., Kozin, S. V., Mino, M., Cohen, K. S., Scadden, D. T., Hartford, A. C., Fischman, A. J., *et al.* (2004) 'Direct evidence that the VEGF-specific antibody bevacizumab has antivascular effects in human rectal cancer', *Nature Medicine*, 10(2), pp. 145–147.

Williams, K. J., Telfer, B. a., Xenaki, D., Sheridan, M. R., Desbaillets, I., Peters, H. J. W., Honess, D., Harris, A. L., Dachs, G. U., Van Der Kogel, A. and Stratford, I. J. (2005) 'Enhanced response to radiotherapy in tumours deficient in the function of hypoxia-inducible factor-1', *Radiotherapy and Oncology*, 75(1), pp. 89–98.

Wilson, W. R. and Hay, M. P. (2011) 'Targeting hypoxia in cancer therapy.', *Nature Reviews Cancer*, 11, pp. 393–410.

Wiltshaw, E. (1979) 'Cisplatin in the Treatment of Cancer', *Platinum Metals Review*, 23(3), pp. 90–98.

Wohlkoenig, C., Leithner, K., Deutsch, A., Hrzenjak, A., Olschewski, A. and Olschewski, H. (2011) 'Hypoxia-induced cisplatin resistance is reversible and growth rate independent in lung cancer cells', *Cancer Letters*, 308(2), pp. 134–143.

Wojcik, K. and Dobrucki, J. W. (2008) 'Interaction of a DNA intercalator DRAQ5, and a minor groove binder SYTO17, with chromatin in live cells - Influence on chromatin organization and histone - DNA interactions', *Cytometry Part A*, 73(6), pp. 555–562.

Wong, A. K. C., Pero, R., Ormonde, P. A., Tavtigian, S. V. and Bartel, P. L. (1997) 'RAD51 interacts with the evolutionarily conserved BRC motifs in the human breast cancer susceptibility gene brca2', *Journal of Biological Chemistry*, 272(51), pp. 31941–31944.

Wozniak, a. J., Glisson, B. S., Hande, K. R. and Ross, W. E. (1984) 'Inhibition of etoposide-induced DNA damage and cytotoxicity in L1210 cells by dehydrogenase inhibitors and other agents', *Cancer Research*, 44(2), pp. 626–632.

Wozniak, a J. and Ross, W. E. (1983) 'DNA damage as a basis for 4'-demethylepipodophyllotoxin-9-(4,6-O-ethylidene-beta-D-glucopyranoside) (etoposide) cytotoxicity.', *Cancer Research*, 43(1), pp. 120–124.

Wyckoff, J., Wang, W., Lin, E. Y., Wang, Y., Pixley, F., Stanley, E. R., Graf, T., Pollard, J. W., Segall, J. and Condeelis, J. (2004) 'A paracrine loop between tumor cells and macrophages is required for tumor cell migration in mammary tumors.', *Cancer Research*, 64, pp. 7022–7029.

Yamanaka, M. and Ishikawa, O. (2000) 'Hypoxic conditions decrease the mRNA expression of proα1(I) and (III) collagens and increase matrix metalloproteinases-1 of dermal fibroblasts in three-dimensional cultures', *Journal of Dermatological Science*, 24(2), pp. 99–104.

Yang, Z. J., Ellis, T., Markant, S. L., Read, T. A., Kessler, J. D., Bourboulas, M., Schüller, U., Machold, R., Fishell, G., Rowitch, D. H., Wainwright, B. J. and Wechsler-Reya, R. J. (2008) 'Medulloblastoma Can Be Initiated by Deletion of Patched in Lineage-Restricted Progenitors or Stem Cells', *Cancer Cell*, 14(2), pp. 135–145.

Yano, K. ichi, Morotomi-Yano, K. and Akiyama, H. (2009) 'Cernunnos/XLF: A new player in DNA double-strand break repair', *International Journal of Biochemistry and Cell Biology*, 41(6), pp. 1237–1240.

Yock, T. I., Yeap, B. Y., Ebb, D. H., Weyman, E., Eaton, B. R., Sherry, N. A., Jones, R. M., MacDonald, S. M., Pulsifer, M. B., Lavally, B., Abrams, A. N., Huang, M. S., Marcus, K. J. and Tarbell, N. J. (2016) 'Long-term toxic effects of proton radiotherapy for paediatric medulloblastoma: A phase 2 single-arm study', *The Lancet Oncology*, 17(3), pp. 287–298.

Yokota, N., Nishizawa, S., Ohta, S., Date, H., Sugimura, H., Namba, H. and Maekawa, M. (2002) 'Role of Wnt pathway in medulloblastoma oncogenesis', *International Journal of Cancer*, 101(2), pp. 198–201.

Yoo, S. (1999) 'Geometry of a complex formed by double strand break repair proteins at a single DNA end: recruitment of DNA-PKcs induces inward translocation of Ku protein', *Nucleic Acids Research*, 27(24), pp. 4679–4686.

You, Z., Chahwan, C., Bailis, J., Hunter, T. and Russell, P. (2005) 'ATM activation and its recruitment to damaged DNA require binding to the C terminus of Nbs1.', *Molecular and Cellular Biology*, 25(13), pp. 5363–5379.

Zagzag, D., Lukyanov, Y., Lan, L., Ali, M. A., Esencay, M., Mendez, O., Yee, H., Voura, E. B. and Newcomb, E. W. (2006) 'Hypoxia-inducible factor 1 and VEGF upregulate CXCR4 in glioblastoma: Implications for angiogenesis and glioma cell invasion', *Laboratory Investigation*, 86(12), pp. 1221–1232.

Zhang, H., Qian, D. Z., Tan, Y. S., Lee, K., Gao, P., Ren, Y. R., Rey, S., Hammers, H., Chang, D., Pili, R., Dang, C. V., Liu, J. O. and Semenza, G. L. (2008) 'Digoxin and other cardiac glycosides inhibit HIF-1 synthesis and block tumor growth', *Proceedings of the National Academy of Sciences*, 105(50), pp. 19579–19586.

Zhang, J., F.G. Stevens, M. and D. Bradshaw, T. (2012) 'Temozolomide: Mechanisms of Action, Repair and Resistance', *Current Molecular Pharmacology*, 5(1), pp. 102–114.

Zhang, Y., Yuan, F., Presnell, S. R., Tian, K., Gao, Y., Tomkinson, A. E., Gu, L. and Li, G. M.

(2005) 'Reconstitution of 5′-directed human mismatch repair in a purified system', *Cell*, 122(5), pp. 693–705.

Zhang, Z., Tang, L., Zhan, R., Tong, Y., Yao, H. and Du, L. (2004) 'Immunotherapy of intracranial G422 glioblastoma with dendritic cells pulsed with tumor extract or RNA.', *J Zhejiang Univ Sci*, 5(10), pp. 1298–1303.

Zhukova, N., Ramaswamy, V., Remke, M., Pfaff, E., Shih, D. J. H., Martin, D. C., Castelo-Branco, P., Baskin, B., Ray, P. N., Bouffet, E., Von Bueren, A. O., Jones, D. T. W., Northcott, P. A., Kool, M., Sturm, D., *et al.* (2013) 'Subgroup-specific prognostic implications of TP53 mutation in medulloblastoma', *Journal of Clinical Oncology*, 31(23), pp. 2927–2935.

Zimmerman, L., Parr, B., Lendahl, U., Cunningham, M., McKay, R., Gavin, B., Mann, J., Vassileva, G. and McMahon, A. (1994) 'Independent regulatory elements in the nestin gene direct transgene expression to neural stem cells or muscle precursors', *Neuron*, 12(1), pp. 11–24.

Zundel, W., Schindler, C., Haas-Kogan, D., Koong, A., Kaper, F., Chen, E., Gottschalk, A. R., Ryan, H. E., Johnson, R. S., Jefferson, A. B., Stokoe, D. and Giaccia, A. J. (2000) 'Loss of PTEN facilitates HIF-1-mediated gene expression', *Genes and Development*, 14(4), pp. 391–396.

Appendix

1.1 Genes, proteins and their full names

Gene Name	Protein Name	Full Name
ABCB1	MDR1	Multidrug resistance protein 1
ABCC1	MPR1	Multidrug resistance-associated protein 1
ABL1	ABL1	Abeison murine leukaemia viral oncogene homolog 1
ACTA2	SMA	Smooth muscle actin
ADM	ADM	Adrenomedullin
AKT	AKT	AKT serine/threonine kinase 1
AMPK		AMP-activated protein kinase
APC	APC	Adenomatous polyposis coli protein
APEX1, 2	APE1, 2	DNA-(apurinic or aprymidinic site) lyase
ATM	ATM	Ataxia telangiectasia mutated
ATR	ATR	Ataxia telangiectasia and Rad3-related
AXIN1	Axin-1	AXIN1
BAX	BAX	BCL2 associated X protein
BCL2	Bcl-2	B-cell lymphoma 2
BID	BID	BH3 interacting domain death agonist
BLM	BLM	Bloom syndrome protein
BRCA1	BRCA1	Breast cancer type 1 susceptibility protein
BRCA1	BRCA2	Breast cancer type 2 susceptibility protein
CA9	CAIX	Carbonic anhydrase 9
CDKN1A	p21	Cyclin-dependent kinase inhibitor 1
CDKN1B	P27	Cyclin-dependent kinase inhibitor 1B
CHEK2	Chk2	Checkpoint kinase 2
CHEK3	Chk3	Checkpoint kinase 3
CREBBP/p300	CREBBP/p300	CREB-binding protein
CTNNB1	CTNNB1	β-Catenin
CXCR4	CXCR4	C-X-C chemokine receptor type 4
CYCLOA	CYCLOA	Cyclophillin A
DCLRE1C	Artemis	Artemis
DDX3X	DDX3X	DEAD-box helicase 3
EGFR	EGFR	Epidermal growth factor receptor
EPO	EPO	Erythropoietin
ERCC1	ERCC1	Excision repair cross-complementation group 1
ERCC4	ERCC4	Excision repair cross-complementation group 4
EXO1	EXO1	Exonuclease 1

FEN1	FEN1	Flap endonuclease 1
FGF	FGF	Fibroblast growth factor
FIF	FIF	Factor Inhibiting HIF
GDF15	GDF15	Growth/differentiation factor 15
GEN1	GEN1	Holliday junction 5' flap endonuclease 1
GLI1	GLI1	Glioma-associated oncogene
GLUT1	GLUT1	Glucose transporter 1
H2AFX	H2AX	H2A histone family member X
IDH1	IDH1	Isocitrate dehydorgenase 1
JMJD1A	JMJD1A	Jumonji domain containing 1A
KDM1A	LDS1	Lysine-specific histone demethylase 1
KDM5B	PLU-1	Lysine-specific demethylase 5B
LIG1	DNA liagse I	DNA liagse I
LIG3	DNA Ligase III	DNA Ligase III
LIGIV	DNA ligase IV	DNA ligase IV
MDM2	MDM2	Mouse double minute 2 homolog
MGMT	MGMT	O^6 methylguanine – DNA Methyltransferase
MLH1	MLH1	MutL homolog 1
MLH3	MLH3	MutL homolog 3
MPG	MPG	DNA-3-methyladenine glycosylase
MRE11	MRE11	MRE11 homolog double strand break repair nuclease
MSH2	MSH2	MutS protein homolog 2
MSH3	MSH3	MutS protein homolog 3
MSH5	MSH5	MutS protein homolog 5
MSH6	MSH6	MutS protein homolog 6
MTOR	MTOR	Mammalian target of rapamycin
MUTYH	MUTYH	MutY homolog
MYCN	N-MYC	N-myc proto-oncogene protein
NBN	NBN	Nibrin
NEIL1,2,3	NEIL1,2,3	Endonuclease VIII-like 1,2,3
NF1	NF1	Nuclear factor 1
NHEJ1	XLF	XRCC4-like factor
NTHL1	NTHL1	Endonuclease III-like 1
OGG1	OGG1	8-Oxoguanine glycosylase
PARP1,2,3,4	PARP1,2,3,4	Poly[ADP-ribose] polymerase 1,2,3,4
PCNA	PCNA	Proliferating cell nuclear antigen
PDGF	PDGF	Platelet-derived growth factor
PHD1,2,3	PHD1,2,3	HIF prolyl-hydroxylase
PI3K	PI3K	Phosphoinositide 3-kinase
PIM1	PIM1	Proto-oncogene serine/threonine-protein kinase

PMS1	PMS1	Mismatch repair endonuclease PMS1
PMS2	PMS2	Mismatch repair endonuclease PMS2
PNKP	PNKP	Bifunctional polynucleotide phosphatase/kinase
POLB	Pol β	DNA polymerase β
POLD1,3,4	Pol δ	DNA polymerase δ
POLE2	Pol ε	DNA polymerase ε subunit 2
POLL	Pol λ	DNA polymerase λ
PRKDC	DNA-Pkcs	DNA dependent protein kinase catalytic subunit
PTCH1	PATCHED1	Protein patched homolog 1
PTEN	PTEN	Phosphate and tensin homolog
RAD23B	RAD23B	UV excision repair protein RAD23 homolog B
RAD50	RAD50	RAD50 homolog
RAD51	RAD51	RAD51 homolog
RAD54L	RAD54L	DNA repair and recombination protein RAD54-like
RBL2	P130	Retinoblastoma-like protein 2
RCF1	RCF1	Replication factor C subunit 1
RCF3	RCF3	Replication factor C subunit 3
RCF4	RCF4	Replication factor C subunit 4
RECQL	RECQL	RecQ-like helicase
RECQL5	RECQL5	RecQ-like helicase 5
RPA	RPA	Replication protein A
SIRT1	SIRT2	Sirtuin 1
SLX4	SLX4/FANCP	Structure specific endonuclease subunit
SMARC4A	SMARC4A	ATP-dependent chromatin remodeler SMARCA4
SMUG1	SMUG1	Single-strand selective monofunctional uracil DNA glycosylase
SNCAIP	SNCAIP	Synphillin-1
SUFU	SUFU	Suppressor of fused homolog
TDG	TDG	G/T mismatch-specific thymine DNA glycosylase
TOP3A	TOP3A	DNA topoisomerase 3-alpha
TOP3B	TOP3B	DNA topoisomerase 3-beta
TP53	p53	Tumour protein P53
TP53BP1	53BP1	Tumour suppression p53-binding protein 1
UBE2T	UBE2T	Ubiquitin-conjugating enzyme 2
UNG	UNG	Uracil-DNA glycosylase
VEGF	VEGF	Vascular endothelial growth factor
VHL	pVHL	von Hippel-Lindau tumour suppressor
WRN	WRN	Werner syndrome ATP-dependent helicase

XRCC1	XRCC1	X-ray repair cross-complimenting 1
XRCC2	XRCC2 (FANCU)	X-ray repair cross-complimenting 2
XRCC3	XRCC3	X-ray repair cross-complimenting 3
XRCC4	XRCC4	X-ray repair cross-complimenting 4
XRCC5	Ku80	X-ray repair cross-complimenting 5
XRCC6	Ku70	X-ray repair cross-complimenting 6

1.2 Genes examined in NanoString assay.

Gene	Accession Number	Alias
ABL1	NM_005157.3	ABL, JTK7, c-ABL, p150
AKT3	NM_005465.4	
ALKBH2	NM_001001655.2	
ALKBH3	NM_139178.3	
APC	NM_000038.3	
APEX1	NM_001641.2	APEX, APE, REF1, HAP1, APX, APEN, REF-1, APE-1
APEX2	NM_014481.2	
ATM	NM_138292.3	ATA, ATDC, ATC, ATD, TEL1, TELO1
ATR	NM_001184.2	
ATRIP	NM_130384.1	
AURKA	NM_003600.2	STK15, STK6, BTAK, AurA, STK7, ARK1, PPP1R47, AIK
BCL2	NM_000657.2	
BCL2L1	NM_138578.1	
BLM	NM_000057.2	
BRCA1	NM_007305.2	
BRCA2	NM_000059.3	FANCD1, FACD, FANCD, FAD, FAD1, BRCC2
BRIP1	NM_032043.1	
BUB1B	NM_001211.4	
CASP8	NM_001228.4	
CCND1	NM_053056.2	BCL1, D11S287E, PRAD1, U21B31

CCND2	NM_001759.2	
CCND3	NM_001760.2	
CCNO	NM_021147.3	CCNU, UDG2, FLJ22422, UNG2
CDK7	NM_001799.2	
CDKN1A	NM_000389.2	CDKN1, P21, CIP1, WAF1, SDI1, CAP20, p21CIP1, p21Cip1/Waf1
CDKN1B	NM_004064.2	
CDKN2A	NM_000077.3	CDKN2, MLM, CDK4I, p16, INK4a, MTS1, CMM2, ARF, p19, p14, INK4, p16INK4a, p19Arf
CDKN2C	NM_001262.2	
CHEK1	NM_001114121.1	
CHEK2	NM_007194.3	RAD53, CDS1, CHK2, HuCds1, PP1425, bA444G7
CREBBP	NM_001079846.1	RSTS, RTS, CBP, KAT3A
CRY1	NM_004075.3	
DDB1	NM_001923.3	
DDB2	NM_000107.1	
DNA2	NM_001080449.2	DNA2L, KIAA0083
EGFR	NM_201282.1	ERBB, ERBB1
ERCC1	NM_001983.3	
ERCC2	NM_000400.2	XPD, MAG, EM9, MGC102762, MGC126218, MGC126219
ERCC3	NM_000122.1	
ERCC4	NM_005236.2	XPF, RAD1, FANCQ
ERCC5	NM_000123.2	
ERCC6	NM_000124.2	CKN2, CSB, RAD26, ARMD5
ERCC8	NM_000082.3	CKN1, CSA
EXO1	NM_006027.3	
FAN1	NM_001146094.1	
FANCA	NM_000135.2	FACA, FANCH, FAA, FA-H, FAH
FANCB	NM_152633.2	

FANCC	NM_000136.2	FACC, FAC, FA3
FANCD2	NM_033084.3	FACD, FANCD, FAD, FA-D2
FANCE	NM_021922.2	FACE, FAE
FANCF	NM_022725.2	
FANCG	NM_004629.1	XRCC9, FAG
FANCI	NM_001113378.1	KIAA1794, FLJ10719
FANCL	NM_001114636.1	PHF9, FLJ10335, FAAP43, Pog
FANCM	NM_020937.2	KIAA1596, FAAP250
FEN1	NM_004111.4	RAD2, FEN-1, MF1
GEN1	NM_182625.3	
GTF2H3	NM_001516.3	
H2AFX	NM_002105.2	
HDAC1	NM_004964.2	RPD3L1, HD1, GON-10
HDAC2	NM_001527.1	
HLTF	NM_139048.2	SNF2L3, SMARCA3, HIP116A, HLTF1, RNF80
HUS1	NM_004507.2	
KRAS	NM_004985.3	KRAS2, KRAS1
LIG1	NM_000234.1	
LIG3	NM_002311.3	
LIG4	NM_002312.3	
MAD2L2	NM_001127325.1	
MDC1	NM_014641.2	
MGMT	NM_002412.3	
MLH1	NM_000249.2	COCA2, HNPCC, FCC2, HNPCC2
MLH3	NM_014381.2	
MNAT1	NM_002431.2	
MPG	NM_001015052.1	
MRE11A	NM_005591.3	MRE11, ATLD
MSH2	NM_000251.1	COCA1, HNPCC, HNPCC1
MSH3	NM_002439.2	
MSH4	NM_002440.3	

MSH5	NM_172165.2	
MSH6	NM_000179.1	
MUTYH	NM_012222.2	
MYC	NM_002467.3	
MYD88	NM_002468.3	
NBN	NM_001024688.1	NBS, NBS1, ATV, AT-V2, AT-V1
NEIL1	NM_024608.2	
NEIL2	NM_145043.2	
NEIL3	NM_018248.2	
NFKB1	NM_003998.2	
NKX3-1	NR_046072.1	NKX3A, NKX3.1, BAPX2
NLRP2	NM_017852.1	NALP2, FLJ20510, PYPAF2, NBS1, PAN1, CLR19.9
NTHL1	NM_002528.5	
OGG1	NM_002542.5	
PARP1	NM_001618.3	PPOL, ADPRT, PARP
PARP2	NM_005484.3	
PARP3	NM_005485.4	ADPRTL3, ADPRT3, IRT1, hPARP-3, pADPRT-3
PARP4	NM_006437.3	ADPRTL1, VAULT3, p193, VPARP, VWA5C
PCNA	NM_002592.2	
PIK3CA	NM_006218.2	
PIK3CB	NM_006219.1	
PIK3R1	NM_181504.2	
PMS1	NM_000534.4	
PMS2	NM_000535.5	PMSL2, H_DJ0042M02.9, HNPCC4
PNKP	NM_007254.2	
POLB	NM_002690.1	
POLD1	NM_002691.2	POLD, CDC2
POLD3	NM_006591.2	
POLD4	NM_021173.2	
POLE	NM_006231.3	

POLE2	NM_002692.2	
POLE4	NM_019896.2	
POLI	NM_007195.2	
POLK	NM_016218.2	DINB1, POLQ, DINP
POLL	NM_001174085.1	
POLM	NM_013284.3	
POLQ	NM_199420.3	
POLR2D	NM_004805.3	
POLR2H	NM_001278698.1	
POLR2J	NM_006234.4	
PRKACB	NM_182948.2	
PRKDC	NM_006904.6	HYRC, HYRC1, DNPK1, p350, DNAPK, XRCC7, DNA-PKcs
PRKX	NM_005044.1	
PTEN	NM_000314.4	BZS, MHAM, MMAC1, TEP1, PTEN1
RAD1	NM_133377.2	
RAD17	NM_133338.1	
RAD18	NM_020165.2	
RAD21	NM_006265.2	
RAD23A	NM_005053.2	
RAD23B	NM_002874.3	
RAD50	NM_005732.2	
RAD51	NM_133487.2	RAD51A, RECA, HsRad51, HsT16930, BRCC5
RAD51B	NM_002877.5	RAD51L1, REC2, hREC2, R51H2
RAD51C	NM_002876.2	
RAD51D	NM_002878.3	RAD51L3, R51H3, Trad, HsTRAD
RAD52	NM_134424.2	
RAD54L	NM_003579.2	
RAD9A	NM_004584.2	
RB1	NM_000321.1	OSRC, RB
RECQL	NM_032941.2	

RECQL5	NM_004259.6	
REV1	NM_016316.2	
RFC1	NM_001204747.1	
RFC3	NM_002915.3	
RFC4	NM_181573.2	
RMI1	NM_024945.2	C9orf76, FLJ12888, BLAP75
RMI2	NM_152308.1	C16orf75, MGC24665, BLAP18
RPA1	NM_002945.3	
RPA3	NM_002947.3	
RPS27A	NM_002954.5	
RRM2B	NM_015713.3	
SIRT1	NM_012238.4	
SLFN11	NM_001104587.1	
SLK	NM_014720.2	
SLX4	NM_032444.2	BTBD12, KIAA1784, KIAA1987, FANCP
SMAD4	NM_005359.3	MADH4, DPC4
SMARCA4	NM_003072.3	SNF2L4, hSNF2b, BRG1, BAF190, SNF2, SWI2, SNF2-BETA, SNF2LB, FLJ39786
SMC1A	NM_006306.2	SMC1L1, DXS423E, KIAA0178, SB1.8, Smcb
SMC3	NM_005445.3	CSPG6, HCAP, BAM, SMC3L1, bamacan
SMUG1	NM_001243789.1	
SUMO3	NM_006936.2	SMT3H1, SMT3A
TDG	NM_003211.4	
TIPIN	NM_017858.2	
TOP3A	NM_004618.3	
TOP3B	NM_003935.4	
TP53	NM_000546.2	
TP53BP1	NM_001141980.1	
TREX1	NM_016381.3	AGS1, DRN3
UBB	NM_018955.2	
UBE2T	NM_014176.3	

UNG	NM_003362.3	DGU, UDG, UNG1, UNG2, HIGM4
USP1	NM_003368.4	
WEE1	NM_003390.3	
WRN	NM_000553.4	
XPA	NM_000380.3	
XPC	NM_004628.3	
XRCC1	NM_006297.2	
XRCC2	NM_005431.1	
XRCC3	NM_001100119.1	
XRCC4	NM_003401.3	
XRCC5	NM_021141.3	
XRCC6	NM_001469.3	G22P1, D22S731, D22S671, KU70, ML8
Internal Reference Genes		
CC2D1B	NM_032449.2	
COG7	NM_153603.3	
EDC3	NM_001142443.1	YJDC, LSM16, FLJ21128, hYjeF_N2-15q23, YJEFN2
GPATCH3	NM_022078.2	GPATC3, FLJ12455
HDAC3	NM_003883.2	
MTMR14	NM_022485.3	C3orf29, FLJ22405, FLJ90311, hJumpy, hEDTP
NUBP1	NM_001278506.1	NBP1, NBP35
PRPF38A	NM_032864.3	
SAP130	NM_024545.3	
SF3A3	NM_006802.2	
TLK2	NM_006852.2	
ZC3H14	NM_001160103.1	

1.3 Matlab script for normalisation

Matlab script for normalisation steps of intensity measurements after laser microirradiation.

```
%% Created by Sophie Cowman University of Liverpool

%%Before you run this make sure you re-name the file output names
correctly to not overwrite data


%%This section deals with raw data - normalisation steps happen -
for each
% for each individual cell a graph is plotted
% calculations have been tested in excel

clearvars
clc


% change this to 1 if want to plot interim graphs to check quality
of data
plot_all_graphs = 0;

FileNames = dir('cell *.xlsx');
% function to delete any old final_data files (allows you to run
this
% script on the same folder multiple times
for i=1:length(FileNames)
    filename = FileNames(i).name;
    if ~isempty(regexp(filename,'.*_final_data', 'once'));
       delete(filename);
    end
end

FileNames = dir('cell *.xlsx');

for i=1:length(FileNames)
    % get the file name:
   filename = FileNames(i).name;
   disp(filename);

   data = xlsread(FileNames(i).name);

   [pathstr,name,ext] = fileparts(filename);

   % naming each column
    DAM = data (:,1);
    NONDAM = data (:,2);
    BG = data (:,3);

     b = size(data,1);
    Total_time = 0:b-1;
```

```
    Total_time = Total_time(:);
    Total_time =  15*Total_time;

    if plot_all_graphs > 0
        Fig_a = figure('Color',[1 1 1]);
        plot (Total_time, DAM, 'MarkerEdgeColor', 'b')
        hold on
        plot (Total_time, NONDAM, 'MarkerEdgeColor', 'r')
        hold on
        plot (Total_time, BG, 'MarkerEdgeColor', 'g')
        hold off
        title (['BGS data ',name])
    end


    % background subtraction
    meanBG = mean(BG);
    BGS_DAM = DAM-meanBG;
    BGS_NUC = NONDAM-meanBG;

    b = size(data,1);
    Total_time = 0:b-1;
    Total_time = Total_time(:);
    Total_time =  15*Total_time;

    % plotting BGS data

    if plot_all_graphs > 0
        Fig_a = figure('Color',[1 1 1]);
        plot (Total_time, BGS_DAM, 'MarkerEdgeColor', 'b')
        hold on
        plot (Total_time, BGS_NUC, 'MarkerEdgeColor', 'r')
        hold off
        title (['BGS data ',name])

        Fig_b = figure('Color',[1 1 1]);
        plot (Total_time, BGS_NUC, 'MarkerEdgeColor', 'r')
        title ([' BGS UN-DAM REGION', name])
    end

% need to determine how many pre-bleach values
% prompt = 'How many pre-bleach values?';
% PBV = input(prompt);

% if know how many pre-bleach values comment out last part and
uncomment
% next

    PBV = 2;

    % averaging pre-damage values
    AVPDDAM = mean(BGS_DAM(1:PBV));
    AVPDNUC = mean(BGS_NUC(1:PBV));

    % normalising to pre-bleach values
    new_DAM = BGS_DAM/AVPDDAM;
    new_NONDAM = BGS_NUC/AVPDNUC;

    if plot_all_graphs > 0
```

```
        Fig_c = figure('Color',[1 1 1]);
        plot (Total_time, new_DAM, 'MarkerEdgeColor', 'b')
        hold on
        plot (Total_time, new_NONDAM, 'MarkerEdgeColor', 'r')
        hold off
        title (['Norm to predam ', name])
    end


    % normalising for photobleaching
    norm_DAM = new_DAM./new_NONDAM;


    % Determing first pre-bleach value
    % PB = norm_DAM(PBV+1);

    % Determining max value
    % highest = max(norm_DAM);

    % scaling pre-bleach to 0 and highest to 1
    % part1 = (norm_DAM - PB);
    % part2 = (highest-PB);
    % Final_data = part1./part2;

    %% Re-organisng data into a new matrix

    % Trimming down the data to remove pre-damage values

    % Final_data = Final_data(PBV+1:end,:);

    Final_data = norm_DAM(PBV+1:end,:);


    % Plotting out all of the data
    b = size(Final_data,1);
    Total_time = 0:b-1;
    Total_time = Total_time(:);
    Total_time =  15*Total_time;

    All_data = [Total_time, Final_data];
    Time = All_data(:,1);
    Intensity = All_data(:,2);

%     Fig_01 = figure('Color',[1 1 1]);
%
% %-- Set the figure position and size to prevent the figure being
too low resolution (X pos, Y Pos, Width, Height)
%     set(gcf,'position',[100 100 800 600])
% %-- Do this to make sure that the figure isn't cut off (or
including other windows) when exporting
%     movegui(gcf,'center')
%
% % '-x' means plot x for all data points
%     plot(Time,Intensity, 'b-x', 'MarkerSize', 3,
'MarkerEdgeColor', [0 .0 .0])
%     axis auto
%     xlabel ('Time (s)', 'FontSize', 12, 'FontName', 'Ariel',
'FontWeight', 'bold')
```

```
%     ylabel ('Intensity (a.u)', 'FontSize', 14, 'FontName',
'Ariel', 'FontWeight', 'bold')
%     grid off
%     title ([name,' Normalised data'])
%     set(gca,'FontSize',12, 'FontName','Ariel', 'Box', 'off',
'TickDir', 'out')

%-- saving as png
%     saveas(Fig_01,strrep(filename,'.xlsx','
normalised_data.png'));

    [pathstr,name,ext] = fileparts(filename);

    final_data_file = [name, '_final_data.xlsx'];
    header = {'Time(s)','Normalised_Intensity'};
    xlswrite(final_data_file, header, 'Sheet1')
    xlswrite(final_data_file, All_data,'Sheet1', 'A2');

%     smoothed_data=smooth(normalised_data,5)

end;
%% Compiling data together
% Tested calcultions on excel - works perfectly

% Inputting data and creating a new matrix

clearvars
clc

FileNames = dir('*_final_data.xlsx');
%this gets all the file names in current directory that have
extension
%.xlsx, as a structure


for i=1:length(FileNames);
    % get the file name:
   filename = FileNames(i).name;
   %disp(filename);
   data = xlsread(FileNames(i).name);
   empty_matrix(:,i) = data(:,2);
end

compiled_data = empty_matrix;


b = size(compiled_data,1);
Total_time = 0:b-1;
Total_time = Total_time(:);
Total_time =  15*Total_time;

xlswrite('Compiled_data.xlsx',compiled_data,'Compiled_data');


Fig_02 = figure('Color',[1 1 1]);
set(gcf,'position',[100 100 800 600])
movegui(gcf,'center')
```

```
plot(Total_time,compiled_data, 'LineWidth', 2)
ylim ([0 7])
xlabel ('Time (s)', 'FontSize', 20, 'FontName', 'Ariel',
'FontWeight', 'bold')
ylabel ('Intensity (a.u)', 'FontSize', 20, 'FontName', 'Ariel',
'FontWeight', 'bold')
grid off
title ('')
set(gca,'FontSize',20, 'FontName','Ariel', 'Box', 'off', 'TickDir',
'out', 'LineWidth', 3)
legend ('off')

saveas(Fig_02,'All_cells_plotted.png');



%% using data in matrix to calculate mean and SEM

average = mean(compiled_data.');
average = average(:);

SEM = std(compiled_data.')/sqrt(size(compiled_data,2));
SEM = SEM(:);

upperint = average+SEM;
lowerint = average-SEM;

final_data = [Total_time,average,SEM, upperint, lowerint];

Time = final_data (:,1);
Meanint = final_data (:,2);
SEM = final_data (:,3);
upperint = final_data (:,4);
lowerint = final_data (:,5);

header = {'Time(s)','Mean','SEM','Upperint','LowerInt'};
%averaged_data_file = [name, 'data.xlsx'];
xlswrite('compiled_data.xlsx', header, 'averaged_data')
xlswrite('compiled_data.xlsx',final_data, 'averaged_data', 'A2')

%% plotting out final figure with mean and SEM

Fig_01 = figure('Color',[1 1 1]);

%-- Set the figure position and size to prevent the figure being too
low resolution (X pos, Y Pos, Width, Height)
set(gcf,'position',[100 100 800 600])
%-- Do this to make sure that the figure isn't cut off (or including
other windows) when exporting
movegui(gcf,'center')

% '-x' means plot x for all data points
% smooth() smooth data based on moving averages - this can be
changed
paleblue = 1/255*[115,164,255];
palered = 1/255*[255,131,153];
```

```
plot (Time, upperint,'Color',paleblue)
x2 = [Time; flipud(Time)];
inBetween = [lowerint; flipud(upperint)];
f = fill(x2, inBetween, paleblue);
set(f,'EdgeColor','none');
hold on

plot(Time,Meanint, 'k-x','Color',[0 .0 .0],'LineWidth', 1,
'MarkerSize', 2, 'MarkerEdgeColor', [0 .0 .0] )
hold on

plot (Time, lowerint, 'Color',paleblue)

hold off
% axis([0 inf 0 inf])
xlabel ('Time (s)', 'FontSize', 12, 'FontName', 'Ariel',
'FontWeight', 'bold')
ylabel ('Intensity (a.u)', 'FontSize', 14, 'FontName', 'Ariel',
'FontWeight', 'bold')
grid off
title ('')
set(gca,'FontSize',12, 'FontName','Ariel', 'Box', 'off', 'TickDir',
'out')

saveas(Fig_01,'Averaged_data.png')
```

1.4 Matlab script for curve fitting

Matlab script for curve fitting and calculating parameters, created by David Mason, University of Liverpool

```
clear all;close all;
%-- get the user to find the MAT file which should contain two
variables data_norm and data_hypo
[inFile,inPath]=uigetfile('*.mat');
%-- load the workspace
load([inPath,inFile]);

%-- do you want to produce plots for quality control? creates a
subplot
makeFig=0; %-- [0,1]

%-- Loop both conditions
for condition=1:2

    %-- load in the relevant dataset
    if condition==1
        data=data_norm;
    else
        data=data_hypo;
    end

    %-- If requested create an output figure
    if makeFig==1
        %-- figure out the dimensions of the subplot
        nPlots=size(data,2)-1;
        sub_cols=floor(sqrt(nPlots));
        sub_rows=ceil(nPlots/sub_cols);
        %-- create the figure
        figure();
        set(gcf, 'Position', get(0, 'Screensize'));
    end
    %-- pull the time data from the first column
    pT=data(:,1);

    %-- loop all traces to produce OUTPUT variable one row per trace
with the following columns
    %1   trace number
    %2   Raw Data Maximum
    %3   Raw Data Index
    %4   Smoothed Maximum
    %5   Smoothed Index
    %6   Smoothed Index Time (sec)
    %7   R squared for off time exp fit
    %8   Intercept for off time exp fit
    %9   Slope for off time exp fit (/sec)
    %10  Calculated t 1/2 for off time exp fit FROM EXPERIMENT START
(sec)
    %11  Calculated t 1/2 for off time exp fit FROM SMOOTHED PEAK
(sec)
    %12  R squared for on time exp fit
    %13  tau value for on time exp fit
```

```
    %14  Half time for recruitment (sec)

    for trace=2:size(data,2)

        pI=data(:,trace);
        output(trace-1,1)=trace-1;
        [maxVal_Raw,maxPos_Raw]=max(pI);
        output(trace-1,2:3)=[maxVal_Raw maxPos_Raw];

        %-- find smoothed maximum

[maxVal_smo,maxPos_smo]=max(smooth(pI,floor(size(pI,1)*0.3)));
        output(trace-1,4:6)=[maxVal_smo,maxPos_smo,pT(maxPos_smo)];

        %-- check there are sufficient off points (some traces peak
at final point)
        if size(pI,1)-maxPos_smo>5
            %-- fit everything past the max point (plus a bit) to an
exponential decay curve

[fitVals,fitAlg,fitGOF]=fit(pT(maxPos_smo+5:end),pI(maxPos_smo+5:end
),'exp1');

            if makeFig==1
                %--select which plot to use
                subplot(sub_rows,sub_cols,trace-1)
                %-- plot the original
                plot(pT,pI,'b.')
                hold on
                %-- Plot smoothed maxima
                plot([pT(1),pT(end)],[output(trace-
1,4),output(trace-1,4)],'-','Color',[0.3 0.3 0.3])
                %-- highlight the points used for decay plot
                plot(pT(maxPos_smo+5:end),pI(maxPos_smo+5:end),'go')
                %-- plot the decay fit
                plot(fitVals,'r--')
                %-- get rid of the legend
                legend 'off'
                title(['C',num2str(condition),' Trace
',sprintf('%03d',trace-1)]);
            end

    %-- calculate the 50% (between peak and first value) off time
(you can select just good fits here or include everything
            if fitAlg.rsquare>0
                output(trace-
1,7:10)=[fitAlg.rsquare,fitVals.a,fitVals.b,(log(((maxVal_smo-
1)/2)+1)/fitVals.a))/fitVals.b];
                output(trace-1,11)=output(trace-1,10)-output(trace-
1,6);
                if makeFig==1
                    plot([output(trace-1,10),output(trace-
1,10)],ylim,'m-');
                end
            end

            %-----------------------------------------------------
-------------------------------------
            %-- Try to fit the on-rate from start to maxPos_smo
```

```
            %-------------------------------------------------------
------------------------------------
            %-- pull the on data
            pT_on=pT(1:maxPos_smo);
            pI_on=pI(1:maxPos_smo);

            %-- two approaches either normalise the data or
incorporate the processing into the fit
            %-- both come out with the same value for tau

            %-- option 1
            if (0)
                %-- unity normalise the Y data to fit the equation
from XXX
                pI_on_norm=(pI_on-1)./(maxVal_smo-1);

                custExp='1-exp(-x/tau)';
                %-- fit the data using 100 (s) as the start point
for the tau paramater

[fitVals_on,fitAlg_on,fitGOF_on]=fit(pT_on,pI_on_norm,custExp,'Start
Point',100);
            end

            %-- option 2
            if (1)
            %custExp='1+(1-exp(-x/tau))*(maxVal_smo-1)';
            custExp=['1+(1-exp(-x/tau))*',sprintf('%.2f',maxVal_smo-
1)];

            %-- fit the data using 100 (s) as the start point for
the tau paramater

[fitVals_on,fitAlg_on,fitGOF_on]=fit(pT_on,pI_on,custExp,'StartPoint
',100);
            end

            %-- record the rsquare for the exp fit
            output(trace-1,12)=fitAlg_on.rsquare;

            if fitAlg_on.rsquare>0

                %-- record the tau value
                output(trace-1,13)=fitVals_on.tau;

                %-- record the half time
                tmp_halfY=(((maxVal_smo-1)/2)+1);
                output(trace-1,14)= -log(1-   (( tmp_halfY -1) /
(maxVal_smo-1)) )  *fitVals_on.tau;

                if makeFig==1
                    %-- plot the curve
                    plot(fitVals_on,'r--');
                    %-- get rid of the legend (again)
                    legend 'off'
                    %-- plot the half time
                    plot([output(trace-1,14),output(trace-
1,14)],[0,tmp_halfY*1.1],'g-');
```

```
                    plot([0,output(trace-
1,14)*1.5],[tmp_halfY,tmp_halfY],'g-');
                end
            end


        else
            %-- NaN empty values
            output(trace-1,7:11)=nan(1,5);
        end %-- loop sufficient off time

    end %-- loop traces


    disp(['Condition ',num2str(condition),' : Mean time to peak:
',sprintf('%.f',mean(output(:,6),'omitnan')),' sec (SD:
',sprintf('%.f',std(output(:,6),'omitnan')),' sec)'])
    disp(['Condition ',num2str(condition),' : Mean off time:
',sprintf('%.f',mean(output(:,11),'omitnan')),' sec (SD:
',sprintf('%.f',std(output(:,11),'omitnan')),' sec)'])

%-- rename the output file per condition
    if condition==1
        output_norm=output;
    else
        output_hypo=output;
    end
    clearvars output;
end %-- loop condition

%clearvars -except output*;

if (0)
    xVals=randn(size(output_norm,1),1)+5;
    plot(xVals,output_norm(:,11),'bo')
    hold on
    xVals=randn(size(output_hypo,1),1)+10;
    plot(xVals,output_hypo(:,11),'ro')
    xlim([-5 20])
end
```

1.5 ATM activation in U251-MG and D566-MG under severe hypoxia

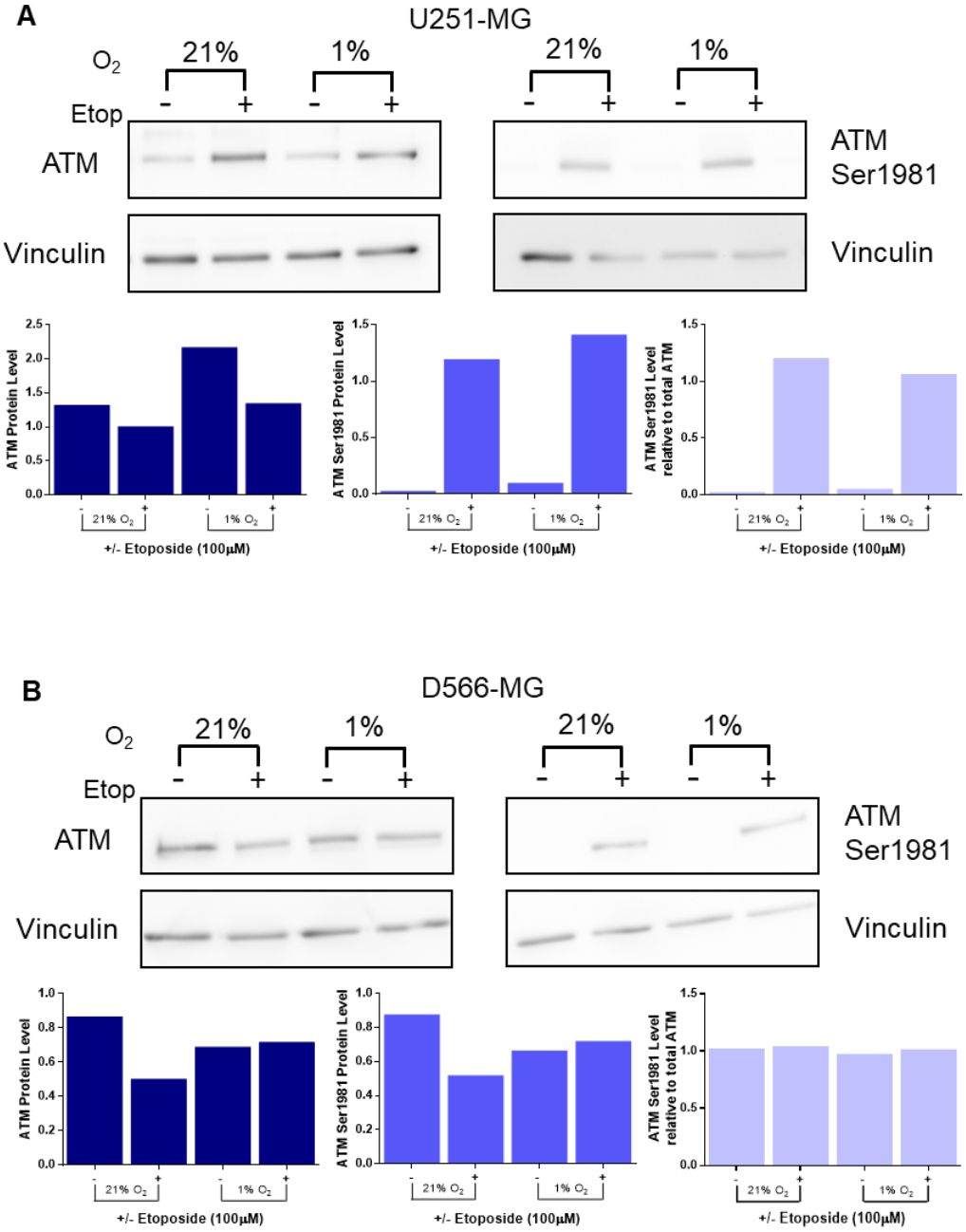

ATM and ATMSer1981 levels in U251-MG and D566-MG incubated in moderate hypoxia. (A) U251-MG and (B) D566-MG cells were incubated in in 1% or 21% O_2 for 5 days before treatment with 50 μM etoposide for 4 h. Protein was extracted and a western blot performed for ATM and ATMSer1981. At least three independent experiments were conducted. Densitometry was performed on a single representative blot using Image J.

1.6 ATM activation in U251-MG and D566-MG under severe hypoxia

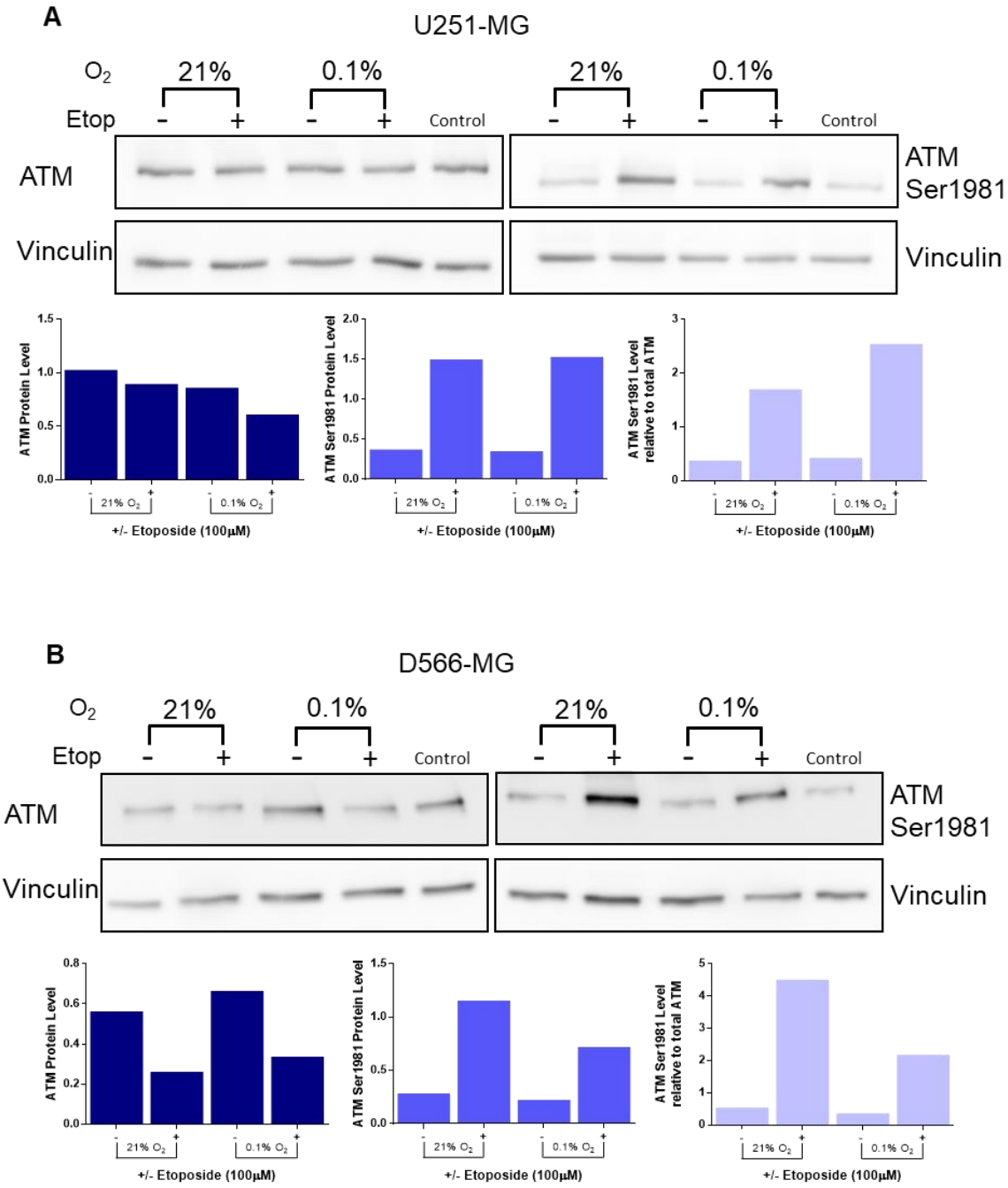

ATM and ATMSer1981 levels in U251-MG and D566-MG incubated in severe hypoxia. (A) U251-MG and (B) D566-MG cells were incubated in in 0.1% or 21% O_2 for 5 days before treatment with 50 μM etoposide for 4 h. Protein was extracted and a western blot performed for ATM and ATMSer1981. At least three independent experiments were conducted. Densitometry was performed on a single representative blot using Image J.

1.7 DNA Ligase IV western blot

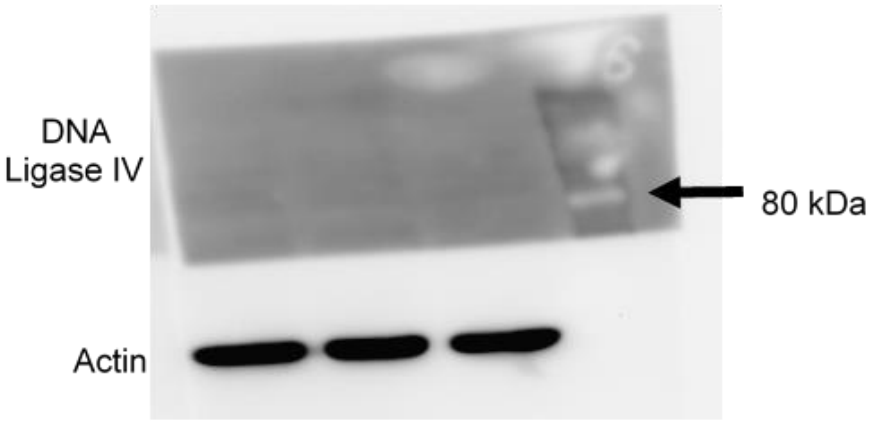

DNA ligase western blot example using Abcam Ab26039 antibody. 30 µg of protein was loaded per well from D566-MG whole cell lysate. Antibody was used at 1 in 1000. Actin was used as a loading control. No bands were observed for DNA ligase IV.

1.8 *PARP1* and *PMS2* expression time course

PARP1 and PMS2 are downregulated by acute and chronic hypoxia

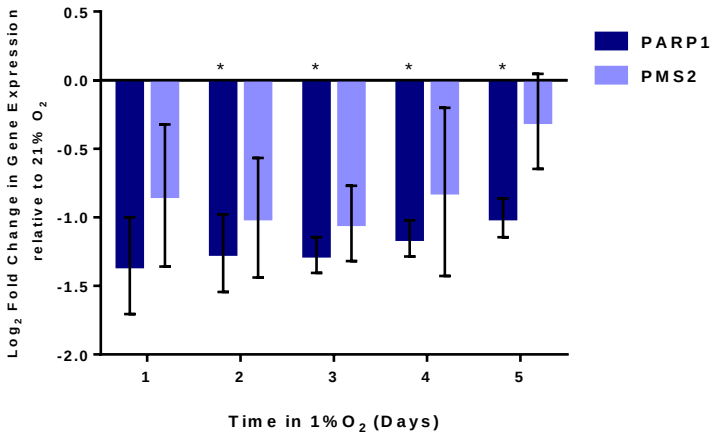

*PARP1 and PMS2 are downregulated after chronic and acute hypoxic exposure. D566-MG cells were incubated in 1% O_2 for 1-5 days, as well as 21% O_2. After incubation, RNA was extracted and converted to cDNA for RT-PCR experiments, probing for PARP1 and PMS1. Data is represented as log_2 fold change in mRNA levels with respect to level for the 21% O_2 samples. Data are the mean of at least three independent experiments, with error bars showing S.E.M. * denotes significant data where $p<0.05$ indicated by one-way student t-test.*

1.9 *PARP1, PMS2* and *WRN* expression after HIF inhibition

HIF inhibition does not restore *PARP1*, *PMS2* or *WRN* expression

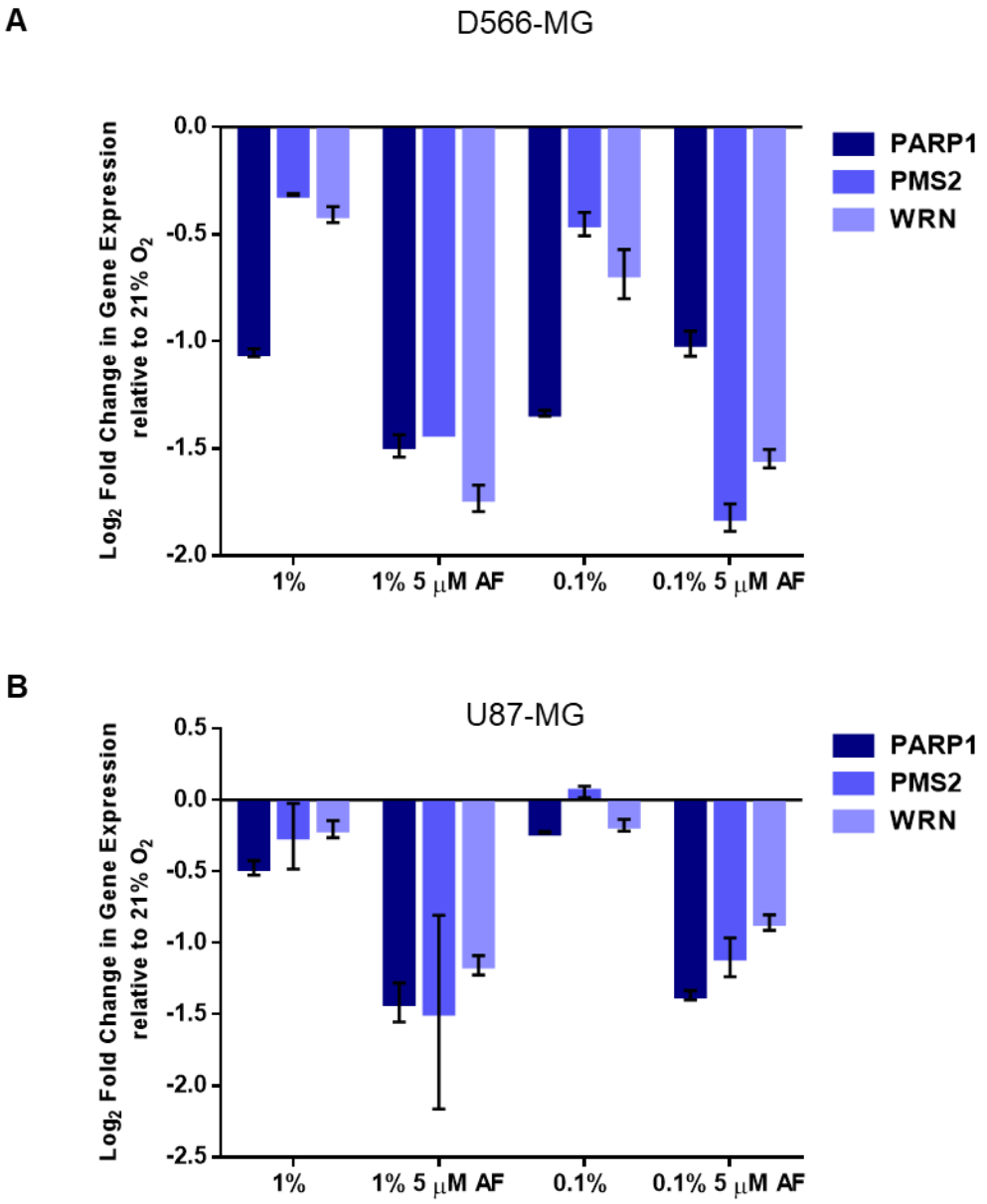

HIF inhibition does not restore PARP1, PMS2 or WRN mRNA levels in hypoxia. (A) D566-MG and (B) U87-MG cells were incubated in 21% and 1% O_2 for 24 h with and without 5 μM Acriflavin. After incubation, RNA was extracted and converted to cDNA for RT-PCR experiments. Data is represented as log_2 fold change in mRNA levels with respect to level for the 21% O_2 samples. Data are the mean of at least three independent experiments, with error bars showing S.E.M.

1.10 Digoxin does not affect HIF-1α levels or HIF transcriptional activity.

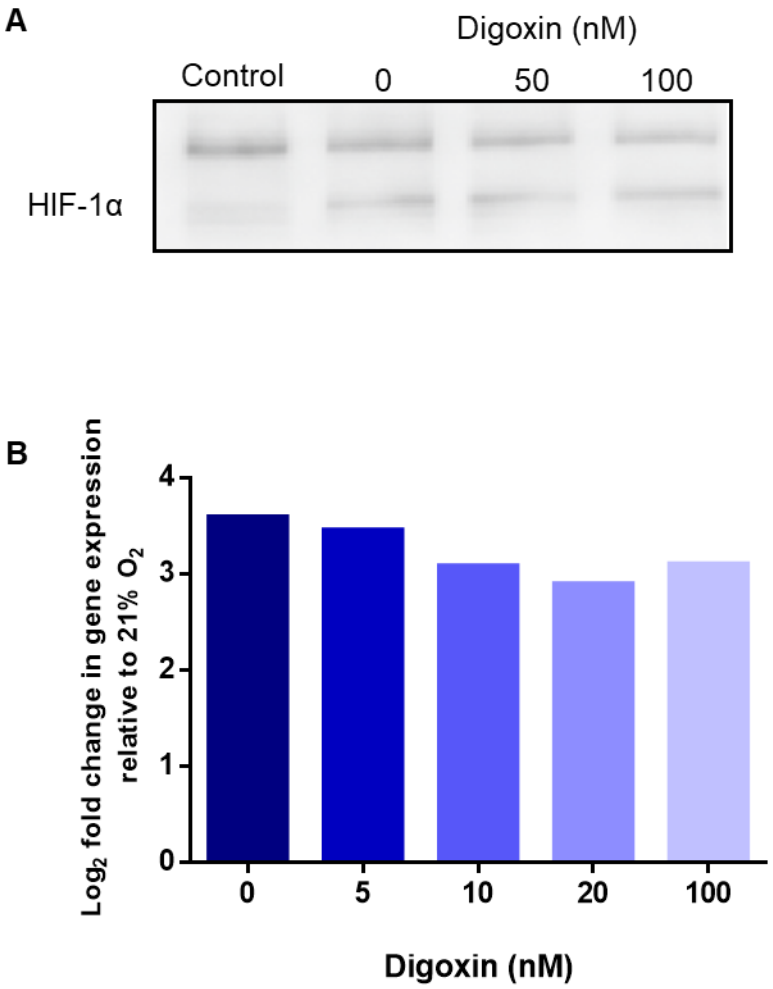

Digoxin does not affect HIF-1α levels or HIF transcriptional activity. D566-MG cells were treated for 8 h with digoxin before incubating in 1% O_2 for 24 h. (A) Western blot of HIF-1α after 0 – 100 nM digoxin treatment. Control represents untreated cells incubated at 21% O_2. (B) RT-PCR of GLUT1 levels after treatment with 0 – 100 nM digoxin. Data is represented as fold change with respect to 21% O_2. Figure represents data from a single experiment.

1.11 MRE11 and NBN localisation

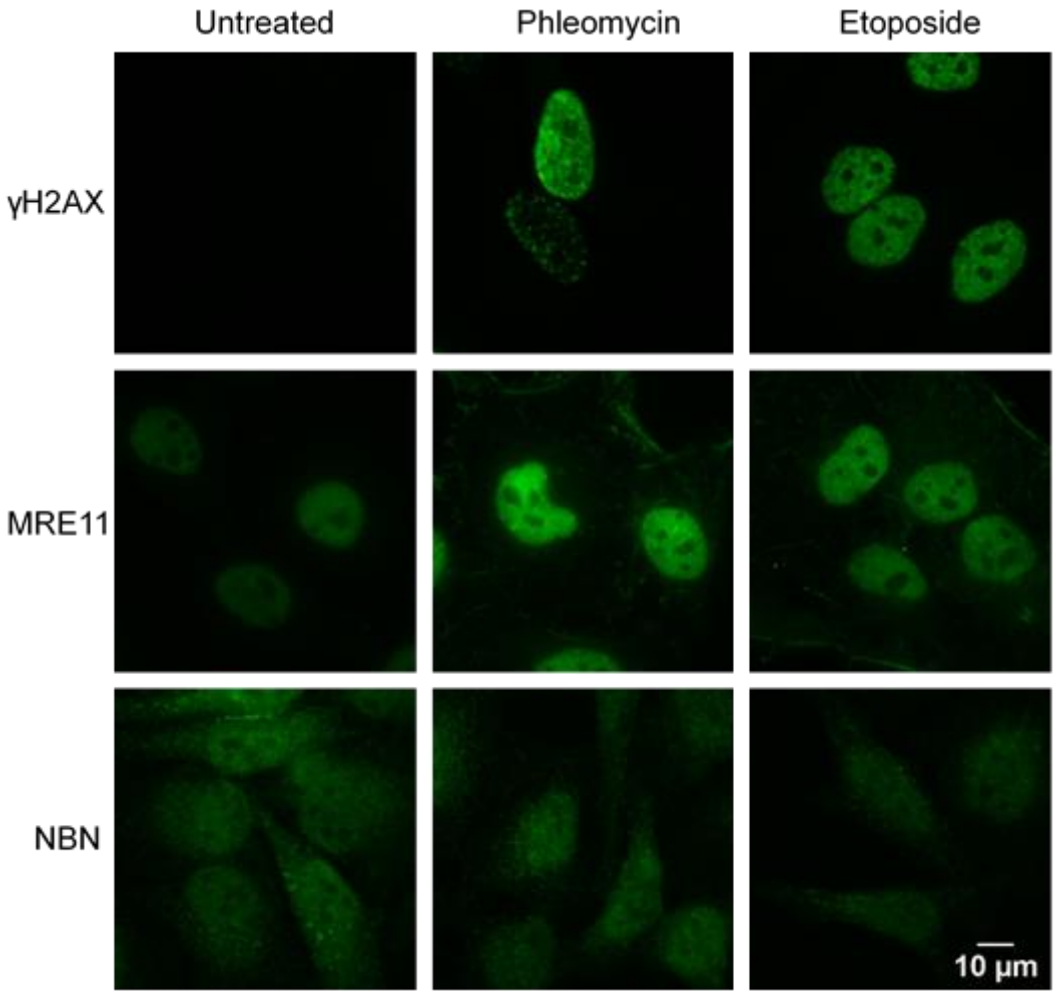

MREl1 and NBN localisation after drug treatment. HeLa cells were treated with 50 µg/ml phleomycin or 50 µM etoposide for 4 h fixing and performing immunocytochemistry for γH2AX, MREl1 and NBN. Imaged on a Zeiss axiovert Epifluorescence microscope using Zeiss 38 HE filter set (GFP) with 100x objective.

1.13 Time to maximal intensity measurements

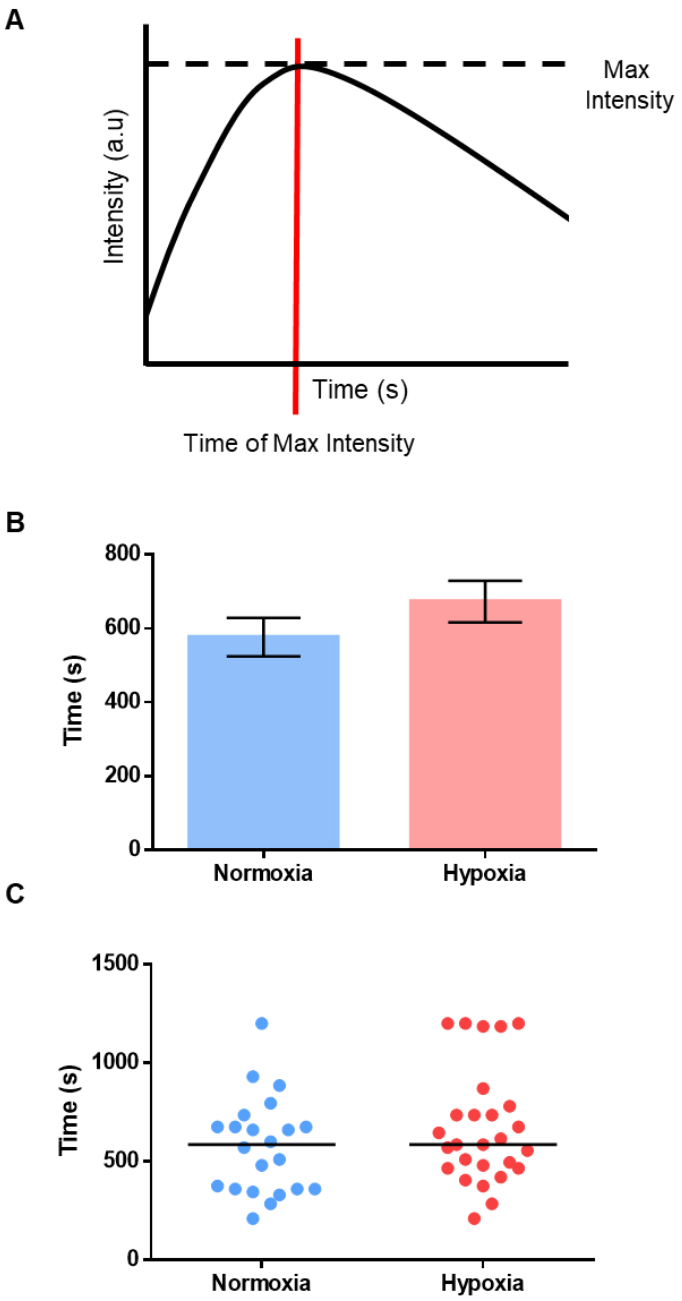

*Time to maximal intensity. D566-MG cells transfected with XRCC4-EGFP were subjected to laser micro-irradiation. Signal intensity was measured for each individual cell. Normalised signal intensity was used to determine the time at which maximal intensity is observed as depicted by the schematic in (A). B) The mean time to maximum intensity for normoxic (n = 22) and hypoxic (n = 27) cells was determined, with error bars representing S.E.M. C) The distribution of time to maximal intensity for each hypoxic and normoxic cell. Line represents the median. * denotes significant data where p<0.05 indicated by student t-test.*

Thesis Output

1. Publications

Decrease of Nibrin expression in chronic hypoxia is associated with hypoxia-induced chemoresistance in medulloblastoma cells.

Sophie Cowman, Yuen Ngen Fan, Barry Pizer, Violaine See. 2018 *Under review in BMC Cancer*

(pre-print: https://www.biorxiv.org/content/early/2017/11/30/227207)

2. Talks

Alteration of DNA Repair Activity in Hypoxic Brain Tumours Underlies Treatment Resistance. *Keystone: Therapeutic Targeting of Hypoxia Sensitive Pathways.* April 2018. Oxford, UK.

How Does Hypoxia Influence DNA Repair? *North West Annual DNA repair Meeting.* April 2018. Liverpool, UK.

Hypoxia, DNA Repair and Brain tumours. *North West Cancer Research Scientific Symposium.* April 2018. Liverpool, UK. Best flash talk prize awarded

3. Poster presentations

Gordon's Research Conference: DNA Damage, Mutation and Cancer. March 2018. California, USA.

Keystone: Therapeutic Targeting of Hypoxia Sensitive Pathways. April 2018. Oxford, UK.

Frontiers in DNA Repair. September 2016. Berlin, Germany.

North West Cancer Research Scientific Symposium. 2015, 2016, 2017, 2018.

Institute of Integrative Biology Away Day. 2015, 2017. Liverpool, UK. Best poster prize awarded.

4. Other

Gibco Cell Culture Hero, Webinar presentation, Hypoxia, DNA Repair and Brain tumours. April 2018.